DEVELOPMENT OF TiAl BASED INTERMETALLICS BY MECHANICAL ALLOYING AND SINTERING

Ph.D. THESIS

by

DEBESH DEVADUTTA MISHRA

DEPARTMENT OF METALLURGICAL AND MATERIALS ENGINEERING
INDIAN INSTITUTE OF TECHNOLOGY ROORKEE
ROORKEE – 247 667 (INDIA)

MAY, 2014

ABSTRACT

This study is a part of larger effort towards the fundamental understanding of structure-property relationship of mechanically alloyed titanium aluminide based nanocomposites containing Cr, Nb and Ni-P coated graphite and carbon powders as second phase reinforcement. The aluminides are synthesized using mechanical alloying and two routes of sintering i.e. pressure less and pressurized sintering. The applications of these aluminides as thermo structural part need strength and in turn densification. Mechanical alloying and the formation of aluminides during sintering hinder the densification process. The formation of aluminides consists of self propagating high temperature reaction, which causes in the bulging of the compacts. The nanograined feature of the compacts though gave higher hardness and strength but the densification were not found desired, which is due to the lack of compressibility of workhardened mechanically alloyed powders.

Morphological and phase analysis of the mechanically alloyed partiecles was studied using TEM, FESEM, and XRD. Archimedes principle was used to study the density of sintered samples and the percentage densification after pressure less and pressurized sintering. The pressurized sintering was carried out in GLEEBLE^{TM} thermo mechanical simulator by the help of plungers. The hardness of the compacts was calculated using Vickers hardness tester. The thermal behavior of the as received powder blends and mechanically alloyed powders were determined using DTA.

As the mechanically alloyed powders having lesser densification, in order to determine the route for better densification, reaction synthesis route is used for the formation of Titanium Aluminides. In reaction synthesis route Titanium and Aluminium powders were mixed in a 50:50 at% composition. To see the effect of particle size on the densification and activation energy, Ti and Al powders were milled separately, to attain particle sizes of 100µ, 25-27µ and 7-9µ. After optimization by milling separately, Ti powders were milled for 1h, 5h and 10h respectively to attain above particle sizes. Al powders were milled for 1h,4h and 7h ton attain above particle sizes respectively. To determine effect of Al particle sizes keeping the Ti particle size constant (44µ), Various particle size of Al were mixed with Ti, to attain Ti-Al (50:50 at%). Similarly to determine the effect of Ti particle size Al powder size were made constant and various particle sizes Ti were mixed with it to prepare powder blends. To determine the cumulative effect of

particle sizes, approximately equal particle sizes of Ti and Al were mixed with each other to prepare powder blends.

The thermal analysis behavior of the powder blends were calculated using DTA and effect of heating rates were determined using three different heating rates. The reaction sintering temperatures (exothermic temperatures) are used to calculate the activation energy of the above mixtures. FESEM analysis was carried out to determine the microstructural evolution. Densification after reaction sintering was detrmined using Archimedes principle.

The above powder mixtures with various Ti particle size, various Al Particle size and cumulative particle size were also subjected to dilatometric calculations. In order to calculate the bulging/expansion during reaction synthesis the dilation behavior is calculated. Dilatometric analyses was calculated at five different soaking temperatures i.e 600^0C,650^0C,700^0C,750^0C and 800^0C to explain solid state sintering, transient liquid phase sintering and formation with completion of Titanium Aluminides.

Using ANN(artificial neural network) and Fuzzy modeling (ANFIS), a model is prepared, where composition, soaking temperature and relative percentage of expansion was given as the input and the average shrinkage rate is the output and the resultis calibrated and validated with 50% of the results.

ACKNOWLEDGEMENT

The author has great privilege and gratification to express his heartiest thanks and deep sense of gratitude to his respected supervisors Dr. V.Agarwala, Professor &Head (centre of nanotechnology), and Dr. R.C. Agarwala, Professor, Department of Metallurgical and Materials Engineering, IIT Roorkee, for their valuable guidance and indefatigable efforts throughout the tenure of this work. They have been an inspiring and driving force where targets appeared to be difficult during the course of work. Their timely help, constructive criticism, positive attitude, painstaking efforts, humanistic and warm personal approaches made the author capable to compile the thesis in its present form. Prof. V. Agarwala helped me grow not only as a researcher, but also as an individual. I am very proud to be one of his students.

Profound sense of appreciation acknowledged to all the members of Student Research Committee (SRC), Dr. B.S.S. Daniel, Chairman, SRC, Dr. K.L. Yadav, External Member and Dr. G.P. Chaudhary, Internal Member for their precious assessment throughout. My special thanks are due to Dr. V.V. Dabhade, Assistant Professor, Metallurgical and Materials Engineering Department, Indian Institute of Technology, Roorkee and Dr. Rama Mehta, Scientist, National Institute of Hydrology, Roorkee, for their ever kind string of help, moral support and encouragement.

Deep sense of admiration acknowledged to the Head, Institute Instrumentation Centre (IIC), for their co-operation in extending the necessary facilities and supports during the course of characterization work. A special thanks to all the IIC faculty and technical staff members for giving their full assistance for all characterization facilities.
The author would like to express his sincere thanks to the technical and administrative staff of Department of Metallurgical and Materials Engineering.

The author wishes to thank his friends and colleagues for their moral support and help to keep things in perspective. Thanks are due to, Dr. Manjeet Singh Goyat, Dr. Abhishek Kumar, Mr. Siddharth Jain, Mr. Prashant Gupta, Mr. Ram Kishore, Mr. Tilak Joshi, Mr.V.M.R. Mutthaiah, Ms. Nidhi Rana, and last but not the least Ms.Preeti Makkar and all the fellows who helped me directly or indirectly during the entire period of this work.

The author expresses his deepest esteem to his father, Shri Bhabani Sankar Mishra and mother, Smt. Satyabati Rajguru Mohapatra for keeping their blessing over me. The author is highly appreciative to his sister Ms. Sushree Smruti Mishra for their encouragement throughout.

Finally, the financial assistance from Department of Science & Technology (DST) of India and Ministry of Human resource Development (MHRD), New Delhi, India also gratefully acknowledged.

Roorkee

Dated: **DEBESH DEVADUTTA MISHRA**

TABLE OF CONTENTS

LIST OF TABLES

LIST OF FIGURES

NOMENCLATURE

Symbol	Description
TiAl	Gamma Titanium Alumnides
Ti_3Al	**α 2** Titanium Aluminides
At%	Atomic percent
T_{MP}	Melting point
MA	Mechanical Alloying
SHS	Self Propagating High Temperature Synthesis
RS	Reaction Synthesis
Wt %	Weight percent
μ	diffusional relation between thickness of the intermetallic compound
D	controlling diffusion rate
t	duration taken for the formation of the compound
FESEM	Field emission scanning electron microscopy
EDAX	Energy dispersive X-ray spectroscopy
TEM	Transmission electron microscopy
AFM	Atomic force microscopy
XRD	X- ray diffraction
FT-IR	Fourier transform infra red
DTA	Differential thermal analysis
TGA	Thermo-gravimetric analysis
Gr	Graphite
B	material constant
Q	activation energy for diffusion
T	absolute temperature
G	grain size
k	the Boltzmann's constant
n	stress exponent

ρ	Density
W_a	weight of sample in air
W_w	weight of sample in air
R	Characteristic of interplaner spacing d_{hkl} of reflecting plane
λ	wavelength of the electron beam
L	distance between the specimen and the screen
HEBM	High Energy Ball Milling
EL	Electroless
F_B	buoyant force
m_L	mass of the liquid displaced
m	Mass of the sample
V	Volume of the sample
HP	Hot Pressed
α	reacted fraction
t	time for transformation
R	gas constant
β	heating rate
T_m	maximum reaction rate point
E	Activation Energy
DTG	Differential Thermal Gravimetry
JCPD	Joint Commission of Powder Diffraction
SCT	Soft Computing Techniques
ANFIS	Artificial Neural Fuzzy Inference System
SCM	Subtractive Clustering Method
FIS	fuzzy inference system
MF	Membership Functions
FLT	Fuzzy Logic Theory
ANN	Artificial Neural Network
r_a	cluster radius
$\|x_i - x_j\|$	Euclidean distance
(p_i^*)	data point with highest potential
D_1^*	first cluster centre

(D_2^*)	second cluster centre
$r_b \quad r_b > r_a \geq 0$	radius that results in measurable reduction in the potential of neighbourhood data points
c_i	is the number of categories in the i^{th} variable

CHAPTER 1

INTRODUCTION

The intermetallics compounds are different from solid solution alloys as it shows ordered structure, where atoms tend to position at specific lattice sites. The dissimilar atomic bonds are having higher strength than the similar atomic bonds, helping in the ordered atomic arrangement (Taub and Fleischer 1989).The tendency to form of alumina covering of these aluminides renders them oxidation resistant (Doychak 1994). Gamma titanium aluminides are potential materials for use upto 1273K, but the α_2 can be used upto 973 K. The density of the gamma alumnides are half of that of the superalloys and have high specific modulus and comparable specific strength at elevated temperatures (Lipsitt et al. 1985, Tetsui 2002 Appel et al. 2003).

Intermetallics of different systems are used in various applications such as chemical, electrochemical, electromagnetic and thermo structural. Nickel, iron and titanium aluminides are potentially preferable materials for thermo structural applications in aerospace, automobile and energy industries (Zhao and Westbrook 2003; Appel et al. 2000; Tetsui 2002; Lipsitt et al. 1985; Sauthoff 1989; Hunt et al. 1990). Iron aluminides i.e Fe_3Al and FeAl have densities as low as 5.4-6.7 g/cc are one of the economically viable materials used for industrial furnace machineries and accessories. Day by day it is replacing stainless steel for high temperature applications upto 873K (Vedula 1994).Generally Ni_3Al (γ') used as second phase strengthening material in nickel based super alloys for thermo structural applications. Due to lower density and better elevated temperature behavior Ni_3Al, NiAl, TiAl and Ti_3Al intermetallics are very attractive materials for aerospace and automotive applications. TiAl is used in applications such as turbine blades, rotor discs, fins, nozzle fins and rotor discs; Mitsubishi is using gamma titanium aluminide in turbocharger rotors in commercial automobiles since 1999.

The poor ambient temperature ductility can be attributed towards the ordered structure of the aluminides; this renders the materials to be processed hardly through ingot metallurgy route (Lipsitt et al. 1985; Taub and Fleischer 1989; Huang and Chesnutt 1994). Elemental segregation, non homogeneous structures, cracking and

requirement of secondary machining are the other difficulties faced during ingot metallurgy route. So Powder metallurgy route is preferably used for processing to attain near net shape components with fine grains and uniform elemental distribution (Whittenbereger 1990; Kim et al. 1999).

The near net shape for titanium aluminides can be achieved by various processes like pre alloying, mechanical alloying and reaction synthesis (RS) in the PM route. Amongst the three processes RS process is comparably simple and can result for the near net shape product easily. Various researchers have made effort for fabrication of nickel and titanium aluminides through RS and its types like synthesis by combustion(Yi and Moore 1988), reactive hot pressing (Rawers and Wrzesinky 1992; Kim et al. 1999; Qian Wang et al. 2000; Wen et al. 2001), reactive hot isostatic pressing (German et al. 1989), XD^{tm} process (Westwood 1988) etc. Most of these reaction synthesis studies are dependent upon stoichiometric compositions. Very little work has been carried out on Ti48Al2Cr2Nb alloy for gamma titanium aluminides used in aerospace and automobile applications.

RS process is advantageous as the process requires low energy, high purity products as outcomes and easy near net shape processing. In titanium aluminides the two phase alloy Ti48at%Al is of practical interest as it shows better ambient temperature ductility due to duplex structural combination of γ and α_2 phases. An increment in ductility for binary alloy is noticed, when alloyed with Cr, Mn and V for 2-5 at%.

Thus, the present work is undertaken with an aim (i) To develop prospective lightweight γ titanium aluminide materials by mechanical alloying with ternary and quaternary compositions of Ti-48at%Al-Nb and Ti-Al-Cr-Nb-Ni-P(Gr/C).(ii) To observe the pressureless sintering and the consolidation through hot pressing on the basis of densification. (iii) To determine the lowest of activation energies for various mixtures of Ti and Al where, the above has been calculated for various particle sizes of Ti(keeping Al particle size constant),Al(keeping Ti particle size constant) and both Ti and Al particle size varying. (iv) To study the % relative expansion, rate of expansion and activation energy calculation for the best ever route to find the reaction synthesis process.

The thesis has been organised in different chapters as follows:

The subject of intermetallics is introduced in the beginning with their properties,

advantages, limitations and various applications. In the second chapter, literature review on various types of aluminides of interest, their crystal structures, alloying additions, property, various microstructures, processing techniques etc. are presented. An overview of reaction synthesis process as compared to other processes is also included in this chapter.

This description leads to the formulation of problem, which has been presented in the third chapter, which defines the total scope of present work.

Experimental details are included in Chapter-4 providing details of raw materials (Ti, A1 Cr, &Nb powders), their mechanical alloying and blending in planetary ball mill, experimental set-up used for sintering(non-reaction synthesis) and reaction sytnthesis of the compacts. The experimental parameters (pressure, temperature and composition) followed for compacts have also been described with the set up of GLEEBLE^{TM} used for hot pressing. The characterisation methods used for density measurement, phases present, microstructure (both optical and TEM), elemental mapping and hardness calculations are included.

In the fifth chapter, results of mechanically alloyed Ti-48Al-Cr-Nb- NI-P/ (Gr, C) are discussed with the morphological characterizations, thermal analysis and phase analysis. This chapter also consists of the mechanical alloying of Ti-48Al-Nb composition and the comparison of sintering on the basis of densification and hardness for pressureless and pressurized (hot pressing) sintering.

Chapter-6 provides results of reaction kinetics studies conducted with temperature and particle size of Ti, Al and (Ti+Al) mixture (Ti-50at%Al composition) during reaction synthesis process. Ti and Al powders were subjected to milling separately for various durations to attain particle sizes of ~100 µ,~25µ and ~7µ and are mixed with each other to observe the effect of particle size of Ti ,Al and (Ti+Al) mixtures on the activation energy and reaction kinetics. The above study also provides an idea about the mixture and lowest/ highest particle size providing lowest activation energy and facilitating the process of reaction kinetics.

The relative percentage expansion, rate of expansion and mean rate of expansion of the various particle size mixtures for the effect of various Ti, Al and (Ti+Al) particle sizes were determined and described in Chapter-7. The activation energy for the above reactions were determined and studied for the least dilation during the reaction synthesis. The above study also gives an idea about the optimized route to

have higher densification and least expansion during reaction synthesis with optimized activation energy.

The conclusions drawn from the results of DTA kinetic studies, RS experiments and the effect of various particle sizes of Ti and Al with the dilatometric behavior are included in the Chapter-8.

In Chapter-9, suggestions for future work in the field are presented based on the Marts of this work.

CHAPTER 2

LITERATURE SURVEY

2.1 Introduction

The ordered crystal structure with constituent atoms preferentially occupying lattice sites is the source of greater strength with dissimilar atoms having better affinity with respect to similar atoms (Taub and Fleischer 1989). The history of the intermetallic compounds depict that includes diverse applications such as cementation, dental amalgam, shape memory alloys and magnets (Westbrook 1977, 1993, Sauthoff 1995).

The brittle characteristics of the intermetallics were the need for the research on various fabrication routes like mechanical alloying (Dutkiewicz et al. 2004; Xinkun et al. 2002; Yinjiang cl al. 2002;Yonggan et al. 2004; Suryanarayana 2001. 2002; Benjamin 1970; Baburaj et al. 2000, Froes et al. 1995), reaction synthesis (Bertolino et al. 2004; Chen et al. 2003; Zhenbin et al. 2003; Minay et al. 2004) and casting (McQuay and Don 1997, Qin et al. 2001; Kuang et al. 2002; Chraponski et al. 2003; Tetsui 2002; Skrotzki et al. 2005; Springgate et al. 2000). The processing rotes also include conventional PM (Dimcic et al. 2005; Mei et al. 2000; Zhao et al. 1995). Some transition metal intermetallics have been developed by using innovative gas reduction route, where metal oxides were reduced at low temperatures for fine grained output. (Morales et al. 2000, 2002; Tilliander et al. 2005, Bustnes et al. 2000; Arvanitidis et al. 2000).

The machining of intermetallics is a difficult task and electro discharge machining (EDM) is widely used (Mohan et al. 2004). The current status of intermetallics and its use as high temperature materials for jet engines have been discussed in various studies (Yamaguchi et al. (2000); Zhao and Westbrook (2003)).

This chapter deals with different intermetallics of interest like iron, nickel and titanium aluminides and their properties, crystal structure, processing routes and relevant phase diagrams are also discussed. An attempt is also made to compare the intermetallics for their behaviors at high temperatures and ambient temperature. A review of transient liquid phase sintering, reaction synthesis has been included discussing the mechanisms and characteristic properties.

2.2 Nickel Aluminides

Owing to the elevated temperature properties along with lower densities than

nickel superalloys, nickel aluminides are the materials of interest from the late 1950's (Westbrook 1959; Liu and Pope 1994; Liu et al. 19S5; Taub et al. 1984; Bertolino et al. 2004; Chen et al. 2003; Zhenbin et al. 2003; Minay et al. 2004). Now –a-days, in aerospace and other sectors nickel aluminides are used commercially (Oak Ridge National Laboratory Review 2002).

The binary phase diagram for Ni-Al system is shown in Fig 2.1 which shows the homogeneity range of Ni_3AI and Ni_3AI intermetallic phases.

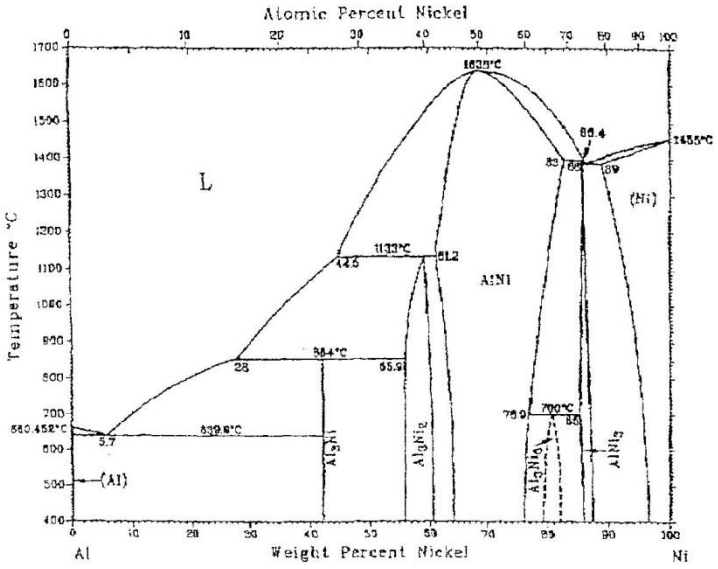

Fig 2.1 Binary Ni-Al phase diagram (Nash, Singleton and Murray 1991)

2.2.1 *Ni_3Al*

Ni_3Al is the most studied phase as it is important for providing strength at elevated temperatures.It is having $L1_2$ ordered, face centered type crystal lattice and four atoms in unit cell with three nickel occupying the face cenre positions and in the corner positions one Al atom is situated,Fig.2.2.

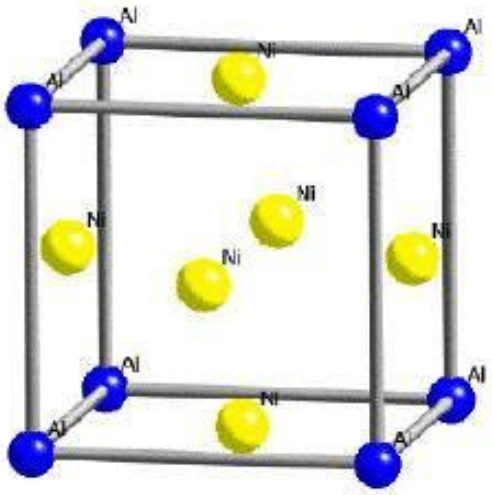

Fig 2.2 Ordered L12 crystal structure of Ni_3Al showing nickel atoms occupying face centered positions with aluminium atoms at the corner positions (Nash, Singleton and Murray 1991)

Nickel aluminides exhibit improve in the yield strength with increase in the temperature and the maxima reaches between 873 to 1073K (Copley and Kear 1967; Thornton et al. 1970; Paidar et al. 1984). The monocrystalline Ni_3Al exhibits better ductility in comparison to the polycrystalline ones. The brittleness of the polycrystalline Ni_3Al is attributed towards the poor cohesive strength of their grain boundaries (Liu 1991) and these materials can be ductilised by microalloying with boron (Liu et al. 1985; Taub et al. 1984).

Some of the processes like air induction melting, inert gas melting and vacuum electron beam melting were used for preparation of some commercial alloys like on Ni- 14 to 18A1- 6 to 9Cr- 0 to 4 Mo- 0.1 to 1.0 Zr/ Hf- 0.01 to 0.2 B(Liu and Pope 1994). The yield strength of an advanced aluminide alloy (Ni-16 Al- 8 Cr- 1.7 Mo- 0.5 Zr- 0.03B) is compared with commercial alloys (In 713C, Haste alloy -X and 316 stainless steel)(Liu and Pope 1994). Direct casting (Sikka 1990) and reaction synthesis (Bose et al. 1988; German et al.1989; Nishimura at al. 1993; Bertolino et al. 2004; Chen et al. 2003; Zhenbin et al. 2003; Minay et al. 2004) were some of the frequently used techniques for near net shape processing for nickel aluminides.

The segregation of boron at grain boundaries in Ni_3Al enhances the cohesive strength which inhibits the grain boundary fracture. With boron addition upto 0.08wt %, the ductility increases in steady manner (Liu and Pope 1994). The increase in ductility is also attributed towards the dimpled fracture in contrast to brittle fracture for the un alloyed Ni_3Al. The alloying of boron has been a starting point for the successful

fabrication of Ni_3Al alloys for elevated temperature applications (Liu et al. 1990). The thermo mechanical treatment on the recrystallisation of boron alloyed Ni_3Al has been studied in detail by Agarwala et al. (Agarwala V. et al. 2000).

The Nickel aluminides are used generally in automotive turbochargers, hydro turbines, cutting tools, pistons and valves for automotive and jet engines, dies and moulds and furnace fixtures (Liu and Pope 1994).

2.2.2 *NiAl*

The other intermetallics phase in Ni-Al system is NiAl which have B2 type crystal structure. The crystal consists of interpenetrating primitive cubic cells where Ni atoms occupy corners of one sub lattice and Al atom occupy corner of another sublattice. Figure 2.3 shows B2 (CsCl) type ordered cubic crystal structure of NiAl (Miracle and Darolia 1994). The discrepancy in the physical and the mechanical properties has been studied by Miracle (Miracle 1993; Miracle and Darolia 1994). The ordered structure of the NiAl remains intact upto 1911K. The Density of the NiAl is 5.9gm/cc and that of the Ni_3Al is 7.5 gm/cc. the polycrystalline NiAl have very less ductility and the addition of boron is not that much effective in improving the same(Reuss and Vehoff 1990).

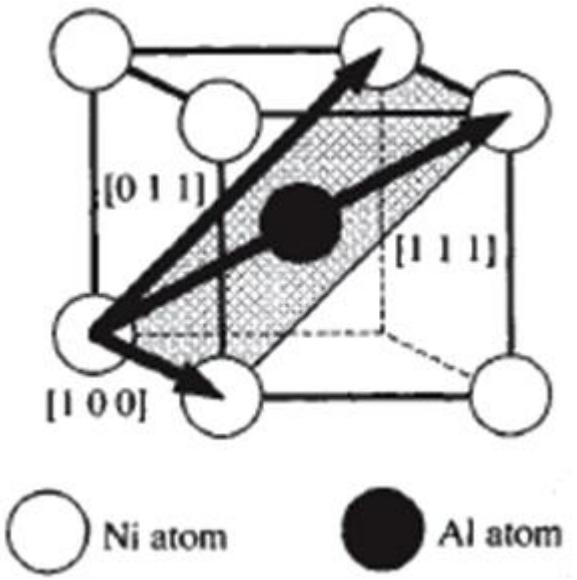

Fig 2.3 Ordered B2 crystal structure of NiAl (CsCl type)
(Miracle and Darolia 1994)

Due to the high ductility and low flow stress of the NiAl alloys above 873K conventional thermo mechanical processes like hot pressing, hot isostatic pressing, swaging, extrusion and hot rolling has been used for the fabrication(Liu and Pope 1994).

The Incapability of boron addition is attributed towards the increase in yield strength way over the fracture strength (George and Liu 1990). The brittleness problem in NiAl has been addressed by Haubold et al by fabricating ultra fine grained material i.e grain size of the order of 10nm(Haubold et al. 1992).

The addition of Be, Ga, Fe and Mo have shown some success in ductilising the NiAl (Baker and Munroe 1990; Darolia et al. 1992a). The compositional effect of these alloying additions on the ductility and yield strength of NiAl is shown in Fig. 2.6 (Darolia et al. 1992a).

2.3 Iron Aluminides

The phase diagram of Fe-Al system is included in Fig. 2.4 (Rabin and Wright 1991). Due to the good oxidation resistance, sulphidation resisitance and economical viability FeAl and Fe_3Al holds main interest amongst the iron aluminides (Vedula 1994).

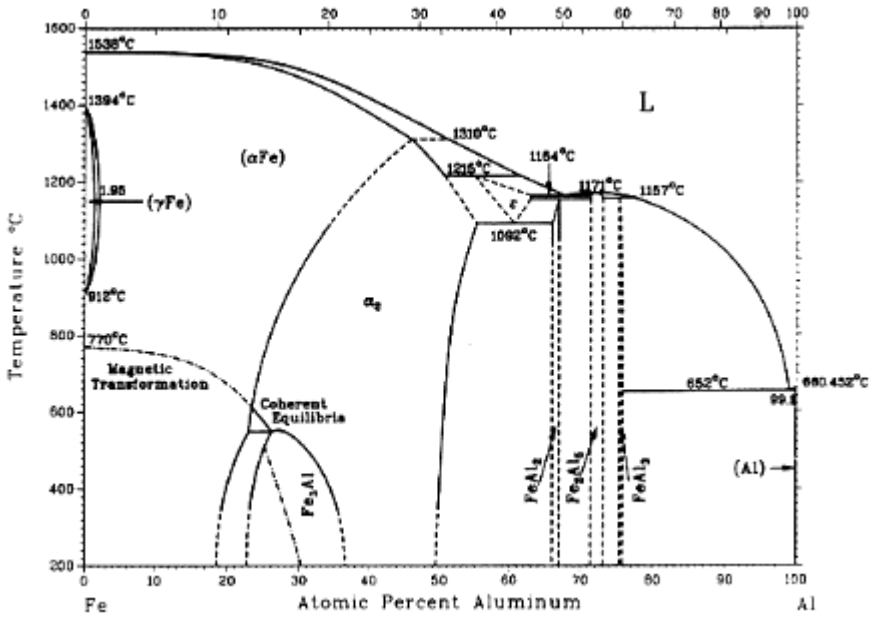

Fig 2.4 Binary Fe-Al phase diagram(Rabin and Wright 1991)

Iron aluminides have been produced by variety of method like melting (Deevi et al. 1997; Bahadur et al. 1995), roll compaction (Hajaligol et al. 1998; Deevi et al. 1999, 2000), reaction synthesis (Gedevanishvili and Deevi 2002) and mechanical alloying (Eelman et al. 1998; Oieszak et al. 1994). Iron aluminides production into thin sheets has been achieved by Mistler et al. (1998).

2.3.1 *Fe_3Al*

As per the phase diagram shown in Fig. 2.5, Fe_3AI phase transforms on cooling

from the disordered bcc solid solution (α), which remains stable till 1073K and then turns into B2 structured FeAl(α_2) and at last to DO_3 structured Fe_3Al phase. The DO_3 ordered crystal structure is shown in Fig. 2.4.

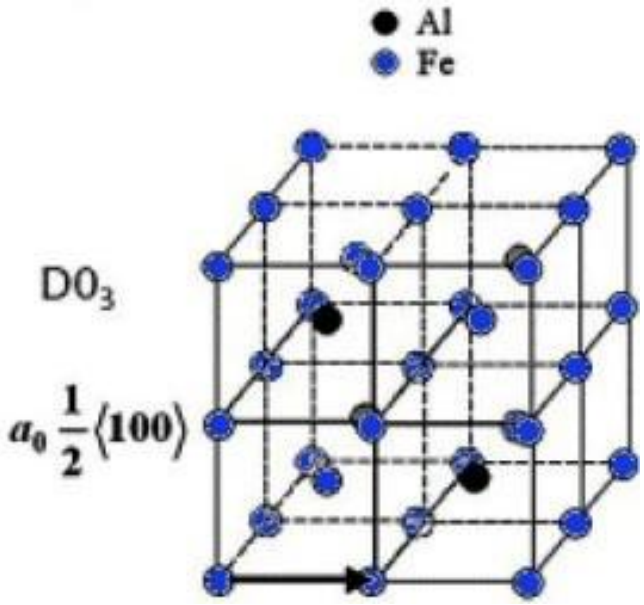

Fig 2.5 Ordered DO3 crystal structure of Fe_3Al (Rabin and Wright 1991)

These alloys are also prepared by electro slag refining, vaccum induction melting and vaccum arc melting from 500gm of melt upto 230kg (Vedula 1994). For fine grained materials powder processing by hot extrusion at 1273K with reduction ratio of 9:1 is also used.

Lots of researchers have worked on the mechanical behavior of Fe_3Al alloys. Ductile Fe_3Al alloys have been successfully produced with Ni and Cr alloying additions (Morris et al. 1991, Sikka et al. 1991; Liu et al. 2003). Sikka et al. has optimized the conventional casting route for the Fe_3Al alloy with Cr, Zr, Nb and C additions for maximum ductility, high temperature strength and sulphidation resistance.

2.3.2 *FeAl*

As shown in the Fig. 2.6 both FeAl and NiAl have structural resemblance of ordered B2 strcuture. In contrast to NiAl, FeAl shows incongruence in melting and exhibits small compression ductility behavior, but hardly tensile (Yamagata and Yoshida 1973).

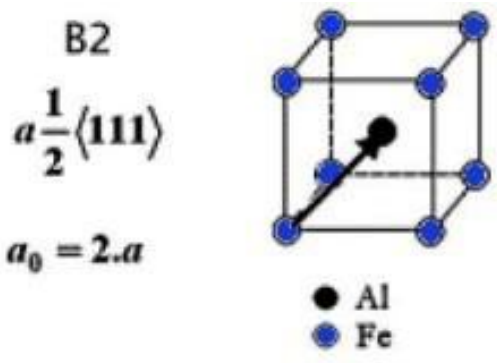

Fig 2.6 Ordered B2 crystal structure of FeAl

Increase in strength and fracture toughness of FeAl has been observed by alloying of boron but the reduction in brittle to ductile temperature is small (Crimp and Vedula 1986). The effect of Zr and B improves ductility and the fabricability is improved in case of Mo, V and C additions (Liu. et al. (1994).Powder processing at 1173K by extrusion has been the most effective processing of fine grained FeAl, while hot pressing and hot isostatic pressing adds to the density of the of FeAl but conventional casting has never been a favourable method (Vedula 1994). Rapid solidification of FeAI has also been attempted but no property enhancements are observed (Baker and Gaydosh 1987). Last few years have seen active research activity in the area of improvement of mechanical properties and sulphidation resistance of iron aluminides. (Henaff et al.2001; Priyadarshi and Balasubramaniam 2001; Liu et al. 2003;Xia 2005).

2.4 Titanium Aluminides

TiAl and Ti_3Al have received tremendous attention from aerospace sector. Specifically Ti_3Al is commercially available from main Ti suppliers like Titanium Metal Corporation, USA. Recently in high performance passenger cars TiAl based alloys are used (Tetsui 2002). The phase diagram ofTi-Al system is included in Fig. 2.7 (Kattneret al. 1992). Although a number of intermetallics exist between titanium and aluminum, mainly there are two aluminides of engineering interest in Ti-AI system exist namely Ti_3Al (α_2), TiAl (γ). The most useful gamma aluminides are of two phase derivatives based on TiAl and Ti_3Al with aluminium content ranging from 36-50 at%. Review of applications and properties of these titanium aluminides have been comprehensively presented (Dimiduk 1999; Djanarthany et al 2001; Das et al. 2004). The other intermetallics feasible as per the phase diagram are Al_3Ti (line compound), AlTi and Ti_2Als (high temperature phase), Fig. 2.7

.

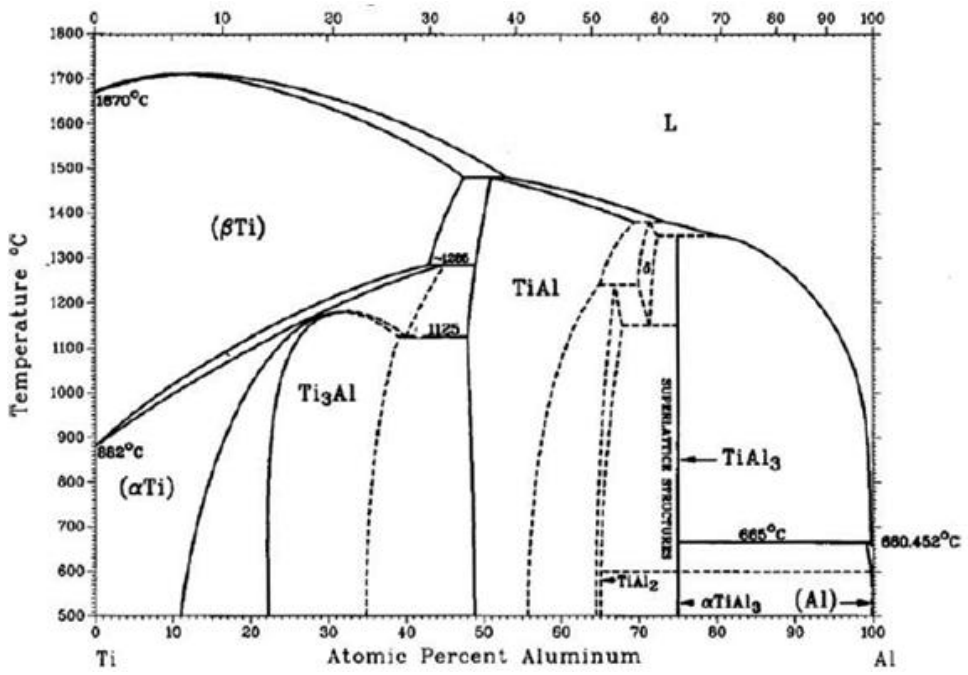

Fig 2.7 Binary Ti-Al phase diagram (Kattneret al. 1992)

As shown in the phase diagram Ti_3Al phase persists in the material for a composition range of 22-39 atomic percent of Al.Ti_3Al or the α_2 phase is having an hexagonal DO_{19} ordered crystal structure and specifically Ti-25Al composition holds its stability upto 1090^0C(Kim and Froes 1990). The density of Ti_3Al is 4.2 g/cc whereas for the alloys of Ti_3AI-based alloys the density is in the range of 4.1 to 4.7 g/cc (Sauthoff 1995).

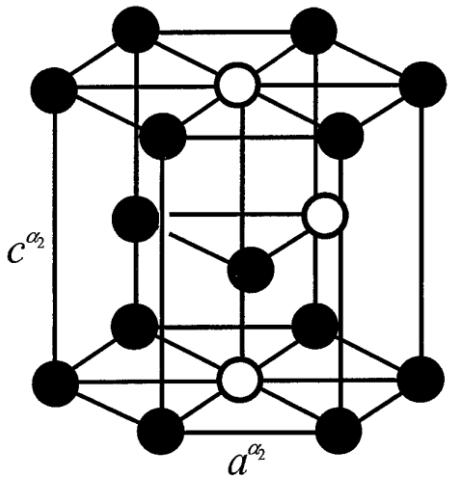

Fig 2.8 Ordered DO_{19} crystal structure of Ti_3Al, where Al-open circles and Ti-filled circles (Sauthoff, Intermetallics 1995)

Ti_3Al when unalloyed is brittle and shows very rare workability at lower

temperatures like 873K (Sauthoff, Intermetallics 1995). Lot of research is aimed at enhancing the strength and ductility by adding of Nb and microstructural evolution (Rowe 1990). Typical alloy compositions with engineering significance are Ti-24Al-1 INb, Ti-25AI-17Nb, Ti-25Al-17Nb-1 Mo (Kim and Froes 1990) and Ti-25AI-10Nb-3V- IMo (Blackburn and Smith 1980).

The Ti_3Al based alloys are classified on the beta stabilizer(Nb,V,Mo) content (Banerjee 1994): (i) Lower Nb content alloys (10-12At% Nb), like Ti- 24A1-1 INb and Ti-25AI-8Nb-2Mo-2Ta, (ii) alloys with medium beta stabilizer content of 14 - 17 At% such as Ti-24Al-15Nb and Ti-24Al-10Nb-3V- IMo and Ti-24Al-17Nb and (iii) recent alloys with 20-30 At% beta stabilizers e.g.Ti-22Al-27Nb and Ti-25Al-24Nb . The first class of alloys consists of two- phase structures of 012 and B2 (ordered p, bcc phase); the second class consists of two phases of α_2 and B2(ordered β, bcc phase): depending on heat treatment, three phases α_2, B2 and O (orthorhombic phase based on Ti_2AlNb). The third class of alloys consists of O and B2 phases entirely and these newer alloys have combination of substantially higher strength and toughness (Rowe 1990; Kumar et al. 1999). Both cast and wrought alloys have been studied for their deformation behavior (Semiatin etal. 1992; Banerjee 1994).

2.4.1*TiAl*

The γ TiAl phase has ordered face centered tetragonal Ll_0 structure with a wide range of homogeneity (49-66 at% Al), Fig. 2.9.

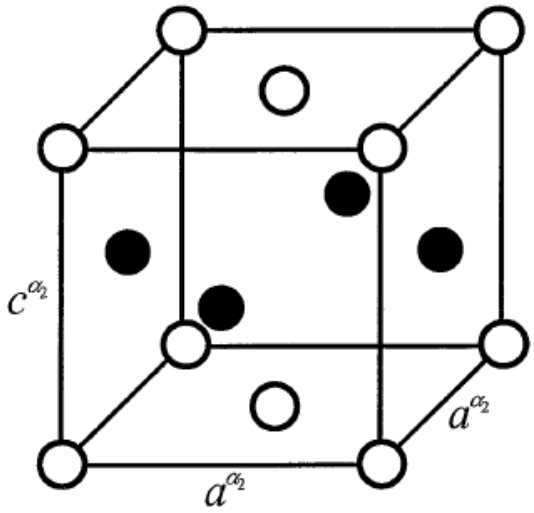

Fig 2.9 Ordered L_{10} crystal structure of TiAl, where Al-open circles and Ti-filled circles

Zhang et al made a comparative study on the physical properties like coefficient of thermal expansion, Young's modulus, electrical resistivity, specific heat and

thermal conductivity of gamma titanium aluminides with other high temperature materials. The ductility and strength of TiAl based alloys depends upon the thermo mechanical processing and composition. These alloys can be classified into two categories: two-phase γplus a2alloys and single γ-phase alloys.

The phase boundary between γandα_2 at 1273K varies around 49at% Al depending upon the type and amount of alloying elements (Fig. 2.10). The alloying of the elements like Nb and Ta helps in increasing the oxidation resistance and elements like Cr, V, Mn and Ni are responsible for the improvement in ductility (Kim and Froes 1990). Further, the oxidation resistance improves with small additions of P (Hanamura et al. 1991; Ramaseshan 1998).

The TiAl phase retains its stability upto its melting pointof 1713K (Huang and Chesnutt 1994). Development of gamma aluminides is being carried out in various countries e.g. in the USA (Lipsitt 1985; Mutoh et al. 1998; Kim and Dimiduk 1991; Huang et al. 1991), in Japan (Tetsui2002; Mutoh et al. 1998; Yamaguchi 1992, 2000), in Great Britain (Peacock 1989), Russia (Bondarev et al. 1991; Imayev et al. 1993a, 1993b, 1997; Salischev et al. 2000a, 2000b; Shagiev et al. 2004), Poland (Baczewska Karwan et al. 1996, 2000) and Germany (Sauthoff 1995, Dogan et al. 1991; Dahms et al. 1991).

There are at least four major pay off areas for γ -TiAl based alloys in advanced turbine engines and other aerospace systems like thermal protection systems:(a) γ-TiAl has a specific stiffness 50% greater than structural materials commonly used in aircraft engines. Stiffness of a material is needed most when clearances are concerned like cases, linings, seal supports and frames (e.g. consisting of honeycomb structures). The acoustically exited vibrations were also shifted towards higher frequencies by higher specific stiffnes materials, which may be useful for turbine blades and parts within the nozzle area used in thermo structural applications. (b) The creep resistance of the TiAl based alloys in the temperature range of 873K to923K enables it to substitute Ni super alloys for high temperature applications. (c) The resistance against Titanium fire also had made it available for the expensive fire resistant designed Ti based alloy components. Skin panel structures in regions that experience temperatures below 1073K for reusable launch vehicles are planned with gamma titanium aluminides. (d) Due to the low density of gamma titanium aluminides the response time for the turbine rotors is reduced, in turn helping in improving the efficiency of the same.

Automotive applications are the other directions of interest for γ alloys. Exhuast engine valves are the ideal application for the gamma based alloys. Generally, there are three major benefits, which could be exploited by the use of lightweight engine valves namely, a) Higher fuel economy, b) Better performance and c) Reduced noise and vibration. Most of the researchers are working on casting and reactive sintering for the fabrication if the gamma based aluminide alloys (Tetsui 1997; Tetsui2002; Rawers and Wrzesinky 1992; Lee et al. 1997).

2.4.1.1 Microstructural studies of γ-TiAl

The Phase diagram of Ti-Al is showing the gamma phase field for alloys of engineering interest in Fig. 2.9 (Appel and Wagner 1998). The three different types of microstructures can be obtained by annealing at different temperatures (Huang and Chesnutt 1994). These can be explained with the help of phase diagram shown in Fig. 2.9. Above 52 at% of Al alloys show single phase gamma structures throughout ambient to elevated temperatures. Alloys in 46-52 at% when heated in the middle region of a+ γ field (-1523K) and cooled, result in two phase duplex structures consisting of γ and lamellar (γ + α_2) grains. Alloys less than 48 at% of Al are heat treated in single alpha region results in fully lamellar microstructures.

The alloys containing lower aluminium with smaller amount of phase behaves more ductile than the single phase alloys (Huang and Chesnutt 1994). The presence of α_2 phase in duplex structure during heat treatment, the γ-phase grain growth is retarded, which enables it as the most ductile microstructure (Huang et al. 1991). Kim has studied (Kim 1992) the effect of microstructure on the mechanical properties of gamma alloy Ti-47Al-lCr-l V-2.5Nb (at %).

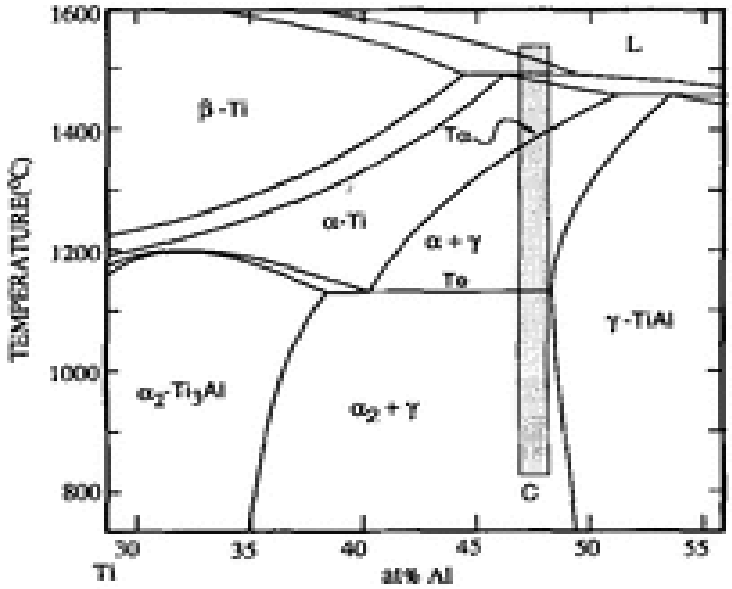

Fig 2.10 Phase diagram showing composition range of γengineering alloys

The duplex structure shows better strength and ductility due to the fine grain size and the presence of α_2 grains, where as the transformed structure is having higher fracture toughness (Huang and Chesnutt , 1994). The presence of α_2 grains helps in the scavenging of oxygen leaving the gamma phase in deformed manner and rendering the the alloys ductile (Huang and Hall 1991). But the higher fracture toughness of the transformed can be explained on the basis of composite toughening effect, where the energy is required higher and the fracture process is delayed due to the interface debonding and deformation blunting (Chan 1992). The lamellar structure has superior creep strength than duplex structure (Huang 1992). Seetharaman and Semiatin (1998) has have studied the hot working and fracture and correlated with grain size of gamma aluminides.

The larger grain size of α_2 laths in the lamellar structures is expected to be soft which help in the superior creep properties (Huang and Chesnutt 1994). The effect of microstructural features like large grain size on mechanical properties has been studied (Takahashi et al. 1990; Appel et al 2000). For as cast alloy Ti-48Al-2V the creep behavior and microstructural characterization studies were carried out by Sujata et al. (2004). The grain size of lamellar structure comes in micron range and becomes fine when the cooling rate is increased and/or holding time is decreased at the temperature of heat treatment.

2.4.1.2 Alloying additions to γ-TiAl

The effect on the ductility of the duplex structured alloys by the additions of V, Mn, Ni and Cr with Al content between 44-52 at% has been studied here. The ductility of lamellar structure material improves by grain refinement, which can be achieved by alloying additions of V, Mn and Cr (Tsuzimoto et al. 1989; Kawabata, et al. 1989). Mn added TiAl show case lamellar structures at higher cooling rates and is an important parameter in the design of the alloys with Mn (Jni et al. 2004). The fact that duplex structure alone can be ductilised by alloying additions and not lamellar or single phase γ structures, rules out the reduction of c/a ratio and unit cell volume as the only reasons for higher ductility (Huang and Hall 1991).

Room temperature tensile ductility is maximum at around Ti-48at%Al (Huang and Chesnutt 1994). Development of gamma aluminides has been contended with composition Ti- (46-52) Al- (1-10) M (At %), where M is at least one element from Cr, V, Mn, Nb, Ta, W and Mo (Kim and Froes 1990). Since, AI, Cr and Nb are the major alloying additions to γ-aluminides; their respective atomic sizes in comparison to Ti are shown in Table-2.1 (Ghosh and Biswas 2002).

Table 2.1: Atomic sizes for alloying elements of interest for γ-aluminides

(Ghosh and Biswas 2002)

Element	Atomic Size
Ti	2.4861
Al	1.3607
Cr	2.2701
Nb	3.2071

The increase in ductility can also be attributed towards the substitution of Al atoms in the ordered lattice rendering the Ti-Al bond less covalent. Cr has the effect of extending the α-phase field towards higher A1 (Huang et al. 1991).Addition of Cr tends to depress γ-solvus and leads to move the γ phase field to the AI-rich side. Cr addition affect mainly by promoting the α-phase at homogenizing temperature , which in turn results in more lamellar content on cooling to room temperature.

The heterogeneous distribution of lamellar structure in duplex structure sfavours in the Further, non-uniform distribution of lamellar structure in the duplex' structure due to ternary additions favours in homogeneous deformation in enhancing ductility. To achieve adequate creep properties and oxidation resistance at high temperatures addition of elements like Nb, W, Mo and Ta is necessary (Huang and Chesnutt 1994) and the most important alloy developed till date is Ti-48Al-2Cr-2Nb being developed mainly through ingot metallurgy route.

2.4.1.3 Mechanical properties of γ-TiAl

As seen in earlier section, there are three main types of microstructures in y- TiAl region. The comparison of properties for as-cast structure with duplex and fully lamellar structures in y-titanium aluminide is listed in Table 2.2(a) while Table-2.2(b) gives optimum microstructure for achieving specific properties (Hamada et al. 2002). Wang and Dahms (1992) have reported highest hardness for lamellar phase and published hardness values of 269±51, 455±33, 468±24 respectively for γ, α_2 and lamellar (γ plus α_2) phases.

Table 2.2 (a): Details of properties of various microstructures in γ titanium aluminides (Hamada et al. 2002)

Property	As Cast	Duplex	Fully Lamellar
UTS Mpa	380	290	190
El, %	0.4	0.4	0.3
K_{max} Mpa√m	18.6	21.0	20.5
K_Q, Mpa√m	14.6	19.0	17.6
Microhardness, Lamellar grain Gamma grain	320 270	270 180	290 -
Grain size, μm Lamellar grain Gamma grain	200-300 120-200	1000-40000 200-300	400-700 -

The microhardness values for gamma grains are lesser than the lamellar regions due to presence of harder TiAl phase in both as-cast and duplex structures (Hamada et al. 2002; Wang and Dahms 1992).

Table 2.2(b): Details of Microstructuresavailable at different condition (Huang and Sih 1991)

Property	**Conditions(temperature and pressure)**	**Preferable microstructure**
Strength	<1033 K	Small grains ⟶ Duplex
Ductility	<1033K	γ/α ratio ⟶ Duplex
Toughness	All temperatures	Lamellar structure ⟶ Fully transformed
Creep and rupture	<923 K	Small grains Lamellar Structure ⟶ Duplex
	>923 K	Large grains Lamellar Structure ⟶ Fully Transformed
High Cycle fatigue	>250 MPa (at 1033 K)	Small grains Lamellar structure ⟶ Duplex

Depending on the condition of the material as seen from the table the tensile strength varies between 190 to 380 MPa and the best structure for the creep behavior below 1033K is duplex structure. The fully transformed lamellar structure is the optimized condition for higher toughness and creep strength above 1033K.In comparison to duplex and single γ phase structures lamellar structures have higher fracture toughness with increasing the Al content (Huang et al. 1994). Planck and Rosenberger (2002) have studied the determination of tensile strength and fatigue properties of γ-titanium aluminide after exposure to elevated temperatures for long duration. Detailed studies on high temperature fretting fatigue behavior of these aluminides have been reported by Hansson et al (2000).

Table 2.3: Details showing the tensile strength achieved by various workers for the binary gamma aluminide processed through various routes

Alloy/Process/Microstructure	UTS MPa	Test temperature (K)	References
Ti-48AI (Duplex) (As-cast) (Fully Lamellar)	290 380 190	300	Hamada et al. (2002)
Ti-48Al (RS)	355	300	Schneider et al. (1997)
Ti-43Al (Plasma skull cast)	363 343	300 1073	Nishiyama et al (1990)

2.4.1.4 Oxidation resistance of y-TiAl

The formation of Protective alumina scale is the most important factor for the high temperature oxidation resistance and the activity of aluminium in the alloy of the formation of scales. Aluminium is more active in case of TiAl than Ti_3Al (Lee and Sanders 1997). The effect of addition of Nb, W and Mo even upto 2 at% depicts the enormous increase in the oxidation resistance. When the alloying of Cr is under 4at% becomes detrimental and when increased above 8 at%, becomes extremely protective. (Perkins et al. 1987). The formation of Al_2O_3 is effectively dependent upon the above elements and also tends to substitute titanium atoms and enhance the diffusivity of Al atoms. The above procedure helps in the formation of a continuous layer of Al_2O_3, which shows influx of oxygen (Shemet et al. 2000). The alloy Ti-48Al-2Cr is ductile but not oxidation resistant, according to the study at NASA Glenn Research Centre at Lewis Field. The Addition of 2 at % Nb to this alloy has led to most notable y-alloy Ti-48Al-2Cr-2Nb (Shih et al. 1991; Landon and Kelly 1991).

The improvement of oxidation resistance by surface modification through shot blasting with WO_3 powder has been studied by Kauwara et al (2002). In this process an adherent layer over the aluminide substrate is formed. The adherent layer helps in the formation of Al_2O_3, when exposed to high temperature, hence enhances the oxidation resistance (Kauwara et al. 2002).

2.5 Processing of Gamma Alloys

Alloying additions, compositions and the control on microstructure are some of the ways to overcome the poor ductility of gamma alloys. The tensile ductility of 1-3 % has been achieved at ambient temperature (Huang and Chesnutt 1994). However, for actual application of the gamma alloys, various issues related to their processing need to be investigated.

2.5.1 *Casting*

The aluminides of potential interest have composition of 45-50 at% Al and solidify with the following peritectic reaction as seen in the phase diagram shown in Fig. 2.10:

$$\alpha + \text{Liquid} \longrightarrow \gamma$$

Heavy segregation and non uniform structures are some of the drawbacks of the above peritectic reaction (Huang and Siemers 1989; Semiatin and Mcquay 1992). That's why though containing ductilising elements like Cr, V, and Mn cast alloys have less ductility (Austin et al. 1993). Ni, Fe and B have been used to increase the castability (Nakagawa et al. 1992), where as higher Nb alloys has already been developed and being used successfully (Tetsui 1997, 2002; Appel et al. 2003).

2.5.2 *Wrought Processing*

The main problem of the wrought processing is to break the coarse and segregated grains of the cast alloys. The non uniform recrystallization and banding of the lamellar structure in the wrought processed alloys are the cause of anisotropy of the yield strength. Lot of studies has been carried out to acquire fine homogeneous structures in gamma based alloys (Huang and Chesnutt (1994)). Large ingots of 360 mm diameter, weighing 250 Kg have been produced commercially (Kim 1995). For secondary processing of these aluminides , isothermal forging is an essential requisite, but in some cases, canned extrusion process or canned non isothermal forging process is used(Appel et al. 2000). Some of the researchers have developed the dynamic recrystallisation due to cyclic isothermal forging at progressively low temperatures (Imayev et al. 1993a; 1993b; Salischev et al. 2000a, 200b). The above processes help in the formation of fine grained aluminide which can withstand large deformations before cracking. Subsequently, thin sheets and foils have been realized by pack rolling techniques (Shagiev et al. 2004; Das et al. 2004; Tetjukhin 2002).

2.5.3 *Polysynthetically Twinned (PST) Crystals*

Special crystal technique (Yamaguchi 1991; Umakoshi et al 1992; Inui et al. 1992; Umakoshi and Nakano l993) was used for synthesizing two phase aluminides with good mechanical properties. PST crystals with good mechanical properties are also prepared in zone melting furnace, where a single set of lamellae can also be grown if the rate is appropriately controlled (Yamaguchi et al. 1990). For example, the alloy with 49.3 at.% Al consists of one or two lamellar grains which are composed of lamellae of the major constituents TiAl and of the secondary phase Ti_3AI. As number of thin twin related lamellae are present in the gamma phase, these crystals otherwise known as polysynthetically twinned crystals. The name is after the phenomenon polysynthetic twinning, mailnly observed in mineral crystals (Yamaguchi et al. 2000).

Accordingly, alloys with this microstructure are called poly synthetically twinned (PST) crystals. This phenomenon introduces the mechanical behavior sensitivity due to the orientation of the crystal and loading direction. Two deformation modes are present, where one is due to shearing across the lamella boundaries and another one is due to the shearing parallel of the lamellar boundaries. The later one is comparatively easier, can withstand tensile elongations of 20% at ambient temperatures. Lamellar microstructural features and fundamental properties of the lamellar microstructure such as microstructural characterisation, deformation, fracture toughness and macroscopic flow behavior have been extensively studied. The study has been carried out by the fact that the PST crystal is in a sense, a single crystal of the fully lamellar polycrystalline alloy. Lot of studies has been carried out on the fatigue properties, characterization of lamellar interfaces and microstructural stability at under creep conditions of PST (Hiroyuki et al. 1997; Wei Zhao and David E. Luzzi 2000; Wegmann and Maruyama 2000). Most of the properties are observed to be sensitive to the relative orientation of the lamellae in PST titanium aluminides.

2.5.4 *Powder Metallurgy (PM)*

Fine grained product, near net shape processing, economical viability and controlled properties are some of the need for the usage of powder metallurgy route (Ibrahim et al. 1991). There are basically two PM approaches based on pre-alloyed and elemental-powder processing techniques respectively to achieve near net shapes in gamma titanium aluminides. In case of pre-alloyed route, high pressure is required for consolidation; moreover interstitial contamination is unavoidable.

Cracking, porosities and coarse grains are some of the main problems in prealloyedmaterials. Hot Isostatic pressing is one of the processes through which comparable microstructures and properties like wrought products have been achieved (Fuchs 1993). Due to the above drawbacks, elemental PM route is attractive for processing of intermetallics.

Table 2.4: Brief comparison of the PM processes

Pre-alloyed PM	**Elemental PM**	
	Mechanical Alloying	**Reaction Synthesis**
Involves melting step Difficult consolidation due to high strength and low diffusivity High cost of powder and limited availability	No melting step Repetitive cold welding-fracture leads to alloying Requires high energy milling at high homologous temperature (T/T_{MP})	No melting step Transient liquid and exothermic heat aids alloying Cheap soft elemental poeders used. Hence, consolidation easy. Monoliths/composites possible by RS variants

As seen from Table- 2.4, reaction synthesis (RS) process is also an attractive process for the production of aluminides. The heat evolved in the process is used for the production. In some processes, oxides of metals are directly reduced at low temperatures, producing fine grained materials. The low temperature reduction process is otherwise termed as gas reduction route, number of transition metal intermetallics are prepared by this method (Morales et al. 2000, 2002; Tilliander et al. 2005, Bustnes et al. 2000; Arvanitidis et al. 2000). A brief review of interesting PM processes for gamma titanium aluminides is presented here.

2.5.5 *Rapid Solidification*

Cooling rate from liquid phase of more than $10^4 Ks^{-1}$ is utilized in rapid solidification The significant undercooling of melt leads to metastable phases (Suryanarayana et al. 1990; Cantor 2001). Rapid solidification has been used to avoid heavily segregated peritectic solidification structure resulting in homogeneous structures (Shechtman et al. 1974; Martin et al. 1983). Though the risk of contamination, it results in homogeneous and finer structures with metastable phases for ductile alloys.(Koch 1988; Vujic et al. 1988 &Mckamey et al. 1995).

2.5.6 *Mechanical Alloying (MA)*

Mechanical alloying (MA) of the powders results in generation of particles with very unique microstructural features. In MA process the powder blends are contained in a vessel of suitable grinding medium with the balls. During MA the plastic deformation and fragmentation of powder takes place and the finer particles gets cold welded, the whole process is repeated time and again until very fine powder is produced. The powders prepared by protective atmosphere MA possess high chemical and structural internal energy, which facilitates the formation of interstitial solid solutions and metastable crystalline or amorphous phases (Pillai et al. 2003).

The fabrication of Al_3Ti by MA from elemental Ti and Al powders has been reported by Srinivasan et al. (1991).But Christman and Jain(1991) studied that for nano phase Ti_3Al-Nb in bulk quantities, MA is also an useful process. Many studies also have been carried out for In-Ga-Se and Al-Ni-Mm systems (Suryanarayana et al. 2001; Hong et al. 2001). The main drawback of the MA powders is the inhibition of the secondary consolidation of the materials, due to heavily plastic deformation. Suryanarayana and Koch (2000) extensively studied and reviewed the processing of nano materials through MA route.

2.6 Comparison of Aluminides - Properties and Applications

Presently, aluminides of nickel, iron and titanium are getting maximum attention for a range of applications. Table-2.5 provides the characteristics of main aluminides and application fields.

Table 2.5: Characteristics and applications of selected aluminides (Sauthoff 1989)

Type	**Characteristics**	**Proposed applications**
Ni_3Al and NiAl	Wear resistance/Low inertia/Creep resistance/lightness	Automobile/Long life heating elements Aerospace
Ti_3Al and TiAl	Low density/high specifice stiffness and comparable specific strength to superaloys	Aerospace- airframe structures, turbine rotors, blades, fins, nozzle seals/ High performance automobiles

Fe_3Al and FeAl	Excellent resistance to oxidation/sulphidation/ lower cost replacement of SS	Fossil energy machinery parts/ applications as cheap replacement for SS

Table-2.6 is included below to give a comparison of properties of these aluminides with their respective density and crystal structure Table-2.7 provides a comparison of physical and mechanical properties for ceramics, metals and aluminides. It can be seen from these tables that aluminides possess properties intermediate to metals and ceramics. Aluminides have low densities and match high temperature properties to a great extent of ceramics while possessing all the advantages of metals.

Table 2.6: Properties of different types of aluminides (Hunt et al. 1990; Lipsitt et al. 1985)

Type	Crystal structure	M.P. ^0C	Density (g/cc)	0.2% YS (MPa)	Modulus (GPa)
Ti_3Al	DO19	1600	4.2	700-900	145
TiAl	L10	1460	3.8	400-650	176
Fe_3Al	DO3	1540	6.7	385-392	141
FeAl	B2	1250	5.6	360-380	261
Ni_3Al	L12	1390	7.5	250-500	179
	B2	1640	5.9	250-475	294

Table 2.7: Comparison showing properties of superalloy, titanium aluminides and ceramic (Si3N4) (Lipsitt et al. 1985; Nishiyama et al. 1990)

Property	Ti_3Al	TiAl	Si3N4	Ni based Superalloy
Density, g/cc	4.15-4.7	3.8	3.2	7.9
Thermal Conductivity Cal/s.cm^{0}C	-	0.05	0.7	0.03
Thermal Expansion Coeff, X10^6/K	5	10.3	2.8	13.1
E, GPa	145	176	310	220
Poisson's Ratio	0.30	0.28	0.24	0.30
Fracture Toughness MPa√m	20	13	6	75
Ductility % Ambient ~ 1073K	 2-5 5-8	 1-2 7-12	 - -	 3-5 10-20

2.7 Self-Propagating High-Temperature Synthesis (SHS) Process

Self propagating high temperature synthesis (SHS) or Reaction synthesis (RS) is a powder metallurgical process through elemental route, where the heat of formation is the driving force for the reaction. Free energy of formation of titanium aluminides of interest is shown in Table-2.8 (Hahn and Lee 1992). Good thermodynamic stability of the intermetallic compound is the driving force for the SHS reaction.

Table 2.8: Free energy for the formation of titanium aluminides (Hahn and Lee 1992)

Intermetallic Compound	Ti_3Al	TiAl	$TiAl_3$
Free Energy of Formation (kJ/mole)	-39	-69	-39

Reactive hot pressing, reactive hot isostatic pressing, combustion synthesis and reactive extrusion are some of the variants of SHS. German (1990); Munir and Anselmi (1989) and Yiand Moore (1990) have extensively reviewed SHS process. Bose et al. 1988 and German et al. 1989 reported the production of Ni_3Al based intermetallics alloys by reaction synthesis with good density and ductility. Some other instances of production of intermetallics are the production of iron aluminides by pressure-less RS process (Gedevanishvili et al. (2002). The studies reveal that the products are of more than 95% density with control of parameters like optimized particle size, heating rate and atmosphere. The study of Nishimura et. al (1993) demonstrates that the uniaxial compressive stress not more than 50 MPa can be useful for achieving product with density at the fullest. Some studies also have been carried out for the production of the TiAl based intermetallics matrix composites by reaction synthesis route (German et. al. 1989 &Wu et. al 2002).

Prasanth et al. (2004) emphasized the production of the intermetallics by RS process carried out in microwave, as the heating rates are higher in case of microwave. Due to imbalanced solubility in Ti-Al system, the pressureless reaction synthesis results in the swelling of the products. According to Savitski and Brutsev (1981), the ratio of solid solubility is as low as 0.003 at% in Al-Ti system, which helps in the swelling of material. The use of pressure during reaction sintering is a need for production of dense near net shaped gamma TiAl (Rawers and Wrzesinky 1992, Lee et al. 1997, Kim et al. 1999, Qian Wang et al. 2000; Wen et al. 2001). Thin foils of 50 mm thick TiAl has been prepared by reaction extrusion (Martin and Hardwick 1994), which in itself is a success over the inherently under malleable intermetallics compound. The reactive synthesis of nano crystalline powders by mechanical alloying route has been reported by Zhu et al. 2002.

The phases prepared from RS of intermetallics were analysed by energy dispersive analysis of X-rays (EDAX) and X-ray diffraction (Park et al. 2002; Rawers and Wrzesinky 1992; Kim et al. 1999). The density of the reacted compacts was commonly determined by Archimedes method (Park et al. 2002; Wen et al. 2001; Nishimura et al. 1993). Some literature is available for oxidation studies for gamma TiAl produced by conventional methods (Retallick et al. 1998).

2.8 Reaction Kinetic Studies of RS

There are many studies relating to development of various intermetallics through RS as described in Section 2.7. Very limited work has been carried out on kinetics of the self propagating exothermic reaction for the formation of intermetallic powders.

The activation energy calculations have been carried out with the help of mathematical modeling and differential thermal analysis datas for the formation of stoichiometric AlTi, Ni_3Al (Sohn and Wang 1996; Wang et al. 1994) and Ni-Al-Fe systems (He et al. 2002) from elemental powders. For the calculation of activation energy from Arrhenius relationship of activation energy with fraction transformed, both isothermal and non isothermal methods have been used (Wang et al. 1994) as follows:

$F(\alpha) = kt = A \exp(-E/RT)$ [isothermal kinetics] ……...2.1

and

$\ln(d\alpha/dt) = k\, g(\alpha)$ ……...2.2

$\ln(d\alpha/dt)/g(\alpha)] = -E/RT + \ln A$[nonisothermal kinetics] ……...2.3

For Al_3Ti and Ni_3Al the activation energies determined are 483 kJ/mol and 283 kJ/ mole respectively (Sohn and Wang 1996). The activation energy for the exothermic reaction is one of the parameters dependent on the reaction temperature (Wang et. al). For AlTi formation Wang et al determined the activation energy of Al_3Ti to be 149 kJ/mole in the temperature range of 963K to 1013K as and the same is calculated as 517kJ/mole in the temperature range 1013K to 1173K. The activation energy value for Ni-Al-Fe system has been determined as 152.42 kJ/mole (Ni-20Al-30Fe (wt %)) at thermal reaction point around 1186K.

2.9 Process Parameters for Reaction Synthesis (RS) Process

Various researchers like Savitski et al. (1980), Savitski and Burtsev (1981) and Bertolino et al. (2003) conducted reactive sintering studies on Ti-Al system,Cu-A1 (Lee and Yoon 1988), Ni-Al (Bose et al. 1988; Nishimura at al. 1993; Guo and Cui 2002), Ti-Ni (Bertolino et al. 2003), Ti-Al-C (Zhenbin et al. 2003) and Fe-Al (Rabin

and Wright 1991; Gedevanishvili et al. 2002). Reaction synthesis involves the step of transient liquid phase sintering for small duration and for fewer amounts, where the step depends upon different process variables that control the sintering mechanism. German (German 1985) has extensively reviewed the liquid phase sintering and reactive sintering and effect of various process parameters, Table-2.9

Table 2.9: Parameters for liquid phase sintering (German 1985)

Variable	**Factor favours swelling**	**Factor favours shrinkage**
Solubility Ratio	Low	High
Particle size	Coarse	Fine
Green density	High	Low
Amount of liquid	Small	Large
Contact angle	Large	Small
Heating rate	Low	High
Atomophere	Insoluble	Soluble
Powder porosity	Low	High

The important process parameters for RS and transient liquid phase sintering (TLPS) processes are described below:,

2.9.1*Additive Content and Particle Size*

Densification of the TLPS depends upon the process variables such as liquid formed and the duration of the stability of the liquid (German 1985). The amount of liquid also have some control over the densities such as too much of liquid introduce pores due to its penetration and generates large pores due to spreading and penetration of the melt away from the additive particle sites. The scarcity in melt liquid leads in lowering of the densification. Characteristics like Kirekendall porosities are seen in case of Ti-Al systems due to the dissimilar diffusivity gradient (Savitski 1980; Savitski and Brutsev 1981). According to Bose et al (1988) an optimum particle size is a requirement for pressure less RS process, where German (1985) reported that the addition of small particle sizes and higher heating rates results in better densified product.

2.9.2 *Effect of Green Density*

The dependence of the resultant porosity upon green density has been studied by Savitski et al.

$$\Omega = \Omega_0 + C(1-\Omega_0) \quad \text{.....2.4}$$

Where, Ω is denoted as the end porosity, Ω_0 represents the green compact porosity and C is the amount of the second phase reacted (Savitski 1980; Savitski and Brutsev 1981). The above equations hold good for the green density levels above 50%.

2.9.3 *Effect of Heating Rate*

The diffusional homogenization during heating helps in pore formation in solid state due to the Kirkendall effect, which is responsible for the swelling (German 1985). The relationship between the liquid volume (V_1), concentration of the additives and the heating rates β is defined as;

$$1 - [V_1/(f)^{1/3} = (T_1/\beta)^{1/2} \quad \text{.....2.5}$$

Thus the higher heating rates produce more liquid phase during RS, where formation of solid state compound inhibits subsequent interdiffusion and hence lowers the density in slower heating rates.

2.9.4 *Effect of Sintering Atmosphere*

In case of vacuum sintering, heating rates hardly have effects on the densification of the Ni_3Al (Bose et al. 1988). However, according to the liquid phase sintering phenomena, high heating rates are needed for better densification in argon and hydrogen atmospheres. Hydrogen in comparison Argon has better solubility in Ni and Al and facilitates in the escaping of gases after the pores get sealed due to densification.

2.9.5 *Effect of Sintering Time*

The process of RS fully depends upon the exothermic heat which leads to intermetallics formation and densifying the product, so the sintering time is not a major parameter. The diffusion is also avoided such as solid state diffusion for better densfication of the products during RS processing. The equation $\mu = (Dt)^{1/2}$ (German 1985) represents the diffusional relation between thickness of the intermetallic compound(μ),duration taken for the formation of the compound (t) and D which is the controlling diffusion rate.

2.9.6 *Effect of Sintering Temperature*

The primary requirements for the reaction RS method is the starting of exothermic reaction within the elemental powders (Nishimura and Liu 1993; German 1985). The temperature is selected for a composition which initiates the exothermic reaction and leads to the formation of compound and densification simultaneously, during the limited presence of the liquid phase (German 1985). Nishimura and Liu (1993) studied that the temperature of RS of aluminides, which is close to the melting point of aluminium and the exothermic heat is used to melt the aluminium for a short duration hence the densification is acquired. Microwave sintering methods can be used for RS at faster heating rates (Prashanth et al. (2004)). Other instances of the systems where RS has been used are TiC powder reaction with Ti (Quinn and Kohlstedt 1984) and SiO_2 reacting with AlN giving Si-Al-0-N compound: (German 1985).

2.9.7 *Effect of External Pressure*

Application of external pressure cause densification and the collapsing of pores in TLPS and RS process (Kingery et al. 1963; Naidich et al. 1974). The transient liquid cannot withstand the shear stress and facilitates the lubrication in particle sliding as induced by external stress (German 1985). Shrinkage rate d (ΔL/Lo)/dt related to applied stress (a) in the final stages of sintering has been given by Kingery et al. (1963) as;

$$d(\Delta L/L_0)/dt = B\sigma^n \exp[-Q/(kt)]/G^3 \quad \ldots\ldots\ldots\ldots\ldots\ldots\ldots\ldots\ldots\ldots\ldots\ldots\ldots\ldots\ldots\ldots 2.6$$

Where, B is a material constant, n stress exponent (~1 for most of system; . Q is activation energy for diffusion, T is absolute temperature, G is grain size and k is the Boltzmann's constant. Thus, for higher a and lower grain size, better densification is achieved.

The perturbations in the sintering behavior can be determined by relatively small pressures of the order of 40 MPa have been shown to describe significant change in sintering behavior (Whittenberger 1990). With pressure-assisted RS process, effect of particle size, sintering atmosphere and initial green density are also studied (German 1985; Nishimura et al. 1993). The densification effect of pressure is higher for transient liquid process like RS as compared to normal sintering process involving no liquid formation (Kingery et al. 1963). Near full density aluminides have been obtained by pressure-assisted RS process and it's variants ike combustion synthesis (Yi and Moore 1988), reactive hot pressing (Rawers and Wrzesinky 1992; Kim et al. 1999), reactive

hot isostatic pressing (German et al. 1989), XD^{tm} process (Westwood 1988). In case of pressure-assisted RS process, heating rate affects the densification by way of changing the kinetics of the process (Lee et al. 1997).

2.10 Properties of Reaction Synthesized (RS) Aluminides

Various mechanical properties of gamma TiAl aluminides synthesized by RS route are determined by Vicker's hardness (Wen et al. 2001), tensile test (Kim et al. 1999; Lee et al. 1997) and transverse rupture stress test (Rawers and Wrzesinky 1992). The comparative study of creep properties for RS TiAl alloy and the conventional cast alloy indicated that the RS TiAl alloy provides better creep properties at steady state (Kim et al. 1999; Worth et al. 1995). The correlation between the heat treatment temperature and the grain growth suggests that higher temperatures (>1643K) results in coarse grains with a declination in the strengths (Lee et al. 1997).

Zhang et al (1996) confirmed the phases at high temperature by high temperature X-ray diffraction studies. Lee et al (1997) found the hardness to be between 25 to 35 Rc by hot hardness measurement of the Ti-46.6Al-1.4Mn-2Mo alloy produced by RS process within room temperature and 1543K.

2.11 Dilatometric Studies of Reaction Synthesised Aluminides

Though mechanical alloying and reaction synthesis are two competitive processes for the development of aluminides, the drawbacks either the work hardnening during mechanical alloying which induces pores, defects into the materials or the bulging of compacts during the sintering process due to the degassing of the materials render the components brittle and worthless. The controlling of path for reaction sintering studies which will provide lesser dilation or bulging during the sintering, have higher activation energies (negative) for the formation of aluminides and finer grain size can only be determined using dilatometric investigations.

Various researchers have studied the linear shrinkage/expansion, rate of expansion and onset of sintering by dilatometric investigations [Dabhade et al 2006; Dabhade et al 2007]. Dabhade et al (2007) studied the onset of sintering temperatures of Ti-TiN composite powders, sinterability and the linear shrinkage rate at constatnt rate of heating. Where as Wang et al studied the same for titanium aluminide compacts fabricated through cold extrusion and have various Al at% of 25-75. Though the dilatometric investigations provide the thermal expansion coefficient, but hardly give any idea about the linear shrinkage/expansion rate of the aluminides formed during

thereaction synthesis process. There is rarely literatures available where the researchers have worked on the dilatometric investigations of titanium aluminides and determined expansion rate, activation energy and percentage linear expansion.

2.12 Summary

For Various high temperature applications like fossil energy, aerospace and automobile sectors aluminides like Fe_3Al, FeAl, NiAl, Ni_3Al, TiAl and Ti_3Al are materials of interest.The progress in the fabrication of aluminides leading the materials towards the successful realization in various high temperature applications. Amongst the aluminides, two phase gamma titanium aluminides with specific composition Ti-48At%Al are the most promising materials for thermo structural applications.The ternary additions such as Nb and Cr in the Ti-48Al binary alloy impart oxidation resistance and ductility respectively. But heavy segregation and non uniform coarse grained structures are the drawbacks of the materials prepared through ingot metallurgy route. Ingot metallurgy also needs machining and secondary working which increase the difficulties for the comparatively brittle materials. Powder metallurgical route allows alleviating the shortcomings and the approach can be progressed through elemental and prealloyed approaches.The mechanical alloying approach and further sintering/consolidation is a better approach in finding the fine grained structure. But finding ultra fine grained structure with a densification of 95-99 % is an uphill task. The elemental blending followed by RS process associated with self propagating high temperature synthesis of aluminides is very efficient, which also avoids the non uniform distribution of phases. One of the other advantages of RS process is the synthesis of fine grained materials with compositional and microstructural homogeneity. The RS process have draw back that with elemental powders achiving fine grained structures is difficult. Specifically the fine grained structures can be achived if the staring powder sizes will be of lesser size.The inherent bulging of the aluminides due to the degasification also hinders the densification during reaction synthesis process. The self propagating high temperature synthesis processes though have an edge of exothermic reaction but the temperature gradient during the small period also is the cause of expansion in the compact.

Examination of dilatometric characteristics was carried out by several researchers in different metal/alloy systems. But for aluminides the studies are very

limited and specifically with various starting particle sizes of Ti/Al aor bith in Ti-Al (50 at %) is almost unavailable. To provide an idea of dilatometric and activation energy calculation for self propagating high temperature synthesis process with various starting particle size of Ti and Al is more important for controlling the reaction synthesis process.

CHAPTER 3

PROBLEM FORMULATION

3.1 Introduction

From the extensive literature survey, it is found that gamma TiAl have potential applications to be used as rtating and thermo structural parts for temperatures upto 1273K. The main concern of these materials is to prepare in useful shapes in ambient temperature. In powder metallurgy route it is possible to attain near net shape, unlike that of other metallurgical processes such as ingot metallurgy. Specifically reaction synthesis route attained a lot of attention for attaining near net shape components.The materials of interest are upon the composition Ti48A12Cr2Nb and some of the researchers have worked on this to achieve better ductility properties. But very limited work has been carried out on any composite with above basic alloy composition with the study of dilation and reaction kinetics which describes a lot about the ductility and porosity of the materials.

The basic aim of this study is to determine the viability of synthesiszing the Ti-48Al-2Nb by mechanical alloying followed by pressure less sintering and hot pressing, to study the development of TiAl intermetallics by dry mechanical alloying of Ti-48Al-1Cr-1Nb-1(C,Gr/Ni-P). The propsed study also comprises of the densification of intermetallics during sintering along with dilatometric characterizations and reaction kinetics studies. The dilation behavior with various particle size mixtures provide us the route through which best densified intermetallics can be achieved.

3.2 Plan of Work

The compositions selected for the study is Ti-50A1, Ti-48Al-1Cr-1Nb-1(C, Gr/Ni-P) and Ti-48Al-2Nb are of engineering interest.

The experimental steps involved in the proposed study are shown in the form of a flow chart and is presented in the Table 3.1.Accordingly the various proposed tasks are given below:

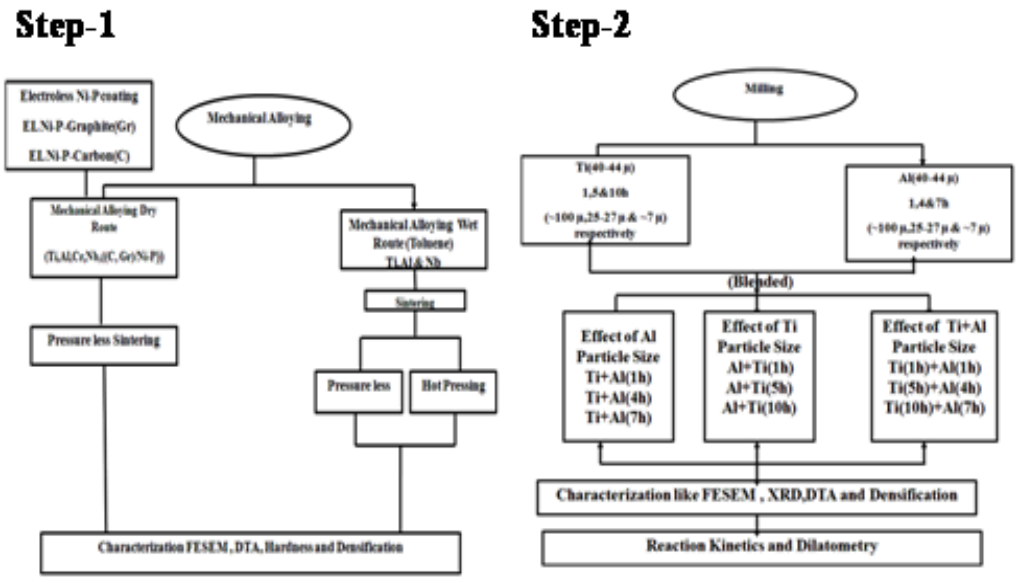

1. The base composition for mechanical alloying is chosen as Ti-48at% Al (Ti-48Al) based on extensive literature survey. This has revealed that alloys of engineering interest are concentrated around this composition. So the mechanical alloying was planned on compositions like Ti-48Al-1Cr-1Nb-1(C, Gr/Ni-P) and Ti-48Al-2Nb.
2. Study of mechanically alloyed powders (dry) for Ti-48Al-1Cr-1Nb-1(C, Gr/Ni-P) and in wet milling in case of Ti-48Al-2Nb compositions using XRD, FESEM and TEM has been planned. There are very rarely studies reported for the above compositions. Although few studies are there for Ti-25Al stoichiometric compositions.
3. To study reaction hot pressing under protective atmosphere or vacuum conditions plungers to be fabricated of the border of 15mm diameter. The plungers to be made up of chromium hardened steels and the reaction hot pressing were planned out in Gleeble^{TM} under 10N load.
4. To carry out reaction hot pressing and sintering 16 mm diameter pellets have been made by 175 Mpa in a hydraulic press. Exothermic temperatures for sintering process to be calculated using DTA technique. Initial experiments have been planned on reaction sintering and hot pressing of Ti-48Al-2Nb composition.
5. Densification to be determined for the above compositions for reaction sintering and hot pressing. The corelation between hardness and densification to be established.

6. After study of the densities of sintered and hot pressed samples of Ti-48Al-2Nb composition, to find a route through which maximum densification and ductility can be achieved reaction kinteics and dilatometry studies has been carried out.
7. Aluminium powders were milled for 1h, 4h and 7h to attain particle sizes of 100µ, 25-27µ and ~7µ. Similarly Ti powders were milled for 1h, 5h and 10h to achieve particle sizes of the above sizes.
8. Various sizes of Al powders with Ti powders of 44µ particle size to be mixedin a ratio of Ti-50at%Al to observe the effect of particle size upon reaction kinetics and activation energy. The above mixtures were planned tosubjected to dilatometric characterizations to determine the lowest dilation and activation energy.
9. Various sizes of Ti powders with Ti powders of Alµ particle size to be mixed in a ratio of Ti-50at%Al to observe the effect of particle size upon reaction kinetics and activation energy. The above mixtures to be subjected to dilatometric characterizations to cqlculate the lowest dilation and activation energy.
10. Similar particle sizes of Al and Ti were mixed in a ratio of Ti-50at%Al to observe the effect of particle size upon reaction kinetics and activation energy. The above characterizations like dilatometric properties and reaction kinetics to be carried out.
11. The above studies with variation of particle size and dilatometric characterizations is rarely been done by any researchers. The processing route and dilatometric study is the innovation in this thesis work.

CHAPTER 4

EXPERIMENTAL DETAILS

4.1 Introduction

The development of TiAl for Ti-48Al-2Nb and Ti-48Al-Cr-Nb-(Ni-P/C/Gr) compositions were carried out using mechanical alloying and reaction sytnthesis route at different temperatures. The developed aluminides were subjected to dilatometry and reaction kinetics studies.For all the above intermetallics the non isothermal reaction mechanism was studied for the exothermic reaction by Differential Thermal Analysis (DTA). The dimension of the compacts for sintering studies after mechanical alloying and the same for dilatometric studies were kept the same as 16.4 mm diameter and 5mm thickness. The dimensions of the compact were kept same to have a comparison of the dilation and densification studies. Densification behaves inversely as the dilation of the material during sintering, so to have the process for highest densification the dilation of the materials must be the lowest. Specifically for aluminides developed through mechanical alloying followed by sintering, are hard due to the ordered phases and it is added upon with the plastic deformation of the materials.The hardness of the phases and the particles hinders the densification process and induces pores and defects in the materials. Therefore, to avoid the harder particles and to have finer grain size the Al and Ti particles were milled separately to attain various particle size range of ~100 µ, 25-27 µ and ~7 µ and were mixed in various proportions. The reaction kinetics of the different compositions and the dilatometric studies were carried out to determine the effect of the particle size upon the percentof relative expansion and activation energies.

4.2 Selection of Raw Materials

Ti (40-44 µm, 99.9% purity), Al (40–44 µm, 99.9% purity),Nb ,Cr (40-44 µm, 99.9% purity) powders were procured from Testbourne UK Limited. The above powders of the given particle size are used for mechanical alloying and sintering processes, where as only Ti and Al powders of the above particle size and purity are used for reaction kinetic studies and dilatometric calculations.

4.3 Compaction and Reaction Synthesis

4.3.1 *Cold pressing of green compacts*

Cold pressing of green compacts was carried out using hydraulic press and a pressure of ~175 MPa. The cold pressing of materials were subjected for both mechanically alloyed powders and blended elemental powders of Ti and Al.To have a comparative study of the processes the dimensions as well as the pressure for the compaction were kept same. The green compacts were maintained the dimensions of the order of ~16.4 mm diameter and ~ 5mm thicknes. For experiments, the die punch set up was made up of Inconel 718 material and to have a lubricated action as well as to protect the die-punch interface, zinc stearate was applied as the lubricant profusely on the wall surfaces of the same. The approximate density of the cold pressed compacts was 60-65 % for various compositions and processes. Accuracy of the furnace for sintering wexperiments was $\pm 2^0$C.

4.3.2 *Hot Pressing Experiments*

Hot pressing was carried out on two different powder mixtures: (1) 100 h-milled (Mechanically alloyed) powders for the non-reactive hot pressing process and (2) blended elemental powders for the reactive hot pressing process. A vacuum of the order of 10^{-4}Torr in Gleeble 3800^{TM} was maintained for hot pressing. The hot pressed samples were ground and polished for the metallographic characterizations.

4.4 Characterisation of Samples

The sintered and as pressed samples were characterized for densification analyses using Archimedes method of water displacement. The samples were submerged in water and displaced water determines the densification of as pressed and sintered samples. The phases after mechanical alloying, compaction and sintering were analyzed by X-Ray diffraction. The morphological analysis and the surface topology of the above samples were observed by field emission scanning electron microscopy. The particle size of the mechanical alloyed powders was calculated using FESEM and TEM. The thermal behavior of mechanically alloyed and the elemental powder blends were calculated using DTA and the study of DTA at various heating rates has helped in determining the rate as well as the activation energy of the process. Hardness of the samples was determined using Vickers hardness.

4.4.1 ***Density Measurement***

The Archimedes principle which was used for the calculation of density of as pressed and sintered samples is defined as

$$\rho = W_{a/}W_{a}.W_{w}$$

WhereW_a denoted as weight of sample in air and W_w denoted as weight of the sample in air. Density measurement kit for Archimedes principle and Sartorius balance has been used for measuring the densification.

4.4.2 ***X-ray Diffraction***

Mechanically alloyed powders, reaction synthesized and sintered samples were characterized for determination of phases by X-ray diffraction analysis. For the compacted and sintered / reaction synthesized samples an approximate dia of 16mm was used. the sample surfaces were cleaned by 1/0 emery papers to remove if any oxide layers were present. For X-Ray diffraction, D8 BRUKER AXS diffractometer with Cu Kα, operating at 40 kV and 30 mA was used. The diffracted beam intensity was traced on a graphical chart at a goniometer speed of 2^0/min. Interplanar spacing for the different phases was determined from their corresponding Bragg's angle 2θ values using Bragg's law of diffraction(Cullity 1967);

$$n\lambda = 2d\ \mathrm{Sin}\theta$$

The wave length of X-ray is denoted as λ , corresponding to the Cu K_α and the value is considered as 1.5405 A^0. The d values calculated, from the Bragg's law were used to identify different phases of titanium aluminides with the help of JCPDS files. Scherer's formula is used to determine the crystallite size with the help of X-ray line broadening:

$$\mathbf{d = 0.9\lambda/\beta\ cos\theta} \ldots\ldots (4.1)$$

$\beta = (\beta^2_M - \beta^2_I)^{1/2}$, where β_M is the full width at half maxima (FWHM), β_I is the instrumental broadening correction factor, θ is the angle of the maxima.

4.4.3 ***Field Emission Scanning Electron Microscopy (FESEM)***

Surface Topography studies and the microstructural evolutions was carried out by FESEM using a QUANTA FEI-200 Field emission scanning electron microscopy with accelerating voltage of 20 kV was used during the elemental mapping.

4.4.4 ***Transmission Electron Microscopy (TEM)***

TEM studies were carried out to characterise the specimens in terms of type and

morphology of phases present in as RS processed condition and after imparting the homogenising treatment. Transmission electron microscopy of selected samples was carried out using Phillips CM12 model at 120kV.

4.4.4.1 Specimen Preparation

TEM samples were prepared from the pellets by first cutting into small piece of approximate size 4mm square section with thickness of about 2 to 3 mm using abrasive cutting machine, The small piece was sliced to obtain a sheet of thickness of 1mm or less using Isomet cutting machine. This sheet was ground and polished by emery papers of various grit sizes (01, 02, 03 &04) to below 0.3 mm thickness. Finally to achieve sample thickness of the order of 1000 angstroms, the sample was electrolytically thinned. The electrolyte used was 6% H_2SO_4 and 94% Methanol cooled with liquid nitrogen to avoid sample oxidation.

4.4.4.2 Structural Analysis

Transmission electron microscopy of selected titanium aluminide samples was carried out to identify various phases present using Phillips model CM12 model at 120kV. The specimens were mounted on the specimen holder and were placed inside the electron beam chamber. Different regions were viewed on the screen and TEM micrographs were taken along with the selected area diffraction (SAD) pattern.

Spot type SAD patterns were obtained and the distance between the diffracted spot and Centre spot (000) from the transmitted beam 'R' is characteristic of interplaner spacing d_{hkl} of reflecting plane and the magnification due to the lense settings i.e. the camera constant λL, where λ is the wavelength of the electron beam and L is the distance between the specimen and the screen. The relation $Rd= \lambda L$ was used to obtain the d values. The d

4.4.5 *Hardness Measurement*

Vickers's hardness measurement was carried out at 20Kg load using Blue Star make hardness tester.

4.4.6 *Thermal Analysis Measurements*

The reaction synthesis of aluminides of titanium-aluminum system is exothermic in nature and hence DTA is a suitable technique to study the reaction kinetics of the process. The base binary composition as well as composite was subjecred to study DTA technique. Exothermic and endothermic temperatures, calculation of activation energy and effect of temperatures on phase transtions were determined using DTA

analyses. PERKIN ELMER PYRIS DIAMOND TG DTA instrument was used for thermal anlysis study. The DTA signal is derived from the differenec in heat between the sample and an inert reference material by reference to a predetermined linearization curve. The unit has a working range from ambient to 1773 K and the equipment has facility for atmospheric control. The microprocessor based DTA lineariser is included as a standard part of the equipment and is not connected to the computer system. Powder mixtures weighing 10 mg was used for the DTA studies. The conversion fraction (a) was calculated for each experimental DTA exotherm by the ratio of the partial reaction heat to the total reaction heat and both the reaction heats were measured by taking the area under the DTA exothermal.

4.5 Construction of the Base Line

Several methods are available to construct the baseline of the exotherms. In the first method, the base points were simply joined by a straight line when the slopes at the beginning and end of the reaction were the same. The second method which was used to construct the baseline of the exotherm by drawing the tangents from the beginning and end points of the exotherm and drawing a perpendicular straight line from the peak of the exotherm. The perpendicular straight line from the peak and the tangent lines gave a stepped baseline and resulted in erroneous measurements of fractional areas of the exotherm. The true baseline at any time was then taken as lying between the extrapolated baselines obtained as above at apposition determined by a lever rule type calculation.

4.6 Dilatometry

The dilatometric analysis was carried out using Linseis data acquisition system. The system consists of sample holder with the highest sample diameter of 14 cm, amplifier, and a cooling circuit. The samples loaded for dilatometric analyses have diameter of the order of 10 cm. The heating consisted of two steps such as the heating to the soaking temperatures with a heating rate of 10^0C/min and the next step as the holding of sample at the soaking temperature.To study both solid state, transient liquid phase sintering and for the calculation of activation energy; the soaking temperatures for the mixtures were kept as 600^0C, 650^0C, 700^0C, 750^0C and 800^0C.

RESULTS AND DISCUSSIONS

CHAPTER 5

DEVELOPMENT OF Ti-Al-X BASED IMCs BY MECHANICAL ALLOYING

5.1 Introduction

This chapter includes the development of the Ti-Al based intermetalic matrix composites by mechanical alloying route. Development of composites included the alloying elements as C, graphite, Cr and Nb.This investigation also includes two different types of sintering such as ; reactive sintering and non-reactive sintering. Above two phenomenons are found during to the sintering of elemental mixtures and mechanically alloyed powders. Consolidation process has been carried out for better densification through hot pressing route.

Section 5.2 includes the development of nanograined Ti-Al-Cr-Nb-X[X= Ni-P coated graphite and carbon reinforced] intermetallic matrix composites by mechanical alloying, where as section 5.3 presents the development of Ti-48Al-2Nb aluminides by mechanical alloying followed by pressure less sintering. The final section 5.4 of this chapter provides an idea about the synthesis of Titanium aluminides by mechanical alloying with hot pressing.

5.2 Synthesis of Nanograined Ti-Al-Cr-Nb-X [X=Ni-P Coated Graphite and Carbon] IMC byMechanical Alloying

The present study deals with the synthesis and characterization of the Titanium Aluminides with reinforcement of carbon and graphite particles coated with Ni-P.

5.2.1 *Experimental Procedure*

5.2.1.1 Coating of Graphite and Carbon Powders with Ni-P

Graphite powder (50 gm) was milled for 5 hours with ball to powder weight ratio of 10:1 at 100 rpm in HEBM upto the size range of -325 ASTM mesh. The elemental carbon and graphite powders were weighed and subjected to account for the bath loading factor (the ratio of surface area of the substrate to the volume of EL coating

bath) of ~25% as reported[Agarwala R.C. et al 1987 &Sharma et al 2002] . The elemental carbon and graphite powders were sensitized by dipping into 0.1% stannous chloride for 2 min, then, dipped in 0.01% palladium chloride solution. Alkaline bath with pH 9 and temperature of the bath around 90 (± 2 ^{0}C) were maintained. The bath constitutes of are nickel sulphate, sodium hypophosphite, ammonium chloride, and tri-sodium citrate. The pH of the bath is maintained by the addition of ammonia solution periodically temperature was maintained constant to avoid variation in coating rate, spontaneous decomposition of electroless nickel solution and to control the reaction. Sodium hypophosphite is used as reducing agent. The coated carbon and graphite powders were characterized by XRD and FESEM.

5.2.2.2 Mechanical Alloying of Elemental Powders

The composite powder mixtures such as Ti-48Al- 1%Cr -1%Nb-1%graphite/Ni-P and Ti-48Al- 1%Cr -1%Nb-C/Ni-P are subjected to mechanical alloying by planetary ball mill at 300 rpm with ball to powder ratio 5:1. The medium was air and toluene is used as process control agent for avoiding the conglomeration of the charge. After an interval of every 25 hours samples (2 gm) were taken out for characterization of synthesis process. The thermal analysis of the alloyed powders milled for different times and as received powders was carried out up to 1400^{0}C. Field emission scanning electron microscopy (FESEM) was used to characterize the morphology of the milled powder and the surface morphology of the samples.

Table 5.1: Milling parameters

Planetary Ball mill Details (Retsch	**Milling Parameters**
Milling Balls- Agate balls	Milling Atmosphere-Air
Milling Jars- Agate jars	Charge to Ball ratio-1:5
Jar capacity- 250 ml	Milling speed- 300 rpm
PCA-Toluene	Total time of milling- 250 h
Weight of initial charge- 30gms	

5.2.3 *Results and Discussion*

The XRD patterns of the compositions Ti-48Al-1Cr-1Nb-1(Ni-P)/ coated carbon are given in the Fig. 5.2(a). Where the phases for different time of milling were determined and results are found such as for 25 hours of milling there were no TiAl phases but there were single phases such as Ti, Al, Al_3Ti, $Ti_3Al(\alpha_2)$. But for the first time TiAl phases were seen in a sample milled for 75 hours. In this milled sample pattern no more single phases of Ti and Al are seen, which reveals that after 75 of milling no more elemental Al or Ti powders are left. In the XRD pattern of 75 h milled sample, the amount of TiAl (γ), Ti_3Al (α_2) been seen to be increased with respect to time i.e, 25h and 50h milled samples. The graphite and carbon powders coated with the Ni-P shows XRD patterns, with different crystallinity. The difference is due to amorphous carbon and crystalline graphite powders. Due to the amorphous electroless coating the XRD pattern of graphite coated with Ni-P display peaks which are not very sharp ones. Presence of microcrystalline Nickel and Phosphorus supports the fact of homogeneous deposition of Ni-P over C and graphite.

In 100 h Milled samples, there exists some other phases such as Ti_3AlC. The XRD patterns of the compositions Ti-48Al-1Cr-1Nb-1(Ni-P) coated elemental graphite powders are given in Figure 5.2(b). TiAl and Ti_3Al phases are seen in 50h milled sample pattern. The Ti_3Al and TiAl amounts increased with increase in milling time and after 100 hours of milling no more peaks corresponding to the original elements like titanium and aluminium are seen. In 100 h milled samples peaks of other phases like Ti_3AlC are found.

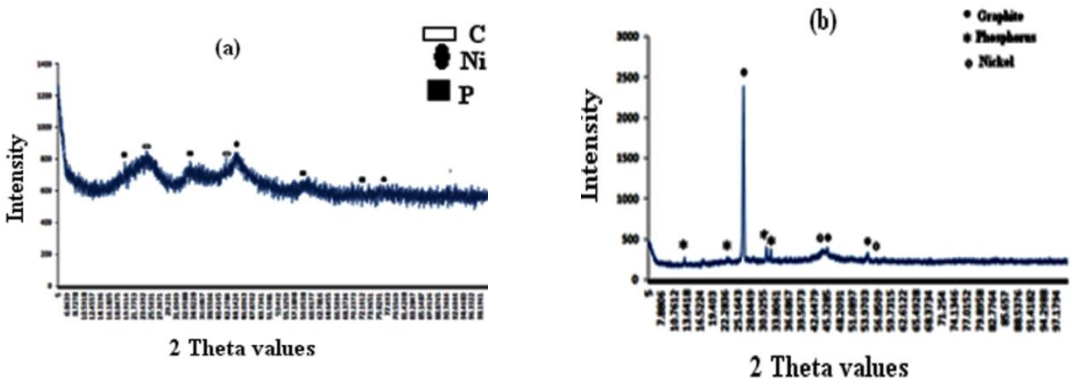

Fig 5.1 XRD patterns of electroless Ni-P coated (a) carbon and (b) graphite powders.

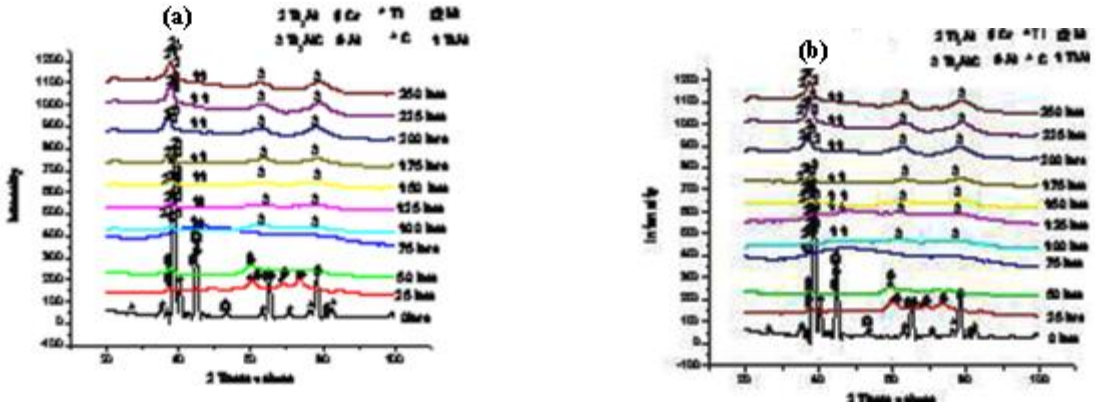

Fig 5.2 X-ray diffraction profiles of (a) mechanically alloyed powders of Ti-48Al-1Cr-1Nb-1(Ni-P) coated carbon (b) mechanically alloyed powders of Ti-48Al-1Cr-1Nb-1(Ni-P) coated

FESEM micrographs of uncoated carbon and Ni-P coated carbon powders are shown in Fig.5.3 (a) and (c) where the particle size are about 1-2 microns for the carbon powders which can be clearly observed.

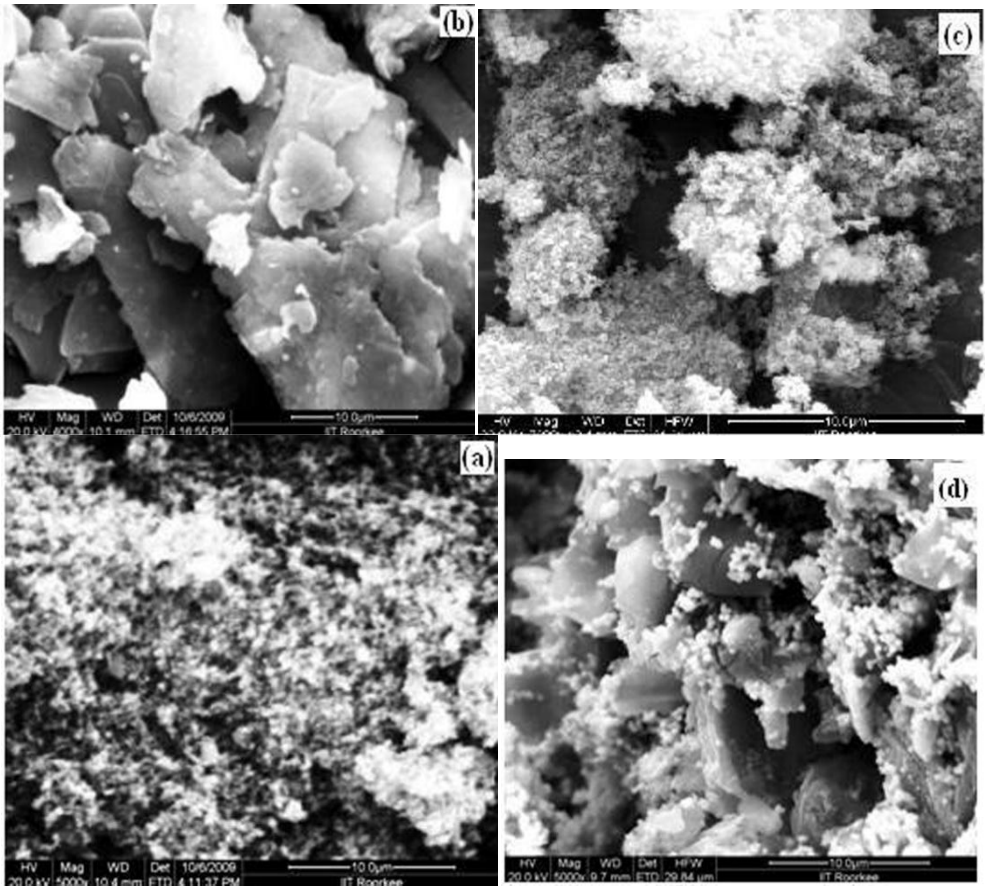

Fig 5.3 FESEM micrographs of (a) elemental carbon powders (b) graphite powders (c) carbon powders coated with Ni-P (d) graphite powders coated with Ni-P

But Fig.5.3 (b) and (d) are showing the uncoated and Ni-P coated graphite powders which are bigger in particle size, and calculated to be 5-10 microns.

The Ni-P coating for carbon and graphite powders is satisfactory due to homogeneous coatings. The uncoated carbon and graphite powders (Fig 5.3 (a) & (b)) can be compared with the coated ones (Fig 5.3(c) & (d)) respectively, where it can be easily noticed that the covering of globules over the particle surfaces (catalytic surface). The covering of the globules is homogeneous which was also reported for graphite by Agarwala R.C. et al (2008). The fracture and cold welding of particles occur due to mechanical energy given by milling. The particle size is getting lowered as the extent of milling increased which is calculated using quantitative metallographic technique.

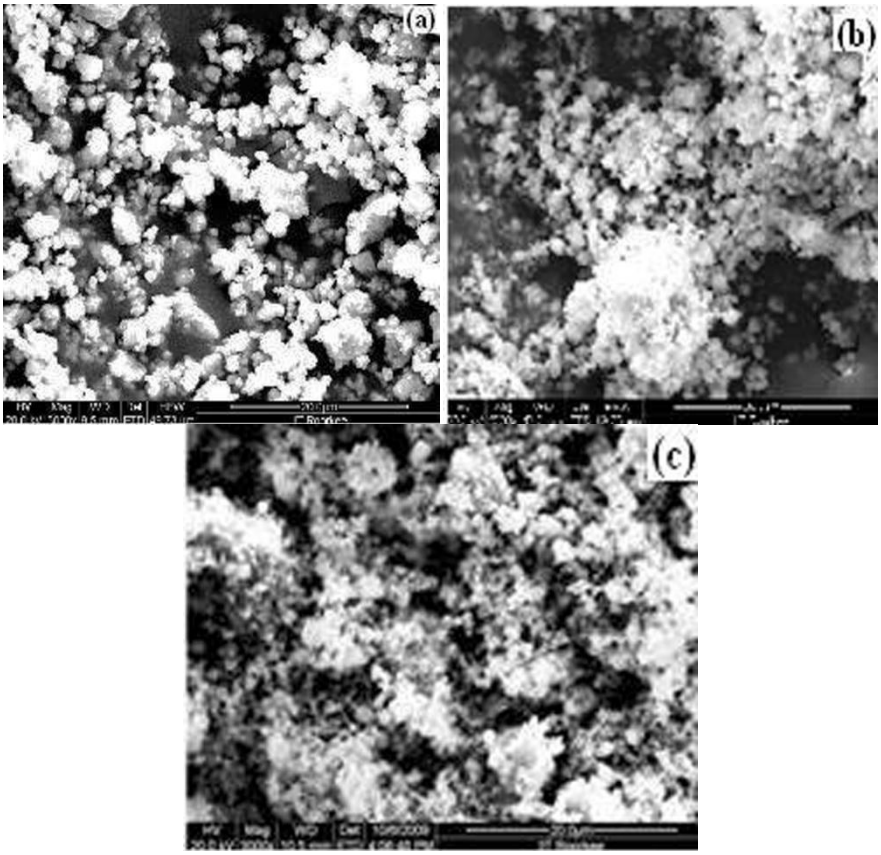

Fig 5.4 FESEM micrographs of Ti-Al-1Cr-1Nb-1(Ni-P) coated carbon powders milled for (a) 25 hours (b) 125 hours and (c) 250 hours

The elemental titanium and aluminum used for mechanical alloying were of the size of ~40 microns. Milling time has two effects on the charge/powders ,firstly breaking of particles then agglomeration of particles occur by cold welding which occur due to diffusion bonding by pressure developed due to the impact of balls. The breaking of powders also attributed towards the work hardening due to the continuous plastic deformation and also the increase in the Gibbs free energy of the system, which facilitates in fracture of the surface to attain lowest potential energy. The formation of nascent surfaces create the chances of cold welding, as it is very short range order the temperature of the system is high enough for welding of fine particles.

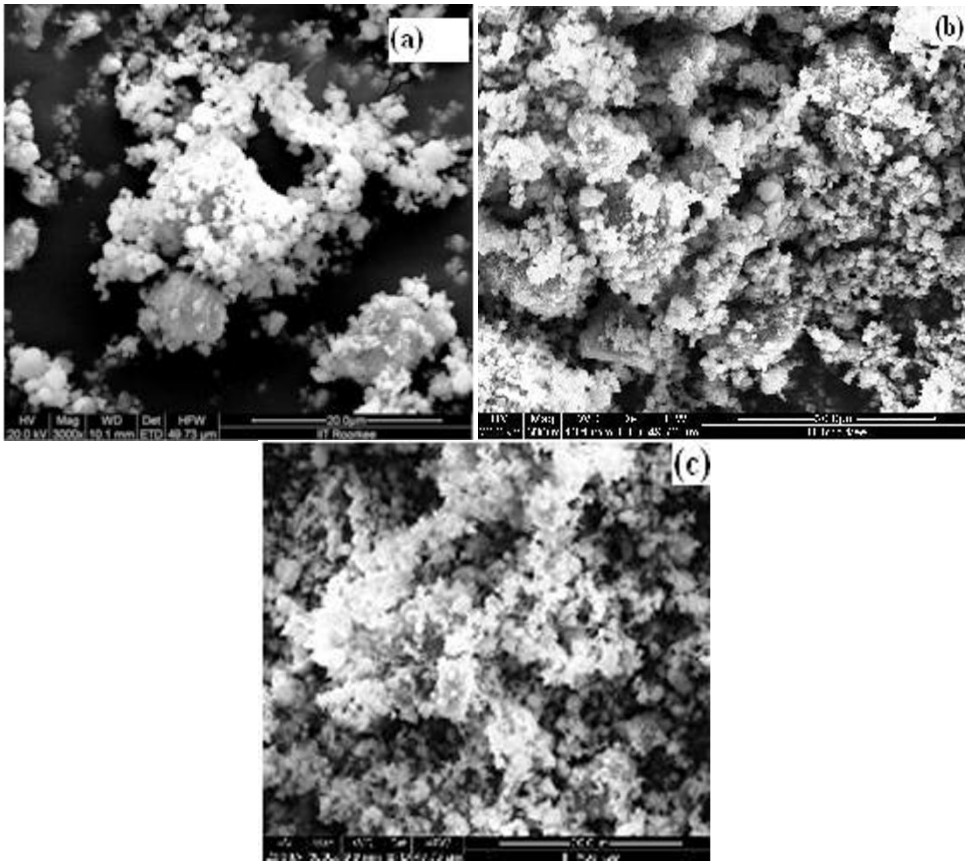

Fig 5.5 FESEM micrographs of Ti-Al-1Cr-1Nb-1(Ni-P) coated graphite powders milled for (a) 25 hours (b) 125 hours and (c) 250 hours

This cycle of cold welding and fracture causes in the formation of intermetallics and the carbon and graphite are used for refinement of grains. The formation of new surfaces due to repeated fracture helps in the alloying of the system constituents as well. The Figs 5.4 & 5.5 shows the lowering of particles after mechanical alloying of the TiAl nanocomposite powders.

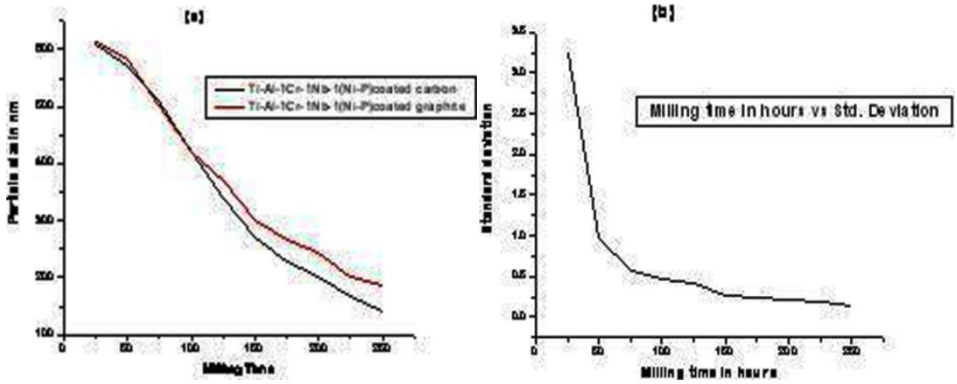

Fig 5.6 With the increase in milling time (a) the change in particle size (b) the change standard deviation of the particle size

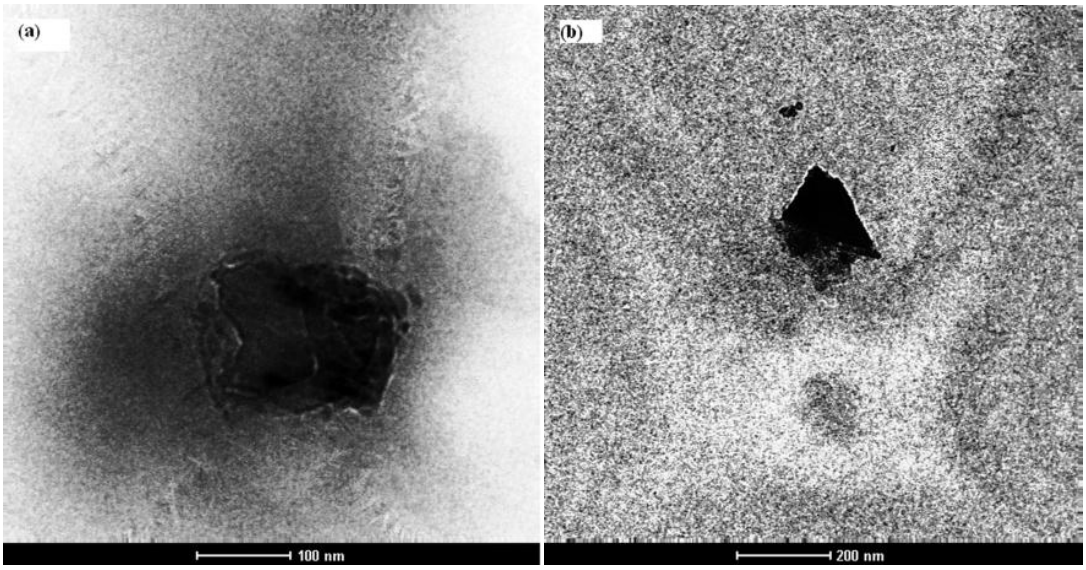

Fig 5.7 Transmission electron micrographs of (a) Ti-48Al-1Cr-1Nb-1(Ni-P) coated elemental carbon powders and (b) Ti-48Al-1Cr-1Nb-1(Ni-P) coated graphite powders

The particle size of both composition are getting lowered and due to the increase in the extent of milling,the particle size of Ti-48Al-1Cr-1Nb-1(Ni-P) coated elemental carbon powders are found ~142 nms and for the Ti-48Al-1Cr-1Nb-1(Ni-P) coated graphite powders are found 169 nms which are shown in Figure 5.6(a).

The Fig 5.7 ((a) & (b)) shows the 250h milled Ti-48Al-1Cr-1Nb-1(Ni-P) coated elemental carbon powders and Ti-48Al-1Cr-1Nb-1(Ni-P) coated graphite powders. The electron micrograph shows the uneven shapes of the powders which can be attributed towards the mechanical milling of the powders, the size of the particles, which can be calculated using volumetric analysis are in the range of 140-180 nms, which are in support of results for particle size calculated using the quantitative metallographic technique. The TEM micrographs reveal the cold welding of particles, because in micrographs the particle shows presence of layers of material. The lowering in decrease of the particle size can be confirmed by TEM micrograph and the prevailing of cold welding over the fracture during mechanical alloying after certain time can be noticed.

5.2.4 *Summary*

Ni-P coating on carbon and graphite powders is possible using alkaline EL bath and can be used for making homogeneous coating on the irregular surfaces of carbon and

graphite powders of the size of 5-10 microns. At least 75 hours to 100 hours of mechanical alloying with 300rpm, 5:1 ball to charge to ratio with agate balls and jars and toluene as PCA is needed for the synthesis of nanograined TiAl and Ti_3Al with an extra phase of Ti_3AlC.From the particle size analysis, it is seen that the particle size and the corresponds standard deviation decreased with increase in milling time, uniform and reduced size (140 to 189 nm) is obtained after 250 h milling for both the composition. The study of XRD patterns of compositions Ti-48Al-1Cr-1Nb-1(Ni-P) coated carbon and Ti-48Al-1Cr-1Nb-1(Ni-P) coated graphite, reveal that after about 75 h milling respectively the broadening of peaks occur. This is because the particles are in amorphous state and it infers that after such time of milling, one could go for sintering and reaction synthesis for further study of mechanical behaviors.

5.3 Sintering Behavior of Mechanically Alloyed Ti-48Al-2Nb Aluminides

Ti-Al intermetallics have been produced using mechanical alloying technique. A composition of Ti-48Al-2Nb at % powders was mechanically alloyed for various durations of 20, 40, 60, 80 and 100 h. At the early stages of milling, a Ti (Al) solid solution is formed, on further milling the formation of amorphous phase occurs. Traces of TiAl and Ti_3Al were formed with major Ti and Al phases after milling at 40 h and beyond. When further milled, phases of intermetallic compounds like TiAl and Ti_3Al were formed after 80 hours of milling and they also found in 100 h milled powders. The powders milled for different durations were sintered at 785^oC in vacuum. The mechanically alloyed powders as well as the sintered compacts were characterized by XRD, FESEM and DTA to determine the phases, crystallite size, microstructures and the influence of sintering over mechanical alloying.

5.3.1 *Materials and Methods*

Ti (40-44µ, 99.9% purity), Al (40–44µ, 99.9% purity) and Nb(40-44 µ,99.9% purity) powders were mixed to give the composition Ti-48-Al-2Nb (at. %) which was then charged into a hardened steel vial with hardened steel balls under wet toluene media i.e. the balls and charge are totally submerged in the toluene. The charge to ball weight ratio (CBR) was 1:5. Milling was performed in a (Retsch PM 400/2) ball mill for periods varying from 0 to 100 h at a milling speed of 300 rpm and vial rotation speed of 600 rpm [Table-5.2].Process control agents, such as toluene was used, which prevent

agglomeration of elemental powders. For the purposes of reactive and non-reactive sintering, Itwas performed on two different series of powders: (1) reactive sintering process done on blended elemental powders, and (2) non-reactive sintering process done on 100 h-milled powders. The powders were sintered under argon environment pure for 2 hours at 450^0C and 800^0 C .Sintered samples were 5 mm in thickness and 16.4mm in diameter. The milled and sintered samples were characterized by of X-ray diffraction (XRD) using a D8 BRUKER AXS diffractometer with Cu Kα operating at 40 kV and 30 mA. Scherer's formula is used to determine the crystallite size with the help of X-ray line broadening (Cullity 1969):

Table 5.2: Milling parameters

Planetary Ball mill Details **(Retsch PM 400/2)**	**Milling Parameters**
Milling Balls- Hardened steel balls	Milling Media-Toluene
Milling Jars- Hardened steel jars	Charge to Ball ratio-1:5
Jar capacity- 500 ml	Milling speed- 300 rpm Vial Speed- 600 rpm
PCA-Toluene	Total time of milling- 100h
	Weight of initial charge- 30gms

$$\mathbf{d = 0.9\lambda/\beta \cos\theta} \quad \text{..... (5.1)}$$

$\beta = (\beta^2_M - \beta^2_I)^{1/2}$, where β_M is the full width at half maxima (FWHM), β_I is the instrumental broadening correction factor, θ is the angle of the maxima, and λ is the

Cu K_α wavelength (= 0.15406 nm).

The thermal analyses of the MA powders of different milling times and as received powders were done up to 1400^0C in PERKIN ELMER Pyris Diamond TG/DTA instrument. DTA measurements were carried out in argon atmosphere to avoid

oxidation. The argon flow rate was kept at 200ml/min and the heating rate was kept 10^0C/min. Using a QUANTA FEI-200 made Field emission scanning electron microscopy (FESEM) was carried out to characterize the morphology of the milled powder and the surfaces of the sintered samples. The densification of the sintered samples was calculated using the Archimedes principle. According to the principle when a body s immersed in a fluid there is buoyant force in upward direction on the body which have the same weight of that of the displaced fluid.

$$\mathbf{F_B = m_L g} \quad \text{.....(5.2)}$$

F_B is buoyant force and m_L is mass of the liquid displaced. The dimensions of the samples were measured by the help of vernier calipers and the mass of the same was measured. Then the density of the samples are measured in air by using the equation

$$\boldsymbol{\rho = m/V} \quad \text{.....(5.3)}$$

Then the sample is submerged in the water and the weight if the sample is taken when submerged.Then the actual density of the sample is calculated by using the equation

$$\boldsymbol{\rho_a = (W_w/(W_a - W_w))} \quad \text{.....(5.4)}$$

Where ρ_a is actual density, W_w is weight in water and W_a is weight in air.

5.3.2 *Results and Discussion*

5.3.2.1 XRD Analysis of Mechanically alloyed powders

The XRD Fig.5.7 depicts the transformation occurred during milling of Ti-48Al-2Nb The XRD pattern of as-received powder is almost similar to that 40 h-milled powders. The peak broadening and lowering in the intensity were observed with increase in extent of milling, due to the decrease in crystallite size occurring from 91-177nm after 20 h to about 12-18 nm after 100hours of milling. Distortion of lattice parameter of Ti results in shifting of the main reflexion of Ti peaks occurring towards higher angles, From the Ti–Al phase diagram (Zou et al 1995), Al has a better solubility in Ti, while the reverse is limited for different temperatures. So as per the expectation, Al largely diffused into Ti in the process of MA up to a certain extent and beyond which an amorphous phase is formed. At this stage peak broadening lead to the overlapping of

peaks, as a result of which different peaks are not easily distinguished. The amorphization of the powders and the lowering of the peak intensities can be attributed towards the external energy supplied to the system by mechanical alloying (Dobbins et al 2009). The amorphization occurs because of the free energy of intermetallics became higher than that of amorphous phase (Zou et al 1995). According to Fig. 5.7, after 40 h of MA, the peaks are broadened between angles of 34–42^0; which indicates the amorphization of powders. Interestingly the free energy curve of the amorphous phase in the Ti–Al system is actually lower than those of the solid solution and intermetallics (Bhattacharya et al 2004). Hence, the amorphous phase is formed first then on further milling, leads to the formation of supersaturated solid solution hcp-Ti (Al) due to the crystallization of an amorphous phase or disordered Ti_3Al, because these two phases present the same unit cell (Bhattacharya et al 2004). The diffraction pattern after 80h MA shows the formation of the TiAl intermetallic compound.

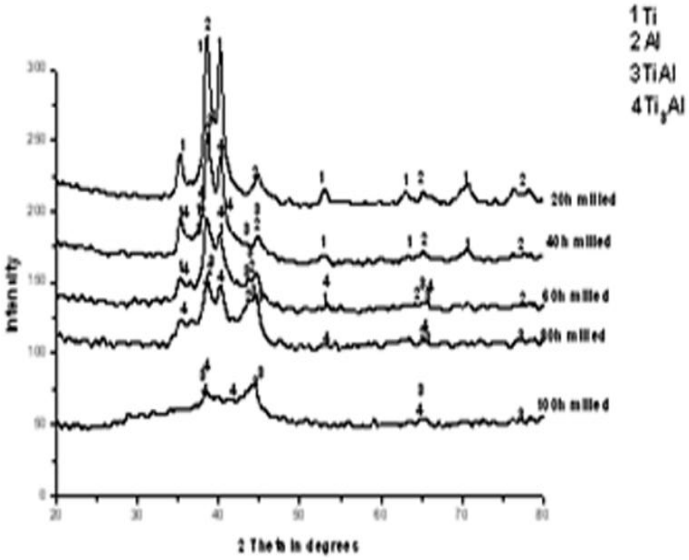

Fig 5.8 XRD patterns of milled powders for different extent

After 100h of MA, both TiAl and Ti_3Al peaks are present in the diffraction pattern. The enthalpy values for the formation of TiAl and Ti_3Al are −75 and −73 kJ/mol respectively (Hay et al 2000 & Froes et al 1995) which is the main cause of formation of intermetallics and further heat treatment is required for crystallization of intermetallics after MA (Dobbins et al 2009). In addition local temperature rises during MA which helps in nucleation and growth of the intermetallic compound. The MA of the powder mixtures results in lowering the crystallite size due to external force applied

by ball milling and plastic deformation occurring. The crystallite size of the as received powder of Ti, Al and Nb were 40-44µ. After MA of 20 hours with 1:5 charge to ball ratio, it came down to 91 nm and 177 nm for Ti and Al respectively. When further MA for 100 hours the crystallite size of the Ti (Al) solid solution, TiAl and Ti_3Al became 12 to 18 nm (Fig.5.8). The crystallite size was determined using Scherer's formula (Eqn. (5.1)).

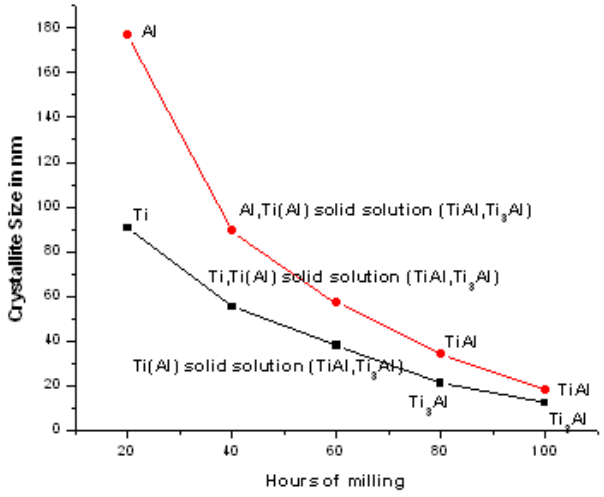

Fig 5.9 Variations of crystallite sizes of the MA Ti-48Al-2Nb at different extent of milling

5.3.2.2 DTA Study

The thermal analysis dataof the as received Ti-48Al-2Nb is shown in Fig.5.9 (a), where at 664^0C Al got molten and at 785^0C there is an exothermic peak, which is the evidence for the formation of TiAl intermetallics. Where the energy released is 39.2 J/g and the exothermic peak shifted to the left with the increase in the extent of milling. The height of the exothermic peak is lowered after 20 hours of milling and the peak temperature came down to the range between 250-450^0C as shown in Fig. 5.9(b). From thermal analysis the sintering temperatures are determined as the 450^0C and 800^0C. So that the TiAl intermetallic phases would be formed and crystallized.

5.3.2.3 Microstructure

The morphology of as-received and MA-ed powders at different milling times was investigated using FESEM, and shown in Fig.5.10. According to Fig.5.10 (a), Ti

powders appear in irregular shapes and in various sizes, but the particles of Al are mainly cylindrical or conical. The agglomeration of powders can be clearly observed in the early stages of MA up to 20h due to the ductility of Al.

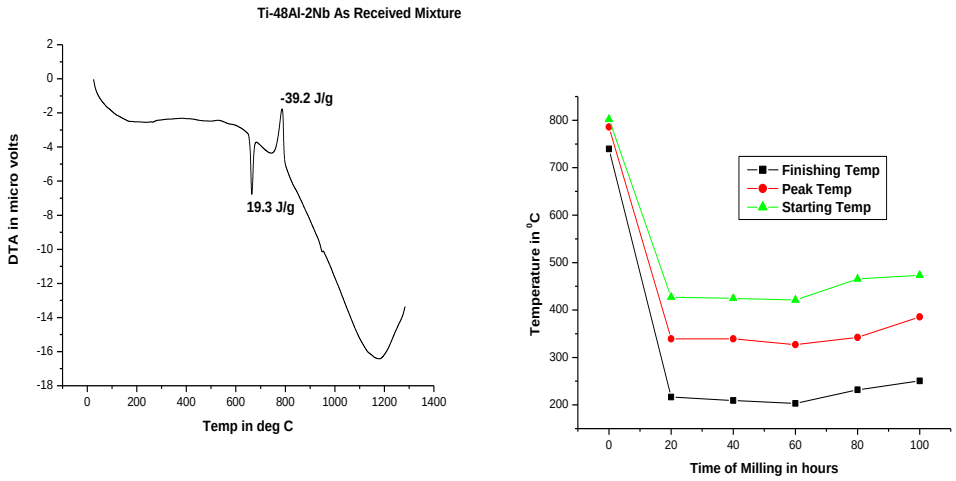

Fig 5.10 (a) Thermal analysis of as received Ti-48Al-2Nb powder mixture and (b) The starting, peak and the finishing temperature of the exothermic peak in the thermal analysis data of powders of different milling times

Work hardening and plastic deformation occurs due to further milling, which results in production of finer particles by fragmenting the agglomerated powders which can be seen for the powders MA from 20h to 80h as shown in Fig.5.10 (b-e). After further milling upto 100h, abrupt reduction of particle size occurs to a dimensionsmaller than 160nm (Fig. 5.10(f)). Due to the formation of the brittle phases, the particle size reduces in sharp manner.

5.3.2.4 XRD Analysis of sintered compacts

According to Fig. 5.11(a) the peaks of the 800^0 C sintered samples for the as received powders shifted to the left showing the formation of TiAl and Ti_3Al phases, Where for the 450^0C sintered and as received samples only Ti and Al peaks were found. Though the 40h MA powders do not show distinct TiAl and Ti_3Al phase but the sintered samples at 450^0C and 800^0C show the phases TiAl, Ti_3Al for 80h and 100h MA.

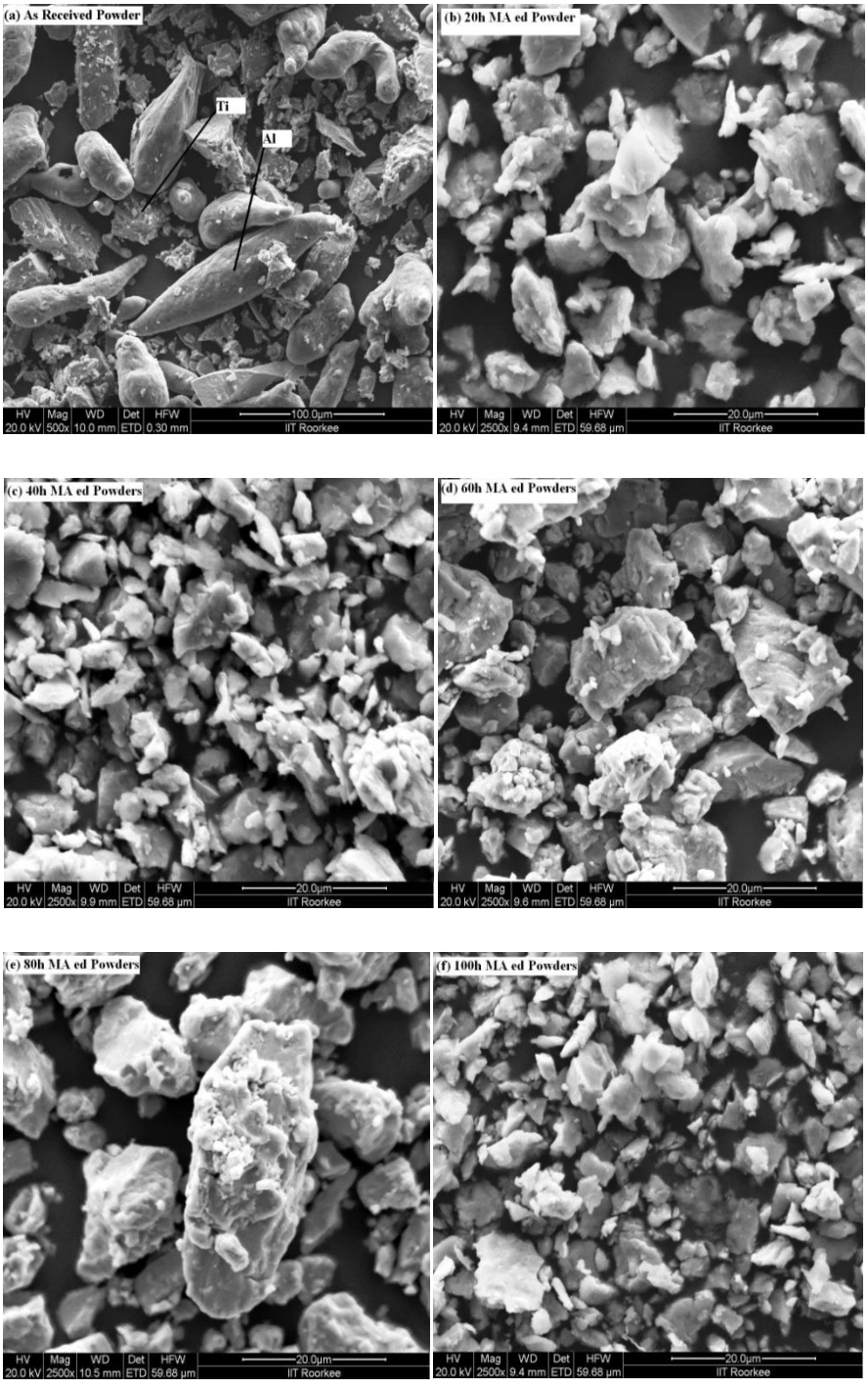

Fig 5.11 FESEM micrographs of as-received and milled powders for different extent of milling (a)As-received powder, (b) 10 h MA powder, (c) 20 h MA powder, (d) 40h MA powder, (e) 60 h MA powder, (f) 80 h MA powder and (g) 100 h MA powder

The MA powders exhibit peaks broadened due to the amorphization occurred by plastic deformation, but the sintered samples show sharp peaks, which is due to recrystallization of the phases. The peaks are matched referring to the JCPD cards for

Al, Ti, TiAl and Ti_3Al respectively Ref code: 00-004-0787, Ref. Code: 00-044-1294, Ref.Code:00-042-1137) and Ref Code: 00-014-0451.

5.3.2.5 Microstructure

According to Figs5.12(a and b) the micrographs of the sintered samples at 450^0C show the phases of Ti, TiAl and Ti_3Al for 80h and 100h MA powders, where the 100h MA ed powders show finer microstructures. The sintered samples were polished using different grit emery papers and etched 1partHNO_3, 1 part HF and rest of water. The sintered samples at 800^0C for both the 80h and 100h MA samples show coarser microstructures compared to the 450^0C sintered samples. Because at higher temperatures recrystallization and grain growth of the intermetallic phases take place.

5.3.2.6 Physical Properties

Table 5.3 shows the density and the amount of porosities during the reactive and nonreactive sintering. The density of the reactively sintered samples is lower than that of the sintered pre-alloyed powder shown in Fig.5.13. As compared reactive and nonreactive sintered possess relatively comparable densities to exhibit considerable mechanical properties [Table 5.3]. Due to the presence of the agglomerated nanocrystalline powders during MA [8 increase in the possibilities of large porosities occurs during sintering. The diffusion distance decreases due to the fine particles.

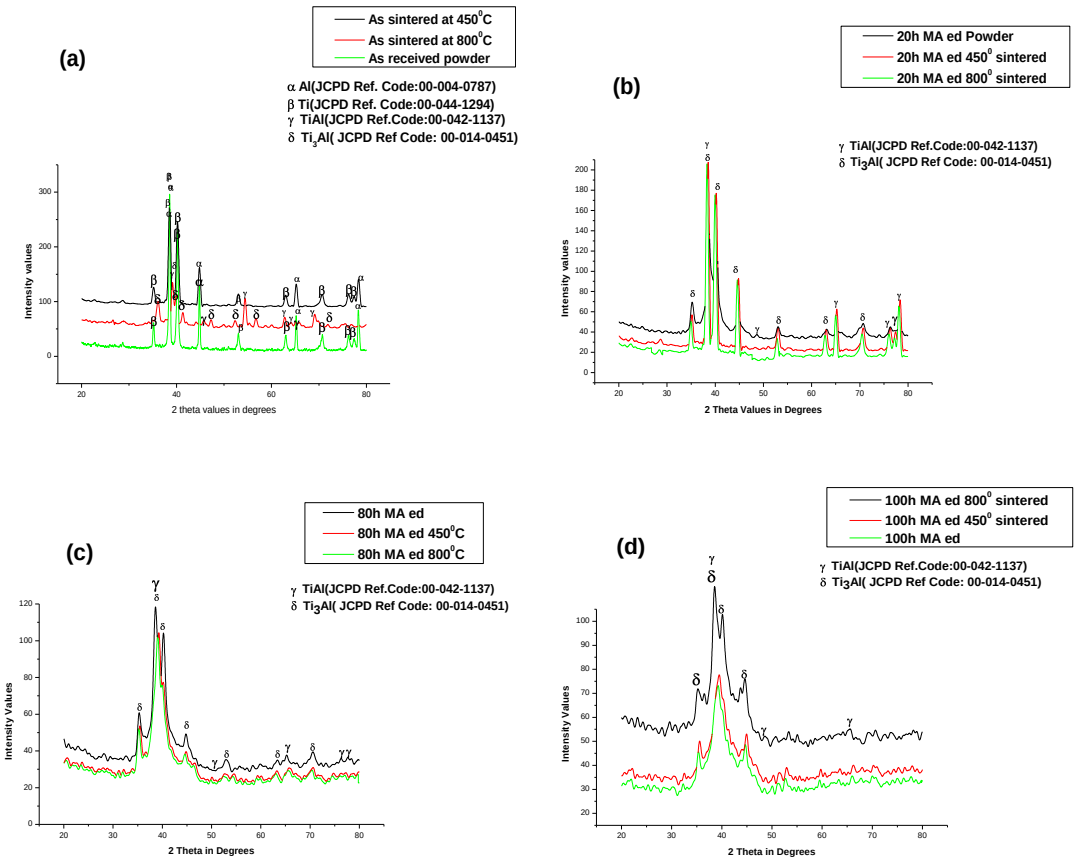

Fig5.12 Comparative XRD patterns of milled and sintered compacts at 450^{0}C and 800^{0}C for (a) as received (b)20h MA (c)80h MA and (d)100h MA

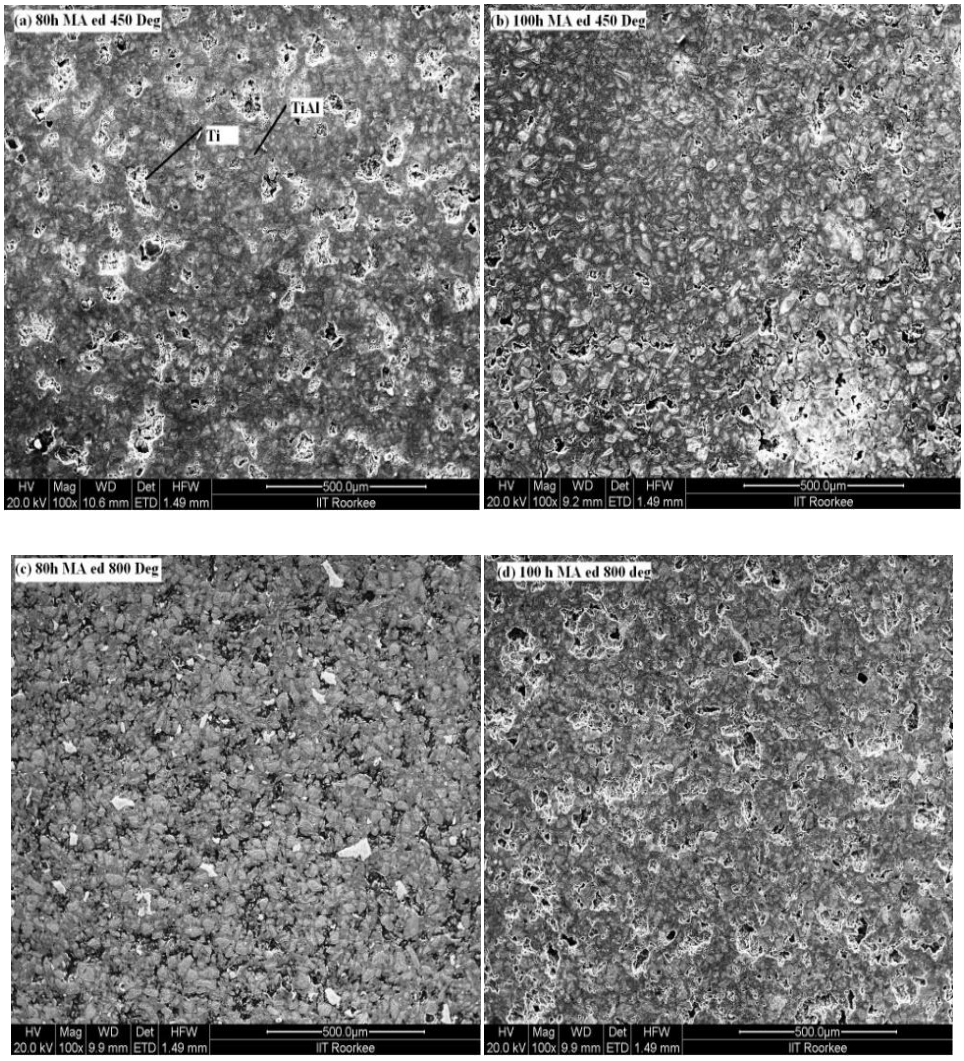

Fig 5.13 FESEM Micrographs of sintered samples (a) 80 h MA at 450^{0}C (b) 100 h MA at 450^{0}C (c) 80 h MA at 800^{0}C and (d) 100 h MA at 800^0 C

Table 5.3: Density comparison of the milled and sintered compacts at (450^{0}C and 800^{0}C) samples

Milling Times	As Milled	% Porosity	Sintered at 450^{0}C	% porosity	Sintered at 800^{0}C	% porosity
0h	3.219	18.6	3.473	12.1	3.619	8.9
20h	3.112	21.3	3.2	19	3.4	14
40h	3.013	23.8	3.093	21.7	3.112	21.3
60h	2.953	25.3	2.991	24.3	3.098	21.6
80h	2.727	31	2.774	30	2.945	25.5
100h	2.688	32	2.717	31.3	2.899	26.7

The area covered by grain boundaries increases due to the fine grained structures, which acts as the site for the nucleation for diffusion path. There occurs increase in the rate of transport for alloy in the presence of chemical potential gradients. Therefore, the density of the sintered pre-alloyed powder is higher than that of the other powders.

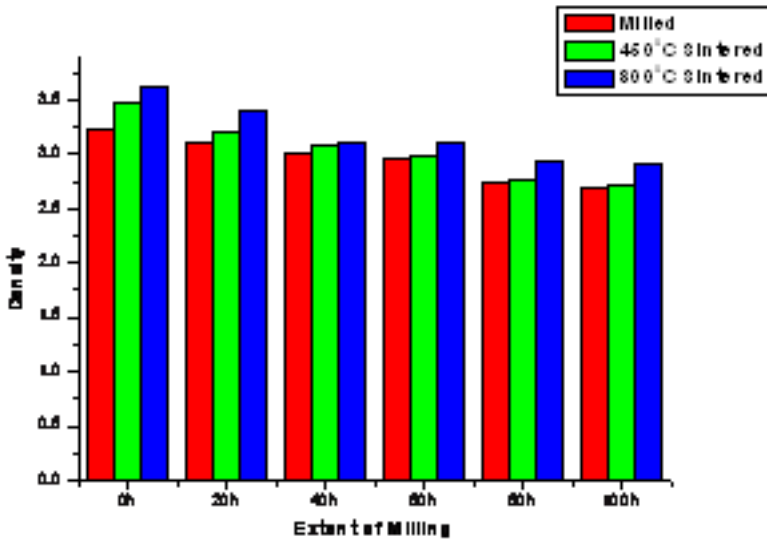

Fig 5.14 Comparison of Density of MA and sintered samples at 450^0C and 800^0 C

The harmful effect of pores and porosities behave directly proportional to the density and hardness. Porosities lead to the weakening of the sample because the reduction available stresses bearing area is lowered and the ability of withstanding the amount of stress.

5.3.3 *Summary*

Titanium aluminide powders can be produced by mechanical alloying of elemental Ti and Al for 80 h. On Increasing MA time the particle size decrease down to less than 160 nm and further decrease in the range of 12-18 nm after 100 h of milling. According to the results the non-reactive sintering process displays better physical properties than reactive sintering.

5.4 A Study on Physical and Mechanical Properties of TiAl Intermetallics Prepared By Mechanical Alloying Followed By Hot Pressing.

A TiAl composite with in situ AlNb2 has been prepared through mechanically alloying of Ti, Al, 2Nb at% and 2Cr at% elemental powder blends for different extents of time 20,40,60,80 and 100 hours. Initially during mechanical alloying, a Ti -Al solid solution

is formed, which is transformed into amorphous aluminides when milled for higher extent. Traces of TiAl and Ti3Al were formed with major Ti and Al phases after milling for 40h. Phases of intermetallic compounds like TiAl, Ti_3Al and $TiAl_3$ started forming after 80 hours of milling. The powders milled for different durations were hot pressed at 30MPa in Gleeble 3800^{TM} at 7850C in vacuum. The samples were characterized by XRD, FESEM and DTA to determine the phases, crystallite size, hardness, and microstructures. The Non-reactively hot pressed powders exhibit fine grained microstructure with respect to reactively ones, and the exothermic peak in the thermal analysis gets lowered.

5.4.1 *Experimental Procedure*

5.4.1.1 Mechanical Alloying

The materials of Titanium, Aluminium and Niobium were taken and the mulling condition applied for this study can be referred from section 5.3.1.

5.4.1.2 Hot Pressing

Hot pressing was performed on two different series of powders: (1) 100 h-milled. (Pre-alloyed) powders for the non-reactive hot pressing process and (2) blended elemental powders for the reactive hot pressing process. The hot pressing was carried out in vacuum of the order of 10^{-4}torr in Gleeble 3800^{TM}. After hot pressing, the samples were ground and polished for the metallographic studies.

Table 5.4: Milling parameters

Planetary Ball mill Details (Retsch PM 400/2)	**Milling Parameters**
Milling Balls- Hardened steel balls	Milling Media-Toluene
Milling Jars- Hardened steel jars	Charge to Ball ratio-1:5
Jar capacity- 500 ml	Milling speed- 300 rpm Vial Speed- 600 rpm
PCA-Toluene	Total time of milling- 100h
	Weight of initial charge- 30gms

5.4.1.3 Characterization

Milled and hot pressed powders were characterized using FESEM, XRD and Archimedes principle which can be referred from section 5.3.2.

5.4.2 *Results and Discussion*

5.4.2.1 XRD Analysis of Mechanically Alloyed Powders

The transformations occurring during milling was shown by XRD. Fig. 5.15 shows the diffraction pattern for Ti-48Al-2Nb-2Cr. XRD pattern of as-received powder is almost similar to that 40 h-milled powders. The peak broadening and lowering in the intensity were observed with increase in extent of milling.The decrease in crystallite size occurred from 90.7-176.8nm after 20h milling to and about 12-18 nm after 100hours of milling. Decrease in the lattice parameter results in the shifting of the main reflexion of Ti peaks towards higher angles. The decrease in the lattice parameter is attributed to the distortion of Ti lattice by Al diffusion. Further milling caused in lowering of the integrated intensity of peaks and result in the complete amorphization of powders (Froes et al 1995). According to Fig. 5.14, after 40 h of MA, the peaks are broadened between angles of 34–42^0; which indicates the amorphization of powders. The free energy curve of amorphous phases lies beneath that of the Ti (Al) solid solution, which causes the formation of the amorphous phases earlier. The diffraction pattern after 80h MA shows the formation of the TiAl intermetallic compound.

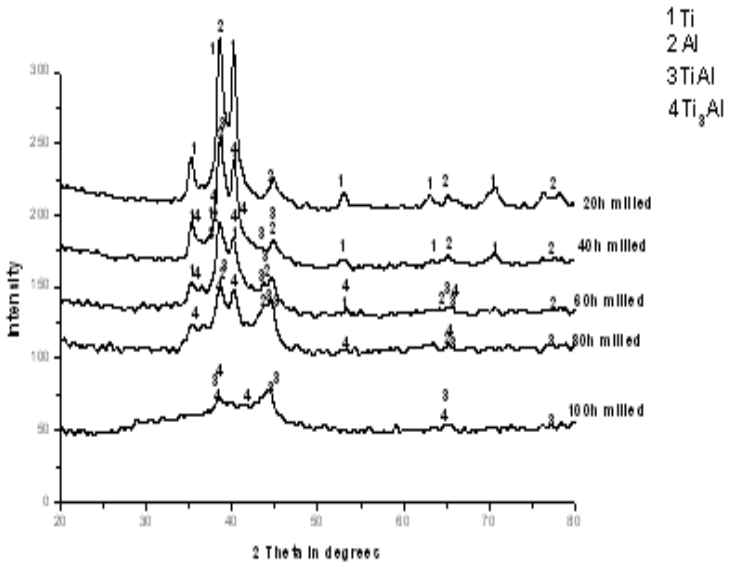

Fig 5.15 XRD patterns of powders milled for different extent

Peaks of TiAl and Ti_3Al intermetallic compounds are exhibited after 100h MA. According to the results obtained in this section, it may be concluded that the formation of intermetallic compounds is possible during MA. The enthalpy values for the formation of TiAl and Ti_3Al are −75 and −73 kJ/mol respectively.This is the main cause for the formation of intermetallics, which gets crystalline after further heat treatment (Froes et al 1995) .

5.4.2.2 DTA Study

Thermal analysis data of the as received Ti-48Al-2Nb-2Cr shown in Fig.5.15 (a), where at 664^0C Al got is molten and at 785^0C there is an exothermic peak, which is the evidence for the formation of TiAl intermetallics. Amount of energy released is 39.2 J/g and the exothermic peak shifted to the left with increasing hours of milling. The exothermic peak is turned into an impression after 20 hours of milling and the peak temperature came down to the range 250-450^0C shown in Fig. 5.15(b), which gives an evidence that the milled powders were given external energy by MA and the difference in the Gibbs free energy between the intermetallics and that of the amorphous phases is smaller compared to the elemental blends. The reactive sintering (sintering of elemental powders), that's why may needed785^0C, where in case of non reactive sintering (sintering of MA powders) may needed temperature is in the of 250^0C-450^0C.

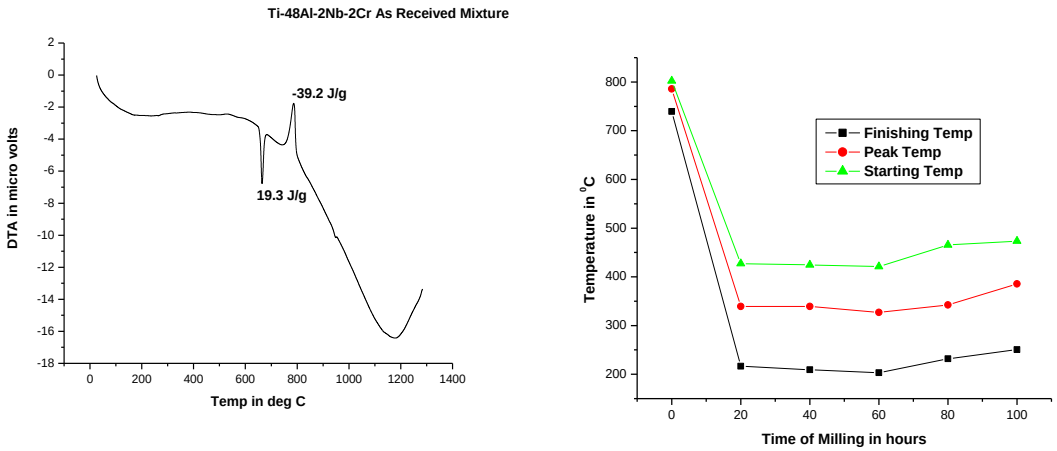

Fig. 5.16 showing (a) Thermal analysis of as received Ti-48Al-2Nb powder mixture and (b) The starting, peak and the finishing temperature of the exothermic peak in the thermal analysis data of powders of different extent of milling

5.4.2.3 Microstructure

Morphology of the as-received and MA powders at different milling times was investigated by FESEM analysis, and shown in Fig.5.16. According to Fig. 5.16(a), Ti powders appear in irregular shapes and in various sizes, but the particles of Al are mainly cylindrical or conical. The agglomeration of powders can be clearly observed in the early stages of MA up to 20h due to the ductility of Al. Work hardening and plastic deformation occurs due to further milling, which results in production of finer particles by fragmenting the agglomerated powders which can be easily seen for the powders mechanically alloyed from 20h to 80h as shown in Figs (3b-3e). Further milling for100h, abrupt reduction of particle size occurs to a dimension smaller than160nm which is attributed towards the formation of brittle phases (Fig. 5.16(f)).

5.4.2.4 XRD Analysis of Hot Pressing Process

According to Fig. 5.17(a) the peaks of the hot pressed samples at 785^0 C for 5,10 and15 mins of the as received powders showing the formation of TiAl, Ti_3Al $TiAl_3$, $TiAl_2$ phases and the formation of $AlNb_2$ with some retained Ti and Al powder peaks. But Fig. 5.17((b) and(c)) show the formation of TiAl, Ti_3Al and $TiAl_3$ for the 80h and 100h MA powders and hot pressed for 5, 10 and 15mins. The mechanically alloyed powders exhibit peaks broadened due to the amorphization occurred by plastic deformation, but the hot pressed samples show sharp peaks, which is due to recrystallization of the phases.

5.4.2.5 Microstructure

According to the Figs5.18(a and b) the micrographs of the 80h and 100h (MA+HP for 15 mins samples at 785^0C) show the phases of Ti, TiAl and Ti_3Al and $AlNb_2$ where the 100h MA ed powders show finer microstructures. It is obvious from Fig. 5.18(a) that TiAl intermetallic compound has the highest amount of the phases though some of the regions show the higher percentage of Ti. Ti_3Al is only found in some isolated islands in TiAl matrix, with some dispersed $AlNb_2$.

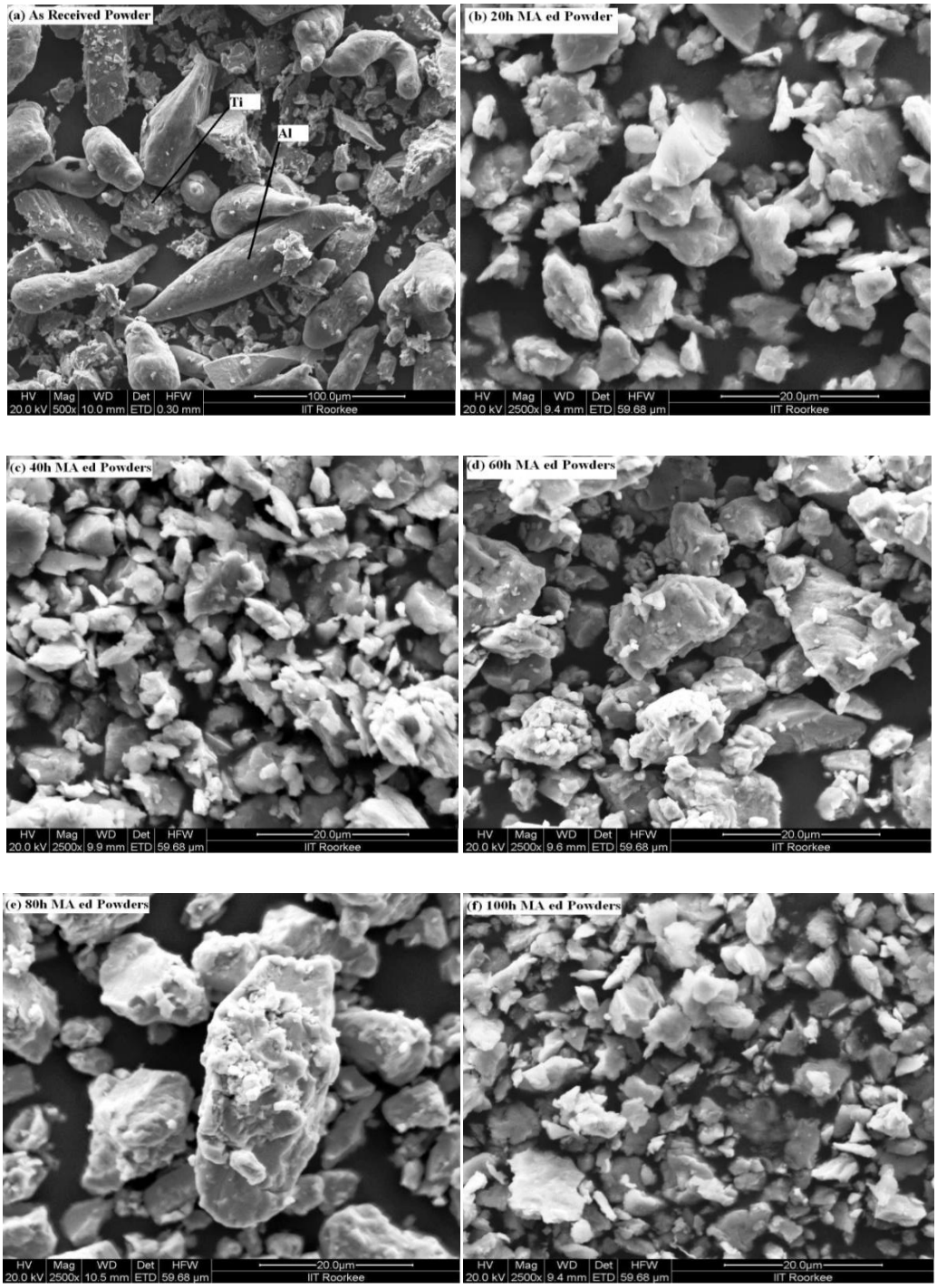

Fig.5.17 FESEM micrographs of as-received and milled powders for different milling times.(a)As-received powder, (b) 10 h MA powder, (c) 20 h MA powder, (d) 40h MA powder, (e) 60 h MA powder, (f) 80 h MA powder and (g) 100 h MA powder

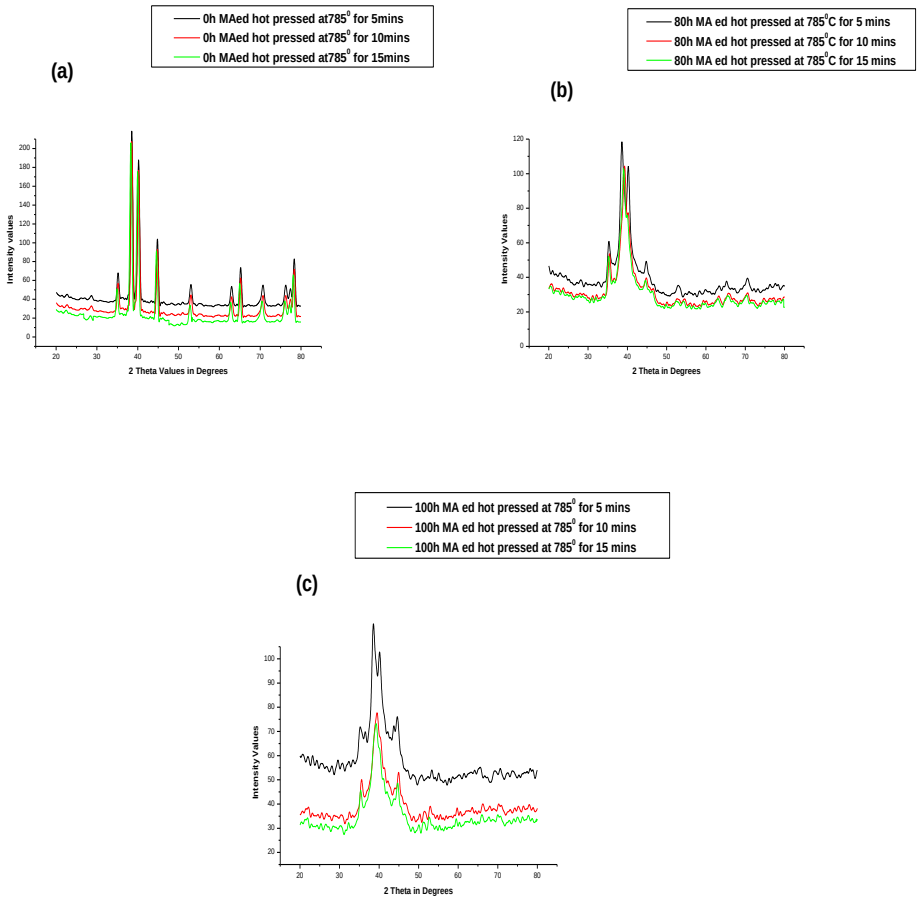

Fig 5.18 Comparative XRD patterns of mechanical alloyed and hot pressed (785 ^{0}C) for different extent of timefor (a) as received (b)80h MA (c)100h MA

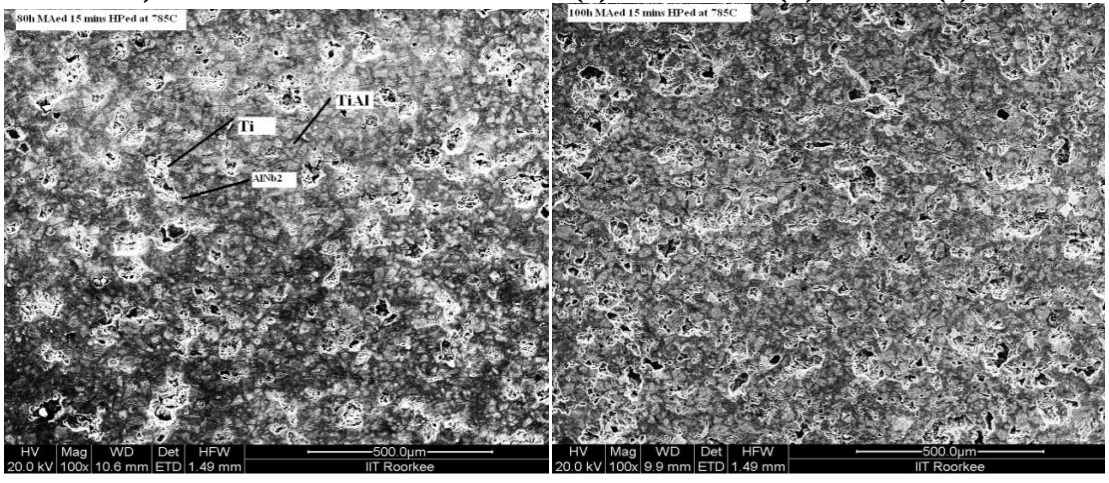

Fig 5.19 FESEM micrographs of mechanically alloyed and hot pressed samples at 785^{0}C for 15 mins (a) 80h MA (b) 100h MA

5.4.2.6 Physical Properties

The density of the sample made with reactive hot pressing (as received) is higher than that of the hot pressed pre-alloyed powder. Both kinds of the hot pressed possess relatively adequate densities to exhibit considerable mechanical properties. Due to the mechanical alloying, lowering of particle sizes and work hardening occurs which is attributed towards the lowering in the densification. The hardness value of the HP pre-alloyed powder (1175 VHN) is almost three times higher than that of the HP elemental one (321 VHN), because of the effect of mechanical alloying, which cause the formation of finer intermetallic phases than the HP elemental powder blends.

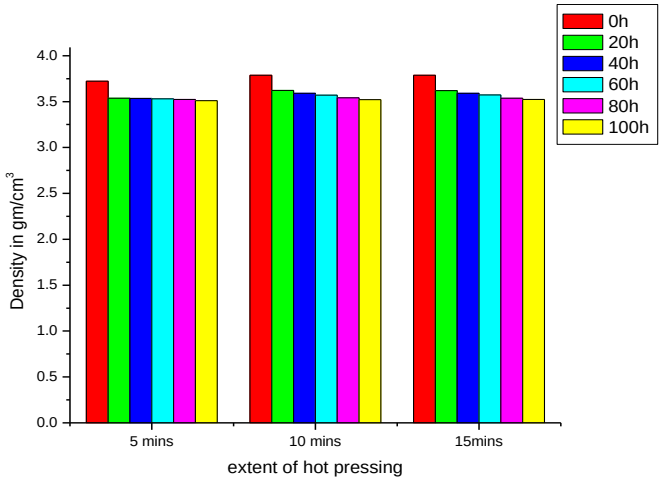

Fig 5.20 Comparison of density of elemental and pre alloyed powder samples hot pressed at785^{0}C for different extent of time

5.4.3 *Summary*

The results of this study show that titanium aluminide based intermetallic matrix composites with $AlNb_2$ phases as reinforcement can be produced by mechanical alloying of elemental Ti and Al powders for times longer than 80 h followed by hot pressing. Increasing mechanical alloying time to 100h lead to a decrease in the particle size of titanium aluminide powders down to about less than 160 nm and crystallite size in the range 12-18 nm after 100 h of milling.The prealloyed powders show lower hot pressing temperature (non reactive) and show comparative physical properties with fine grains.

CHAPTER 6

REACTION KINETICS STUDY OF Ti-Al INTERMETALLICS WITH VARIOUS PARTICLE SIZES

6.1 Introduction

Reaction kinetics and activation energy of any system provides an idea about the feasibility of the reactions,rate at which reaction will occur and stability of the phases formed.Ti-Al intermetallics though showed nano grained structure by processing through mechanical alloying,but the compaction and sintering density were not found desirable. The lesser densification with respect to other processes can be attributed to plastic deformation and incompressibility of the powders due to mechanical alloying.

Section 6.2 of Chapter 6 consists of the study of reaction kinetics of Ti-Al intermetallics processed by reaction synthesis with various particle sizes of Al. The effect of various Al particle size is seen on activation energy. The next section 6.3 comprises of the effect of particle sizes of Ti powders on the activation energy, where study of reaction kinetics has been carried out for Ti-Al intermetallics. To have the best composition with optimized particle size mixtures, equivalent particle sizes of Ti and Al powders were mixed and processed through reaction synthesis. The same has been characterized to determine activation energy and study reaction kinetics of the system in the final section 6.4 of this chapter.

6.2 Effect of Al Particle Size on The Reaction Kinetics and Densification of TiAl Intermetallics

The present investigation deals with response of the particle size of aluminium on the reactive sintering of Ti-Al intermetallics and subsequently on their reaction kinetics and densification behavior. Aluminium powders of initial average particle size of 44μm were milled for various durations in a planetary ball mill to produce average particles sizes of 100, 28 and 7μm. These aluminum powders of various particle sizes i.e. 100, 28, and 7μm were mixed with titanium powder of average particles size of 44μm in the ratio of 1:1 corresponding to the Ti-Al intermetallic composition. The reactive sintering temperatures of the mixtures were determined by DTA and the effect of change in

particle Al particle size has been determined for the activation energy of the self propagating reaction. The effect of Al particle size on the sintering was determined by studying density and microstructure.

6.2.1 *Experimental Procedure*

Titanium (99.9% purity) of average particle size of 44 µ and aluminum (99.9% purity) of average particle size 44 µ were obtained from Testbourne (UK). The aluminum powder received was milled in a planetary ball mill (RETSCH PM 400/2) for various duration of 1, 4 and 7h. Hardened steel balls were used as the milling media and charge to ball weight ratio kept as 1:5.Toluene was used as the process controlling agent for milling, where balls and charge were totally submerged in toluene. The Al powder milled for durations of 1, 4 and 7h exhibited an average particle size of 100, 28 and 7µ respectively. Milled aluminum powder of 100, 28 and 7µ particle size were mixed individually with titanium powder of 44 µ to prepare mixture of 50:50at%. Mixing was carried out in a mortar and pestle for 5mins followed by mixing in a planetary mill at 70 rpm for 30 min in a dry condition in argon atmosphere. Henceforth the mixed samples will be denoted as follows: Ti (~44µ)-Al (~44µ) as Ti-Al (0h), Ti (~44µ)-Al (~100µ) as Ti-Al (1h), Ti (~44µ)-Al (~28µ) as Ti-Al (4h) and Ti (~44µ)-Al (~7µ) as Ti-Al (7h). The cold compaction was carried out in a hydraulic press using a pressure about 175 MPa. The powders were sintered under ultra high pure argon environment for 1 hour at785^{0}C, 763^{0}C, 758^{0}C and 696^{0}C for Ti-Al(0h), TiAl(1h), Ti-Al(4h) and Ti-Al(7h) mixtures respectively. The sintering temperatures were determined by analyzing the DTA results of the respective mixtures. The sintered samples were 16.4mm in diameter and 5mm in thickness. The heating rate for sintering was kept 10^{0}C/min, and the samples after sintering were annealed in the furnace. After sintering, the samples were ground and polished. The milled and sintered samples were characterized by means of X-ray diffraction (XRD) using a D8 BRUKER AXS diffractometer with Cu Kα, operating at 40 kV and 30 mA. The thermal analyses of the Ti-Al mixtures of different Al particle size were carried out up to 1400^{0}C in a PERKIN ELMER Pyris Diamond TG/DTA. Using a QUANTA FEI-200 Field emission scanning electron microscopy (FESEM) was carried out to characterize the morphology of the surfaces of the sintered samples. The density of the sintered samples was determined using the immersion method in distilled water based on Archimedes principle.

The reaction rate of solid state transformation obeying John-Mehl-Avrami(JMA) kinetic model can be written in the following form

$d\alpha/dt = An (1-\alpha) [\ln 1/ (1-\alpha)^{(n-1/n)} \exp (-E/RT)]$……(6.1)

Where, α is the reacted fraction; t is time for transformation; T is the absolute temperature; R is the gas constant = 8.314 J/mol/K;

n is Avrami index parameter depending on the nucleation mechanism and number of growth dimension; E is the activation energy; A is the pre exponent factor. The above equation is differentiated and equated to zero

($d^2\alpha/dt^2=0$) for maximum reaction rate at T_m temperature to obtain final equation as follows;

$\ln \beta/T_m^2 = -E/RT_m+C_1$.....(6.2)

Where, β is the heating rate;

T_m is maximum reaction rate point;

C_1 is a constant.

For all the different heating rates Tm is calculated from the DTA plots with the assumption that the peak of respective DSC plot for a particular heating rate (β) is maximum reaction rate point. The plot for $\ln \beta /T_m^2$ versus $1/T_m$ is linear and slope of this curve gives the activation energy E. Integrating equation (1) and taking double natural logarithm and using Doyle's approximation (German 1985).

$\ln[\ln (1/1- \alpha)] = C_2-1.05 nE/RT$ ……(6.3)

Where C_2 is a constant

Thus, slope of the ln[ln(1/1 - α)] versus 1/T plot gives the value of nE. Ratio of slopes of this plot and E (slope of plot for $\ln \beta/T_m^2$ versus $1/T_m$) would thus give value of 'n' for the reaction under a particular heating rate.

6.2.2 *Results and Discussion*

6.2.2.1 XRD Analysis of Sintered compacts

The evolution of the transformations occurring during sintering was followed by XRD. Fig. 6.1 shows the diffraction pattern for Ti-Al (of various Al particle sizes) compacts sintered at their respective reactive sintering temperatures. The XRD pattern of Ti-Al mixture for Ti-Al (1h) Al sintered at 763^0C depicts that there is formation of TiAl and Ti_3Al phases with reference to the JCPD code No. 00-042-1137 and 00-014-0461 respectively. But in case of the Ti-Al mixtures Ti-Al(4h) and Ti-Al(7h) though both of the intermetallic phases are formed but due to the pre-milling of Al powders the peaks are slightly broadened (Cullity 1969 & Guo et al 1990). This infers the formation of refined TiAl and Ti_3Al intermetallic phases. The peak broadening and lowering in the intensity were observed with increase in extent of milling, due to the decrease in crystallite size of Al.As the milling of Al powders were carried out at lower rpm and for lesser extents so shifting of the peaks were not noticed though the lattice parameter is decreased upto a certain amount.

The enthalpy values for the formation of TiAl and Ti_3Al are −75 and −73 kJ/mol respectively (Hay et al 2000 & Froes et al 2001).The DTA graphs show the presence of exothermic peaks at 763^0C, 758^0C and 696^0C for Ti-Al (1h), Ti-Al (4h) and Ti-Al (7h)respectively.

6.2.2.2 Morphological Analyses

The morphology of Al powders milled for different durations i.e 1h, 4h and 7h is shown in Fig. 6.2 (a-c). Al powder during milling is flattened at early stages of milling due to plastic deformation and attains an approximate size of 100µ. On further milling the work hardened splats are fragmented to approximate size of 28µ and 7µ for 4h and 7h milling respectively.

6.2.2.3 DTA Study

DTA of Ti-Al mixtures of different Al particle size were carried out at three different heating rates, 10^0C/min, 20^0C/min and 50^0C/min to determine the effect of heating rate upon self propagating high temperature synthesis [Fig.6.3 & Fig6.4]. The endothermic peaks in the DTA traces refer to the melting point of Al particles. The DTA plot of

TiAl mixtures for particle size (~44µ), records the value of melting point of Al at 664^0C for 10^0C/min, but the endothermic peaks of the TiAl mixtures of Al particle size 1h milled (~100µ), 4h milled (~28µ) and 7h milled (~7 µ) are 672^0C,673^0C and 671^0C respectively for 10^0 C /min.

Table 6.1: Milling and mixing parameters

Planetary Ball mill Details **(Retsch PM 400/2)**	**Milling Parameters**
Milling Balls- Hardened steel balls	Milling Media-Toluene
Milling Jars- Hardened steel jars	Charge to Ball ratio-1:5
Jar capacity- 500 ml	Milling speed- 200 rpm Vial Speed- 400 rpm
PCA-Toluene	Total time of milling-1h,4h&7h
	Weight of initial charge-30gms
Mixing parameters	
Milling Balls- Hardened steel balls	Charge to Ball ratio-1:3
Milling Jars- Hardened steel jars	Milling speed- 70 rpm Vial Speed- 140 rpm
Jar capacity- 500 ml	Total time of mixing-30mins
Argon atmosphere	Weight of initial charge-30gms

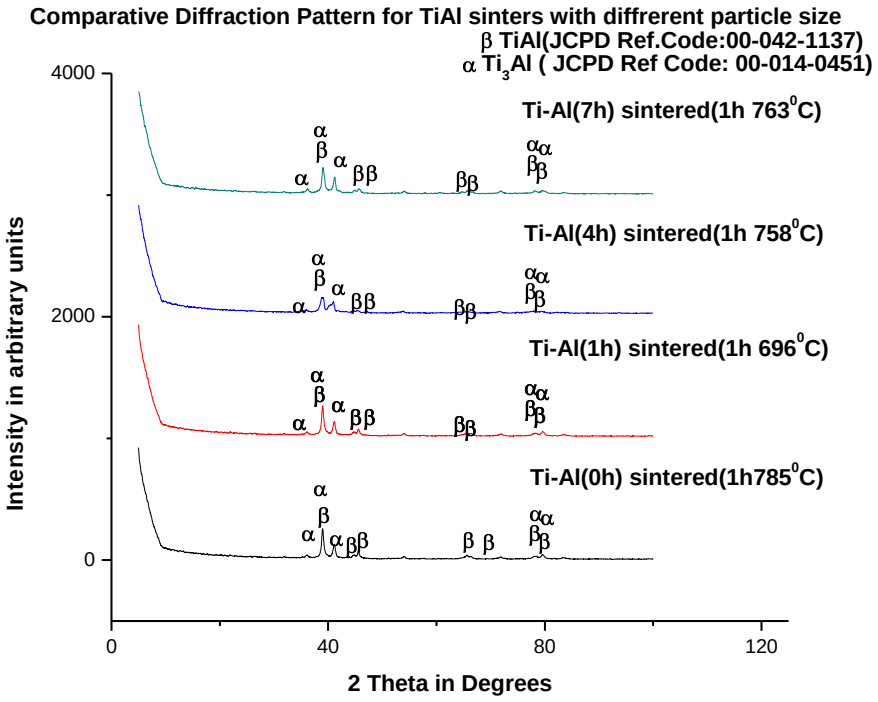

Fig 6.1 XRD pattern of Ti-Al (0h), Ti-Al (1h), Ti-Al (4h) and Ti-Al (7h) mixtures sintered at their respective temperatures

The melting point of Al of the above mixtures is lower in comparison to ~44µ mixtures for 30^0C/min heating rate, but for the rate of 50^0 C /min, the melting temperature is increased. The above heterogeneous characteristics is due to the milling of Al and the heating rate, in one way it is lowering the melting point of Al for 30^0 C /min and on the other way the 50^0 C /min helps in overshooting of the temperature. The above optimization infers that 30^0 C /min rate gives the lowest temperature of the liquidus Al for various Ti-Al mixtures.

The DTA trace of the Ti-Al (0h) mixture shows an exothermic peak at 785^0C, and for Al powder sizes with 1h milled (~100µ), 4h milled (~28µ) and 7h milled (~7 µ) in Ti+Al mixtures the same is shifted to 763^0C, 758^0C and 696^0C respectively. The exothermic temperatures are due to the phase transformation forming titanium aluminides, which can be confirmed by the XRD patterns of the sintered TiAl mixtures (Fig 6.1) resulting in the formation of TiAl and Ti_3Al.

6.2.2.4 Effect of Particle Size

The lowering of exothermic temperatures is attributed to the milling/particle size of Al. Milling induces plastic deformation and external energy to the Al powders which in

turn helps in decreasing the Ti-Al sintering temperatures. The reduction of Al particle size also helps in increasing the surface area of reaction which is in accordance with the lowering of exothermic peaks. The exothermic temperatures in the above said behavior for only heating rate of 10 ^{0}C /min(Fig 6.5), but in case of the rates like 30 ^{0}C /min and 50 ^{0}C /minthe exothermic points deviate for the Ti-Al (0h) and Ti-Al (1h) mixtures, the later show higher exothermic temperatures due to the formation of bigger 100µ Al particles which in turn helps in overshooting of temperature for higher heating rates. DTG values such as -39.2 mJ/mg for Ti-Al (0h) (10^0C/min) mixtures depicts the rate at which the heat loss has occurred at 786^0C. Similarly from the observation for different particle sizes with a particular heating rate infers that with decrease in particle size the rate of heat loss increases. The heat loss occurs due to the incipient diffusion of the two nascent surfaces. The lowering in the particle sizes, increases the nascent surface area of the reaction, as a result of which the speed and hence the rate of diffusion is increased. The DTG results are as follows:

(a) For heating rate 10^0C/min, Ti-Al (0h) < Ti-Al (1h) < Ti-Al (4h) < Ti-Al (7h).
(b) For heating rate 30^0C/min, Ti-Al (0h) < Ti-Al (1h) < Ti-Al (4h).
(c) For heating rate 50^0C/min, Ti-Al (0h) < Ti-Al (1h) < Ti-Al (4h).

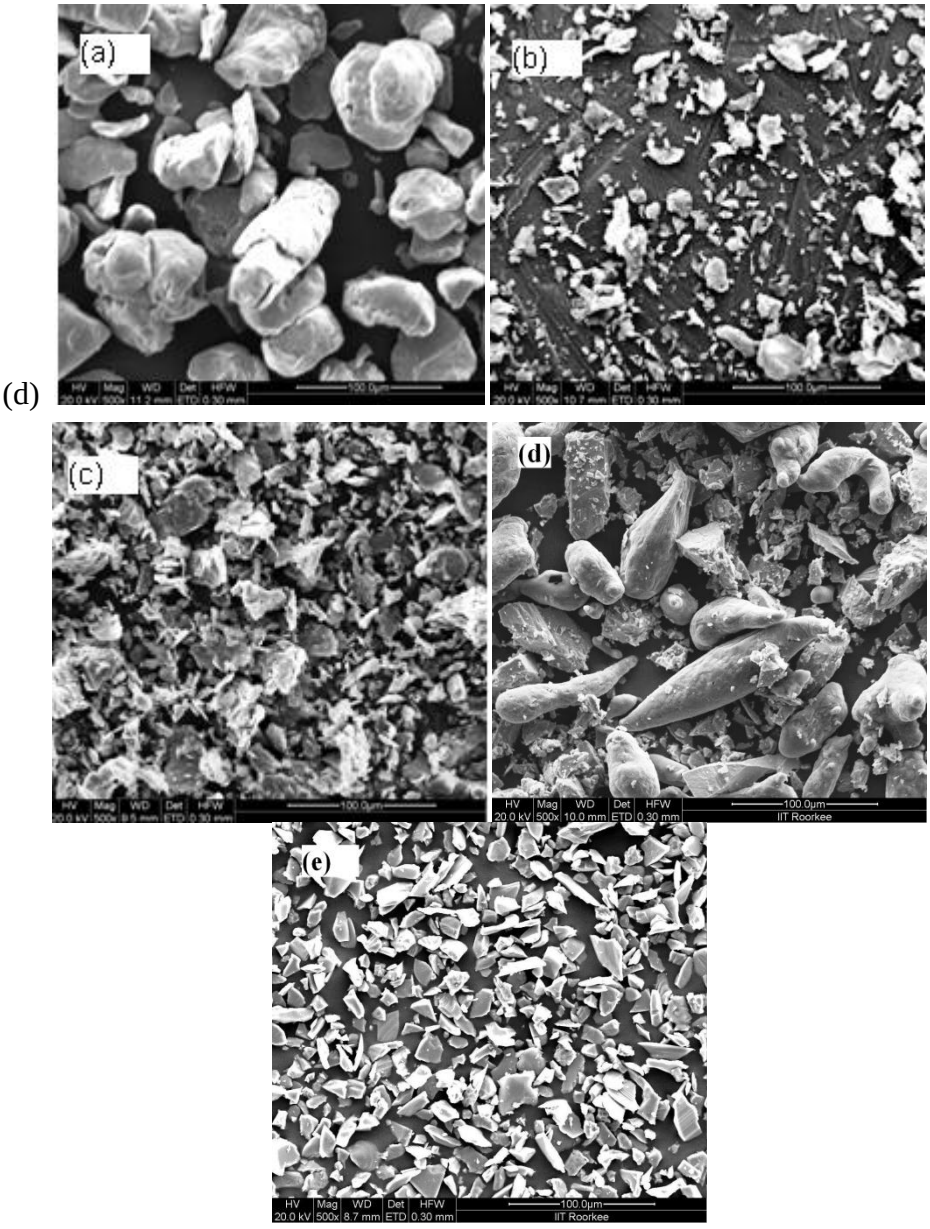

Fig 6.2 FESEM micrographs of milled Al powders for different extent of milling (a) 1h, (b) 4h, (c) 7h,(d) "as received" Al powder and (e) "as received" Ti powder

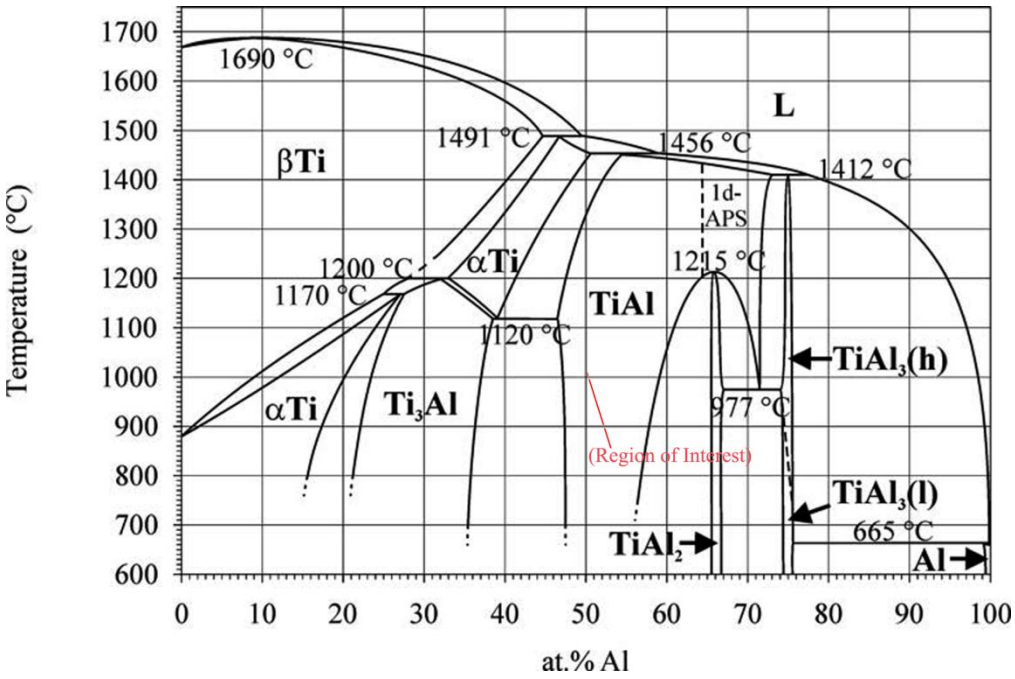

Fig 6.3 Phase diagram of Ti-Al binary system

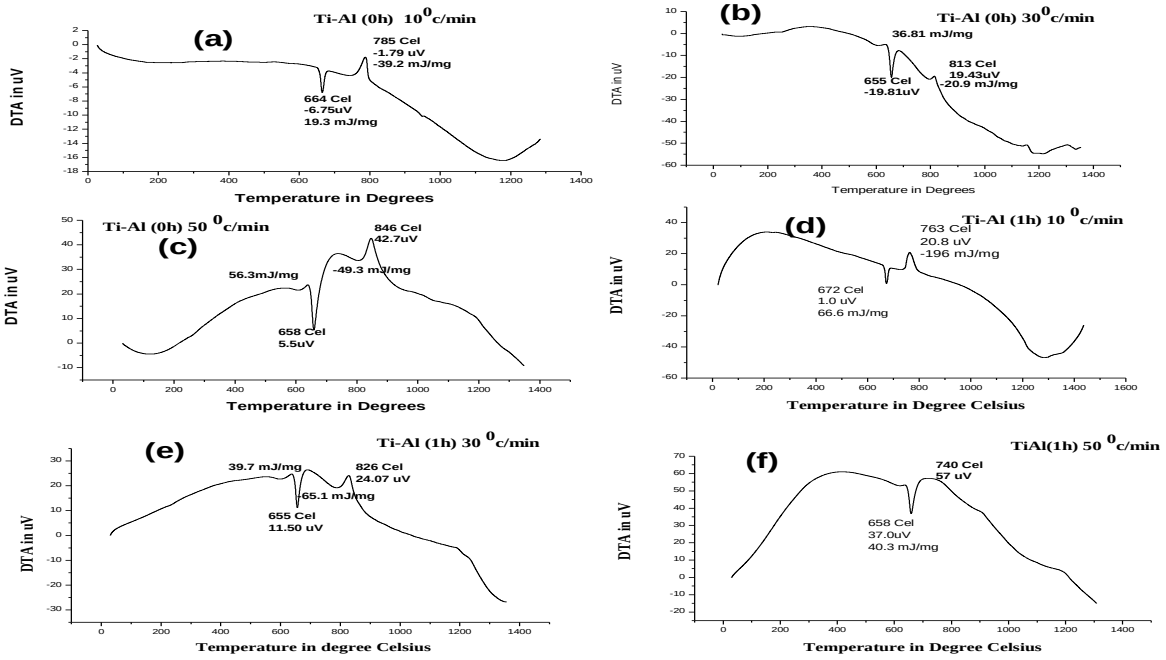

Fig 6.4 Thermal analysis plots of Ti-Al (0h) mixtureswith different heating rates (a) 10^0C /min (b) 30^0C /min (c) 50^0C /min and Ti-Al (1h) mixture at (d) 10^0C /min (e) 30^0C /min and (f) 50^0C /min

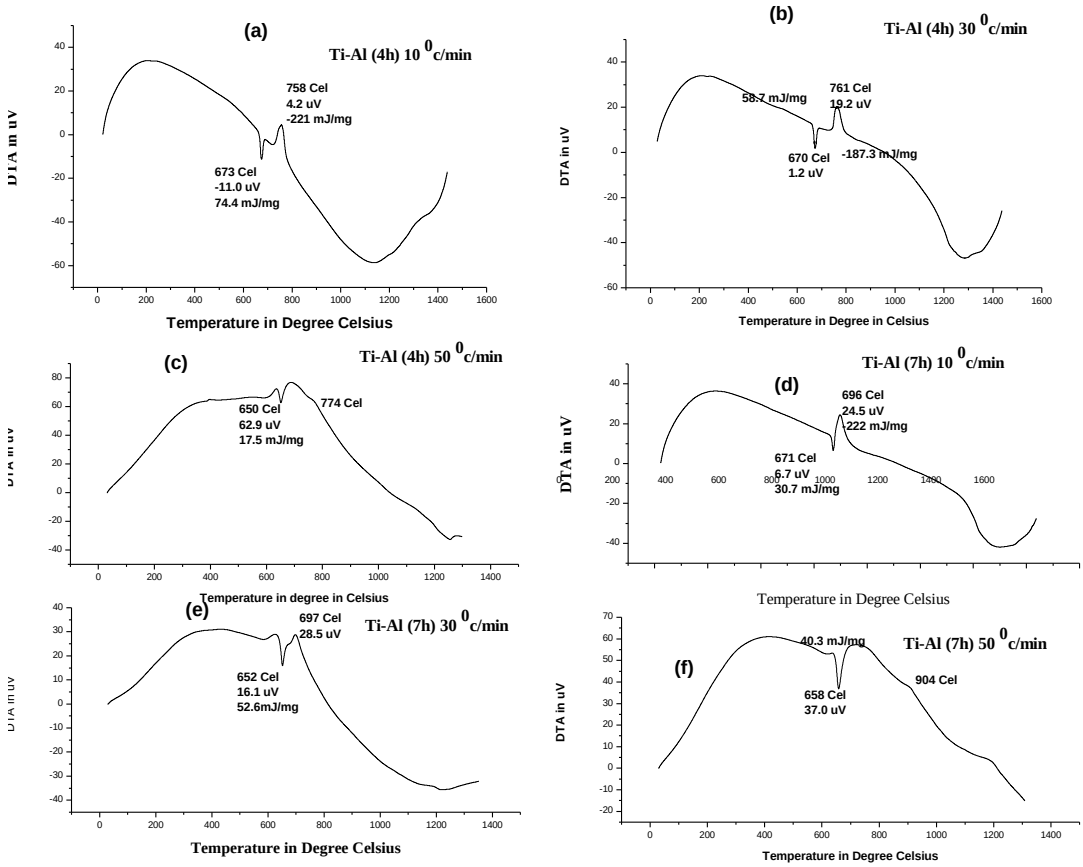

Fig. 6.5 Thermal analysis plots of Ti-Al (4h) mixtureswith different heating rates (a) 10^0C /min (b) 30^0C /min (c) 50 degrees/min and Ti-Al (7h) mixture at (d) 10 ^{0}C /min (e) 30 ^{0}C /min (f) 50 ^{0}C /min

6.2.2.5 Effect of Heating Rate

Heating rates affect the exothermic points linearly, i.e with increase in the rates, the temperatures are increased. The elevation in the exothermic points corresponds to overshooting of temperature, which is found higher for higher particle size and the gap becomes negligible for the lowest particle size mixture. This fact supports the discrepancy in the effect of particle size for the Ti-Al (0h) and Ti-Al (1h) mixtures at the higher heating rates. The lowest particle size mixture confirms the ease of formation of liquidus Al, which facilitates the sintering, formation of titanium aluminides and the trend of dropping temperature gap, is the evidence of facilitated formation of aluminides.

6.2.2.6 Determination of Activation Energy, E

As per equation 6.2, according to the non isothermal kinetics the slope of plot of $\ln\beta/T_m^2$ vs $1000/T_m$ will provide the value for the empirical activation energy. In Fig 6.6 slope of the plots give the E value is -16,788 kJ/mol,-0.149kJ/mol,-0.01681 kJ/mol and -0.00886kJ/mol. The E value suggests the amount of energy taken out from the system for the formation of the phases as these phases form due to the exothermic reaction. The magnitude of the activation energy is lowered as the milled Al particles are introduced in the TiAl mixtures and decreases with increase in the extent of milling of Al. This clarifies that for Ti-Al (7h) mixture needs very less energy to be taken out of the system for the formation of aluminide phases, where the amount of energy is highest for the Ti-Al (0h) mixture.

6.2.2.7 Physical Properties

The density and amount of porosities obtained during reactive sintering is shown in Fig 6.7 The density of the reactive sintered powder is around 2.9~3.1 g/cm^3 which is near about 50% higher than that of the green density. The particle size of Al powders is one of the parameter for controlling the densification. The analyses of the densification depicts that % porosities behaves inversely towards the % interface of Al-Ti.

Finer particles lower the diffusion distances and also increases the concentrations of grain boundaries which act as preferential nucleation site for the diffusion path and also increase the rate of transport for alloy in the presence of chemical potential gradients. The finer particles of Al though create the preferential nucleating site for the diffusion path, but don't show commendable difference between the sintered densities of Ti-Al (4h) and Ti-Al (7h) mixtures. Ti-Al (4h) mixture gives considerably low exothermic temperature, low activation energy and better control over particle size and highest density amongst all the tested mixtures.

6.2.2.8 Microstructural Evolution

FESEM micrographs (Fig 6.8 (a-d)) show that the microstructures contain bright Ti rich regions and dark Al rich regions. The interface as represented in Fig 6.10 depicts the diffusion of Al into Ti rich regions during the reactions in reaction sintering. The sintering process leads to various phases in the structure with different grey contrast.

Darker the shade higher is the Al content in the phases. Most probably the microstructure can be described as the Ti (bright region) islands are inside the Ti_3Al grain locale. XRD patterns depict the formation of the TiAl and Ti_3Al, which can be clearly seen in the microstructures with Ti rich region forming TiAl and Al rich region are in the perimeter of the Ti rich region forming Ti_3Al. The interface though small in content can be attributed towards the formation of intermediate phases.

Table 6.2: Details of Ti-Al mixtures with different heating rates

Specification	**Heatingrates ^{0}C/Min**	**Melting temperaturesin ^{0}C**	**Reaction sintering temperatures in ^{0}C**
Ti-0hAl	10	664	785
	30	655	813
	50	658	846
Ti-1hAl	10	672	763
	30	666	826
	50	658	740
Ti-4hAl	10	673	758
	30	670	761
	50	650	774
Ti-7hAl	10	671	696
	30	662	697
	50	668	-

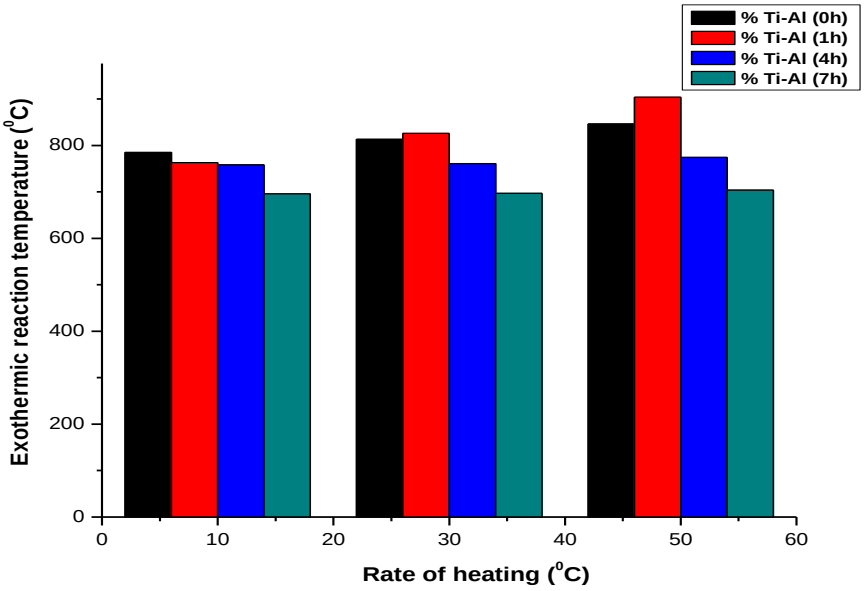

Fig 6.6 Comparison of exothermic reaction temperatures with rate of heating of Ti-Al particulate mixtures having various Al particle sizes

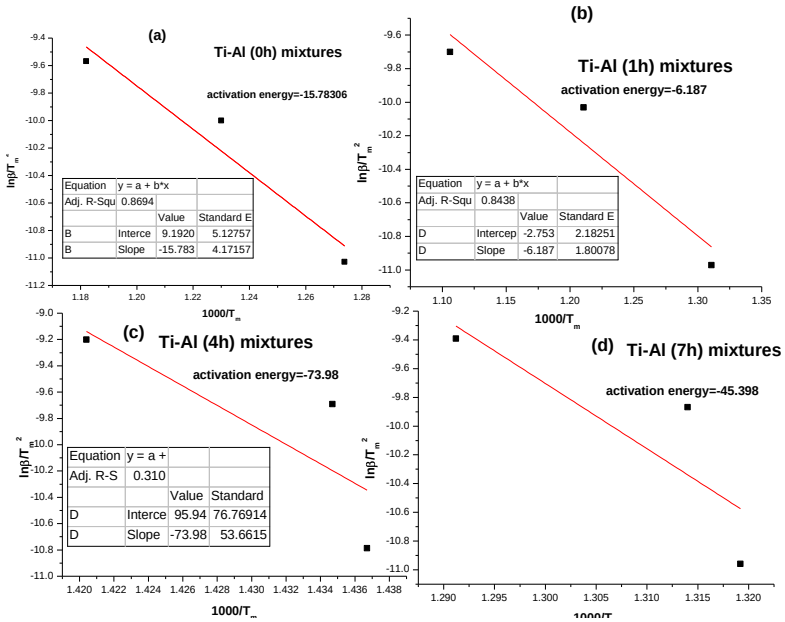

Fig 6.7 Variation of $\ln\beta/T_m^2$ vs $1000/T_m$ for Ti-Al particulate mixtures having various Al particle sizes, (a) Ti-Al (0h) (b) Ti-Al (1h) (c) Ti-Al (4h) and (d) Ti-Al (7h) mixtures

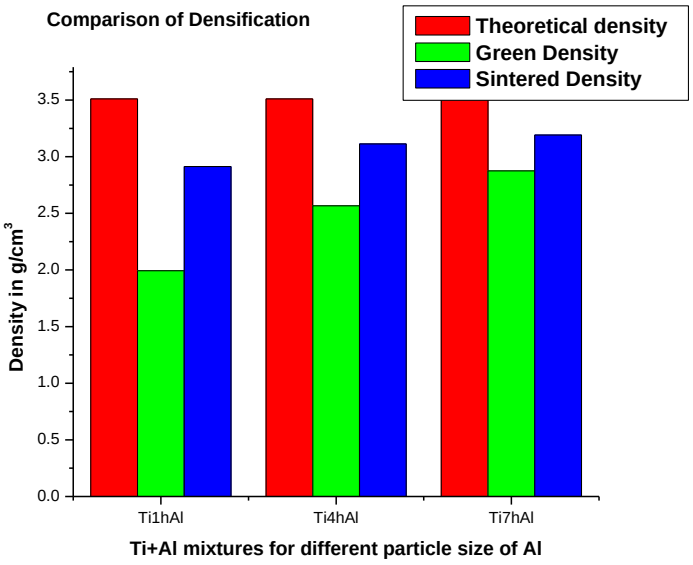

Fig 6.8 Comparison of densification of sintered samples with green density

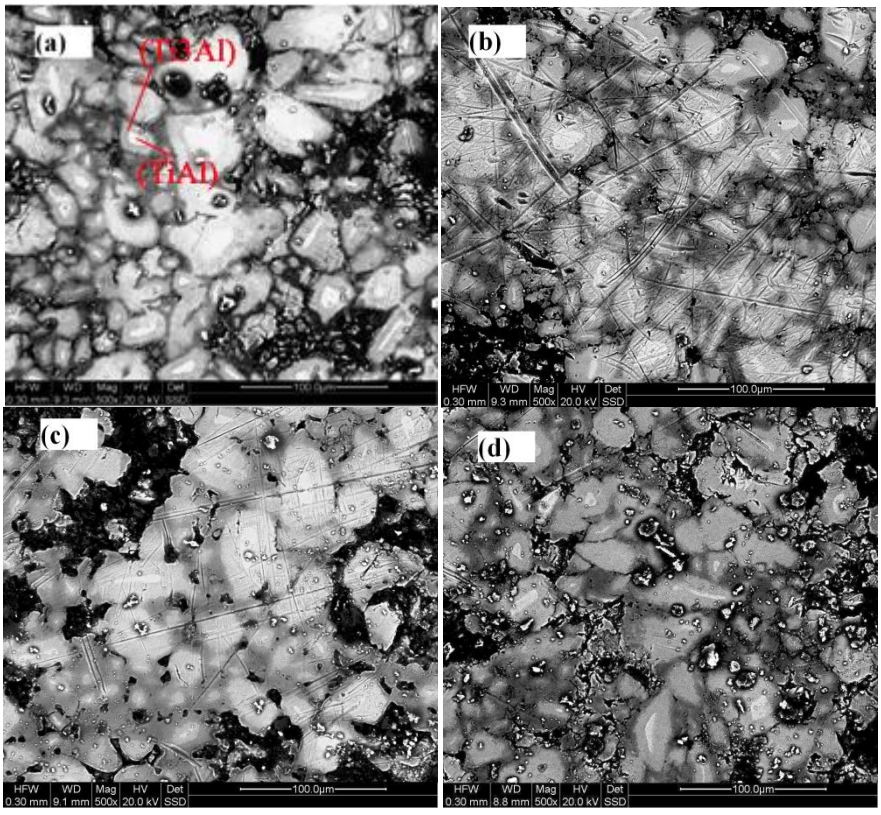

Fig 6.9 FESEM micrographs of sintered Ti and Al mixtures with different extent of milling of Al (a) Ti-Al (1h), (b) Ti-Al (4h) (c) Ti-Al (7h) and (d) Ti-Al (0h)

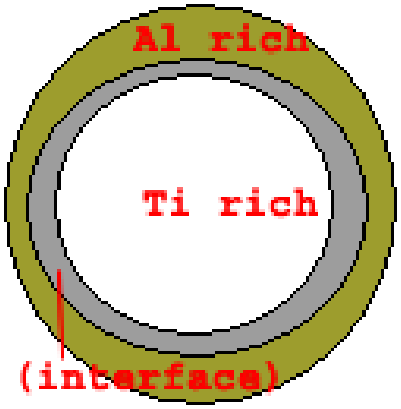

Fig 6.10 Schematic diagram representing Ti rich and Al rich regions and the interface

6.2.3 *Summary*

Here we have compared the exothermic temperatures, heating rates, activation energy and density with various Al particle size containing TiAl mixtures. After the study of above results, Ti-Al (4h) mixtures show the optimized result for 30^0C/min heating rate. The above TiAl mixture records activation energy of -73.98 kJ/mol and highest density of 3.129g/cm^3. The exothermic temperatures recorded for 30^0C/min is 761^0C. The Exothermic temperature range for Ti-Al (4h) for different heating rates is considerably low in comparison to that of the Ti-Al (0h) and Ti-Al (1h) and also not that much higher than that of the Ti-Al (7h) mixtures.

6.3 Effect of Ti Particle Size on the Reaction Kinetics and Densification of TiAl Intermetallics

Most useful gamma titanium aluminides are centered around Ti-50at% Al composition. These aluminide can be tailored to have a variety of microstructures by way of heat treatment resulting in the desired properties. Specifically the reaction kinetics of formation of intermetallics compound affect the microstructures and density as well.

Just above the temperature of lowest eutectic in the Ti-Al phase diagram, the exothermic process takes place and works as a self propagating reaction, with the formation of liquid melt and increase in the densification by travelling of liquid melt by capillary force action (Mishra et al 2013(a); Mishra et al 2013(b); German 1985 & German et al 1986). Parameters like temperatures at which self propagating reaction occurs plays a pivotal role in the reaction sintering process (Wang et al 2008). Green density, particle size, rate of chemical kinetics and rate of heating are some of the main parameters that control the extent of densification. As per Bose et al. the heterogeneity in densification is found in the synthesis of Ni_3Al through reaction sintering due to various particle sizes of Al (Bose et al 1988). Control on particle sizes, sintering temperature, heating rate and composition can result in products with density as high as 95% of the theoretical density. The short lived liquid melt plays the controlling hub in sintering and densification of the samples by flowing in the capillary pores (Cullity 1969).

The present investigation deals with response of the particle size of titanium on the reactive sintering of Ti-Al intermetallics and subsequently on their reaction kinetics and densification behavior. Titanium powders of initial average particle size of 44μm were milled for various durations in a planetary ball mill to produce average particles sizes of 100, 28 and 7μm. These titanium powders of various particle sizes i.e. 100, 28, and 7μm were mixed with titanium powder of average particles size range of40-44μm in the ratio of 1:1 corresponding to the Ti-Al intermetallic composition. The reactive sintering temperatures of the mixtures were determined by DTA and the effect of change in particle Al particle size has been determined for the activation energy of the self propagating reaction. The mixtures of Ti and Al blends of various Ti particle size has been compacted and subsequently sintered at reaction sintering temperatures for 1h in

argon atmosphere. The porosity levels as well as the microstructure studies were carried out to determine the influence of the particle size of aluminium on the reactive sintering of Ti-Al. The compacts were further characterized by X-ray diffraction to determine the extent of phase formation. The influence on hardness was also determined with respect to densification and Titanium particle size.

6.3.1 *Experimental Procedure*

The Titanium and Aluminium powders taken for milling and the milling condition described can be referred from section 6.2.1.

The milling parameters and the details of milling condition are shown in Table 6.1.The Ti powders milled for time extents of 1, 5 and 10h resulted a mean particle size approximately of 100, 25-28 and 7-9µ respectively. The Titanium powder of various particle sizes were blended with aluminum powder of average particle size of 44 µ to prepare blends of 50:50at%. The blending of powders was carried out in mortar and pestle for 5 mins followed by blending in ball mill for 30 mins at 70 rpm in dry condition. The powder blends of Ti (1h)-Al, Ti (5h)-Al and Ti (10h)-Al were sintered in high pure inert environment (argon) for 1 hour duration at 677^0C, 725^0C and 747^0C respectively where the temperatures for sintering were decided by studying the thermal analytical results of the blends. The powder mixtures were compacted at 175 MPa to a cylindrical shape of the dimensions of 16.4 mm diameter and 5mm thickness. The sintered samples were polished and ground with different grits emery papers followed by polishing cloths. The characterization of XRD, FESEM, Archimedes principle and reaction kinetics phenomenon subjected to the samples can be referred from section 6.2.1.

6.3.2 *Results and Discussion*

6.3.2.1 XRD Analysis of Sintered compacts

The phase evolutions occurred during sintering was explored by XRD and shown in Fig.6.10. It shows the diffraction patterns of sintered compacts of Ti-Al mixtures of various Ti particle sizes. The diffraction pattern of Ti-Al mixture of Ti (1h)-Al sintered at 677^0C reveals the synthesis of TiAl and Ti_3Al phases, which referred from the JCPD code numbers 00-042-1137 and 00-014-0461 respectively for phase analysis. In

comparison with the mixtures Ti(0h)-Al and Ti(1h)-Al ; Ti(5h)-Al, Ti(10h)-Al show slightly broadened peaks, though in all the cases both the intermetallics phases are formed. The formation of comparatively broadened peaks of intermetallic phases in the diffraction pattern is attributed towards the amorphization of Ti powders at higher extent of milling. The decrease in intensity of those peaks also can be explained on the basis of the formation of finer Ti particles at higher extent of milling which in turn infers the synthesis of the refined Ti_3Al and TiAl intermetallic phases.As the milling of Ti powders were subjected at lower rpm and only upto 10 hours, the shifting of peaks were unnoticeable, though the lattice parameter has been lowered by certain percentage.

Table 6.3: Milling and mixing parameters

Planetary Ball mill Details (Retsch PM 400/2)	**Milling Parameters**
Milling Balls- Hardened steel balls	Milling Media-Toluene
Milling Jars- Hardened steel jars	Charge to Ball ratio-1:5
Jar capacity- 500 ml	Milling speed- 200 rpm Vial Speed- 400 rpm
PCA-Toluene	Total time of milling- 1h,5h&10h
	Weight of initial charge- 30gms
Mixing parameters	
Milling Balls- Hardened steel balls	Charge to Ball ratio-1:3
Milling Jars- Hardened steel jars	Milling speed- 70 rpm Vial Speed- 140 rpm
Jar capacity- 500 ml	Total time of mixing-30mins
Argon atmosphere	Weight of initial charge- 30gms

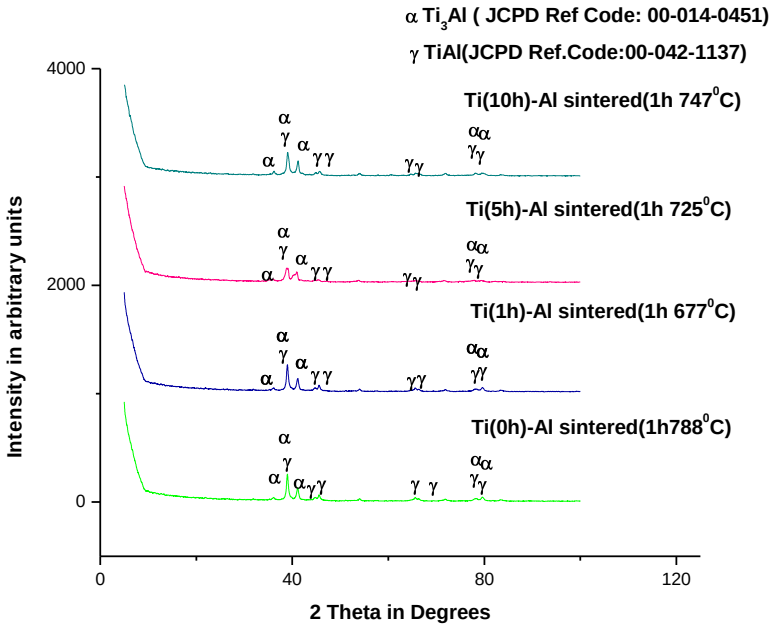

Fig 6.11 XRD pattern of Ti (0h)-Al, Ti (1h)-Al, Ti (5h)-Al and Ti(10h)-Al mixtures sintered at their respective temperatures

The enthalpy values for the formation of TiAl and Ti_3Al are −75 and −73 kJ/mol respectively and the DTA graphs show the presence of exothermic peaks at 677^0C, 725^0C and 747^0C for Ti (1h)-Al, Ti (5h)-Al and Ti (10h)-Al respectively.

6.3.2.2 Microstructure of milled powders

The Morphological evolution of the Ti powders milled for various durations are displayed in Figs 6.11 (a-c). The Ti powders are milled for 1h, 5h and 10h. The milled powders showed the fractured surfaces due to plastic deformation by ball-particle-ball collisions, ball-jar (wall)-ball collisions. The milling process involves the phenomenon of agglomeration and fracture.The milling of particles first show the process of cold welding, which can be attributed towards the formation of nascent surfaces of the particles. The free energy of the nascent surfaces is high that it immediately forms the cold welding which in turn induces the agglomeration of the powders. When the powders were subjected to increased extent of milling, the work hardening of the particles overrules the free energy of the nascent surfaces and agglomerated clumps, which starts to increase the fracturing of the surfaces in comparison to the simultaneous process of agglomeration. Thus the higher extent of milling helps in lowering the particle size. The lowering of particle size can be described as the comparative process

between two phenomena of agglomeration and fractures. After some time of milling both the phenomena sets up an equilibrium, which inhibits further lowering of particle sizes. The morphology of Ti powders milled for 1h reveals the fact that the powders are agglomerated and flattened due to plastic deformation this and can be attributed towards the ductility of the powder particles. The morphological study depicts the approximate particle size attained by 1h milled Ti powders are 100 µ. The work hardened splats of Ti powders when further milled upto 5h, the particle sizes get reduced to an approximately of 28µ. As shown in Fig.6.11(c) Ti particles milled for 10h, produces particles of the order of ~7µ. The uneven particle morphology of the milled powders is due to the fractured surfaces created during the collisions.

6.3.2.3 DTA Study of Powder blends

The study of the thermal analysis of Ti-Al mixtures has been carried out at low heating rates for efficient calculation of the activation energy (Vyazovkin et al 2011). Ti-Al mixtures of different Ti particle sizes were characterized by thermal analysis with three different heating rates of 3^0K/min, 6^0K/min and 9^0K/min. Different heating rates has been used to determine the activation of energy of the exothermic reaction and the effect of heating rates on it Figs [6.12, 6.13, 6.14& 6.15]. The melting point of Al particles is shown as endothermic peaks in the thermal analyses plots. The DTA behavior of Ti (0h)-Al provides the result that the melting point of Al is almost same for 3^0K/min, 6^0K/min and 9^0K/min. The Ti powders have no influence on the melting of the Al powder, so the melting point is found to be almost same for all the heating rates.

The DTA plots of Ti-Al mixtures show exothermic peaks at 788^0C, 677^0C, 725^0C and 747^0C for Ti (0h)-Al, Ti (1h)-Al, Ti (5h)-Al and Ti (10h)-Al respectively for 9^0C/min heating rate. The exothermic temperatures are due to the phase transformation to titanium aluminides, which are confirmed by the XRD patterns of the sintered TiAl mixtures (Fig 6.10) resulting in the formation of TiAl and Ti_3Al.

6.3.2.4 Effect of Particle Size

The particle size of the mixtures affects the sintering temperatures. The effect of different particle sizes of Ti directly affects the void space or the diameter of the capillaries through which the liquid aluminum flows. The sintering of Ti-Al mixtures is

facilitated by lower diameter of capillaries. The lower the diameter of capillaries, higher will be the reaction of Al melt with Ti particles and better would be the sintering. Milling of Ti particles increased the surface area of the reaction interface by decreasing the particle size and increasesGibbs free energy of the system by providing energy to the system during milling. So the reaction sintering temperatures (exothermic temperature) are lowered for Ti (1h)-Al, Ti (5h)-Al and Ti (10h)-Al mixtures. Specifically the lowering of sintering temperature for Ti (1h)-Al, refers to the inclusion of external energy provided through milling of Ti particles. Reducing of particle size facilitates the finer voids which used as finer capillaries for the flow of Al melt and in turn provides better densification. The study of DTG values provides the clear idea of sinterability of the mixtures of different Ti particle sizes. The DTG values reveal the rate at which the heat loss occurred. This also have influence on the reaction rate at a particular heating rate. For highest heating rate, lower the particle size elevated will be the rate at which the heat is lost. Reduction of DTG values for higher particle size mixtures can be explained as the rate of capillary flow of Al melt controls the rate of heat loss of the reaction. But the heterogeneity in this trend is noticed in the 3^0C/min and 6^0/min heating rates.

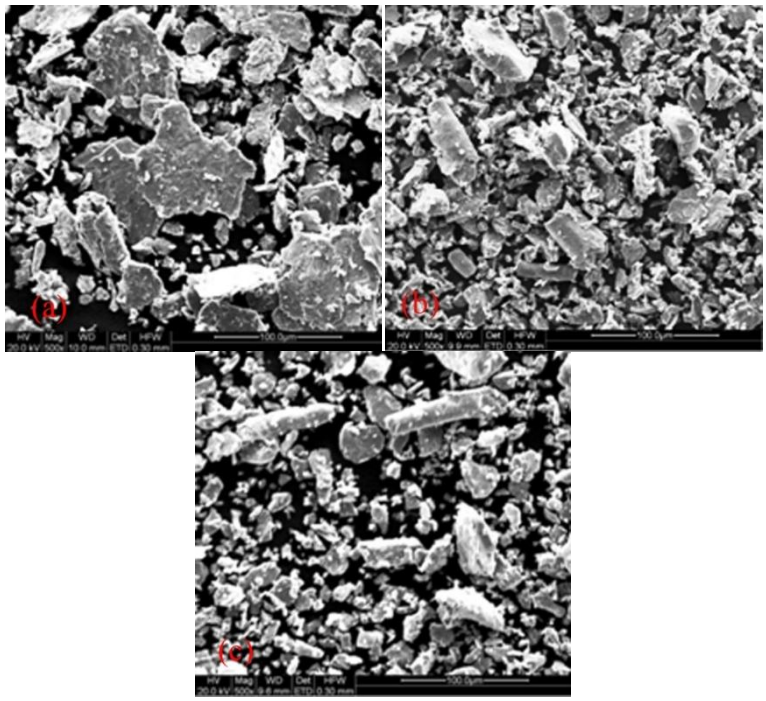

Fig.6.12 FESEM micrographs of milled Ti powders for different extent of milling (a) 1h milled (b) 5h milled & (c) 10h milled

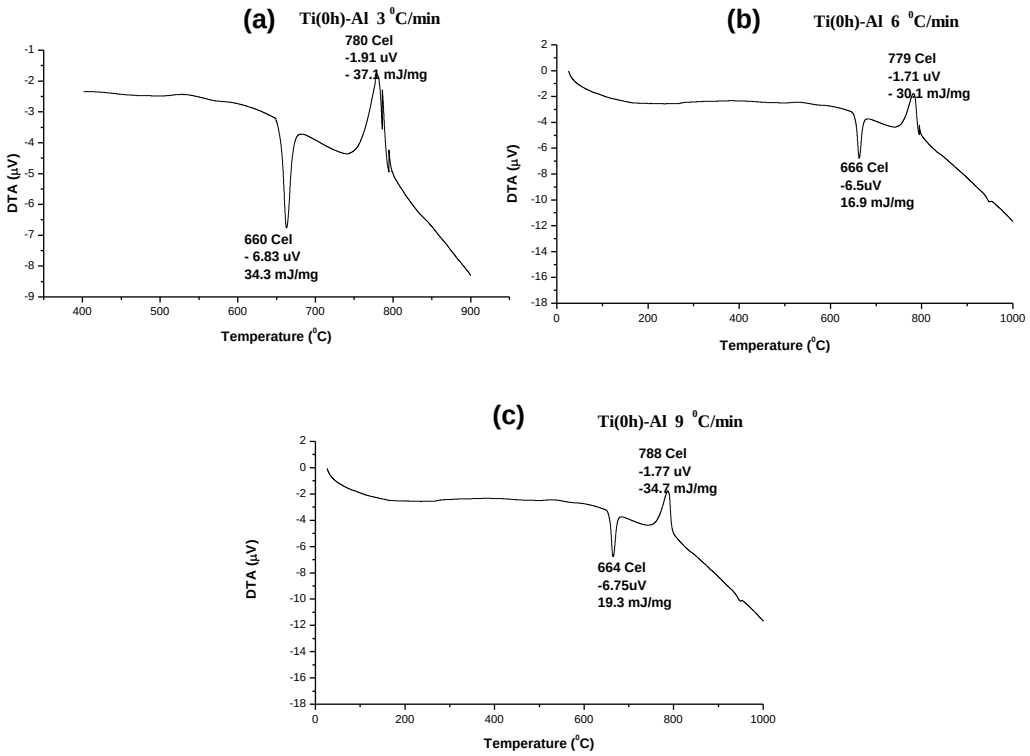

Fig.6.13 Thermal analysis plots of Ti (0h)-Al mixture with different heating rates, (a) 3^0C/min (b) 6^0C/min (c) 9^0C/min

The discrepancies in the DTG values show that Ti (1h)-Al > Ti (5h)-Al for 3^0C/min and Ti (5h)-Al >Ti (10h)-Al for 6^0/min heating rates. If noticed the DTG values are almost same having a little difference and that can also be attributed towards the exothermic temperatures very near to the melting point of Al, which give an resultant amount of DTG values, because melting involves the heat gain and exothermic temperatures involves heat loss.

(a) For heating rate 3^0C/min, Ti (0h)-Al <Ti (1h)-Al >Ti (5h)-Al <Ti (10h)-Al.
(b) For heating rate 6^0C/min, Ti (0h) -Al <Ti (1h) -Al <Ti (5h) -Al >Ti (10h)-Al.
(c) For heating rate 9^0C/min, Ti(0h)-Al < Ti(1h)-Al < Ti(5h)-Al <Ti(10h)-Al

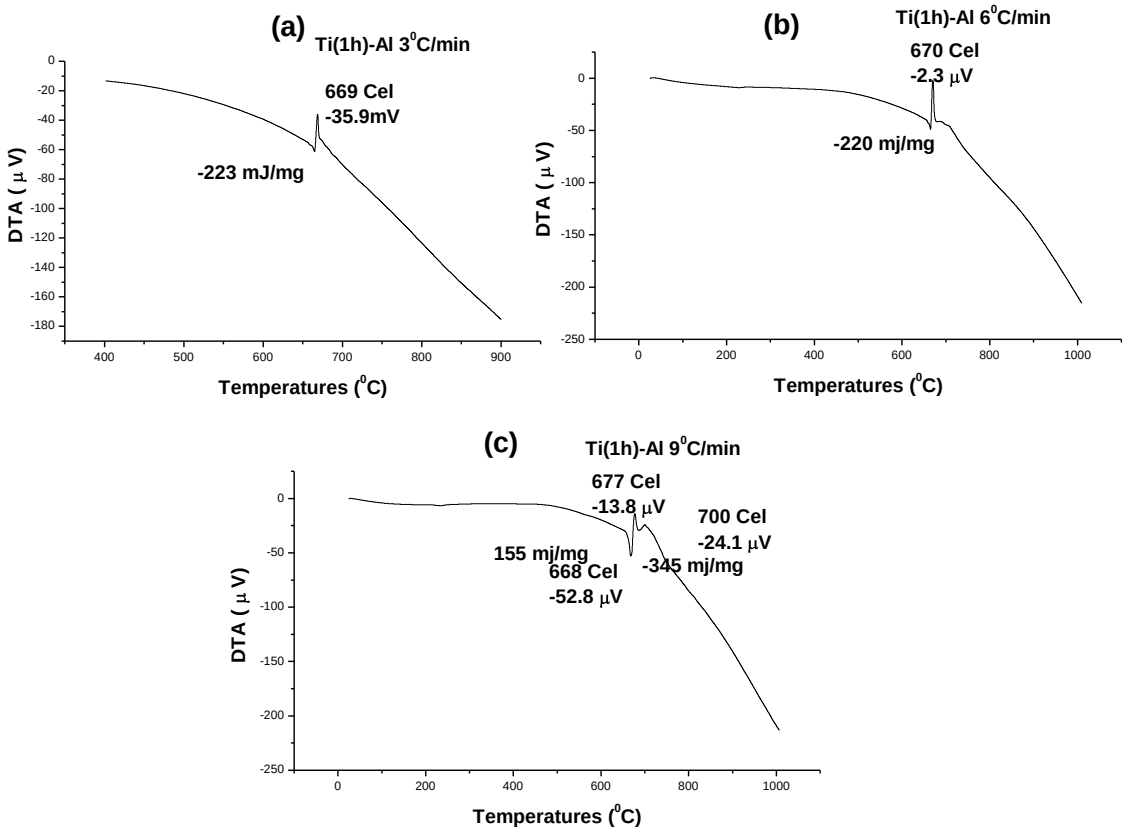

Fig 6.14 Thermal analysis plots of Ti (1h)-Al mixture with different heating rates, (a) 3^0C/min (b) 6^0C/min (c) 9^0C/min

6.3.2.5 Effect of Heating Rates

The effect of heating rates is almost nullified or can be said as the exothermic points are hardly affected for the Ti(0h)-Al powder mixtures(Fig 6.16).For the Powder mixtures Ti(1h)-Al the exothermic temperatures are almost same for 3^0C/min and 6^0C/min. But for 9^0/min heating rate an elevation in the exothermic points are seen, which can be attributed towards the overshooting of temperatures during higher rate of heating (Table-6.4). For Ti (1h)-Al mixtures also the trend of overshooting of temperatures for higher rate of heating is observed. But the discrepancy comes in case of the lower particle size mixtures like Ti (5h)-Al and Ti (10h)-Al. In both the mixtures the elevation in exothermic temperatures are seen for 3^0C/min with respect to 6^0/min heating rate. The behavioral discrepancies can be explained on the basis of heat evolved during the reaction. When observed in Figs (6.15 &6.16), the exothermic peaks at 3^0C/min, evolves the highest amount of heat such as 40.7μV, and 35.5 μV for Ti(5h)-Al and Ti(10h)-Al mixtures respectively. The higher heat evolved is responsible for increasing the exothermic temperature of the Ti-Al systems of the above mixtures. The

phenomenon is supported by capillary action of the Al melt in the pores created by Ti particles. The pores are actually the void space created by Ti particles. For Ti (5h)-Al, Ti (10h)-Al mixtures the void space created is lower as compared to the other two Ti-Al mixtures taken .Because the particle sizes are smaller as a result of which the void space/size of the space created is lower in compared to Ti(0h)-Al and Ti(1h)-Al which helps in increasing the capillary action. The capillary action is increased due to the decrease in size of the voids which otherwise can be described as the diameter of the capillaries. When Ti (5h)-Al and Ti (10h)-Al heated at 9^0C/min, the exothermic temperatures have increased upto 725^0C and 747^0C. The lower Ti particle size mixture confirms the formation of lower diameter capillaries which would have increased the evolved heat content but the trend is not maintained which can be explained as the over shooting of temperatures at higher heating rate. At highest heating rates lower the particle size higher the exothermic temperature and the temperature gaps between6^0C/min and 9^0C/min also increased.

Table 6.4: Details of Ti-Al mixtures with different heating rates

Sample Name	**Heatingrates Degrees/Min**	**MeltingTemperaturesin Celsius**	**Reaction Sintering Temperatures in Celsius**
Ti(0h)-Al	3	660	780
	6	666	779
	9	664	788
Ti(1h)-Al	3	664	669
	6	663	670
	9	668	677
Ti(5h)-Al	3	666	683
	6	664	671.
	9	668	725
Ti(10h)-Al	3	666	697
	6	668	695
	9	668	747

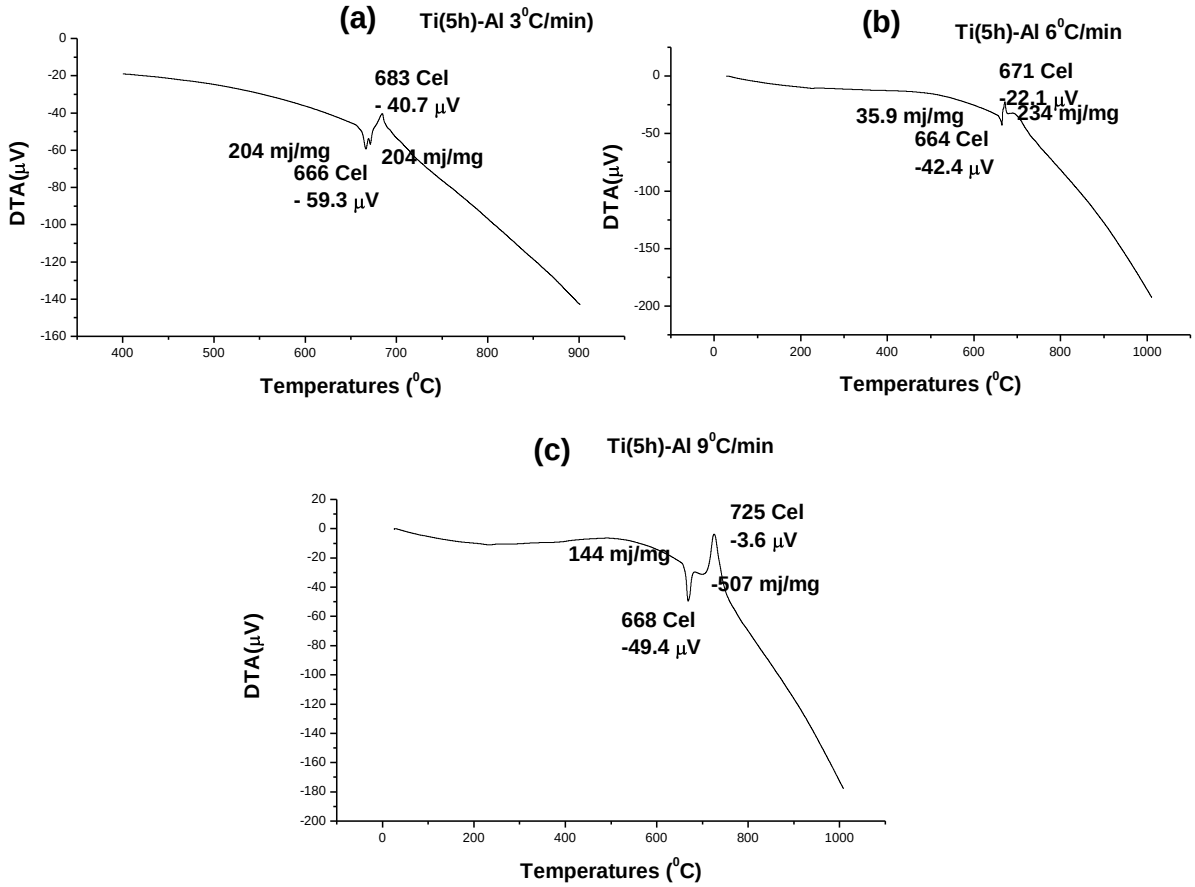

Fig 6.15 Thermal analysis plots of Ti (5h)-Al mixture with different heating rates, (a) 3^0C/min (b) 6^0C/min (c) 9^0C/min

6.3.2.6 Determination of Activation Energy, E

Non isothermal kinetics shown in equation (6.5) defines the empirical activation energy as the slope of the $\ln\beta/T_m^2$ vs $1000/T_m$ plot. The slope determined in the Fig 6.17 provides the activation energy E as -81.95865kJ/mol, -75.51176 kJ/mol,-11.57914 kJ/mol and -6.009kJ/mol. The activation energy values determined are in negative numbers, this suggest that the energy or the Gibbs free energy is in excess and the process will be feasible only if that amount of energy will be taken out from the system. The values of activation energy were found to be higher for finer particulate mixtures, which suggest that the finer particulate mixtures facilitate the sintering process. The feasibility of the process increased on increase in the percentage of active surface area. In case of lower size particulate blends the active surface area is higher and the sizes of the voids are finer, which provides the driving force for the sintering and formation of

the intermetallics. The magnitude for the activation energy is highest for the Ti (5h)-Al and the lowest is for Ti (1h)-Al (Fig 6.18), that confirms the fact that Ti (5h)-Al mixture is more favorable for the formation of intermetallics.

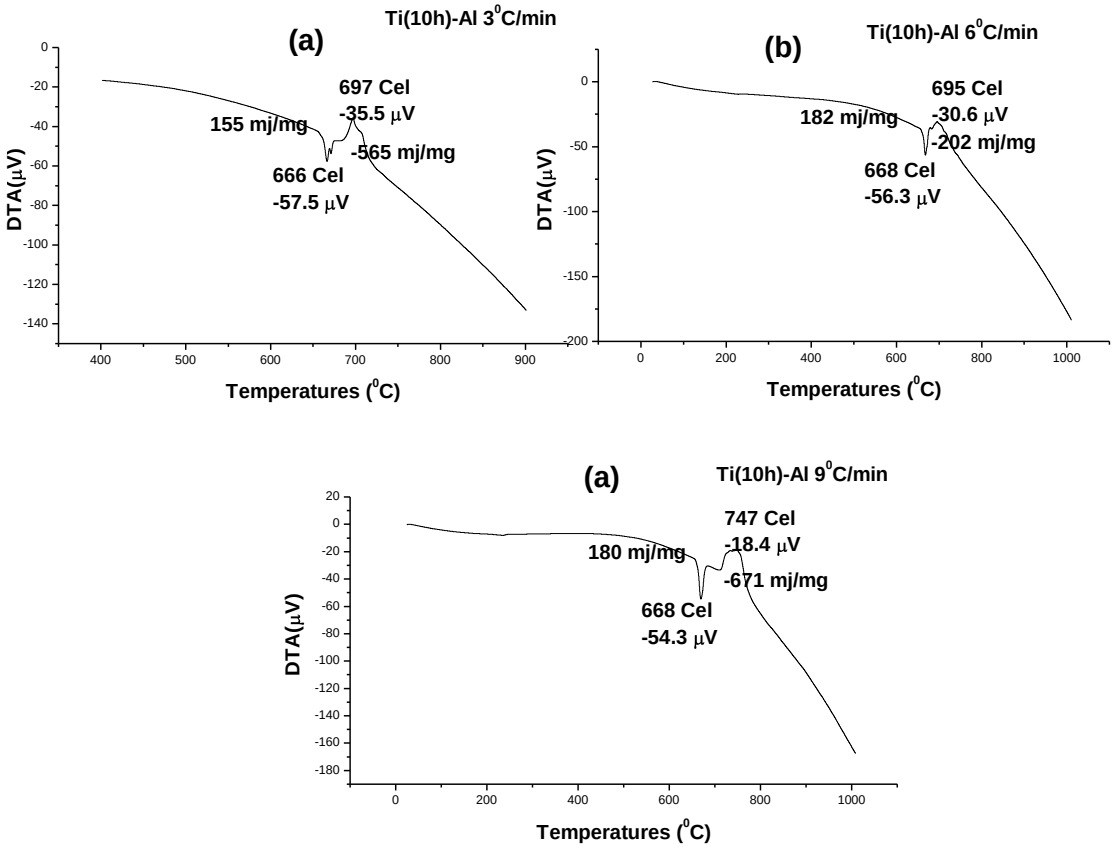

Fig 6.16 Thermal analysis plots of Ti (10h)-Al mixture with different heating rates, (a) 3^0C/min (b) 6^0C/min (c) 9^0C/min

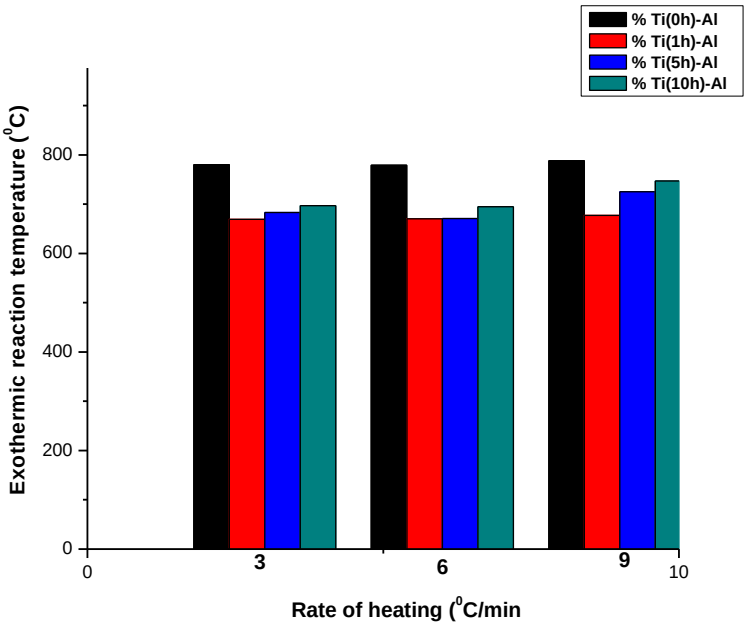

Fig 6.17 Comparison of exothermic reaction temperatures with rate of heating of TiAl particulate mixtures having various Ti particle sizes

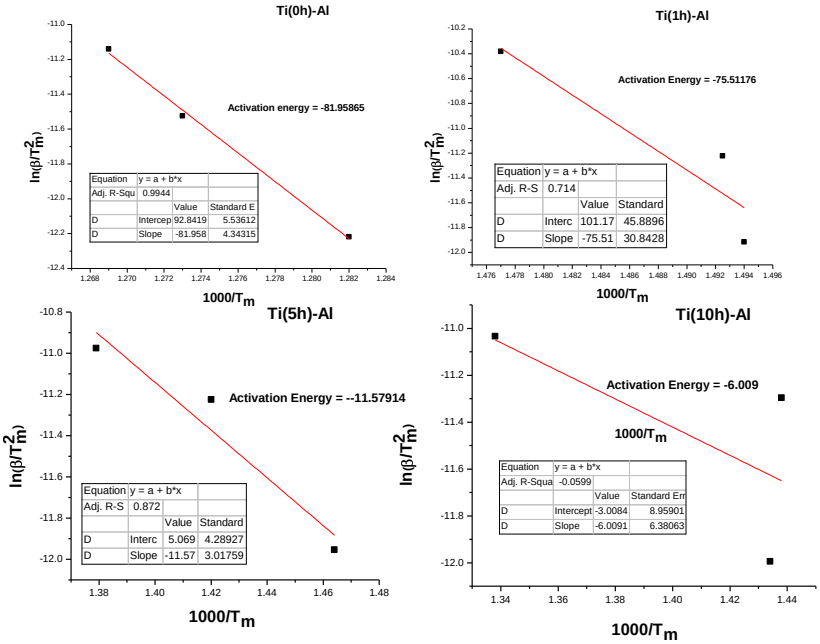

Fig 6.18 Variation of $\ln\beta/T_m^2$ vs $1000/T_m$ for Ti-Al particulate mixtures having various Ti particle sizes (a) Ti(0h)-Al (b) Ti(1h)-Al (c) Ti(5h)-Al and (d) Ti(10h)-Al mixtures

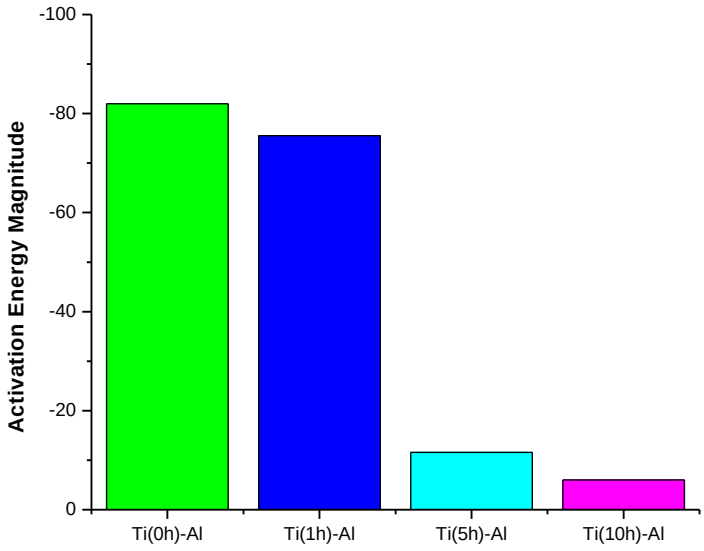

Fig 6.19 Variation of activation energy with Ti particle sizes in Ti-Al mixtures

6.3.2.7 Physical Properties

The densification and porosities during reactive sintering are presented in Fig 6.19.The densification of the reactively sintered powders is in the range of 2.9-3.1 g/cm^3, which is found to be a two fold increase over the green density. The particle size of Ti powders is the main influencing parameter for the densification. The percentage of porosities behave inversely proportional towards percentage interface of Ti-Al. The diffusion distances are lowered incase of finer particles, increase the rate of alloy transport in the chemical potential gradients. The small size particles although provide the large number of nucleation sites for the diffusion process, but remarkable differences between the sintered densities of Ti(5h)-Al and Ti(10h)-Al mixtures are not seen. Ti (5h)-Al powder blends show highest sintered density, low activation energy, low reaction sintering temperatures as compared to other powder blends.

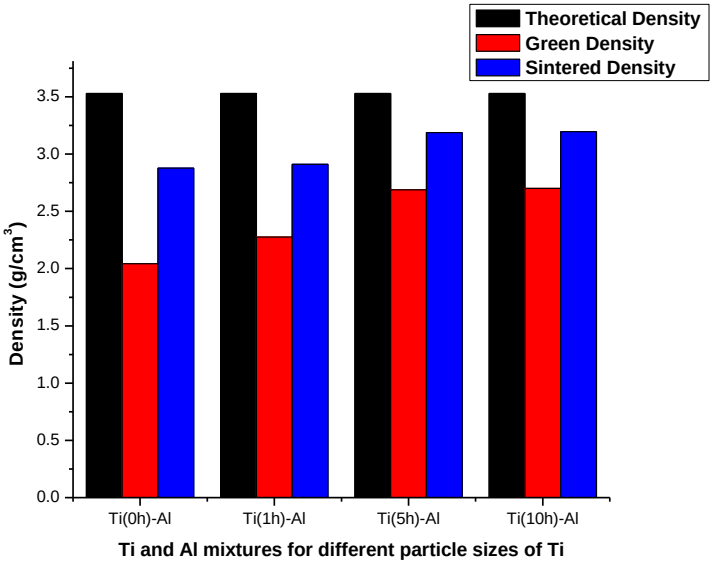

Fig 6.20 Comparison of Densification of Samples sintered at different temperatures with the green density

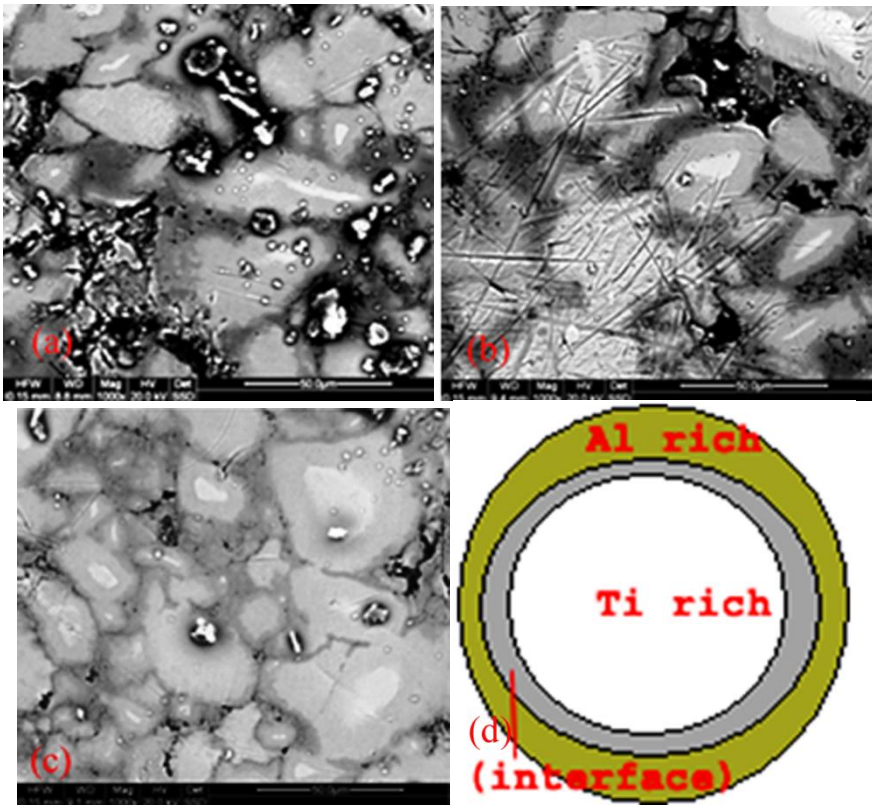

Fig 6.21 FESEM micrographs of sintered samples (a) Ti (1h)-Al , (b) Ti (5h)-Al (c) Ti (10h)-Al & (d) Schematic diagram representing Ti rich and Al rich regions and the interface Microstructural Evolution

FESEM micrographs in Figs 6.20 (a-c), show the sintered microstructures containing bright Ti rich and dark Al rich regions. Diffusion of Al into Ti rich regions is clearly seen in the microstructures, with various grey contrasts. The grey contrast shows the presence of various intermetallic phases. Darker the phases, higher are the Al content. The microstructures can be explained as the islands of Ti (bright region) are fitted in the Ti_3Al grain locale. The XRD pattern (Fig 6.10) also reveals the formation of Ti_3Al and TiAl, which are formed in the perimeter of Ti rich regions.

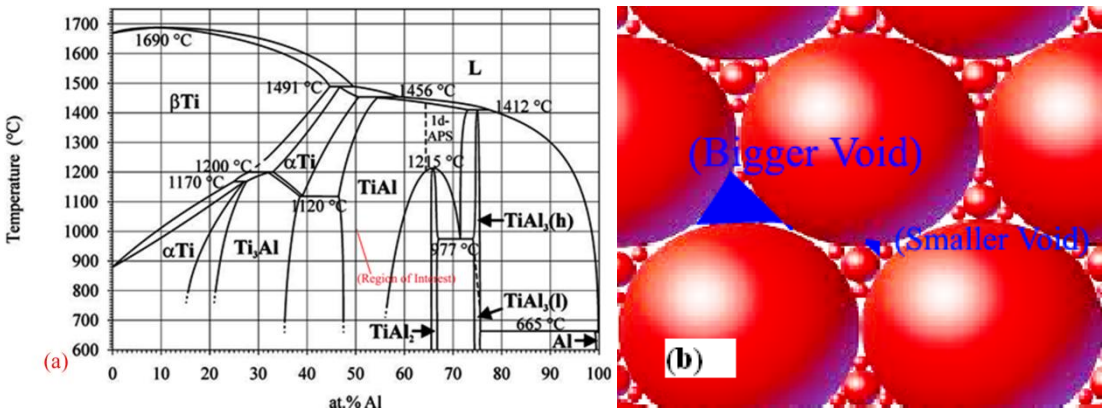

Fig 6.22 shows (a) A systematic phase diagram of Ti-Al binary system (b) Thematic diagram explaining size of voids with change in particle sizes.

6.3.3 *Summary*

In this study the comparison of exothermic temperatures, heating rates, effect of particle size and determination of activation energy were carried out. After the study of the above results, Ti (5h)-Al provides optimized results for 6^0C/min rate of heating. Ti (5h)-Al powder blends records-11.57914kJ/mol kJ/mol activation energy and optimized density of 3.188g/cm^3. The reaction sintering temperature observed for the above mixture is 671^0C for heating rate of 6^0/min. The temperature range for exothermic peaks is the lowest for Ti (5h)-Al with respect to Ti (0h)-Al, Ti (1h)-Al and Ti (10h)-Al mixtures.

6.4 Effect of Ti and Al Particle Size on the Thermal Analytical behavior and Densification of TiAl Intermetallics

The present study determines the effect of particle size of Aluminum and Titanium powders on the reactive sintering of Ti-Al based intermetallics as well as the subsequent reaction kinetics and densification behavior. Titanium and Aluminum powders of average particle size were milled separately for different extents to produce average particle sizes of 100, 28 and 7 μm. Both the powders were mixed with each other having nearly similar particle sizes in the ratio of 1:1 at% intermetallic composition. The reactive sintering temperatures of the mixtures were determined by DTA and the effect of change in particle sizes has been determined for the activation energy of the self propagating reaction. The mixtures of Ti and Al blends of various particle size has been compacted and subsequently sintered at reaction sintering temperatures for 1hr in argon atmosphere. The density / porosity levels as well as the microstructural evolution were carried out to determine the influence of the particle size on the reactive sintering of Ti-Al. The compacts were further characterized by X-ray diffraction to determine the extent of phase formation. The influence on hardness was also determined with respect to densification and various particle size mixtures.

6.4.1 *Experimental Procedure*

Section 6.2.1 can be referred for the size and make of titanium and aluminium powder used. The milling equipment and the manufacturers can be referred from the same. The Titanium powder obtained was milled in a RETSCH PM 400/2 planetary ball mill for different time extent of 1, 5 and 10h. The hardened steel balls and jars were used as the medium for milling and the ball to charge weight ratio were kept as 5:1. To avoid the agglomeration of powders during milling, toluene is used as the process control agent. The charge and the balls were totally submerged in the toluene during milling condition to avoid oxidation of powders (Guo et al 1990; Hay et al 2000 & Froes 1995). The milling parameters and the details of milling condition are shown in Table-1.The Ti powders milled for time extents of 1, 5 and 10h resulted a mean particle size approximately of 100, 25-28 and 7-9μ respectively. The Al powder milled for durations of 1, 4 and 7h exhibited an average particle size of 100, 28 and 7μ respectively. Milled aluminum powder of 100, 28 and 7μ particle size were mixed individually with

titanium powder of similar size to prepare mixture of 50:50at%. The powder blends of Ti (1h)-Al(1h), Ti (5h)-Al(4h) and Ti (10h)-Al(7h) were sintered in high pure inert environment (argon) for 1 hour duration at 717^0C, 695^0C and 713^0C respectively where the temperatures for sintering were decided by studying the thermal analytical results of the blends. The powder mixtures were compacted at 175 MPa to a cylindrical shape of the dimensions of 16.4 mm diameter and 5mm thickness. The sintered samples were polished and ground with different grits emery papers followed by polishing cloths.

The characterizations like FESEM, XRD, DTA, Archimedes principle and reaction kinetics phenomena can be referred from 6.2.2.

6.4.2 *Results and Discussion*

6.4.2.1 XRD Analysis of Sintered compacts

Milling introduces plastic deformation and renders the crystallinity in short range order.Sintering after milling includes process of recrystallization and growth.Specifically reactive sintering forms the phases and densifies the compacts. When the sintered samples were characterized using XRD (Fig.6.22), formation of TiAl and Ti_3Al phases are confirmed.The mixtures of Ti (5h)-Al(4h) and Ti(10h)-Al(7h) display slightly broadened peaks with respect to Ti(0h)-Al(0h), Ti (1h)-Al(1h) mixtures. The phases were confirmed with JCPD code numbers 00-042-1137 and 00-014-0461 respectively. The broadening and decrease in the intensity of the peaks can be attributed towards the milling of Ti and Al powder.

Table 6.5: Milling and mixing parameters

Planetary Ball mill Details **(Retsch PM 400/2)**	**Milling Parameters**
Milling Balls- Hardened steel balls	Milling Media-Toluene
Milling Jars- Hardened steel jars	Charge to Ball ratio-1:5
Jar capacity- 500 ml	Milling speed- 200 rpm Vial Speed- 400 rpm
PCA-Toluene	Total time of milling- 1h,5h&10h(Ti) 1h,4h, & 7h (Al)
	Weight of initial charge- 30gms
Mixing parameters	
Milling Balls- Hardened steel balls	Charge to Ball ratio-1:3
Milling Jars- Hardened steel jars	Milling speed- 70 rpm Vial Speed- 140 rpm
Jar capacity- 500 ml	Total time of mixing-30mins
Argon atmosphere	Weight of initial charge- 30gms

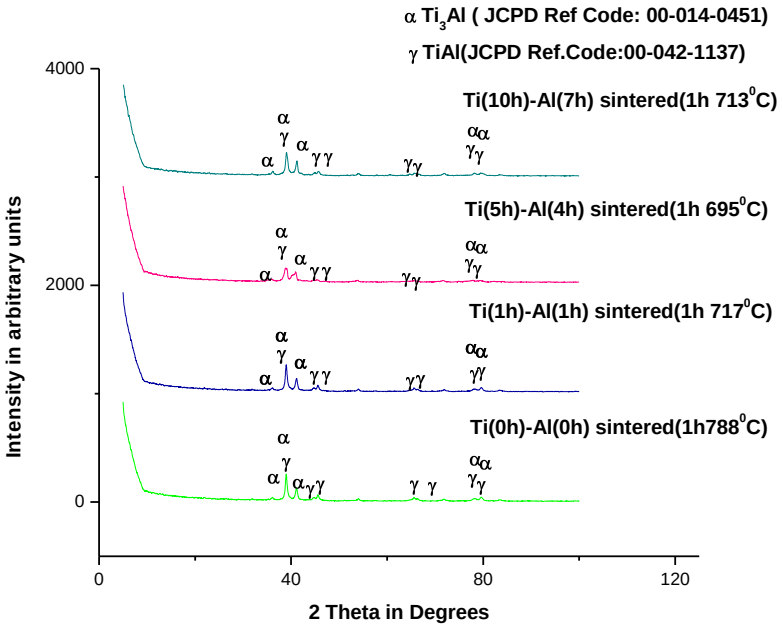

Fig 6.23 XRD pattern of Ti (0h)-Al(0h), Ti (1h)-Al(1h), Ti (5h)-Al(4h) and Ti(10h)-Al(7h) mixtures sintered at their respective temperatures

The shifting of peaks is unnoticeable, as the milling of the powders was carried out at lower rpm and for small duration though the lattice parameter has been lowered to certain percentage.

For the mixtures Ti (1h)-Al (1h), Ti (5h)-Al (4h) and Ti (10h)-Al (7h), exothermic peaks are recorded at 717^0C, 695^0C and 713^0C respectively. The heat of formation of TiAl and Ti_3Al are −75 and −73 kJ/mol respectively (Baek et al 1985 & Wang et al 2008)

6.4.2.2 Microstructure

Milled powders of Ti and Al are displayed in Figs. 6.23 &6.24. Milling of Ti and Al powders show fractured and uneven morphology. Milling process contains two processes such as cold welding and fracture. The formation of new surfaces during milling has higher surface energy which is responsible for cold welding of the particles so as to decrease the free energy. The morphological studies of the milled Ti powders are displayed in Fig 6.23 (a-c). Fracture and cold welding are two processes which occur during milling and the breakage is the resultant. Ti powders are subjected to 1h, 5h and 10h of milling. The fracturing phenomenon of the powders is due to work hardening introduced by higher extent of milling, which help in overcoming the free

energy of nascent surfaces and agglomerated clumps for their breakage. Thus the higher extent of milling helps in lowering the particle size. After certain duration of milling the equilibrium of the above two process is set in such a way that the further lowering of particle sizes are inhibited. Ductility of Ti powder is the cause of flattening and agglomeration of particles after 1h of milling. The approximate particle size attained by 1h milled Ti powders was ~100µ. The work hardened splats of Ti powders when further milled to 5h, the particle sizes get reduced to an approximate size of 28µ. As shown in Fig 6.23(c) Ti particles milled for 10h, produces particles of the order of ~7µ. The uneven particle morphology of the milled powders is due to the fractured surfaces created during the collisions. The morphology of Al powders milled for different duration i.e 1h, 4h and 7h and as received Al and as received Ti powderare shown in Figs 6.24 (a-e). Al powders upon milling is flattened at early stages of milling due to plastic deformation and attains an approximate size of 100µ (1h miling)and upon further milling the work hardened splats fracture to an approximate size of 28µ and 7µ for 4h and 7h of milling respectively.

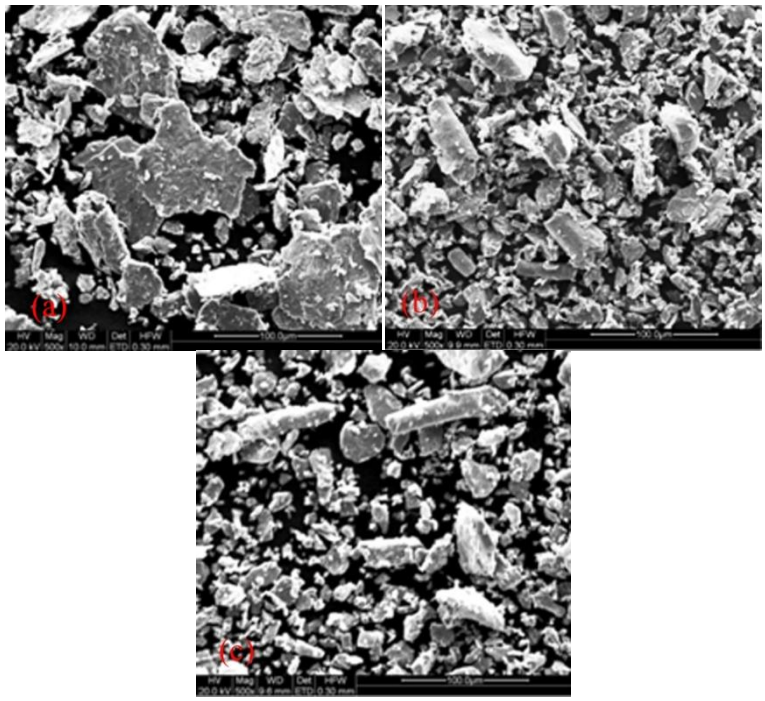

Fig 6.24 FESEM micrographs of milled Ti powders for different extent of milling (a) 1h milled (b) 5h milled & (c) 10h milled

6.4.2.3 DTA Study

The study of the thermal analysis of Ti-Al mixtures has been carried out at low heating rates for efficient calculation of the activation energy (Vyazovkin et al 2011). Ti-Al mixtures of different particle sizes were studied by thermal analysis with three different rates of heating i.e, 3^0C/min, 6^0C/min and 9^0C/min. Different heating rates has been used to determine the activation of energy of the exothermic reaction and the effect of

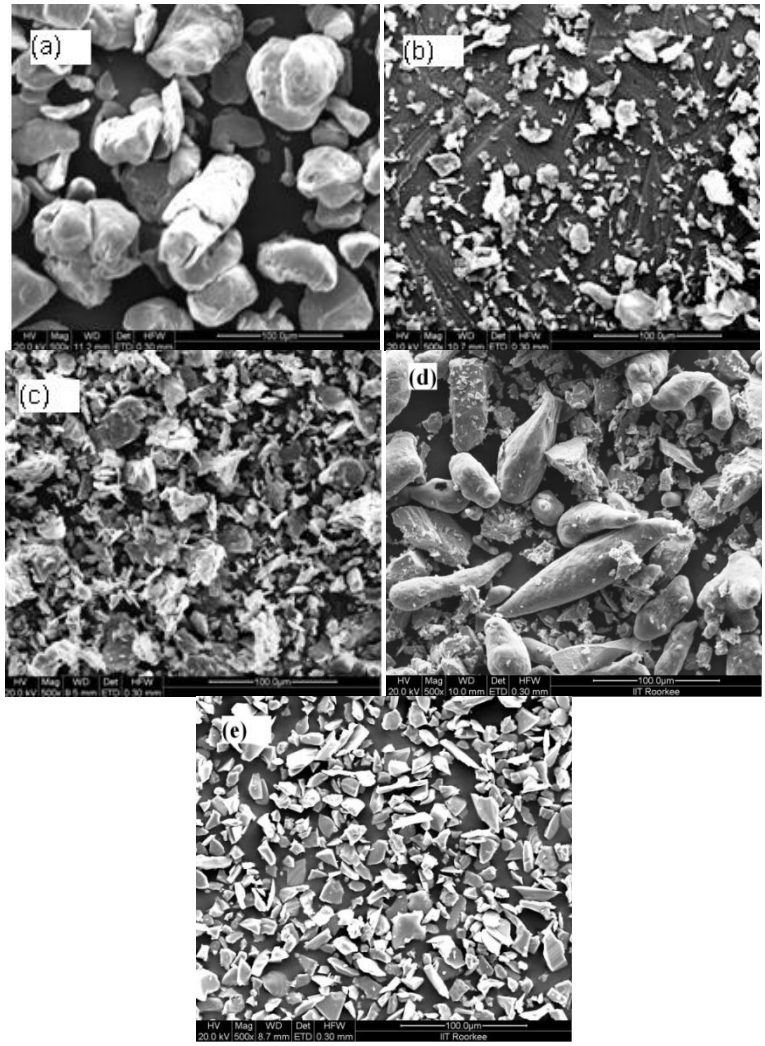

Fig 6.25 FESEM micrographs of milled Al powders for different extent of milling (a) 1h, (b) 4h, (c) 7h,(d) "as received" Al powder and (e) "as received" Ti powder

heating rates on it [Figs 6.25, 6.26, 6.27 & 6.28]. The melting of Al particleis displayed by endothermic peaks in the thermal analyses graphs. The thermal analytical behavior of Ti (0h)-Al (0h) gives the result that the melting temperature of Al is almost the same as for 3^0C/min; 6^0C/min and 9^0C/min. Ti powders have no influence on the

melting of the Al powder, so the melting point is found to be almost same for all the heating rates.

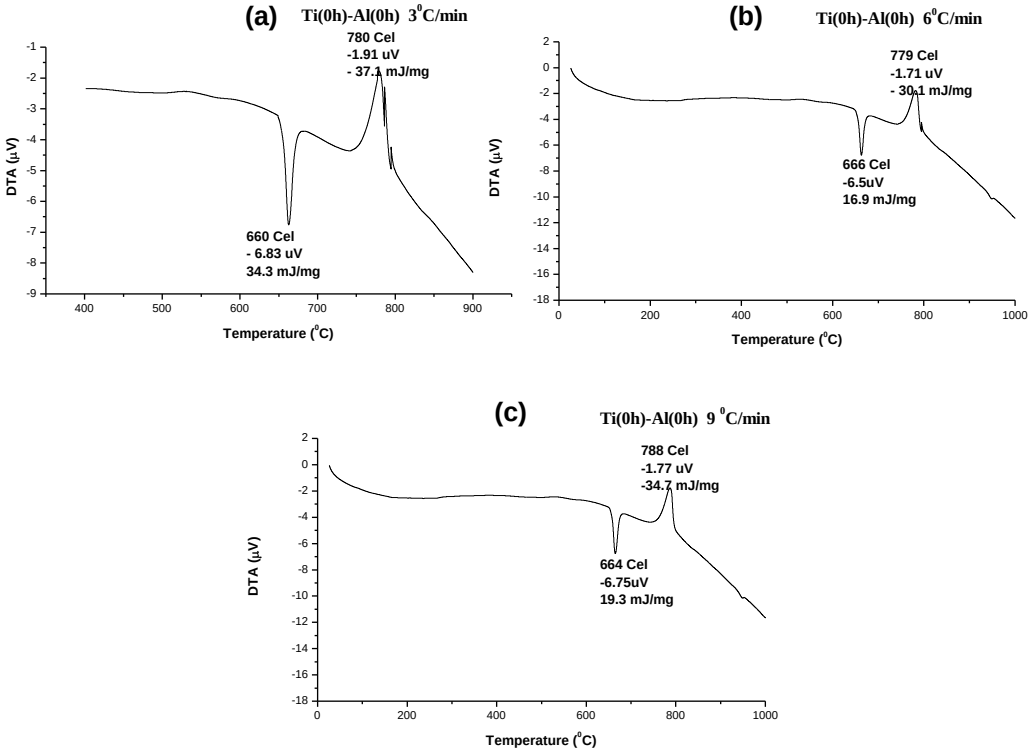

Fig 6.26 Thermal analysis plots of Ti (0h)-Al mixture with different heating rates, (a) 3^0C/min (b) 6^0C/min (c) 9^0C/min

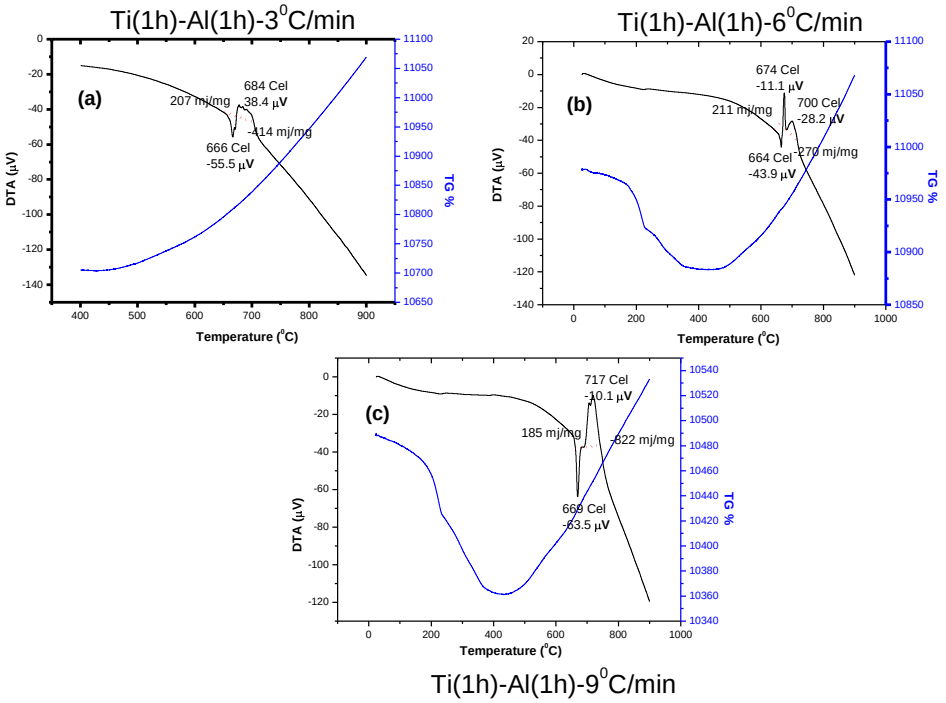

Fig 6.27 Thermal analysis plots of Ti (1h)-Al (1h) mixture with different heating rates, (a) 3^0C/min (b) 6^0C/min (c) 9^0C/min

The DTA plots of Ti-Al mixtures show exothermic peaks 788^0C, 717^0C, 697^0C and 713^0C for Ti (0h)-Al(0h), Ti (1h)-Al(1h), Ti (5h)-Al(4h) and Ti(10h)-Al(7h) respectively for the heating rate of 9^0C/min. The exothermic peaks are the characteristics of phase transformation of titanium aluminides which were confirmed by the diffraction patterns of the sintered Ti-Al blends (Fig 6.22) resulting in the formation of TiAl and Ti_3Al.

6.4.2.4 Effect of Particle Size

The particle size of the mixtures affects the sintering temperatures. The effect of different particle sizes of Ti and Al directly affects intermediate space or the diameter of the capillaries through which liquid Al flows. The sintering of intermetallics is enhanced by finer diameter of capillaries. The rise in the capillaries and the amount of capillaries behave directly with the percentage densification. Milling of Ti and Al particles increased the area of the reaction interface by lowering the particle size and hence Gibbs free energy of the system is increased. This causes reaction sintering temperatures (exothermic temperature) to be lowered for Ti (1h)-Al(1h), Ti (5h)-Al(4h) and Ti (10h)-Al(7h) mixtures. Specifically the lowering of sintering temperature for Ti

(1h)-Al(1h), refers to the inclusion of external energy provided through milling of Ti and Al particles. Reduction of particle size is the establishment factor for finer voids for the flow of Al melt and in turn provides densified product. The analysis of differential thermal gravimetric values provides clear idea of sinterability of the mixtures of different Ti and Al particle sizes. The rate at which heat loss or gain has occurred can be determined from DTG values. This also have influence on the reaction rate at a particular heating rate. For highest heating rate, lower the particle size elevated will be the rate at which the heat is lost. Reduction of DTG values for higher particle size mixtures can be attributed towards the rate of capillary flow of Al melt.

6.4.2.5 Effect of Heating Rates

The effect of heating rates is almost nullified or can be said as the exothermic points are hardly affected for Ti(0h)-Al(0h) powder mixtures(Fig 6.29).For the powder mixtures Ti(1h)-Al(1h) the exothermic temperatures are almost same for 3^0C/min and 6^0C/min. But for 9^0/min heating rate an elevation in the exothermic temperature is seen, which can be attributed towards the overshooting of temperatures during higher rate of heating (Table-6.6). For Ti (1h)-Al (1h) mixtures also the trend of overshooting of temperature for higher rate of heating is observed. But the discrepancy comes in case of lower particle size mixtures like Ti (5h)-Al (4h) and Ti (10h)-Al (7h). In both the mixtures the elevation in exothermic temperatures are seen for the heating rate of 3^0C/min as compared to 6^0/min heating rate. The behavioral discrepancies can be explained on the basis of heat evolved during the reaction. When observed in Figs(6.27&6.28), the exothermic peaks of3^0C/min heating rate, evolves the highest amount of heat recorded as 40.7µV, and 35.5 µV for Ti (5h)-Al and Ti(10h)-Al mixtures respectively. The higher heat evolved is responsible for increasing the exothermic temperature of Ti-Al systems. The phenomenon is supported by capilliary action of Al melt in the pores created by Ti particles. The pores are actually the void space created by Ti particles. For Ti (5h)-Al(4h), Ti(10h)-Al(7h) mixtures the void space created is lower in compared to the other two Ti-Al mixtures taken .Because the particle sizes are smaller as a result of which the void space created is lower as compared to Ti(0h)-Al and Ti(1h)-Al which helps in increasing the capillary action. The capillary action is increased due to the decrease in size of the voids which otherwise can be described as the diameter of the capillaries. When Ti (5h)-Al (4h) and

Ti (10h)-Al (7h) areheated at the heating rate of 9^0C/min, the exothermic temperatures have increased to 725^0C and 747^0C respectively. The lower Ti particle size mixture confirms the formation of lower diameter capillaries which would have increased the evolved heat content but the trend is not maintained this can be explained as the over shooting of temperatures at higher heating rate. At highest heating rates lower the particle size higher is the exothermic temperatures. The temperature gap in exothermic peaks increase with increase in heating rate i.e. 6^0C/min and 9^0C/min.

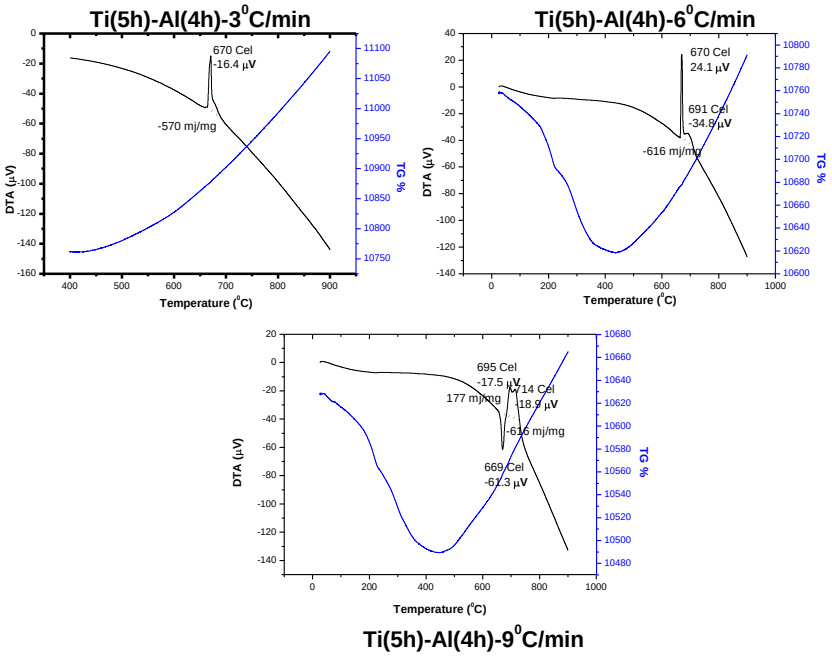

Fig 6.28 Thermal analysis plots of Ti (5h)-Al(4h) mixture with different heating rates (a) 3^0C/min (b) 6^0C/min (c) 9^0C/min

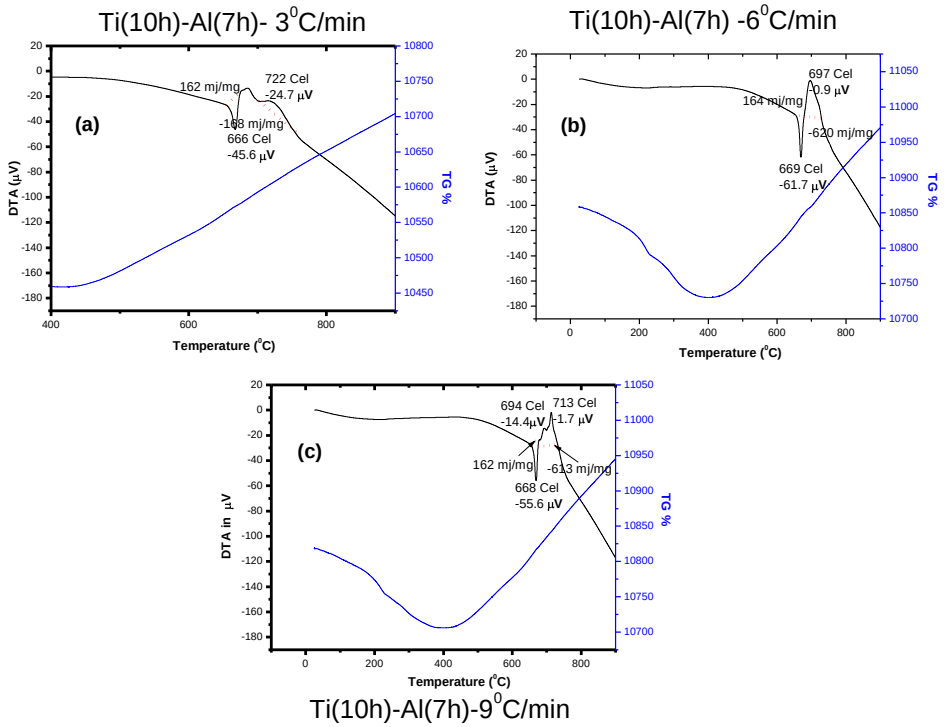

Fig 6.29 Thermal analysis plots of Ti (10h)-Al(7h) mixture with different heating rates (a) 3^0C/min (b) 6^0C/min (c) 9^0C/min

6.4.2.6 Determination of Activation Energy, E

Non isothermal kinetics as shown in equation (6.8) defines the empirical activation energy as the slope of the $\ln\beta/T_m^2$ vs $1000/T_m$ plot. The slope determined in the Fig 6.29 provides the activation energy. The activation energy values determined are in negative numbers, suggest that the energy or the Gibbs free energy is in excess and the process will be feasible only if that amount of energy will be taken out from the system. The values of activation energies were found to be higher for finer particulate mixtures, which suggest that the finer particulate mixtures facilitate the sintering process. The feasibility of process increases on increase in the percentage of active surface area. In case of lower size particulate blends the active surface area is higher and the sizes of the voids are finer, which provides the driving force for sintering and the formation of the intermetallics. The magnitude for the activation energy is highest for the Ti(5h)-Al and the lowest is for Ti(1h)-Al(Fig 6.31), that ascertains the fact that Ti(5h)-Al mixture are more favorable for the formation of intermetallics and sintering.

6.4.2.7 Physical Properties

The densification and porosities during reactive sintering are presented in Fig.6.32.The densification of the reactively sintered powders is in the range of 2.9-3.1 g/cm^3, which is found to be a two fold increase over the green density. The particle size of Ti powders is the main influencing parameter for densification. The percentage of porosities behaves as inversely proportional to percentage interface area of Ti-Al. The diffusion distances are lowered incase of finer particles, increase the rate of alloy transport in the concentration gradients. The lower size particles although provide large number of nucleation sites for the diffusion process, but remarkable differences between the sintered densities of Ti (5h-Al and Ti (10h)-Al mixtures are not seen. Ti (5h)-Al powder blends show cases of highest sintered density, low activation energy, low reaction sintering temperatures with respect to other powder blends.

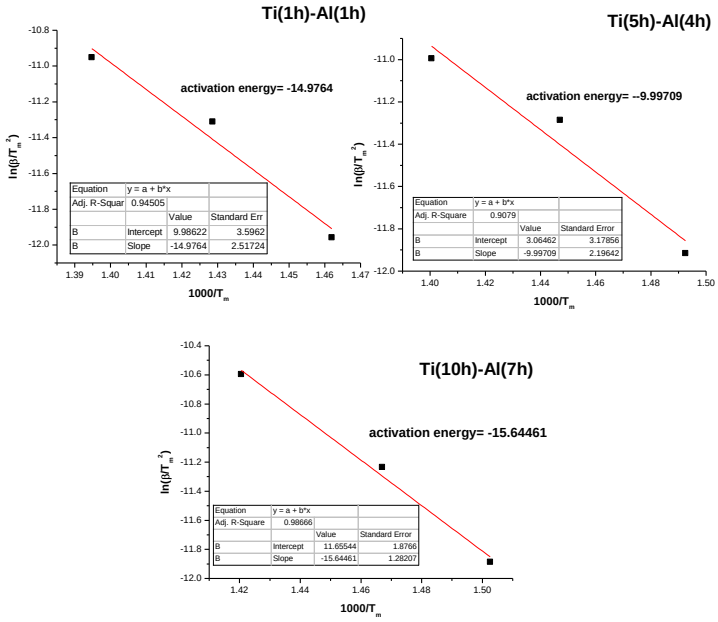

Fig 6.30 Variation of $\ln\beta/T_m^2$ vs $1000/T_m$ for Ti-Al particulate mixtures having various Ti and Al particle sizes (a) Ti(1h)-Al(1h) (b) Ti(5h)-Al (4h) and (c) Ti(10h)-Al(7h) mixtures

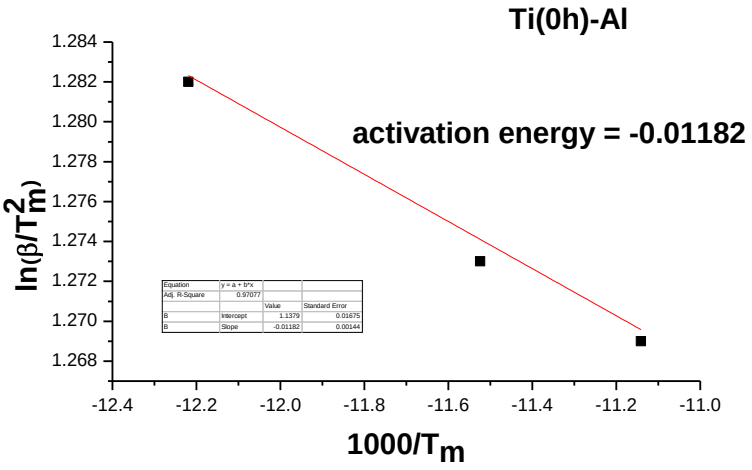

Fig 6.31 shows the determination of E, from $\ln\beta/T_m^2$ vs $1000/T_m$ for Ti(0h)-Al(0h)

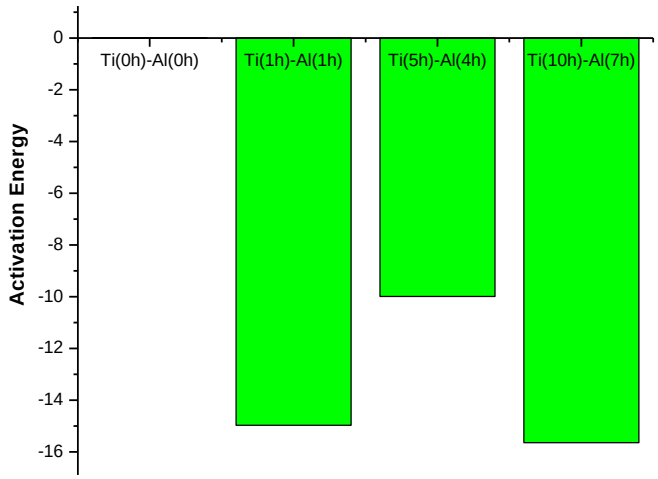

Fig 6.32 Variation of activation energy with Ti particle size in Ti-Al mixtures

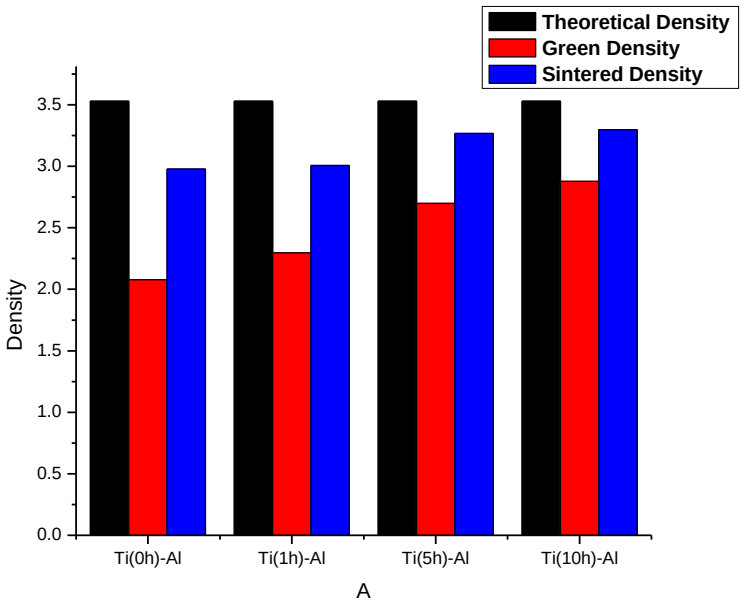

Fig 6.33 Comparison of Densification of Samples sintered at different temperatures with green density

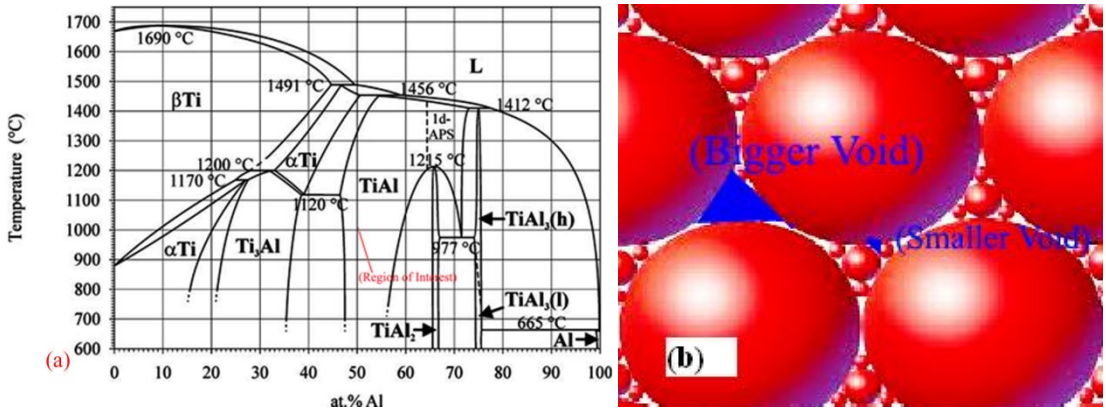

Fig 6.34 shows (a) A systematic phase diagram of Ti-Al binary system (b) Thematic diagram explaining size of voids with change in particle sizes

6.4.2 *Summary*

In this study the comparison of exothermic temperatures, heating rates, effect of particle size and the determination of activation energy were carried out. After studying above results, Ti (5h)-Al (4h) provides optimized results for 6^0C/min rate of heating. Ti (5h)-Al (4h) powder blends provides lower activation energy and optimized density of 3.188g/cm^3. The reaction sintering temperature observed for the above mixture is 670^0C for the heating rate of 6^0/min. The temperature range for exothermic peaks is lowest for Ti (5h)-Al (4h) as compared to Ti (0h)-Al (0h), Ti (1h)-Al (1h) and Ti (10h)-Al (7h) mixtures.

CHAPTER 7

DILATOMETRIC STUDY OF THE Ti-Al INTERMETALLICS WITH VARIOUS PARTICLE SIZES OF Al, Ti AND THEIR MIXTURES

7.1 Introduction

The feasibility of the formation of Ti based intermetallics and the rate with which the above reaction taking place (reaction synthesis and mechanical alloying) has been studied by reaction kinetics and activation energy of the system. Mechanical alloying though as process providing the output as fine grained structures, but it is a non equilibrium process and the hardening of powders hinders the densification. In sections 5.3, 5.4, it is noticed though the densities are optimized, but to apply as component, the densification must be higher than 95 %. With reaction kinetics, varying particle size and composition lowest of activation energy of the system is derived (sections 6.2, 6.3 & 6.4). Densification of Ti-Al intermetallics can only be effective if and only if the bulging during reactive sintering is controlled. Dilatometric characteristics will give an clear idea about the bulging during reaction sintering. The lowest expanded Ti-50Al composition with lowest activation energy will provide us the path for highest densification. Hence, other parameters like effect of varying soaking temperature with varying particle sizes of Al, Ti and their mixtures are dealt in the following sections.Section 7.2 of Chapter 7 consists of the study of dilatometric characteristics of Ti-Al intermetallics processed by reaction synthesis with various particle sizes of Al. Section 7.3 comprises of the effect of particle sizes of Ti powders on the dilation during reaction sintering.

To have the best composition with optimized particle size mixtures, similar particle sizes of Ti and Al powders were mixed and processed through reaction synthesis. The same has been characterized to determine expansion/shrinkage and study reaction kinetics of the system in the final section of 7.4 of this chapter.

7.2 Dilatometric Behavior of the Ti-Al Intermetallics Containing Various Al Particle Size

The optimized density, high stiffness, oxidation resistance and high strength to weight ratio are the key characteristics in making the Ti-Al based intermetallics, a desired material for the industrial applications in gas turbines and aerospace industries.

Powder metallurgical processes have an edge upon other processes due to economical viability of the method and fabrication of near net shape product. Reaction synthesis and Mechanical alloying are two competitive processes for synthesis of aluminides. Work hardening during mechanically alloying and bulging of compacts during reaction sintering are the main drawbacks of the above processes. As mechanical alloying is a non equilibrium process, so work hardened materials will hardly show higher densification. When the starting materials were lowered in size, through reaction synthesis finer grain structures can be achieved. Dilatometric characterization will provide the idea of material which will have lowest bulging during sintering. Various researchers have carried out experimentation on linear shrinkage/expansion,onset of sintering and rate of expansion [Dabhade et al 2006 & Dabhade et al 2007]. Dabhade et al (2007) calculated the onset of sintering temperatures of Ti-TiN composite powders, linear shrinkage rate at constant rate of heating and sinterability. Wang et al studied the same for titanium aluminide compacts fabricated through cold extrusion and have various Al at% of 25-75. Though the dilatometric investigations provideddata regarding thermal expansion, but hardly gave any idea about the linear shrinkage/expansion rate of the aluminides formed during thereaction synthesis process. There is rarely literatures available where the researchers have worked on the dilatometric investigations of titanium aluminides and determined expansion rate, activation energy and percentage linear expansion.

The present study deals with the effect of particle size of Aluminium and temperatures over the sintering and dilatometric behavior of Ti-Al mixtures. The above study also provides an idea about the expansion rate and activation energy of the process carried

out.Aluminum powders were milled separately for various durations to produce average particle sizes of 100, 28 and 7 μm. The milled powders were then mixed with Titanium powders of average particle size of ~44 μm in the ratio of 1:1 at% intermetallic composition. The exothermic reaction temperatures were determined using DTA. The effect of changes in particle sizes in Al on the dilatometric behavior, activation energy and expansion rates were analyzed. The samples were further characterized for microstructural evolution by FESEM and phases present in the sinters were determined by using XRD.

7.2.1 *Experimental Procedure*

Titanium and Aluminium of mean particle size 44μ and 99.9% purity procured from Testbourne (UK) were used as the starting materials. The Aluminium powder obtained was milled in a planetary ball mill (RETSCH PM 400/2) for various durations of 1, 4 and 7h. Hardened steel balls and jars were used as the media for milling, where ball to charge ratio was kept as 5:1.Toluene as the process control agent was used as the dispersant to avoid agglomeration and prevent oxidation. The toluene was used in such a way that the charge and balls mixture was totally submerged inside the reagent (Froes et al 1995; Hay et al 2000 & Guo et al 1990). The Al powders produced after milling for durations of 1h, 4h and 7h resulted to have an average particle sizes of 100, 25-28 and 7-9μ respectively. The Al powder of different sizes was mixed along with Ti powder of approximate particle size of 44 μ to prepare mixtures of 50:50at%. The mixing of powders was done firstly for 5 mins by mortar and pestle followed by mixing in planetary ball mill at 70 rpm for 30 mins in atmospheric condition. The sintering of powders were carried out under ultra high pure inert environment of argon for 1 hour at 763^0C, 758^0C and 696^0C for Ti-Al (1h), Ti-Al(4h) and Ti-Al(7h) mixtures according to data analyzed from the thermal analysis. The sintering temperatures were determined by analyzing the DTA results of the respective mixtures. The diameter of samples for sintering was 16.4 mm and about 5mm thickness. The rate of heating for sintering process was kept as 10^0C/min and the sintered samples were furnace cooled. For examining microstructural evolution the sinters were ground and polished with different grits of emery paper and cloths. The milled and sintered samples were subjected to of X-ray diffraction (XRD) using a D8 BRUKER AXS diffractometer with Cu Kα, operating at 40 kV and 30 mA to characterize the phases present.. Thermal

behavior was calculated by heating the samples upto 1400^0C in a PERKIN ELMER Pyris Diamond TG/DTA. FESEM was done using Using a QUANTA FEI-200 Field emission scanning electron microscopy (FESEM). The dilatometric analysis was carried out using Linseis data acquisition system. The system consists of sample holder with the highest sample diameter of 14 mm, amplifier, and cooling circuit. The samples loaded for dilatometric analyses have the diameter of the order of 10 mm. The heating consisted of two steps such as the heating to soaking of temperatures with a heating rate of 10^0C/min and the next step as the holding of sample at the soaking temperature. To study both solid state, transient liquid phase sintering and for the calculation of activation energy, the soaking temperatures for the mixtures were kept as 600^0C, 650^0C, 700^0C, 750^0C and 800^0C.

Table 7.1: Milling and mixing parameters

Planetary Ball mill Details (Retsch PM 400/2)	**Milling Parameters**
Milling Balls- Hardened steel balls	Milling Media-Toluene
Milling Jars- Hardened steel jars	Charge to Ball ratio-1:5
Jar capacity- 500 ml	Milling speed- 200 rpm Vial Speed- 400 rpm
PCA-Toluene	Total time of milling- 1h,4h&7h
	Weight of initial charge- 30gms
Mixing parameters	
Milling Balls- Hardened steel balls	Charge to Ball ratio-1:3
Milling Jars- Hardened steel jars	Milling speed- 70 rpm Vial Speed- 140 rpm
Jar capacity- 500 ml	Total time of mixing-30mins
Argon atmosphere	Weight of initial charge- 30gms

7.2.2 *Results and Discussion*

7.2.2.1 XRD Analysis of reaction sintering process.

X-ray diffraction patterns were analyzed to determine the phase evolutions occurred during sintering process. There is absolute synthesis of TiAl and Ti_3Al phases occurred for Ti-Al (1h) mixtures sintered at 763^0C. The phases were matched with the reference of JCPD code No. 00-042-1137 and 00-014-0461. The slight broadening of peaks can be clearly seen incase of Ti-Al(4h) and Ti-Al(7h) due to pre milling of Al but both the intermetallic phases are clearly found (Bose et al 1988 & Guo et al 1990). Increase in extent of milling of Al powders induced the broadening of the peaks. The shifting of the peaks were not that much prominent as the milling was carried out in a very low rpm.

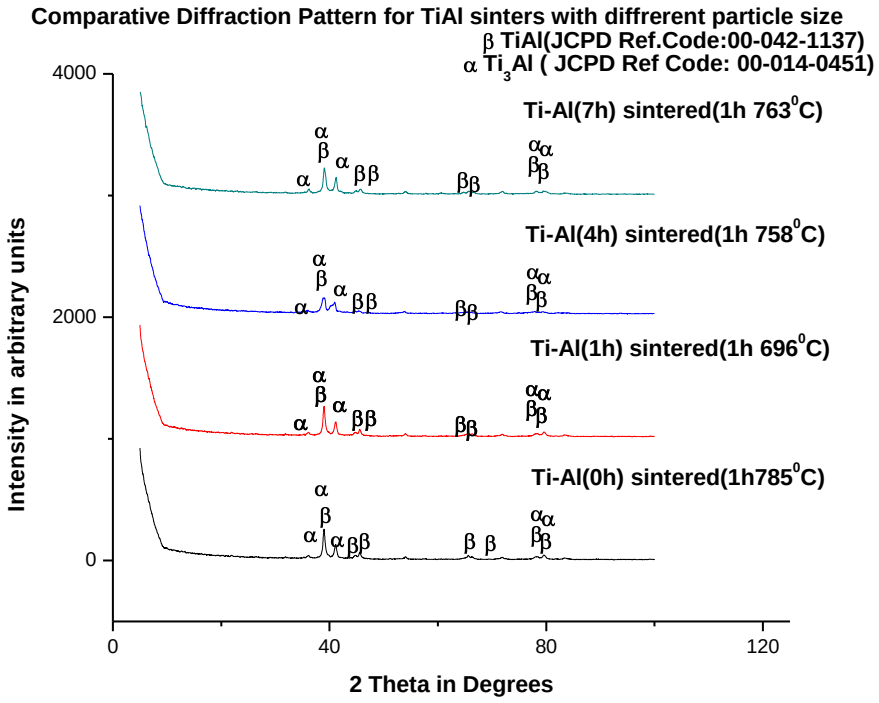

Fig 7.1 XRD pattern of Ti-Al (0h), Ti-Al (1h), Ti-Al (4h) and Ti-Al (7h) mixtures sintered at their respective temperatures

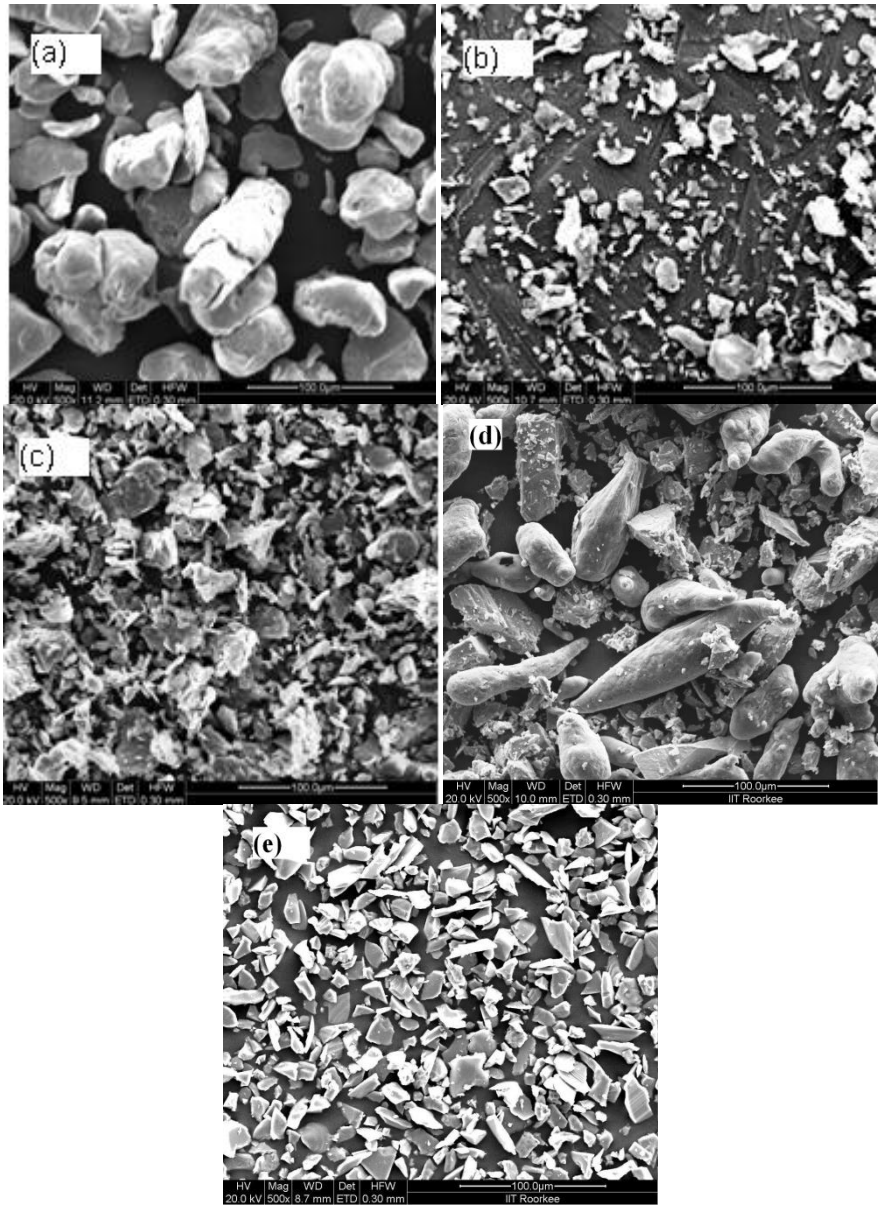

Fig 7.2 FESEM micrographs of milled Al powders for different extent of milling (a) 1h, (b) 4h, (c) 7h,(d) "as received" Al powder and (e) "as received" Ti powder

7.2.2.2 Morphological Analyses

The morphology of Al powders milled for different durations i.e 1h, 4h and 7h is shown in Fig 7.2 (a-c). The Al powders upon milling is flattened at early stages of milling due to plastic deformation and attains an approximate size of 100µ and upon further milling the work hardened splats fracture to approximate size of 28µ and 7µ for 4h and 7h milling respectively.

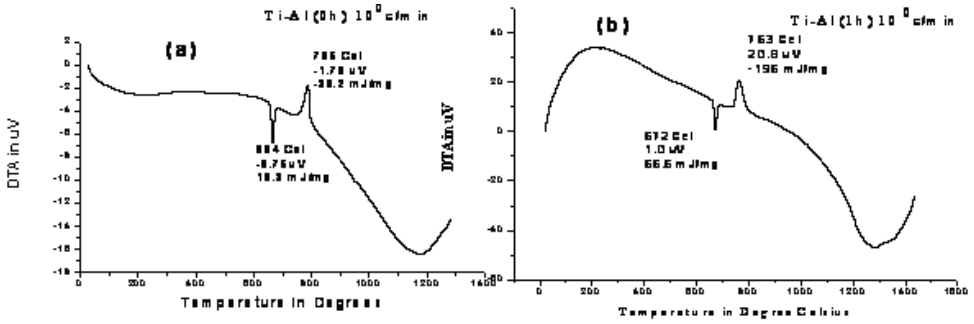

Fig 7.3 Thermal analysis plots of (a) Ti-Al (0h) mixture and (b) Ti-Al (1h) mixture at 10^0C /min

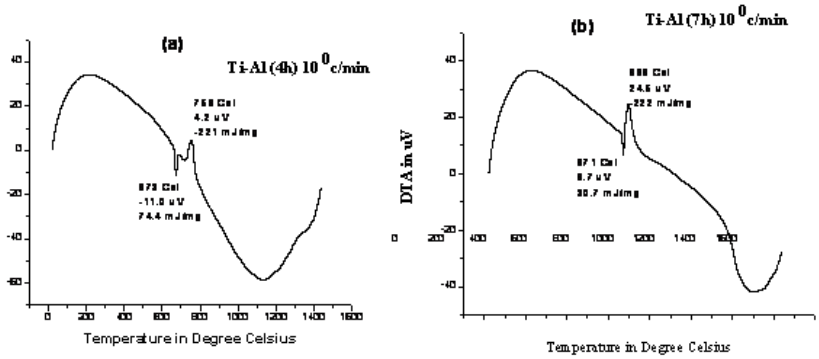

Fig 7.4 Thermal analysis plots of (a) Ti-Al (4h) mixture and (b)Ti-Al (7h) mixture at 10^0C /min

7.2.2.3 DTAStudy

The melting of Al powder was revealed by the endothermic peaks present in the figures. The melting point for Ti-Al (0h) is 664^0C, but for the other compositions it is 672^0C, 673^0C and 671^0C. The melting point of aluminium would have shown a decreasing trend but the milling increasedthe nascent surface area which when mixed with titanium gets coated with it and delays the process.

7.2.2.4 Dilatometric Study

The dilatometric behavior of mixtures with various Al particle size are displayed in Fig 7.5,7.6 & 7.7 for temperatures 600^0C, 650^0C, 700^0C, 750^0C & 800^0C. The above figures depict the comparative patterns of relative percentage of expansion/shrinkage and coefficient of thermal expansion. The relative percentage of expansion and coefficient of thermal expansion though provides the facts about physical behavior of thermal expansion but in turn explains the characteristics of sinterability of the

materials. Because the process consists of various soaking temperatures include two types of sintering such as; 1.Solid phase sintering, 2.liquid phase sintering. Process of sintering was decided on the basis of the temperatures above or below the melting point of the Al. The mixtures contain 50 at% of Al which decides about the sinterability of the materials. In Fig 7.5, 7.6& 7.7 the green and blue plot represents coefficient of thermal expansion & relative percentage of expansion respectively. The nature of the plots clearly displays the difference between solid phase and liquid phase sintering when the plots for 600^0C and other temperatures are observed. The relative % of expansion for 600^0C for all the mixtures (Ti-Al (1h), Ti-Al (4h) & Ti-Al (7h)) is almost directly proportional with the temperature and shows a steep increase when held for 1h. The steep increase in relative expansion can be attributed towards the coefficient of thermal expansion of Al. The thermal behavior shows a different pattern when the onset of liquid phase sintering occurs. It can be seen starting of liquid phase sintering in 650^0C for all the Ti-Al mixtures (Figs (7.5 (b), 7.6(b) &7.7 (b)). Though melting point of Al is 664^0C, due to milling of powder, Gibb's free energy of the system increases which is responsible for premature liquid phase formation of Al in the system. Ti-Al mixtures are more prone to self propagating high temperature synthesis of aluminides when liquid phase is formed. The small dip in the relative expansion just before 650^0C for the Ti-Al mixtures gives an idea of the formation of Al melt. The melt formed travels through the interparticulate voids which act as tiny capillaries for the sintering of the material. The sintering provides small dip for the coefficient of thermal expansion and the relative expansion. When it is held at 650 ^{0}C for 1h for soaking a steep increase in expansion is observed. The expansion can be attributed towards the expansion coefficient of the aluminides formed due to self propagating high temperature process and the gases evolved during the sintering process. Ti and Al have HCP and FCC crystal lattice, where as the intermetallics have bigger ordered structure like TiAl (L_{10} face centered tetragonal,), Ti_3Al (DO_{19}) and $TiAl_3$ (DO_{22}). These ordered structures have c/a ratio higher than that of the crystal structures of Ti and Al. For other temperatures like 700^0C, 750^0C and 800^0C for all Ti-Al mixtures the steep increase in the relative expansion during the soaking time can be described as the opportunity for the materials to complete the formation of intermetallics. For the above temperatures, a clear formation of step is found at 650^0C in the relative expansion behavior. This confirms the onset of liquid phase sintering near to 650^0C. But for the patterns above

650^0C displays the completion of formation of intermetallic phases. The part of the plots after the steep increase shows either a flattened part or a declined part during soaking time for 700^0C, 750^0C and 850^0C. The flattened part/ declined part of the plot can be attributed towards the stoppage in the formation of intermetallics. No more formation of intermetallics in turn helps in inhibiting the expansion. The inhibition of expansion / shrinkage in the materials can be explained by studying the behavior of shrinkage rate with temperature [Fig 7.8, Fig 7.9 & Fig 7.10].

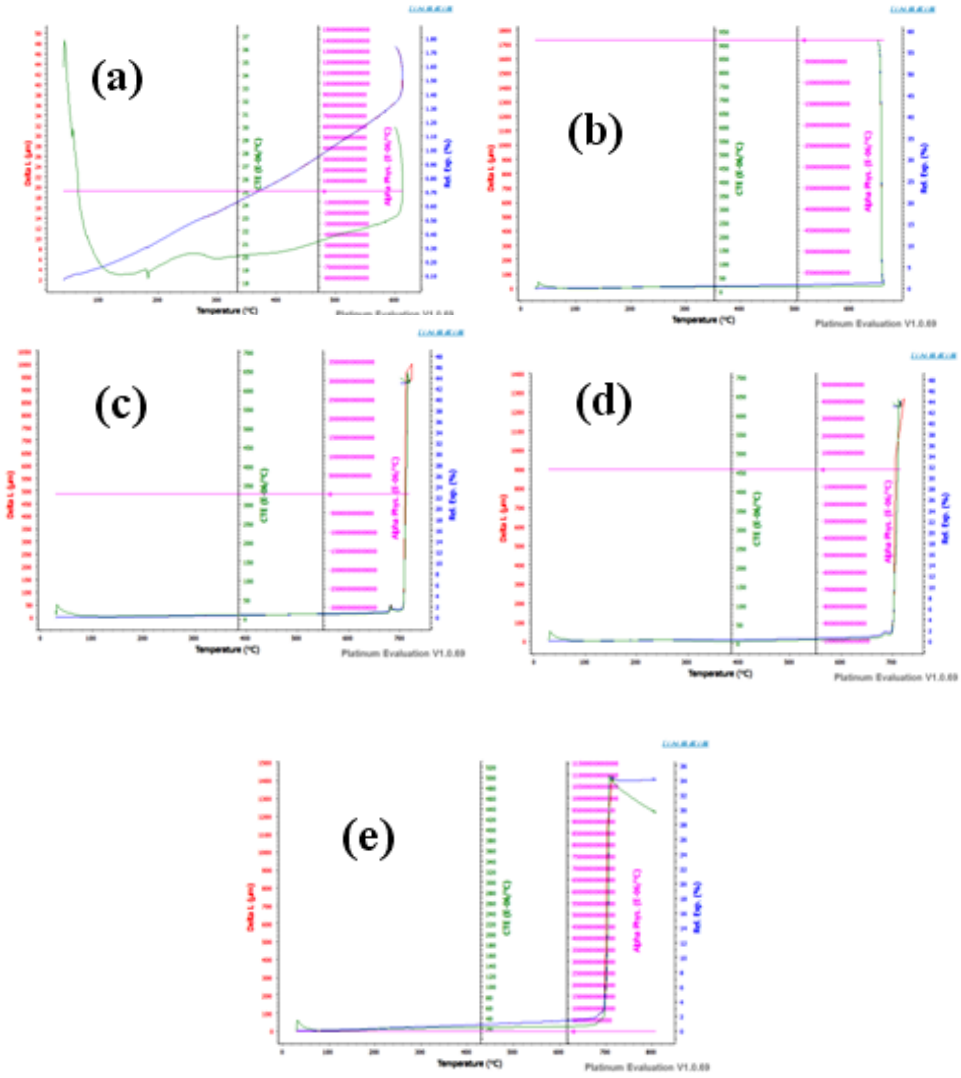

Fig 7.5 Dilatometric plots of Ti-Al (1h) Al mixture at (a) 600^0C (b) 650^0C (c) 700^0C (d) 750^0C and (e) 800^0C

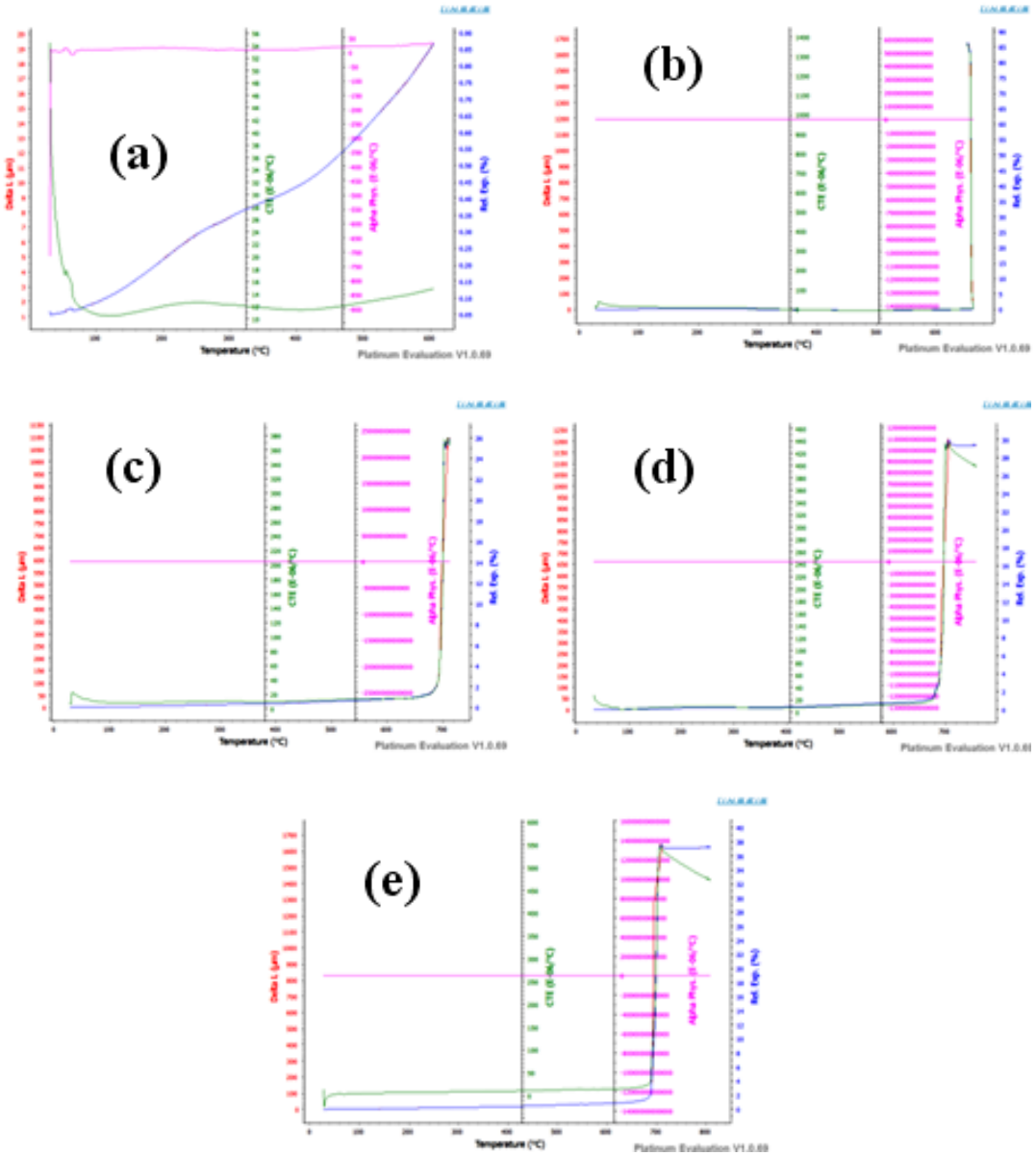

Fig 7.6 Dilatometric plots of Ti-Al (4h) Al mixture at (a) 600^{0}C (b) 650^{0}C (c) 700^{0}C (d) 750^{0}C and (e) 800^{0}C

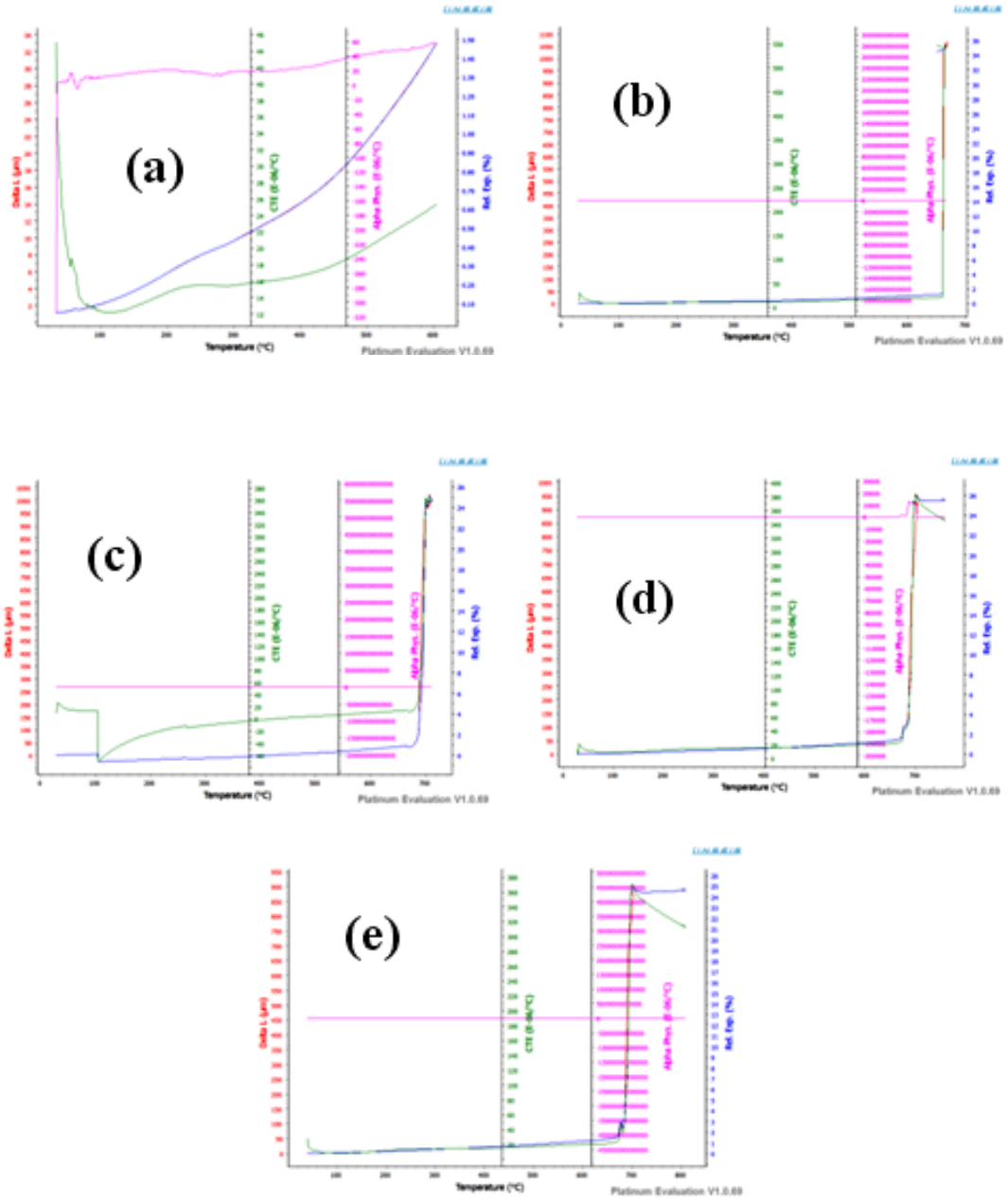

Fig 7.7 Dilatometric plots of Ti-Al (7h) Al mixture at (a) 600^{0}C (b) 650^{0}C (c) 700^{0}C (d) 750^{0}C and (e) 800^{0}C

7.2.2.5 Shrinkage/Expansion Rate Vs Temperature

The rate of expansion for the mixtures behaves directly with the increase in temperature. For 600^{0}C and 650^{0}C the behavior of graph shows both expansion and shrinkage unevenly. But for other temperatures the patterns show a part of constant rate

upto 690^0C and then a steep increase in rate is noticed which is having a maxima at 700^0C. The steep increase is followed by dip in the plots for the above temperatures. The nature of the patterns can be described on the basis of relative percentage expansion. The relative expansion data provides the fact that after steep increase the expansion is either nullified or shrinkage is started. The above nature describes the steep fall in the plots after inclination. The rate of the expansion is also the process rate which can be used for calculating the activation energy of the process. Though the relative expansion for 650^0C of all the mixtures confirms the onset of liquid phase sintering, but the expansion rate patterns are not similar with other higher temperatures. The heterogeneity in the nature is due to the onset of Al melt formed in the system, which travels through the pores. But at higher temperatures the Al melt is already formed at 650^0C, so the melt gets ample time to sinter the samples and form intermetallic phases. Specifically the increase in expansion rate with temperature is exponential and the leap is the highest when the same has been compared with 650^0C and 700^0[Fig 7.8, Fig 7.9 & Fig 7.10]. This deviation in expansion rate can be attributed for the process is of formation and completion of the ordered structures.

7.2.2.6 Average Shrinkage/Expansion Rate Vs Temperature

The behavior of average expansion rate with temperature decides the smoothness and the feasibility of the process. The rate of expansion of the process also gives an idea of the activation energy and the rate of the process. Fig 7.11(a) shows the variation of average expansion rate for various soaking temperatures for Ti-Al mixtures. The curve showing pattern for Ti-Al (4h) mixtures is smooth, without any undesired dip or inclination and have a constant behavior at the end. The smoothness of the curve can be attributed towards self propagating synthesis occurring during sintering. The particle sizes are also small enough to have improvement in the expansion when heated at higher temperatures. This fact is supported by the calculated activation energies, where for Ti-Al (4h) mixtures the magnitude is highest. The magnitude of the activation energy provides the easiness of feasibility of the process and the negative value confirms the exothermic reaction.

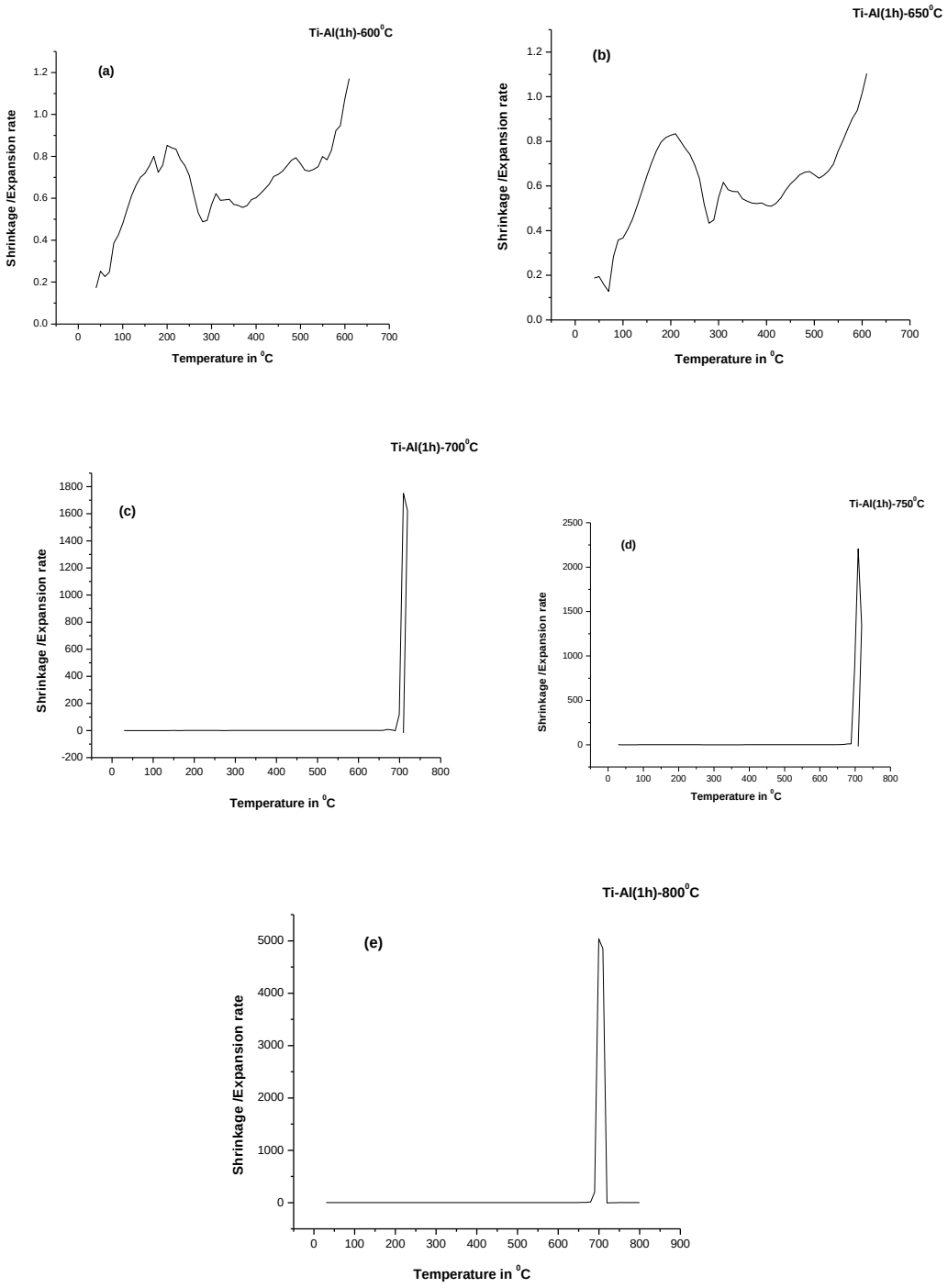

Fig 7.8 Variation of shrinkage/expansion with temperature for Ti-Al (1h) Al mixture at (a) 600^{0}C (b) 650^{0}C (c) 700^{0}C (d) 750^{0}C and (e) 800^{0}C

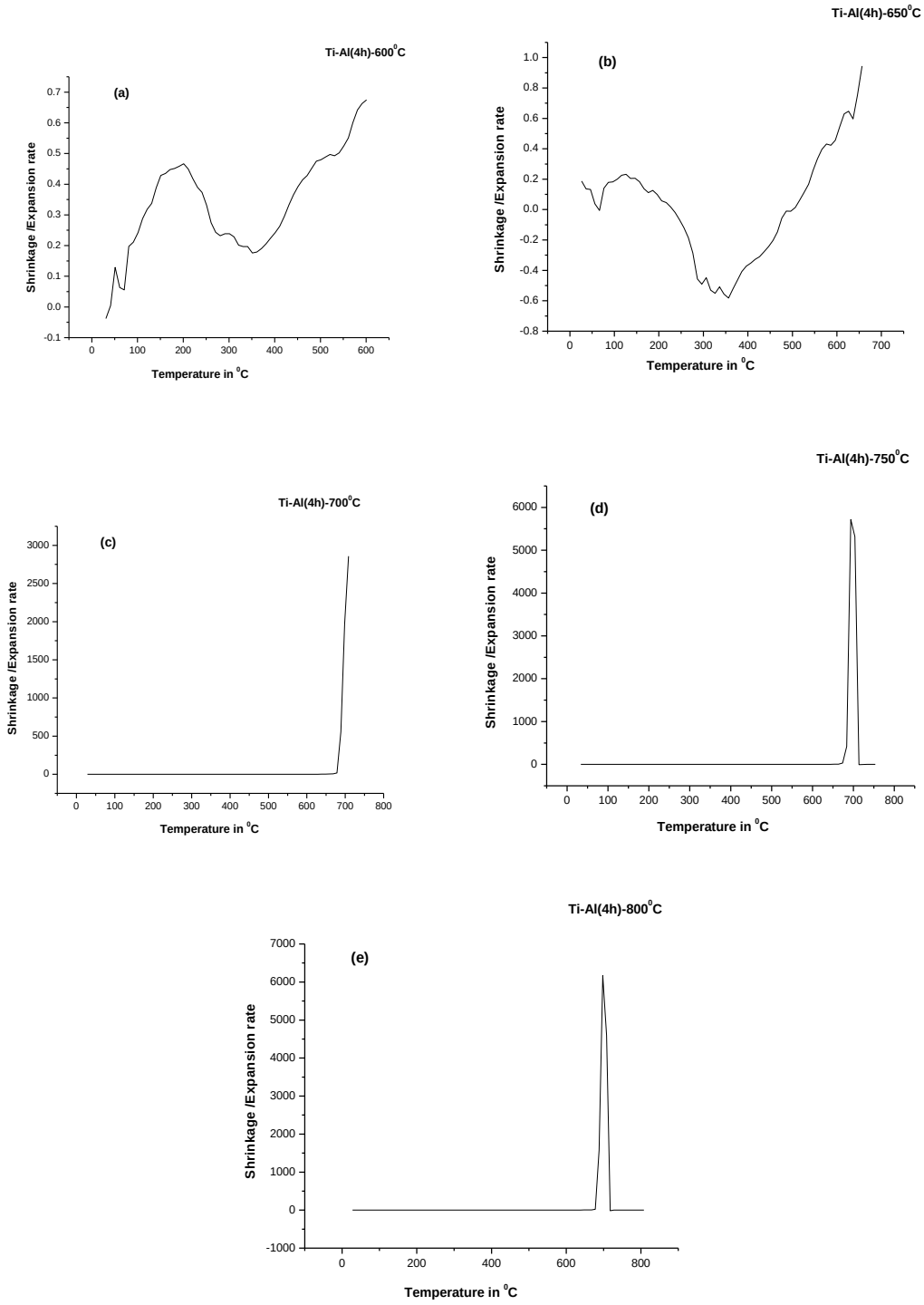

Fig 7.9 Variation of shrinkage/expansion with temperature for Ti-Al (4h) Al mixture at (a) 600^{0}C (b) 650^{0}C (c) 700^{0}C (d) 750^{0}C and (e) 800^{0}C

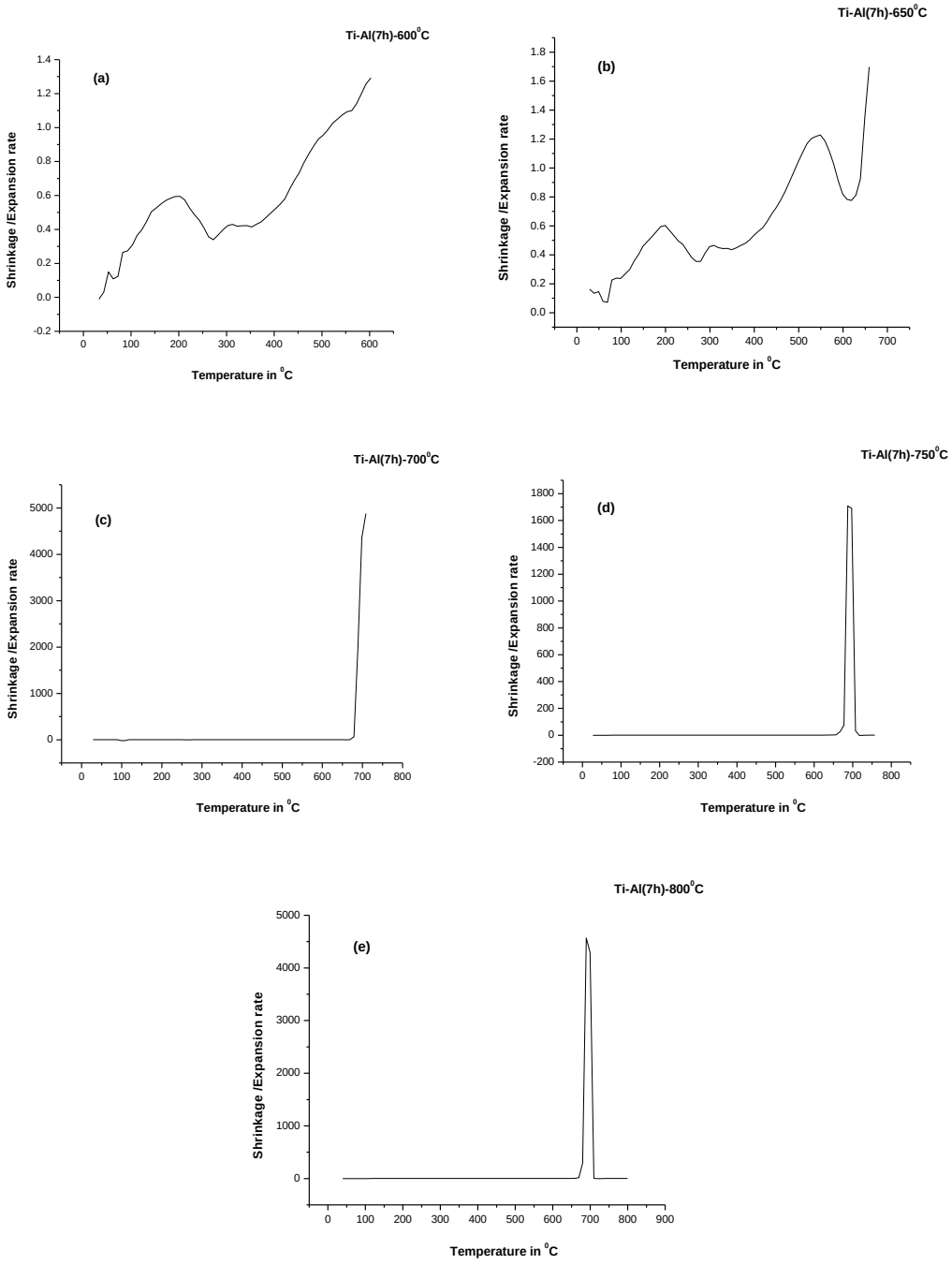

Fig.7.10 Variation of shrinkage/expansion with temperature for Ti-Al (7h) Al mixture at (a) 600^{0}C (b) 650^{0}C (c) 700^{0}C (d) 750^{0}C and (e) 800^{0}C

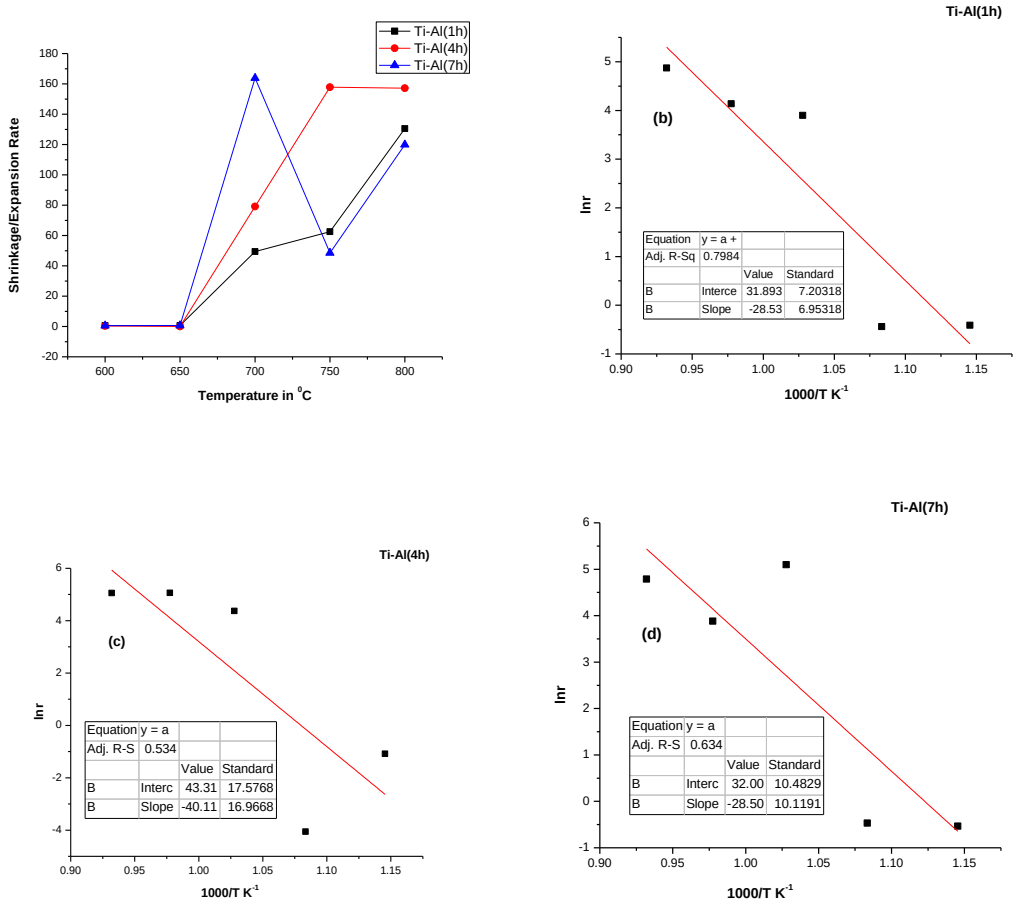

Fig 7.11 shows (a) comparative average shrinkage/expansion rate vs Temperature and activation energy of (b) Ti-Al (1h) (c) Ti-Al (4h) (d) Ti-Al (7h)

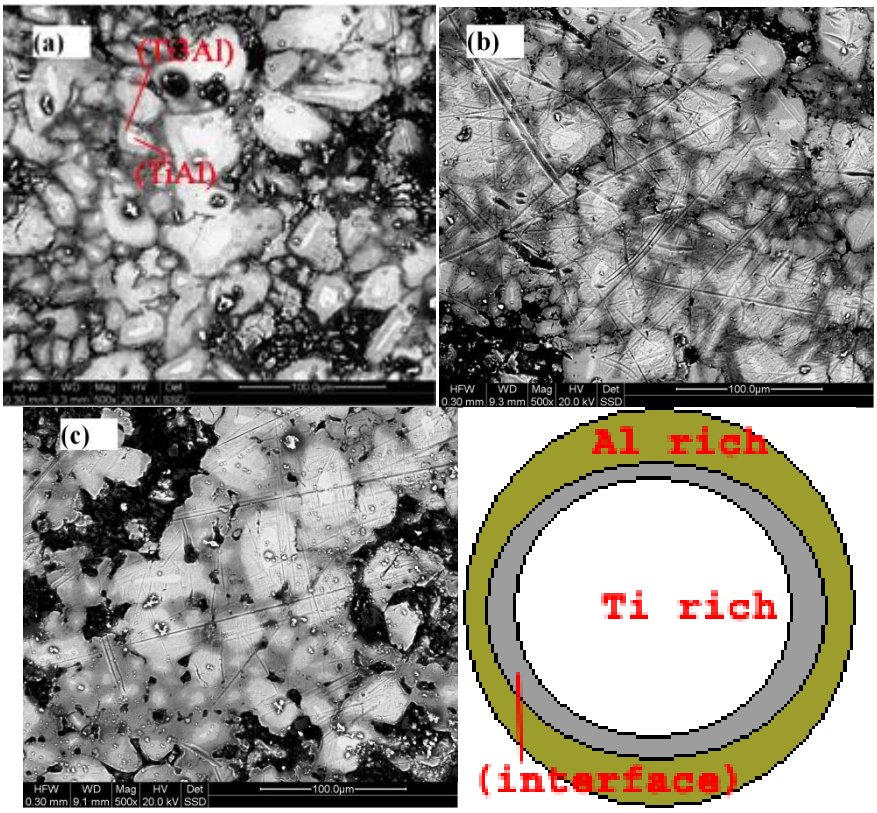

Fig7.12 FESEM micrographs of sintered samples (a) Ti-Al (1h), (b) Ti-Al (4h) (c) Ti-Al (7h)& (d) Schematic diagram representing Ti rich and Al rich regions and the interface

7.2.2.7 Microstructural Evolution

The FESEM micrographs (Figs (7.12 (a-d)) show that the microstructures contain bright Ti rich regions and dark Al rich regions. The interface as represented in Fig7.12 depicts the diffusion of Al into Ti rich regions during the reactions in sintering. The sintering process leads to various phases in the structure with different grey contrast. Darker the shade higher is the Al content in the phases. Most probably the microstructure can be described as the Ti (bright region) islands inside the Ti_3Al grain locale. XRD patterns depict the formation of the TiAl and Ti_3Al, which can be seen in the microstructures with Ti rich region forming TiAl and Al rich region are in the perimeter of the Ti rich region forming Ti_3Al. The interface though small in content can be attributed towards the formation of intermediate phases.

7.2.3 *Summary*

In this section, the exothermic temperatures, activation energy, and percentage relative expansion with various particle sizes of Al in Ti-Al mixtures were compared. After the study of the above results, Ti-Al (4h) mixtures show the optimized behavior for percentage relative expansion with highest of activation energies. The above Ti-Al mixture evolves activation energy of - 40.11 kJ/mol. The microstructures also provide the information of lack of pores in case of Ti-Al (4h) mixtures.

7.3 Dilatometric Behavior of the Ti-Al Intermetallics Containing Various Ti Particle Size

The sintering of Ti-Al intermetallics was studied by dilatometric analysis. Ti powders of various particle size were prepared by planetary ball milling. The Ti powders of initial particle size of ~44 μm were milled in a planetary ball mill for 1h, 5h and 10h. The resultant particle sizes of the above were approximately 100, 28, and 7μm respectively. These Ti powders were mixed with Al powders of the order of ~44 μm separately in in the compositional ratio of 1:1 at%. The thermal behavior of the mixtures was calculated by DTA. The reactive sintering temperatures of the mixtures were determined using DTA and the transformation of phases was studied using powder diffraction. Using FESEM, microstructural evolution was explored due to sintering. Dilation of the sinters, % relative expansion and coefficient of thermal conductivity was determined using dilatometry of the mixtures. Solid state sintering and transient liquid phase sintering studies were done to calculate the behaviors of the mixtures with various Ti particle size.

7.3.1 *Experimental Procedure*

The Titanium and Aluminium powders taken for milling and the milling condition described can be referred from section 7.2.1

The Titanium powder obtained was milled in a RETSCH PM 400/2 planetary ball mill for different time extent of 1, 5 and 10h. The hardened steel balls and jars were used as the medium for milling and the ball to charge weight ratio were kept as 5:1. To avoid the agglomeration of powders during milling, toluene is used as the process control agent. The charge and the balls were totally submerged in the toluene during milling

condition to avoid oxidation of powders. The Ti powders milled for time extents of 1, 5 and 10h resulted a mean particle size approximately of 100, 25-28 and 7-9µ respectively. The Titanium powder of various particle sizes were blended with aluminum powder of average particle size of 44 µ to prepare blends of 50:50at%. The blending of powders was carried out in mortar and pestle for 5 mins followed by blending in ball mill for 30 min at 70 rpm in dry condition. The powder blends of Ti (1h)-Al, Ti (5h)-Al and Ti (10h)-Al were sintered in high pure inert environment (argon) for 1 hour duration at 677^0C, 725^0C and 747^0C respectively where the temperatures for sintering were decided by studying the thermal analytical results of the blends. The powder mixtures were compacted at 175 MPa to a cylindrical shape of the dimensions of 16.4 mm diameter and 5mm thickness. The sintered samples were polished and ground with different grits emery papers followed by polishing cloths. The characterization of XRD, FESEM, Archimedes principle and Dilatometric phenomenon subjected to the samples can be referred from section 7.2.1

7.3.2 *Results and Discussion*

7.3.2.1 XRD Analysis of sintered compacts

The phase evolutions occurred during sintering was explored by XRD which is shown in Fig7.13. Fig7.13 shows the diffraction patterns of the sintered compacts of Ti-Al mixtures of various Ti particle sizes. The compacts were sintered at their respective sintering temperatures. The diffraction pattern of Ti-Al mixture of Ti(1h)-Al sintered at 677^0C reveals the synthesis of TiAl and Ti_3Al phases, which referred from the JCPD code numbers 00-042-1137 and 00-014-0461 respectively for the phases.

Table 7.2: Milling and mixing parameters

Planetary Ball mill Details (Retsch PM 400/2)	**Milling Parameters**
Milling Balls- Hardened steel balls	Milling Media-Toluene
Milling Jars- Hardened steel jars	Charge to Ball ratio-1:5
Jar capacity- 500 ml	Milling speed- 200 rpm Vial Speed- 400 rpm
PCA-Toluene	Total time of milling- 1h,5h&10h
	Weight of initial charge- 30gms
Mixing parameters	
Milling Balls- Hardened steel balls	Charge to Ball ratio-1:3
Milling Jars- Hardened steel jars	Milling speed- 70 rpm Vial Speed- 140 rpm
Jar capacity- 500 ml	Total time of mixing-30mins
Argon atmosphere	Weight of initial charge- 30gms

In comparison with the mixtures Ti(0h)-Al and Ti(1h)-Al , Ti(5h)-Al, Ti(10h)-Al showcase slightly broadened peaks, though in all the cases both the intermetallics phases are formed. The formation of the comparatively broadened intermetallics phases in the diffraction pattern is attributed towards the amorphization of Ti powders at higher extent of milling. The decrease in intensity of those peaks also can be explained on the basis of the formation of finer Ti particles at higher extent of milling which in turn infers the synthesis of the refined Ti_3Al and TiAl intermetallics phases. As the milling of Ti powders were subjected at lower rpm and only upto 10 hours, the shifting of peaks were unnoticeable, though the lattice parameter has been lowered to certain percentage.

The enthalpy values for the formation of TiAl and Ti_3Al are −75 and −73 kJ/mol respectively and the DTA graphs show the presence of exothermic peaks at 677^0C, 725^0C and 747^0C for Ti(1h)-Al, Ti(5h)-Al and Ti(10h)-Al respectively.

7.3.2.2 Microstructure

The Morphological evolution of the Ti powders milled for various durations are displayed in Fig7.14 (a-c). The Ti powders are milled for 1h, 5h and 10h. The milled powders showed the fractured surfaces due to plastic deformation by ball-particle-ball collisions, ball-jar (wall)-ball collisions. The milling process involves the phenomenon of agglomeration and fracture.The milling of particles, first show the process of cold welding, whichis attributed towards the formation of nascent surfaces of particles.The free energy of the nascent surfaces is such high that it immediately forms the cold welding which in turn induces the agglomeration of the powders.

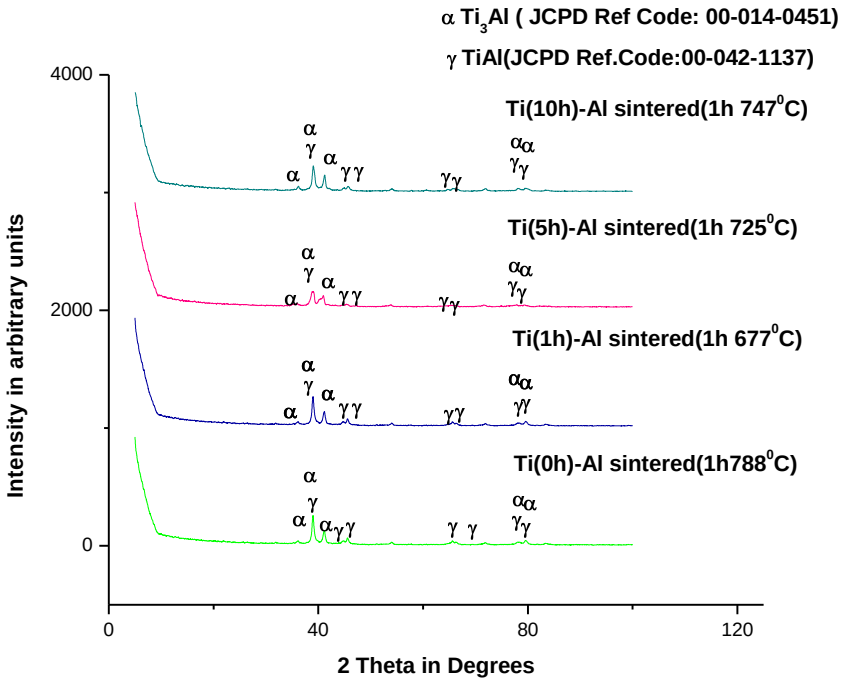

Fig 7.13 XRD pattern of Ti (0h)-Al, Ti (1h)-Al, Ti (5h)-Al and Ti(10h)-Al mixtures sintered at their respective temperatures

When the powders were subjected to increased extent of milling, the work hardening of the particles overrules the free energy of the nascent surfaces and agglomerated clumps, which starts to increase the fracturing of the surfaces in comparison to the simultaneous

process of agglomeration. Thus the higher extent of milling helps in lowering the particle size. The lowering of particle size can be described as the comparative process between two phenomena of agglomeration and fractures. After time of milling both the phenomena sets up an equilibrium, which inhibits the further lowering of particle sizes. The morphology of Ti powders milled for 1h reveals the fact that the powders are agglomerated and the flattened due to plastic deformation of the powders and also can be attributed towards the ductility of the powder particles. The morphological study depicts the approximate particle size attained by 1h milled Ti powders are 100 µ. The work hardened splats of Ti powders when further milled upto 5h, the particle sizes get reduced to an approximate size of 28µ. As shown in Fig 7.14(c) the Ti particles milled for 10h, produces particles of the order of ~7µ. The uneven particle morphology of the milled powders is due to the fractured surfaces created during the collisions.

7.3.2.3 DTA Study

The melting of Al powderwas revealed by endothermic peaks present in the plots. The melting poit for Ti (0h)-Al is 664^0C, but for the other compositions it is 668^0C. The melting point is not affected as the external energy is applied to the system by the milling. The exothermic temperatures show an increasing trend.

7.3.2.4 Dilatometric Study

The relative percentage of expansion and the coefficient of thermal conductivity is studied using dilatometry (Fig 7.16, 7.17 & 7.18). The characteristics of dilation also have been studied by varying temperature. The effect of Ti particle size and temperature also has been analyzed using the expansion rate and activation energy of the process to have optimized route as the resultant.

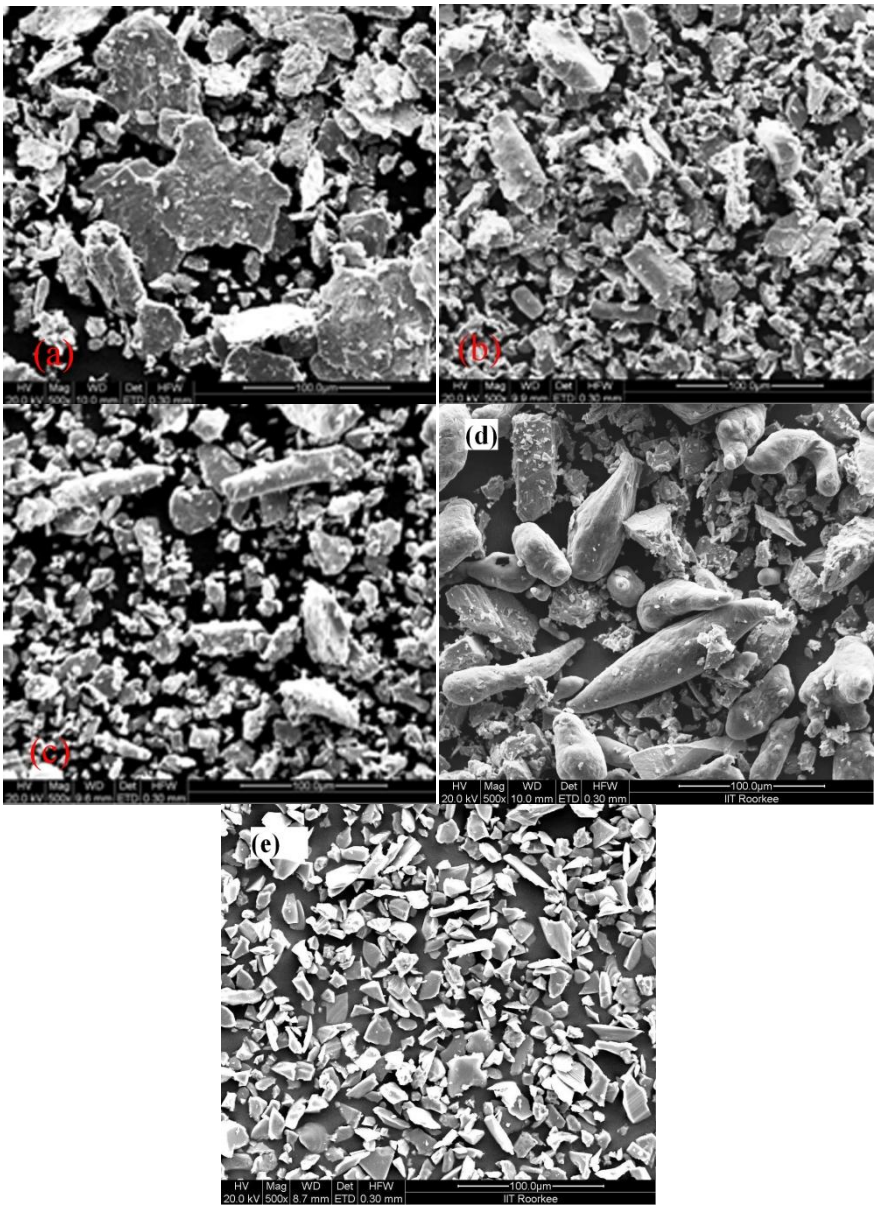

Fig 7.14 FESEM micrographs of milled Al powders for different milling times (a) 1h milled, (b) 5h milled, (c) 10h milled,(d) As received Al & (e) As received Ti powders

The dilation behavior of the compacts was explored for 600^0C, 650^0C, 700^0C, 750^0C & 800^0C temperatures. The dilation characteristics of the compacts not only describe the coefficient of thermal expansion and also explain about the route with extent of sintering process. The temperatures for dilation behavior were taken on the basis of the melting point of Al and the exothermic peaks describing the self propagating high temperature synthesis of Ti-Al intermetallics. Two different type of sintering behavior were seen in this process.

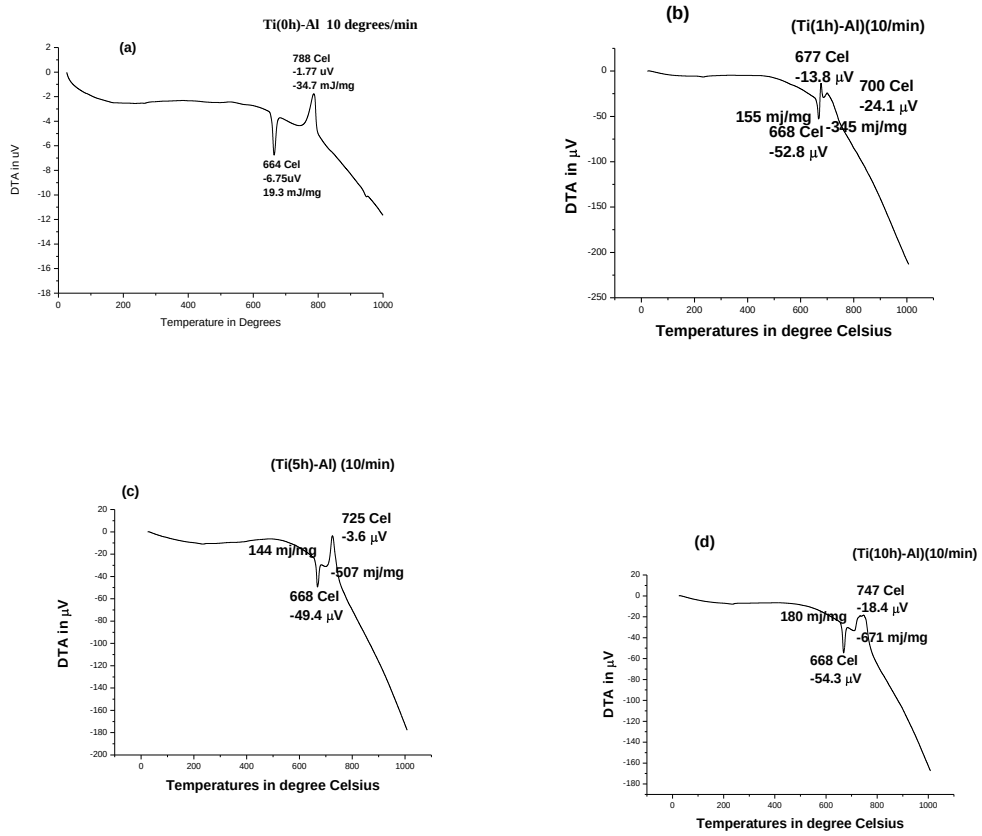

Fig 7.15 Thermal analysis plots of Ti-Al mixture at 10^0C /min (a) Ti(0h)-Al (b) Ti(1h)-Al (c) Ti(5h)-Al and (d) Ti(10h)-Al

Due to the absence of Al melt for the samples heated at 600^0C, solid state sintering occurs. But for higher temperatures, molten Al plays a vital role in sintering processes and transient liquid phase sintering dominates the whole process. The transient liquid phase sintering is also facilitated due to the traversing of molten Al through the fine pores or interparticulate voids created by Ti particles. Though the melting point of Al is 664^0C, but the semi liquid phase is formed before that's why the samples heated at 650^0C display the transient liquid phase sintering.

The plots of Figs 7.16, 7.17 and 7.18 represent the relative percentage of expansion and coefficient of thermal conductivity of Ti (1h)-Al, Ti (5h)-Al and Ti (10h)-Al respectively. The solid state sintering behavior of the intermetallics can be clearly studied for the materials heated at 600^0C. The relative percentage of expansion for the samples heated at 600^0C show a maximum of 2.8 % for Ti (1h)-Al mixture. For other mixtures the percentage of expansion for the same temperature is getting lower due to

the size of Ti powder. The size of Ti for the mixture Ti (1h)-Al is ~100 μ but for the particle size before the sintering is lesser, which is the main cause of lesser % of expansion. The % of expansion for other temperatures increases as the holding temperatures are increased. This proportionality behavior can be attributed towards the increase in the time of heating. Especially for temperatures higher than 650^0C a step is noticed in the plots for relative percentage of expansion. At higher temperatures the steps can be attributed towards the onset of sintering which can be studied the plots of soaking temperatures of at 650^0C. The effect of Ti particle size on relative expansion can be depicted as directly proportional. This characteristics show that with decrease in the particle sizes of Ti, the percentage relative expansion is decreasing. The dip just before the steep increase in the plots at the soaking temperatures confirms the onset of sintering. Though the process of liquid phase sintering suggests the shrinkage of the compacts, the expansion process is predominant. The expansion in the materials can be partly due to the formation of gases that renders the porosities inside the samples. But the main reason of bulging of the compacts can be given to the formation of intermetallics during the sintering. Formation of Ti-Al during reactive sintering by self propagating high temperature synthesis process, which forms TiAl (L_{10} type face centered tetragonal), Ti_3Al (DO_{19}) and $TiAl_3$ (DO_{22}) ordered structures. The c/a ratio of the above compounds is higher than that of the lattice structures Ti and Al, which causes the expansion in the compacts.

The formation of intermetallics occurred during the steep increase in the relative expansion plots in soaking process. After the completion of synthesis, the relative expansion shows either a constant or declined trend. The constancy or shrinkage can be attributed towards the stoppage of formation of intermetallic phases, which prevents further expansion of compacts. The rate of the process will provide better idea about the expansion and activation energy [Figs 7.19, 7.20, 7.21 & 7.22].

7.3.3.5 Shrinkage/Expansion Rate Vs Temperature

The rate of expansion for Ti-Al mixtures at 600^0C displays unevenly placed dips and inclination in the plots. The rate of expansion can be described as the rate of the sintering process. The rate of expansion shows a common trend as the rate remains constant upto 650^0C.

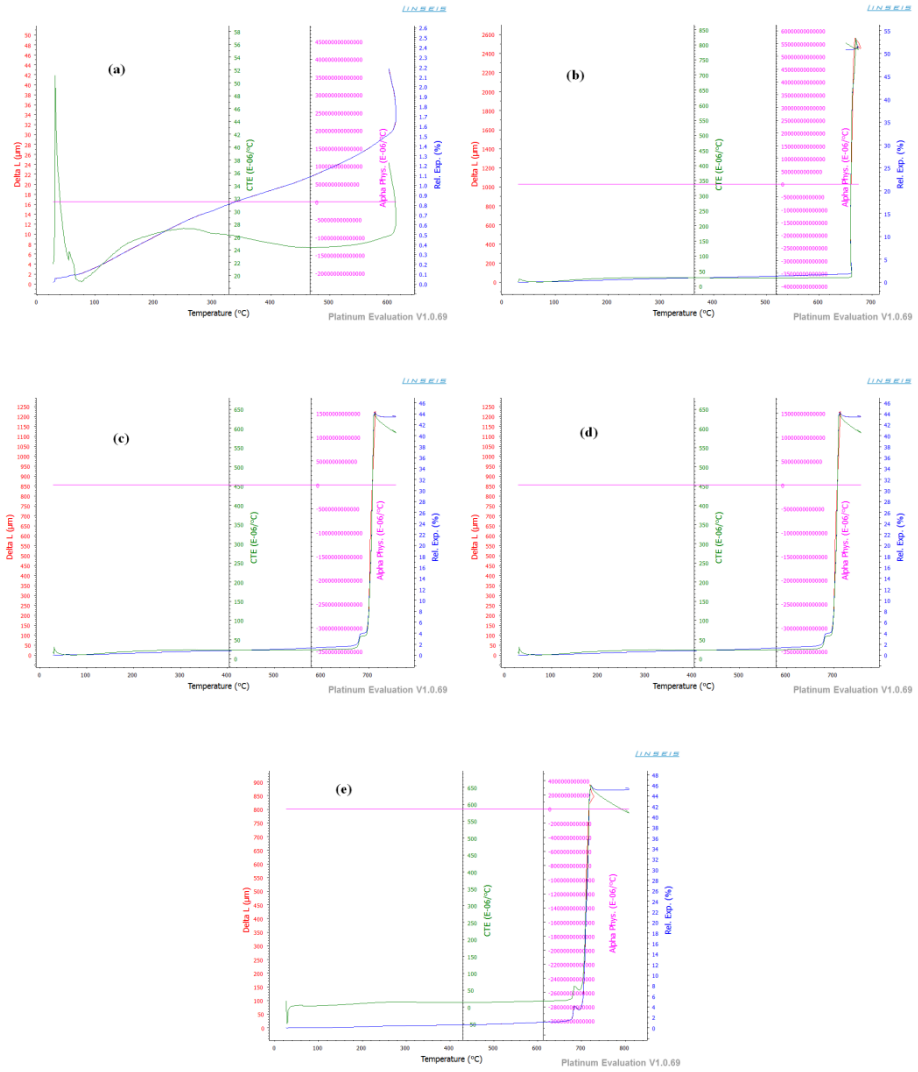

Fig 7.16 Dilatometric plots of Ti(1h)-Al Al mixture at (a) 600^{0}C (b) 650^{0}C (c) 700^{0}C (d) 750^{0}C and (e) 800^{0}C

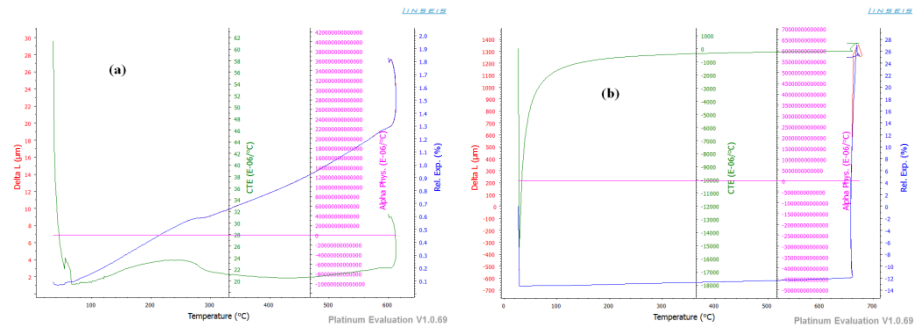

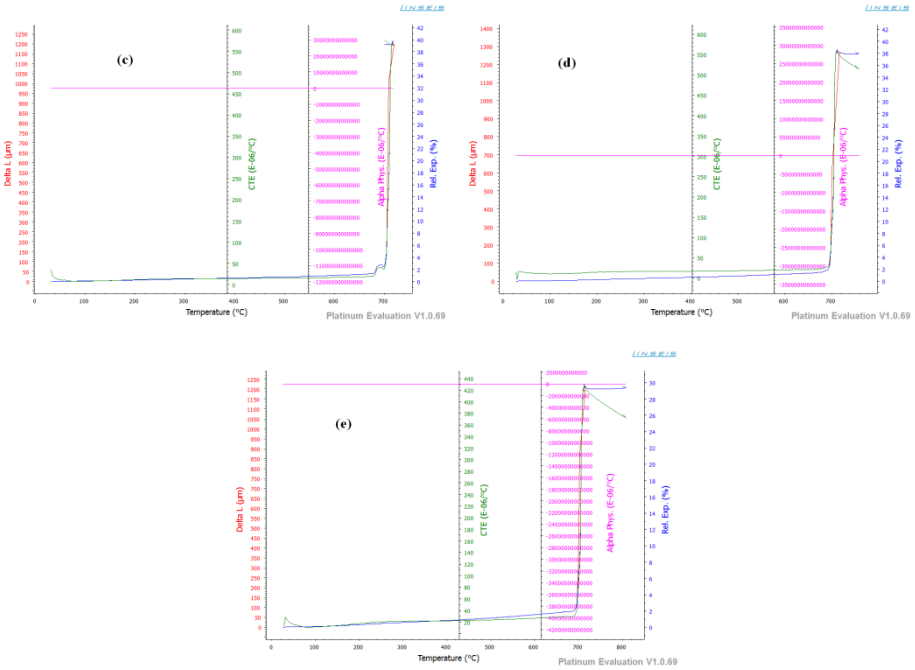

Fig 7.17 Dilatometric plots of Ti (5h)-Al Al mixture at (a) 600^{0}C (b) 650^{0}C (c) 700^{0}C (d) 750^{0}C and (e) 800^{0}C

But the onset of liquid phase sintering brings steep increase in the rate due to the formation of ordered intermetallic structures simultaneously. For all the Ti-Al mixtures the maximum expansion rate was found at 700^{0}C.The maxima at above temperature can be described as the maximum formation of intermetallic phases or the rate of formation of intermetallic phases is the highest.

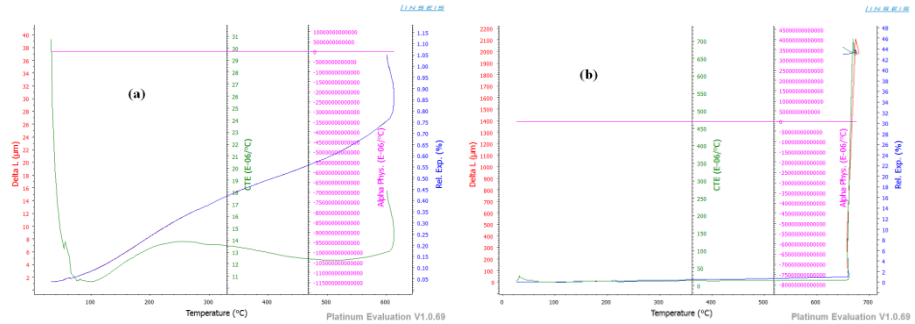

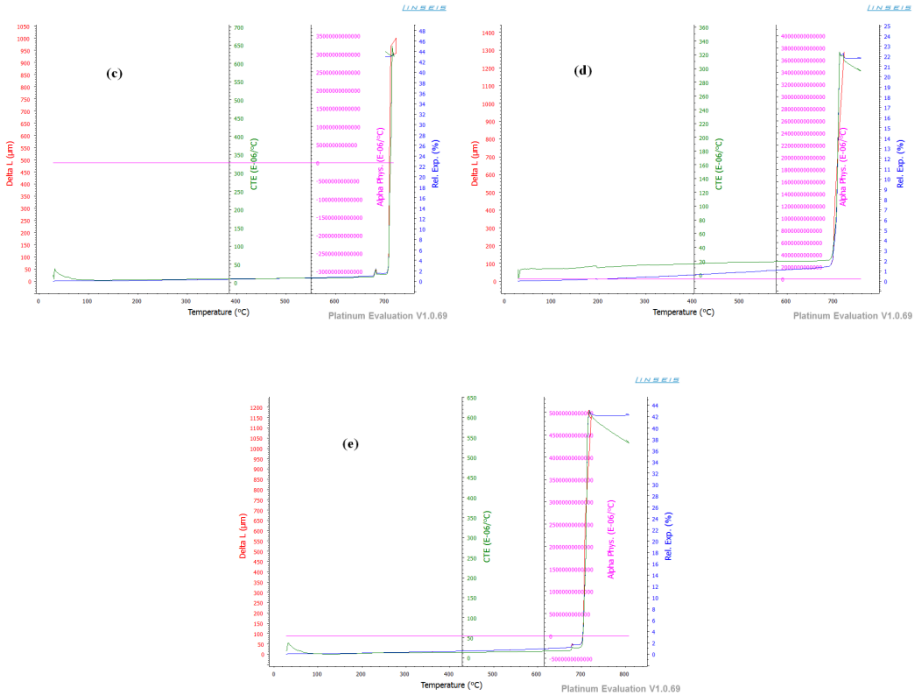

Fig 7.18 Dilatometric plots of Ti (10h)-Al Al mixture at (a) 600^{0}C (b) 650^{0}C (c) 700^{0}C (d) 750^{0}C and (e) 800^{0}C

The inclination of the plot of expansion rate is followed by a dip. The dip in the expansion rate can be explained as the inhibition for further expansion. The completion in the formation of intermetallic phases, leads to the prevention of expansion. The smaller part in the plots of relative expansion after the steep increase is the reason for steep decrease in the rate of expansion. For all the mixtures of Ti-Al, the Ti (5h)-Al mixture shows the highest rate of expansion. The increase in the rate of expansion can be explained as the ease of traversing of liquid Al through the interparticulate voids of Ti resulting in increase in the rate of reaction of forming of aluminides.

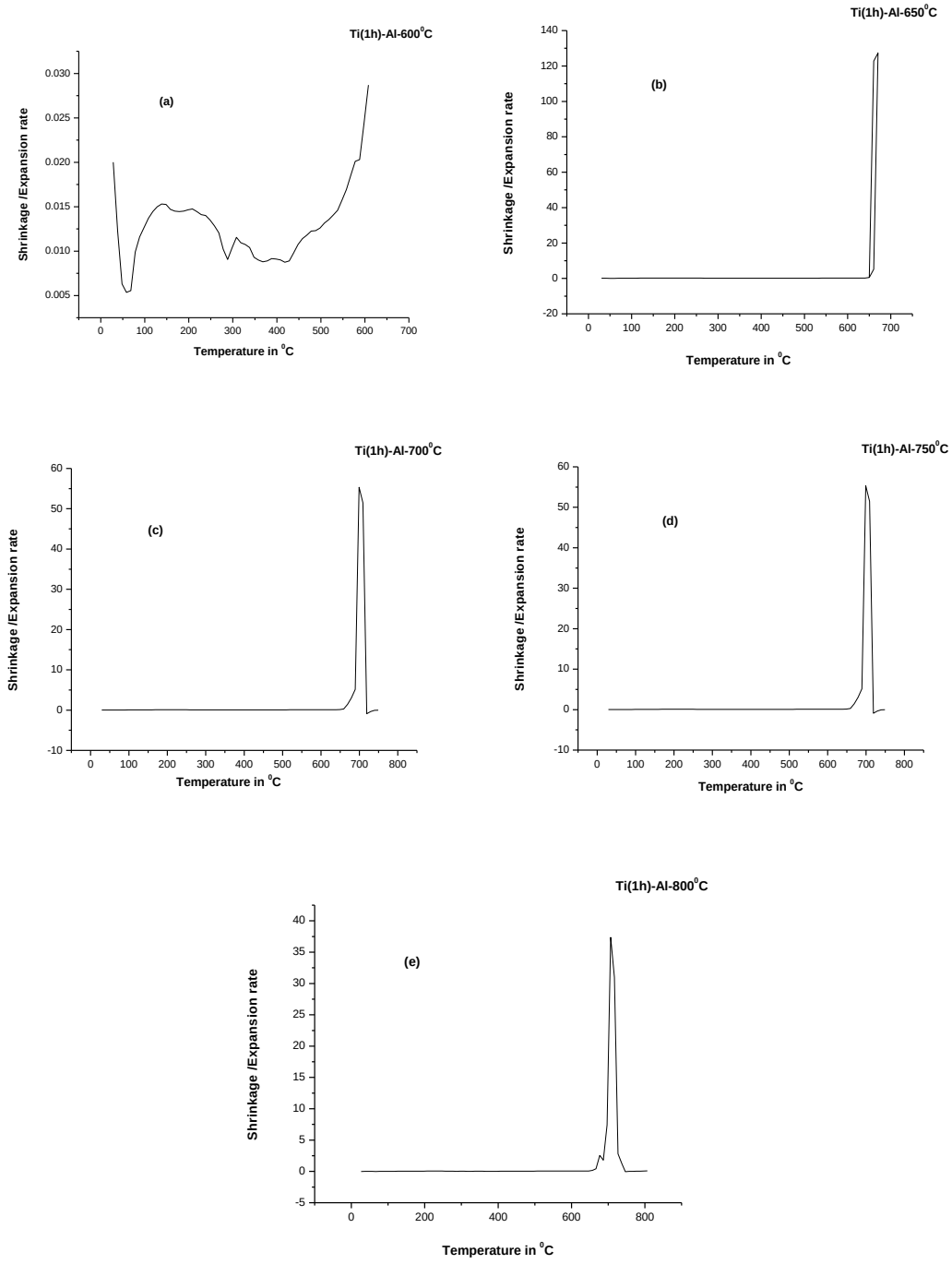

Fig 7.19 Variation of shrinkage/expansion with temperature for Ti (1h)-Al mixture at (a) 600^{0}C (b) 650^{0}C (c) 700^{0}C (d) 750^{0}C and (e) 800^{0}C

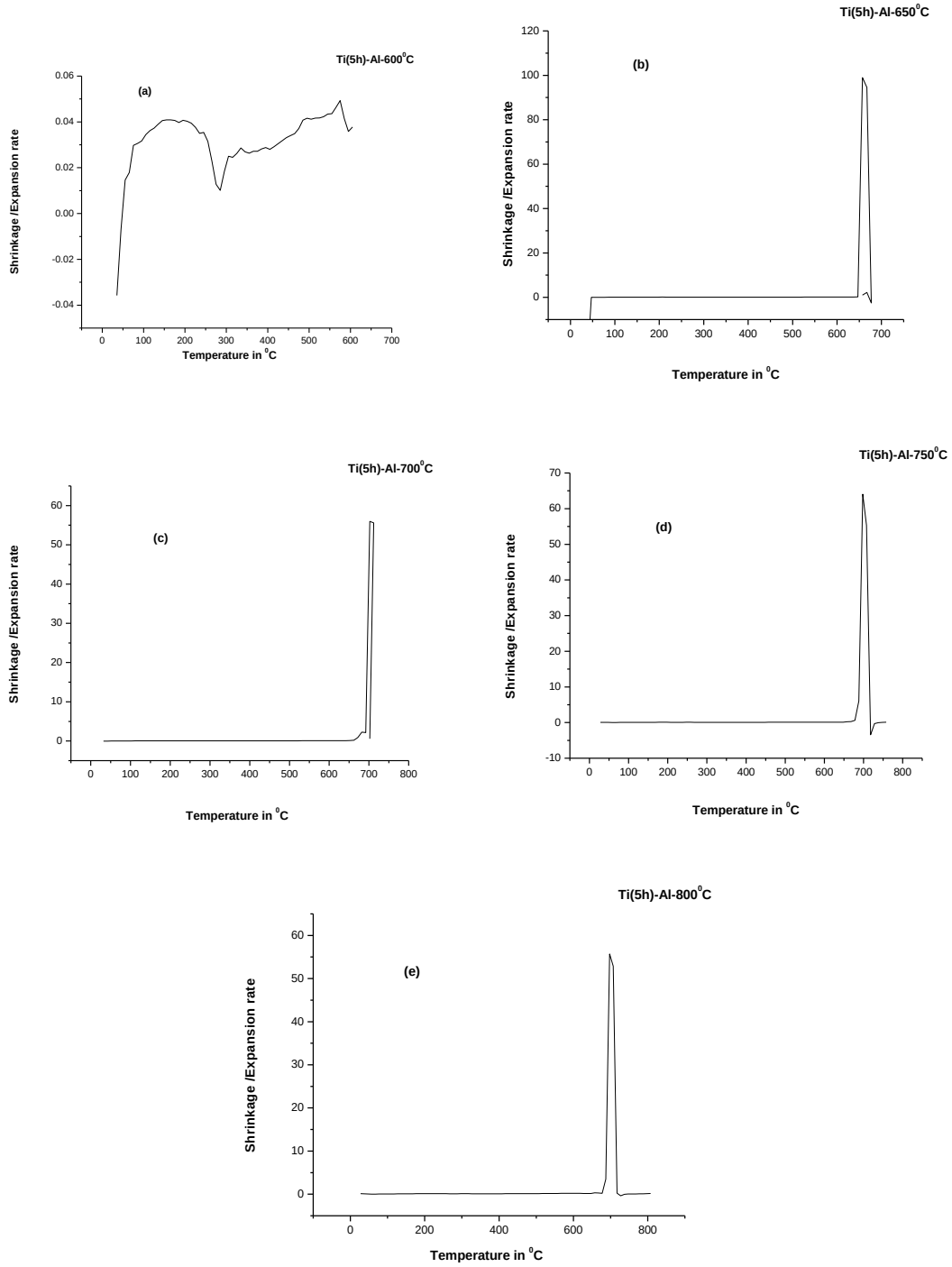

Fig 7.20 Variation of shrinkage/expansion with temperature for Ti(5h)-Al mixture at (a) 600^{0}C (b) 650^{0}C (c) 700^{0}C (d) 750^{0}C and (e) 800^{0}C

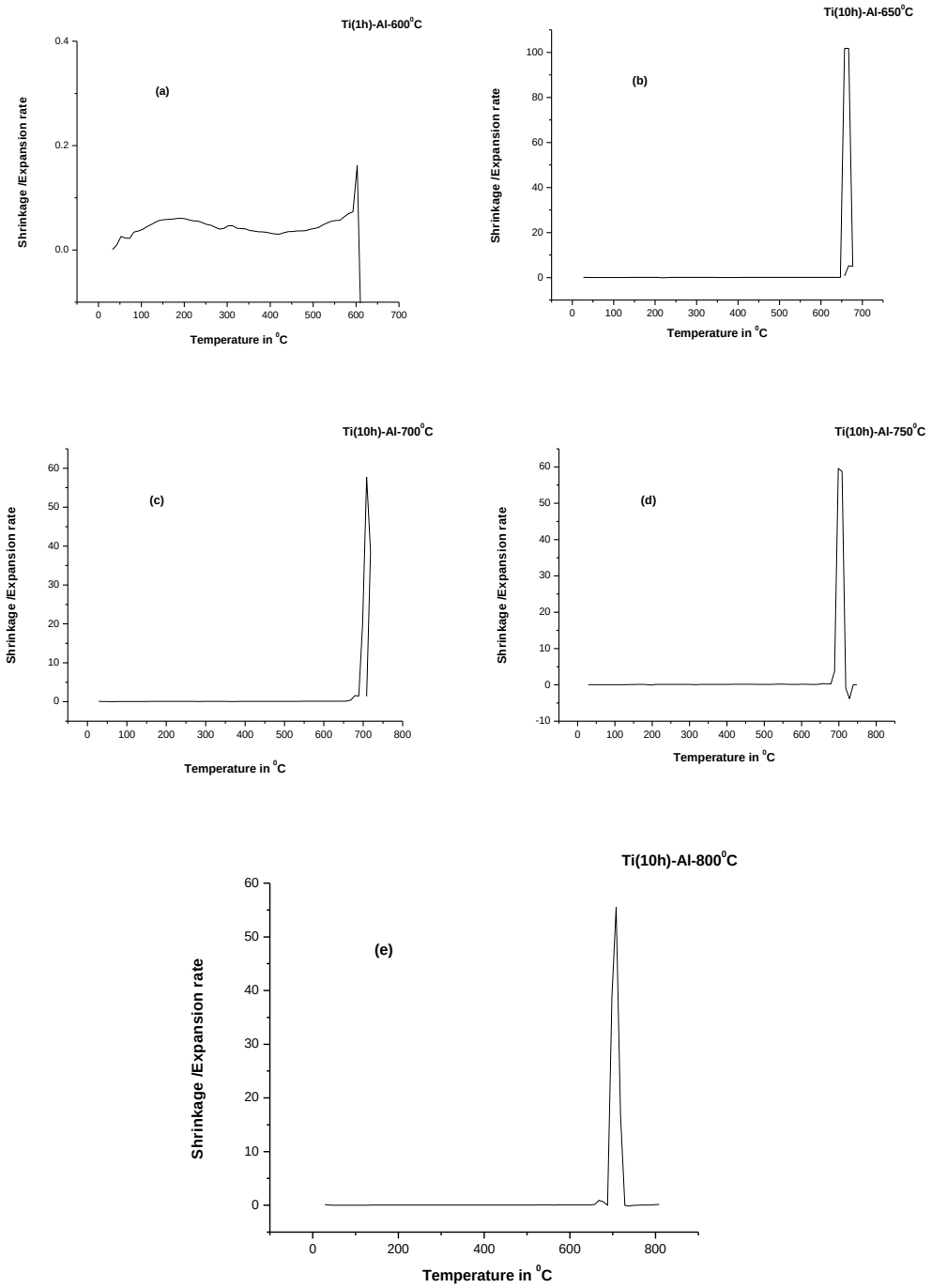

Fig 7.21 Variation of shrinkage/expansion with temperature for Ti(10h)-Al mixture at (a) 600^{0}C (b) 650^{0}C (c) 700^{0}C (d) 750^{0}C and (e) 800^{0}C

7.3.3.6 Average Shrinkage/Expansion Rate Vs Temperature

The effect of temperature on mean expansion rate depicts the feasibility and smoothness of the reaction. Activation energy and rate of the reaction also can be explained on the basis of rate of expansion. The traces in the Fig 7.22 (a) display the effect of particle size on the expansion rate at various holding temperatures. The graph

showing smooth characteristics for Ti (5h)-Al mixture as compared to other mixtures. Optimized activation energy of -15.5 kJ/mole is also a factor for better results of Ti (5h)-Al mixtures (Fig 7.22). Particle size of Ti is small enough for Ti (5h)-Al mixtures which provide voids for easy traversing of liquid Al melt. The magnitude of the activation energy explains the ease of the process and the negative value confirms the exothermic reaction.

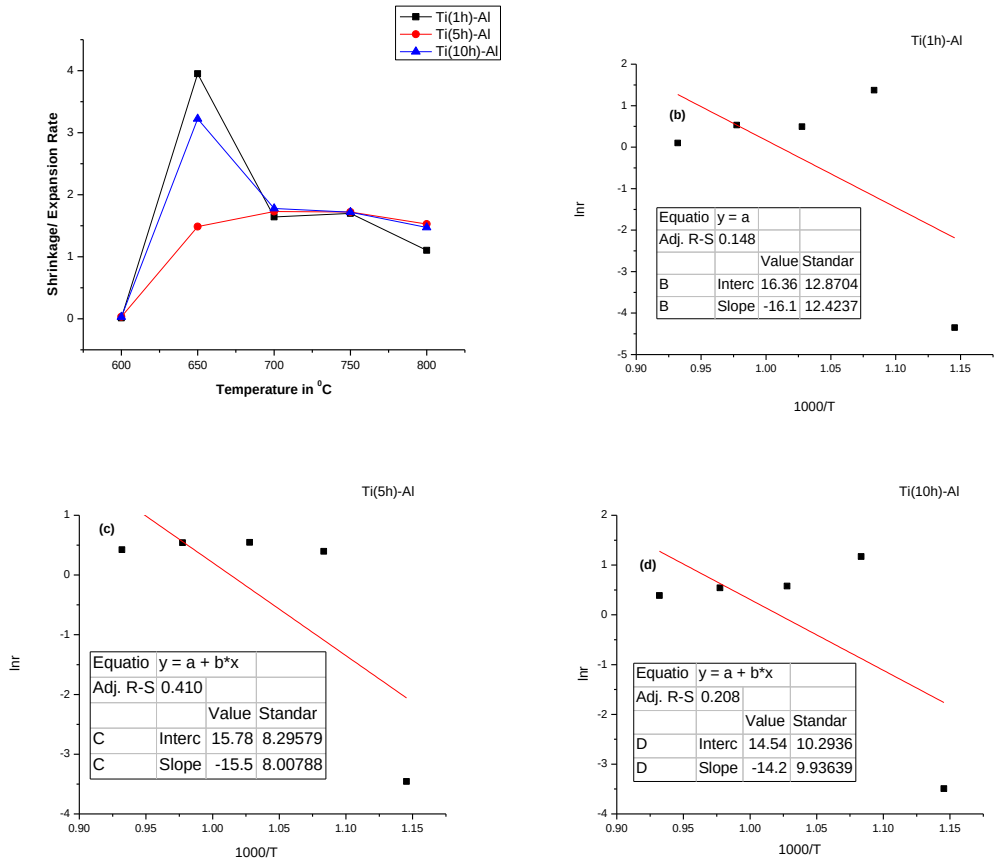

Fig7.22 shows (a) comparative average shrinkage/expansion rate vs Temperature and activation energy of (b) Ti(1h)-Al (c) Ti(5h)-Al) (d) Ti(10h)-Al

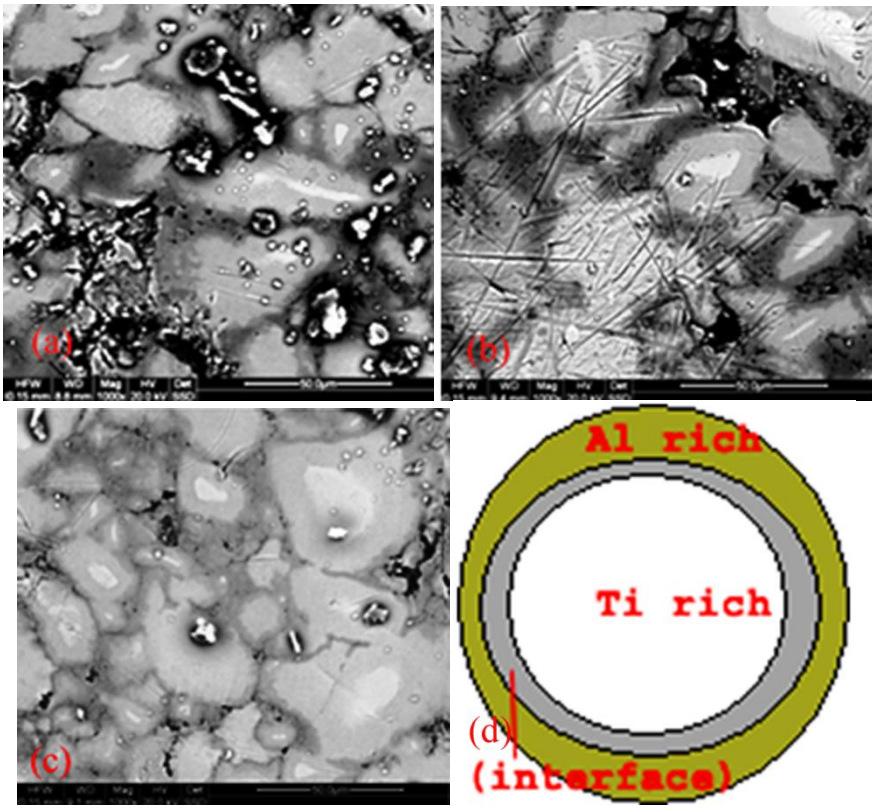

Fig 7.23 FESEM micrographs of sintered samples (a) Ti (1h)-Al , (b) Ti (5h)-Al (c) Ti (10h)-Al & (d) Schematic diagram representing Ti rich and Al rich regions and the interface

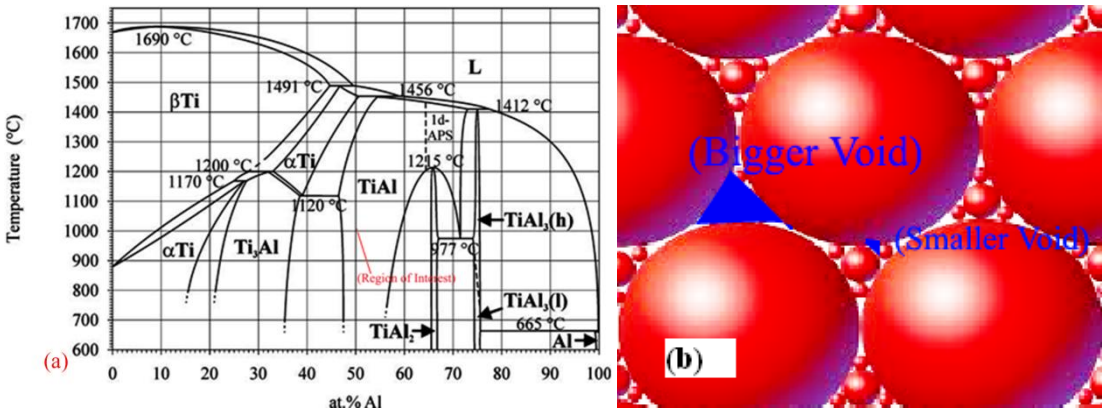

Fig 7.24 shows (a) A systematic phase diagram of Ti-Al binary system [28] (b) Thematic diagram explaining size of voids with change in particle sizes

7.3.3.7 Microstructural Evolution

FESEM micrographs in Fig 7.22 (a-c) show the microstructures of sintered compacts which containing bright Ti rich and dark Al rich regions. The diffusion of Al into Ti rich regions is clearly seen in the microstructures, with various grey contrasts. The grey

contrast shows the presence of various intermetallics phases. Darker the phase, higher is the Al content. The microstructures can be explained as the islands of Ti (bright region fitted in the Ti_3Al grain locale. The XRD pattern (Fig7.13) also reveals the formation of Ti_3Al and TiAl, in the perimeter of Ti rich regions.

7.3.4 *Summary*

In this section, the exothermic temperatures, activation energy, and percentage relative expansion with various particle sizes of Al in TiAl mixtures. After the study of the above results, Ti (5h)-Al mixtures show the optimized behavior for percentage relative expansion with highest of activation energies. The above TiAl mixture evolves activation energy of - 15.5 kJ/mol. The microstructures also provide the information of lack of pores in case of Ti (5h)-Almixtures.

7.4 Dilatometric Behavior of the Ti-Al Intermetallics Containing Various Ti and Al Particle Size

Section 7.2 and 7.3 discuss about dilatometric characteristics titanium aluminides prepared through reaction sintering process. Specifically the effect of Ti and Al powder size separately on the same is discussed. But the main aim is to get an optimized mixture of Ti and Al powders of similar particle sizes. The above mixture should have the desired dilation characteristics with activation energy.

The present study determines the effect of particle size of Aluminum and Titanium powders on the reactive sintering of Ti-Al based intermetallics as well as the subsequent reaction kinetics and densification behavior. Titanium and Aluminum powders of average particle size were milled separately for different extents to produce average particle sizes of 100, 28 and 7 μm. Both the powders were mixed with each other having nearly similar particle sizes in the ratio of 1:1 at% intermetallic composition. The reactive sintering temperatures of the mixtures were determined by DTA. The mixtures of Ti and Al blends of various particle size has been compacted and subsequently sintered at reaction sintering temperatures for 1hr in argon atmosphere. The compacts were further characterized by X-ray diffraction to determine the extent of phase formation. The influence on hardness was also determined with respect to densification and various particle size mixtures. Dilatometric characterization

was done to examine the expansion rate, activation energy and relative expansion of the process during sintering.

7.4.1 Experimental Procedure

Section 7.2.2 can be referred for the size and make of titanium and aluminium powder used. The milling equipment and the manufacturers can be referred from the same. The Titanium powder obtained was milled in a RETSCH PM 400/2 planetary ball mill for different time extent of 1, 5 and 10h. The hardened steel balls and jars were used as the medium for milling and the ball to charge weight ratio were kept as 5:1. To avoid the agglomeration of powders during milling, toluene is used as the process control agent. The charge and the balls were totally submerged in the toluene during milling condition to avoid oxidation of powders. The milling parameters and the details of milling condition are shown in Table-1.The Ti powders milled for time extents of 1, 5 and 10h resulted a mean particle size approximately of 100, 25-28 and 7-9µ respectively. The Al powder milled for durations of 1, 4 and 7h exhibited an average particle size of 100, 28 and 7µ respectively. Milled aluminum powder of 100, 28 and 7µ particle size were mixed individually with titanium powder of similar size to prepare mixture of 50:50at%. The powder blends of Ti (1h)-Al (1h), Ti (5h)-Al(4h) and Ti (10h)-Al(7h) were sintered in high pure inert environment (argon) for 1 hour duration at 717^0C, 695^0C and 713^0C respectively where the temperatures for sintering were decided by studying the thermal analytical results of the blends. The powder mixtures were compacted at 175 MPa to a cylindrical shape of the dimensions of 16.4 mm diameter and 5mm thickness. The sintered samples were polished and ground with different grits emery papers followed by polishing cloths.

The characterizations like FESEM, XRD, DTA, and dilatometric phenomena can be referred from 6.2.2.

Table 7.3: Milling and mixing parameters

Planetary Ball mill Details (Retsch PM 400/2)	**Milling Parameters**
Milling Balls- Hardened steel balls	Milling Media-Toluene
Milling Jars- Hardened steel jars	Charge to Ball ratio-1:5
Jar capacity- 500 ml	Milling speed- 200 rpm Vial Speed- 400 rpm
PCA-Toluene	Total time of milling- 1h,5h&10h
	Weight of initial charge- 30gms
Mixing parameters	
Milling Balls- Hardened steel balls	Charge to Ball ratio-1:3
Milling Jars- Hardened steel jars	Milling speed- 70 rpm Vial Speed- 140 rpm
Jar capacity- 500 ml	Total time of mixing-30mins
Argon atmosphere	Weight of initial charge- 30gms

The Phases present were determined by means of X-ray diffraction using a D8 BRUKER AXS diffractometer. The Cu $K_{\alpha,}$ target was used for the XRD, operating at 30 mA current and 40 kV. The thermal behavior of powder blends were determined using DTA upto 1400^0C in argon environment in a PERKIN ELMER made Pyris Diamond TG/DTA. The morphology of milled powders and the surface topology of the sintered samples were studied using a QUANTA FEI-200 field emission scanning electron microscopy (FESEM). The dilatometric analysis was carried out using Linseis data acquisition system. The system consists of sample holder with the highest sample diameter of 14 cm, amplifier, and cooling circuit. The samples loaded for dilatometric analyses have the diameter of the order of 10 cm. The heating of consisted of two steps such as the heating of the soaking of temperatures with a heating rate of 10^0C/min and

the next step as the holding of sample at the soaking temperature. To study both solid state, transient liquid phase sintering and for the calculation of activation energy, the soaking temperatures for the mixtures were kept as 600^0C, 650^0C, 700^0C, 750^0C and 800^0C.

7.4.2 *Results and Discussion*

7.4.2.1 XRD Analysis of Sintered Compacts

The phases formed after sintering were determined using XRD, which is shown in Fig7.25. The compacts were sintered at their respective sintering temperatures. The diffraction pattern of Ti-Al mixture of Ti (1h)-Al (1h) sintered at 717^0C depicts the formation of TiAl and Ti_3Al phases, which is referred from the JCPD code numbers 00-042-1137 and 00-014-0461 respectively for the phases. In comparison with the mixtures Ti(0h)-Al(0h), Ti (1h)-Al(1h), Ti (5h)-Al(4h) and Ti(10h)-Al(7h) display slightly broadened peaks, where as the formation of intermetallic phases are same for all the patterns. The comparatively broadened peaks of intermetallic phases can be attributed towards the amorphization of Ti and Al powders for higher duration of milling. The lowering in intensity of peaks also can be described on the basis of the breakage of Ti and Al particles at higher extent of milling which in turn confirms the formation of intermetallics phases. The shifting of peaks are un noticeable ,as the milling of the powders were carried out at lower rpm and for small duration though the lattice parameter has been lowered to certain percentage.

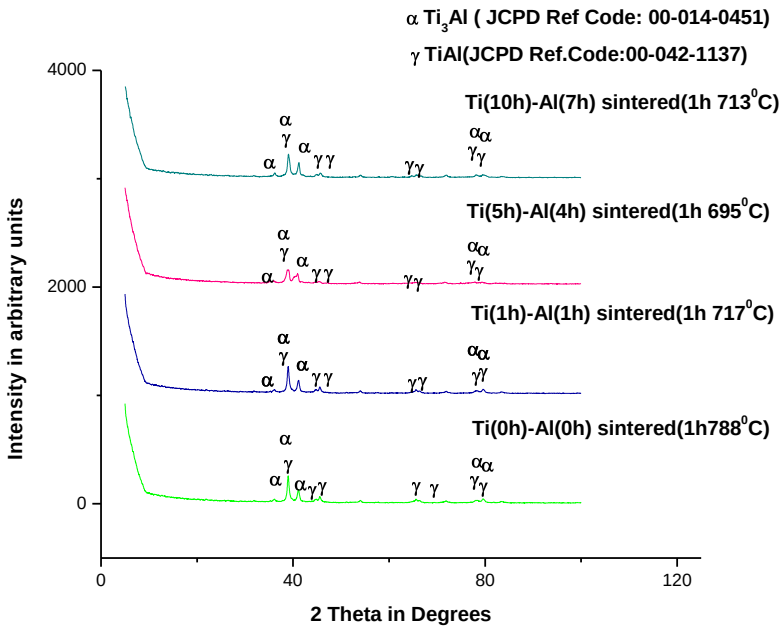

Fig 7.25 XRD pattern of Ti (0h)-Al(0h), Ti (1h)-Al(1h), Ti (5h)-Al(4h) and Ti(10h)-Al(7h) mixtures sintered at their respective temperatures

The heat change values for the synthesis of TiAl and Ti_3Al are −75 and −73 kJ/mol respectively and the DTA graphs show the presence of exothermic peaks at 717^0C, 695^0C and 713^0C for Ti (1h)-Al (1h), Ti (5h)-Al (4h) and Ti (10h)-Al (7h) respectively.

The Morphological studies of the milled Ti powders for are displayed in Fig.2 (a-c). The Ti powders are subjected 1h, 5h and 10h of milling. The milling results in the formation of fractured surfaces due to plastic deformation introduced by ball-particle-ball collisions, ball-jar (wall)-ball collisions. The milling process includes the steps of agglomeration and fracture. Cold welding of the particles is first seen due to the formation of nascent surfaces. The available free energy on the nascent surfaces is sufficient for the immediate formation of cold welding, which helps in agglomeration of the powders. The fracturing phenomenon of the powders is due to work hardening introduced by higher extent of milling, which help in overcoming the free energy of nascent surfaces and agglomerated clumps for their breakage. Thus the higher extent of milling helps in lowering the particle size. The lowering of particle size can be described as the comparative process between two phenomena of agglomeration and fractures. .After certain duration of milling the equilibrium of the above two process is set in such a way that the further lowering of particle sizes are inhibited. The ductility

of the Ti powder is the cause of flattening and agglomeration of particles after 1h of milling. The approximate particle size attained by 1h milled Ti powders was ~100µ. The work hardened splats of Ti powders when further milled upto 5h, the particle sizes get reduced to an approximate size of 28µ. As shown in Fig.2(c) the Ti particles milled for 10h, produces particles of the order of ~7µ. The uneven particle morphology of the milled powders are due to the fractured surfaces created during the collisions. The morphology of Al powders milled for different durations i.e 1h, 4h and 7h,as received Al and as received Ti powders were shown in Fig 7.26 (a-e). The Al powders upon milling is flattened at early stages milling due to plastic deformation and attains an approximate size of 100µ and upon further milling the work hardened splats fracture to approximate size of 28µ and 7µ for 4h and 7h milling respectively.

7.4.2.2 DTA Study

The melting of Al powders were revealed by the endothermic peaks present in the traces. The melting point for Ti (0h)-Al (0h) was 664^0C, but for the other compositions it is 668^0C. The melting point is not affected as the external energy is applied to the system by the milling. The exothermic temperatures show an increasing trend.

7.4.2.3 Dilatometric Study

The dilatometric behavior of various particle size Ti-Al mixtures were studied using relative percentage of expansion of the compacts. The effect of varying soaking temperature over the expansion rate of the mixtures is also determined. Activation energy of the process was calculated to have a better idea of reaction kinetics of the heating as well as high temperature synthesis process (Fig 7.29, 7.30& 7.31).

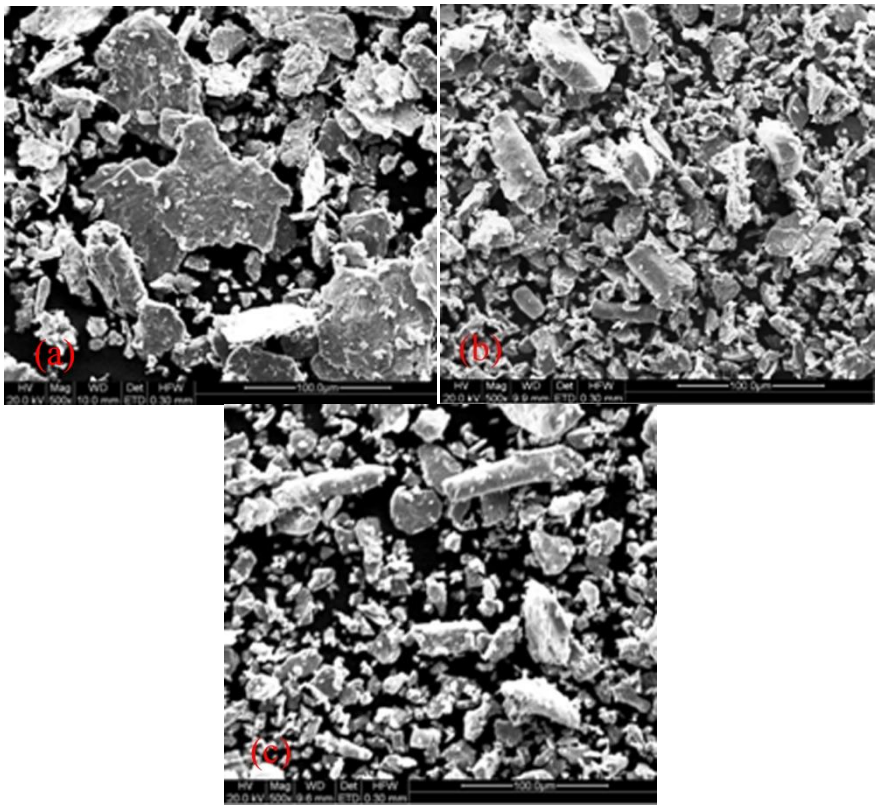

Fig 7.26 FESEM micrographs of milled Ti powders for different milling times (a) 1h milled (b) 5h milled & (c) 10h milled

The dilation characteristic describes the route of and extent of sintering method. Various temperatures like 600^0C, 650^0C, 700^0C, 750^0C & 800^0C are kept as the holding point for the sintering and dilation process. Both the materials have vital role in expansion and reaction rate of the dilatometry. Molten Al plays the role of bridging the gap or filling the interparticulate pores in the material, which in turn decides the sintering and formation of the intermetallics. As the process is a transient liquid phase sintering, so only Al is molten but Ti powder predominantly decide the traversing of liquid melt. The pores/voids within the particles act as fine capillaries which help in the capillary flow of liquid melt. The diameter of the capillaries decreases with lowering of the particle size. The lowering of the particle size decreases the interparticulate voids and also increases the number of voids in the materials. Various temperatures of soaking display solid state and transient liquid phase sintering. Solid state sintering process is exhibited at 600^0C, but for the mixtures heated at 650^0C show the onset of liquid phase sintering process for the soaking temperatures, due to onset of Al melting process. When the plots for the temperatures higher than 650^0C observedthey show the

formation of step at 650^0C. The step formed at the above temperature for relative percentage of expansion can be attributed towards the formation of intermetallics and the onset of transient liquid phase sintering.

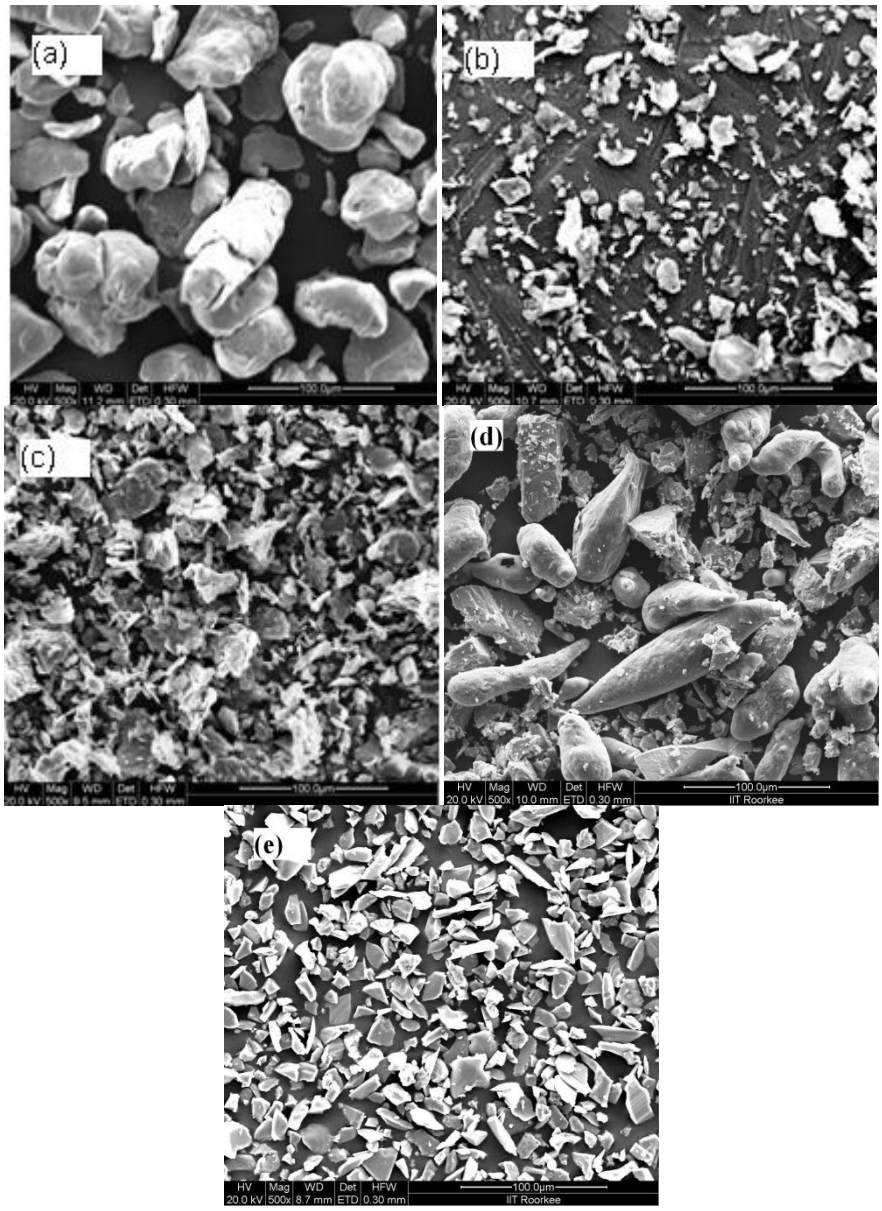

Fig 7.27 FESEM micrographs of milled Al powders for different milling times (a) 1h milled, (b) 4h milled, (c) 7h milled,(d) As received Al & (e) As received Ti powders

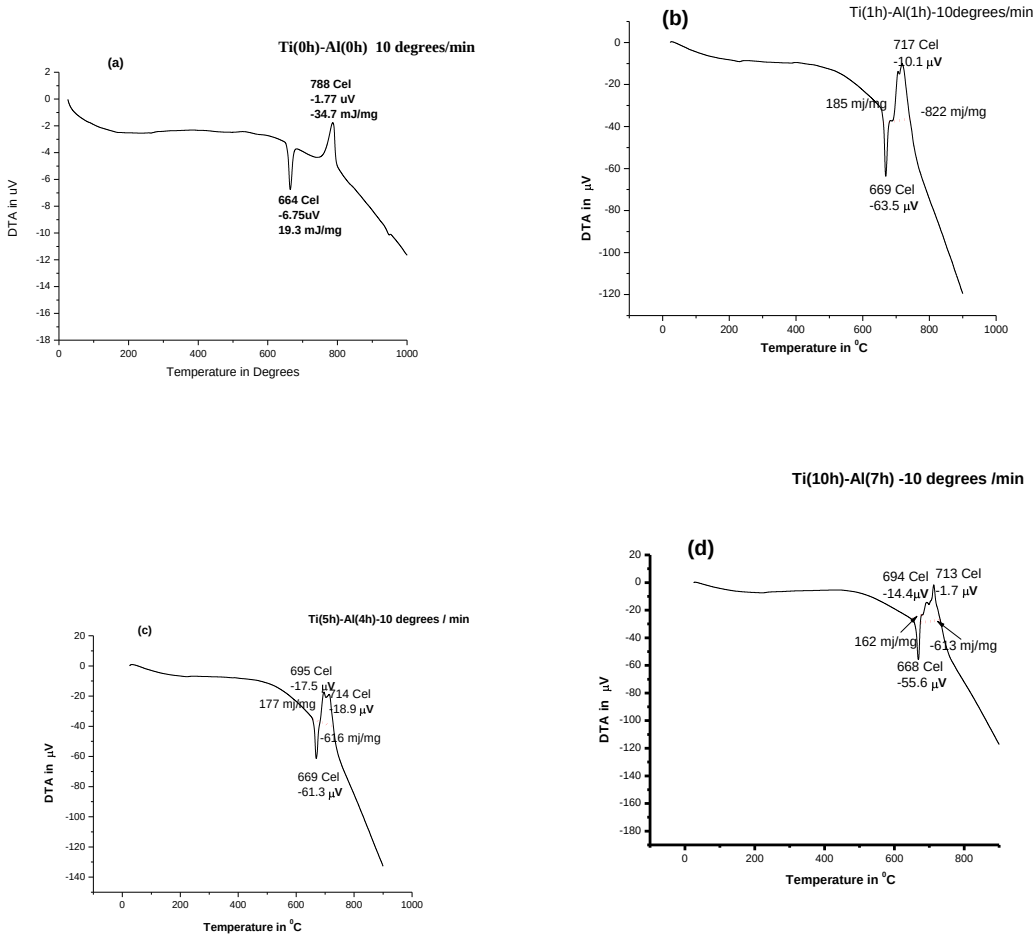

Fig 7.28 Thermal analysis plots of Ti-Al mixture at 10^0C /min (a) Ti(0h)-Al(0h) (b) Ti(1h)-Al(1h) (c) Ti(5h)-Al(4h) and (d) Ti(10h)-Al(7h)

Expansion in the compacts were noticed due to the formation of TiAl , Ti_3Al and $TiAl_3$ intermetalics. As the intermetalics have lattice structures of L_{10} type face tetragonal, DO_{19} type and DO_{22} type ordered structures respectively. The above structures have higher c/a ratio, which is the main reason for the expansion during dilatometric studies. Relative percentage expansion of the mixtures is higher for the samples heated at 650^0C, but for higher temperatures it is lowered by 30 to 45%. Higher percentage expansion in case of the samples heated at 650^0 C can be explained as the formation of the intermetallics,as the process is spontaneous and self propagating. But for the higher temperatures, the percentage expansion is decreasing with increase in temperatures. Expansion in the higher temperatures is lowered due to sintering and shrinkage taking place inside the compacts. Process of the sintering can be described as two parts, firstly the formation of intermetallics and then the sintering of the compacts. Therefore the

step at 650^0C, describes the onset of liquid formation, transient liquid phase sintering and the formation of intermetalics. Formation of intermetallics dominates the percentage of relative expansion and then comes the sintering into action and the shrinkage takes place. For temperatures like 750^0C and 800^0C, the completion of sintering and the synthesis process is clearly noticed. The flatter part of the plot after the steep increase in the above soaking temperatures describes the completion of self propagating high temperature synthesis process. For mixtures Ti (5h)-Al (4h) and Ti (10h)-Al (7h) the percentage expansion are almost the same as in case of 650^0C,but the composition Ti(1h)-Al(1h) shows percentage expansion upto 75 %. Though the earlier ones have higher free energy in the system due to milling, but the initial particle size of the materials (~100μ) plays an important role in the percentage expansion. Expansion rate and average expansion rate would provide a better idea of the sintering process showing optimized expansion and activation energy.

7.4.2.4 Shrinkage/Expansion Rate Vs Temperature

The expansion rate of the Ti-Al mixture compacts for various particle sizes may have different maxima, but the characteristics of curves showing the rates are similar. The rate of expansion is the sum of the rate of expansion of the compacts which is rate of shrinkage and the rate of flatter part of the curve showed in relative expansion. The Effective expansion rate also can be depicted as the rate of the whole process. The rate curve shows unevenly dips and inclination for the 600^0C soaked compacts, but for the other temperatures the common behavior of the curve displays constant characteristics in the beginning and the steep inclination at the end.

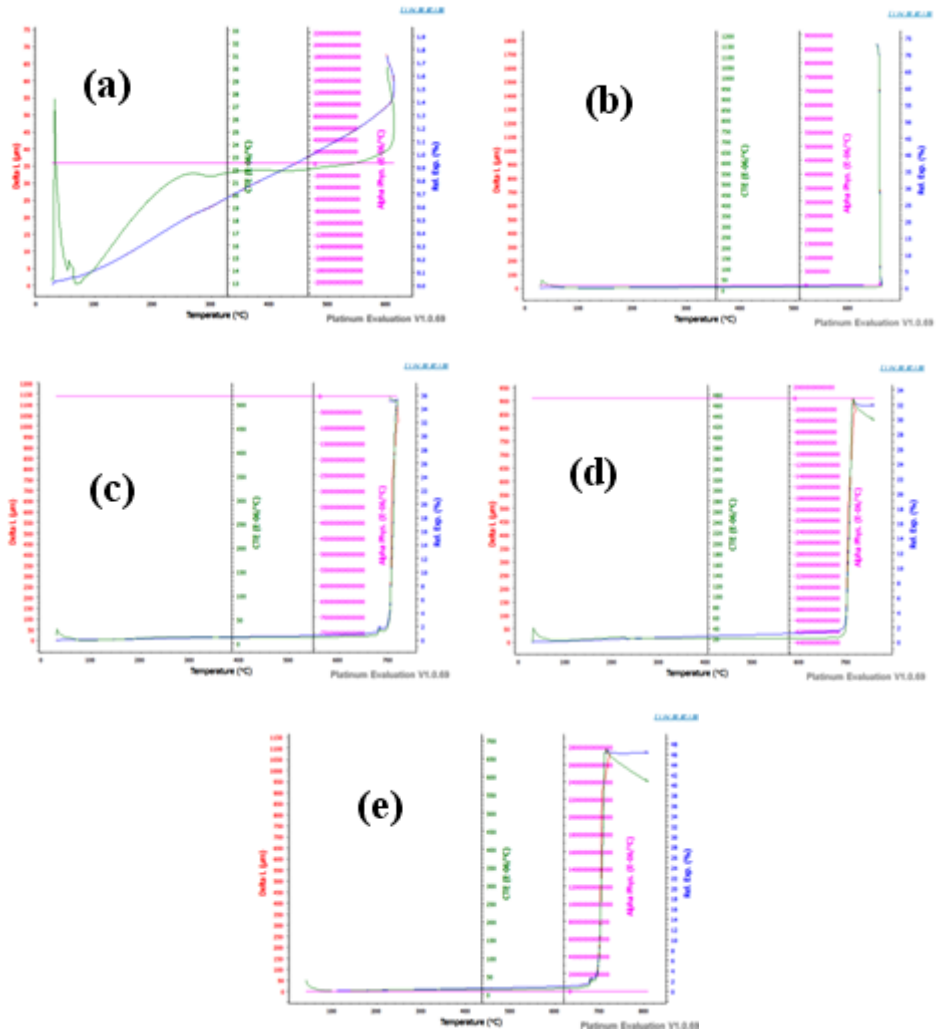

Fig 7.29 Dilatometric plots of Ti (1h)-Al(1h) Al mixture at (a) 600^{0}C (b) 6500C (c) 700^{0}C (d) 750^{0}C and (e) 800^{0}C

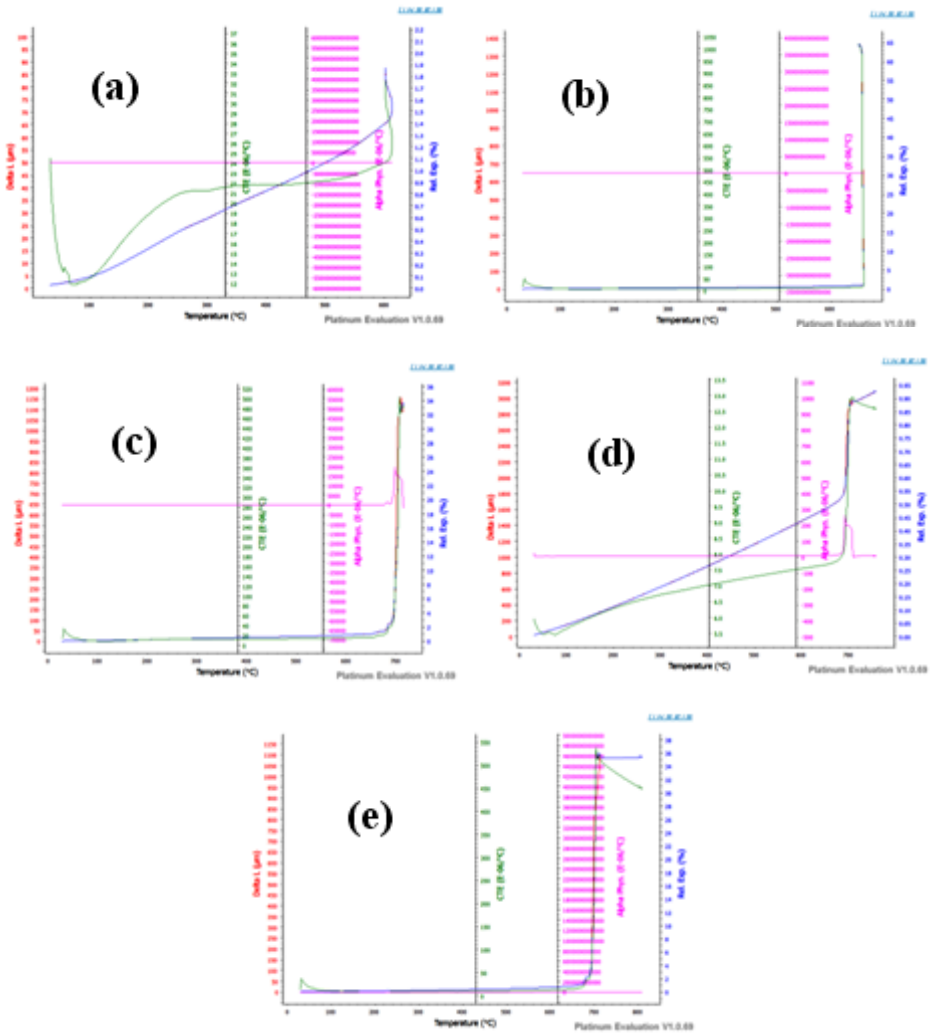

Fig 7.30 Dilatometric plots of Ti (5h)-Al(4h) Al mixture at (a) 600^{0}C (b) 6500C (c) 700^{0}C (d) 750^{0}C and (e) 800^{0}C

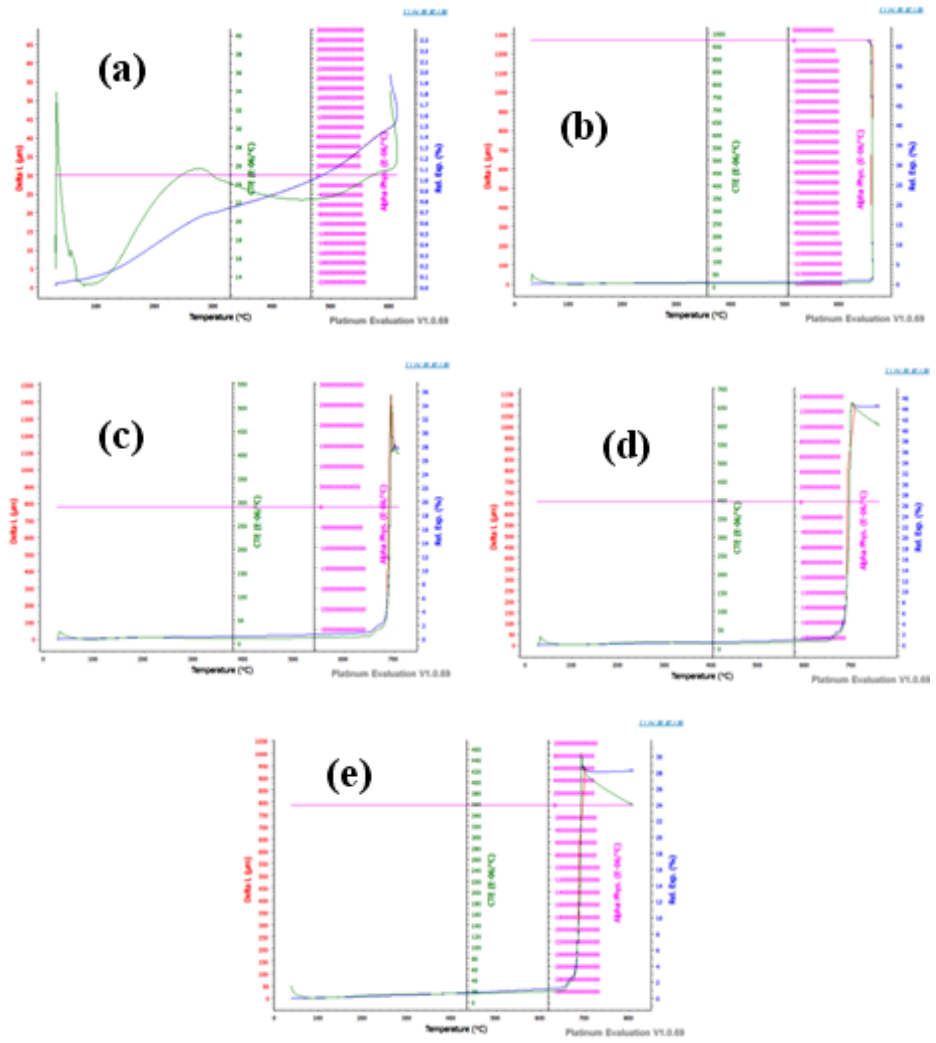

Fig 7.31 Dilatometric plots of Ti(10h)-Al(7h) mixture at (a) 600^{0}C (b) 6500C (c) 700^{0}C (d) 750^{0}C and (e) 800^{0}C

The uneven curves for 600^{0}C can be explained as the sintering process in the solid state which forms the dips but the coefficient of thermal expansion show the inclination or the ups in the curves. The steep inclination at higher temperatures can be attributed towards the steep increase of relative expansion at the soaking temperatures (Figs7.32, 7.33& 7.34). The rate increases nearly 10 times for 650^{0}C in comparison with 600^{0}C compacts. But the same happens when compared for 650^{0}C and higher temperatures. The increase in rate is due to the increase in relative expansion, but for higher temperatures the effective rate is the sum of rate of expansion and the rate of

shrinkage. This rate of shrinkage confirms the sintering process and the completion of the formation of intermetallics. The study of average shrinkage rate and the activation energies of various mixtures would give the best possible route for sintering and the optimized kinetics of the process.

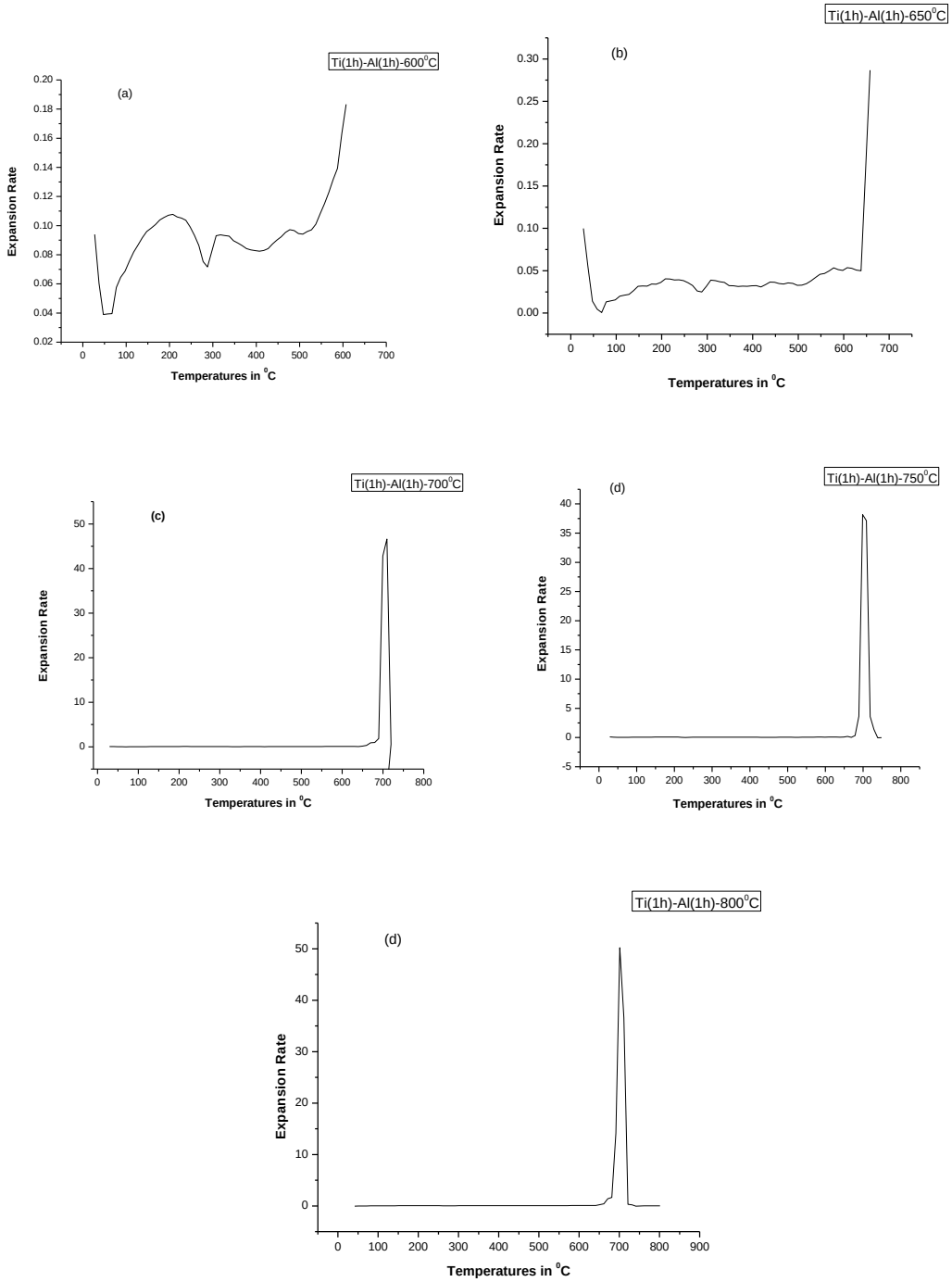

Fig 7.32 Variation of shrinkage/expansion with temperature for Ti(1h)-Al(1h) mixture at (a) 600^{0}C (b) 6500C (c) 700^{0}C (d) 750^{0}C and (e) 800^{0}C

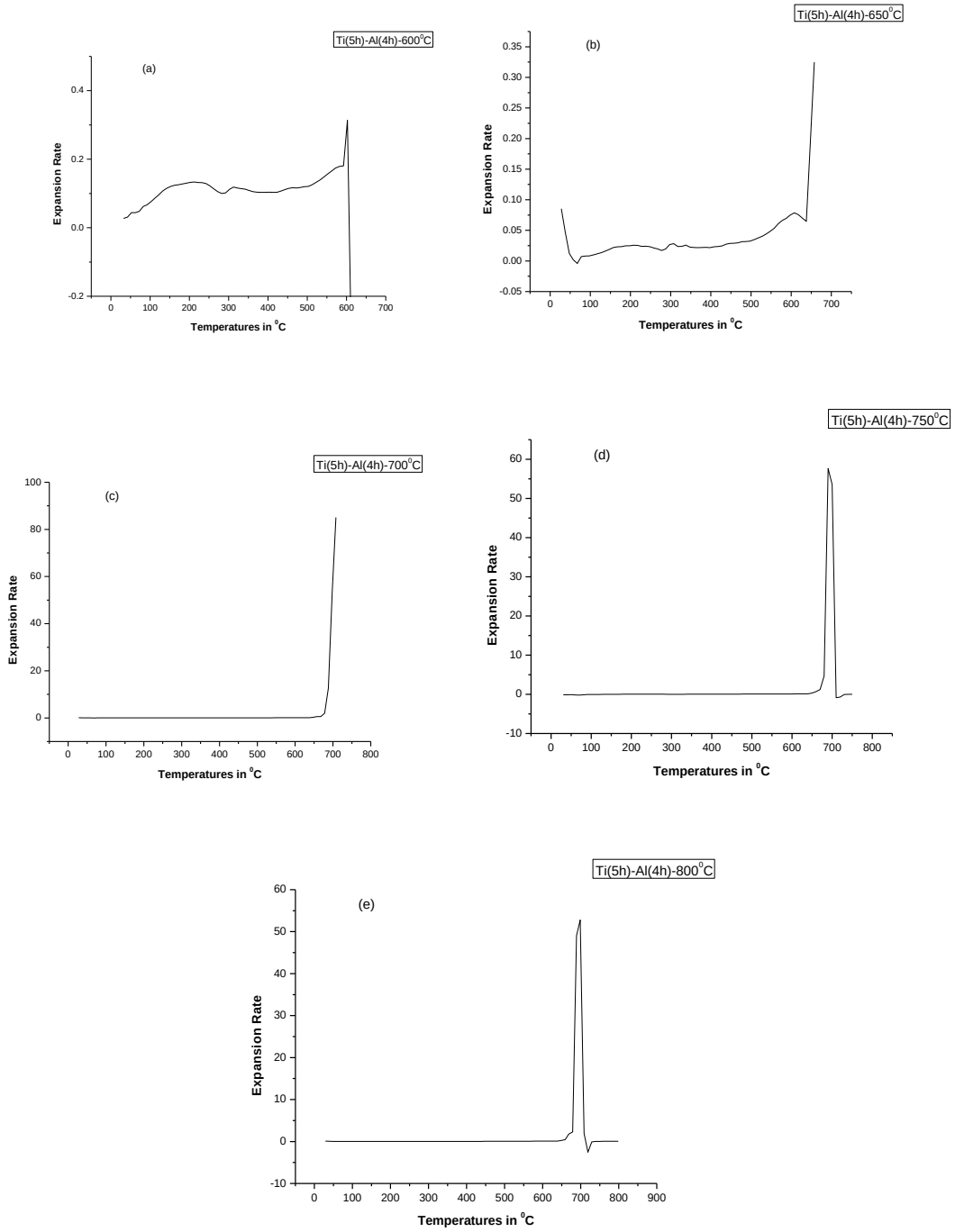

Fig 7.33 Variation of shrinkage/expansion with temperature for Ti (5h)-Al (4h) mixture at (a) 600^0C (b) 6500C (c) 700^0C (d) 750^0C and (e) 800^0C

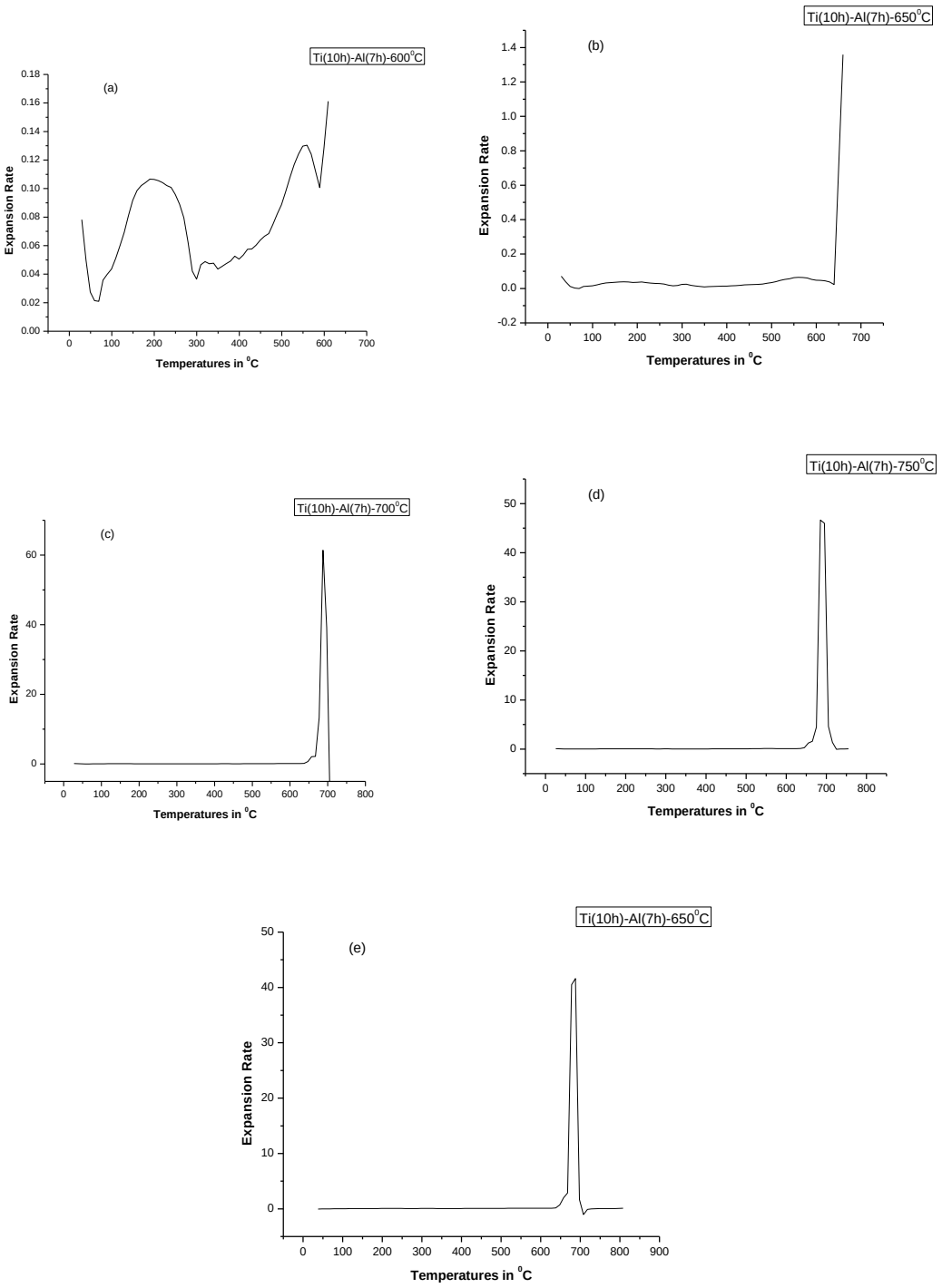

Fig 7.34 Variation of shrinkage/expansion with temperature for Ti(10h)-Al(7h) mixture at (a) 600^{0}C (b) 650^{0}C (c) 700^{0}C (d) 750^{0}C and (e) 800^{0}C

7.4.2.5 Average Shrinkage/Expansion Rate Vs Temperature

The effect of temperatures over the average expansion rate explains the possibility of the sintering and smoothness in the process. The activation energy of the process

describes the ease of the process; the magnitude of the activation energy explains the available free energy in the system for the feasibility of the process. The negative magnitude describes about the excess energy or that amount of the energy should be taken out of the system for the process to complete. The Fig 7.35(a) describes the comparative average expansion rate, which can also be depicted as the smoothness of the process. Analyzing the average expansion rate of three mixtures, it is quite clear thatTi (5h)-Al (4h) mixture has the smoothest of the traces and follows a path without any dip or inclination unlike others. Comparing the activation energies of the various mixtures, Ti (5h)-Al (4h) has the highest of them. The activation energy of the above mixture is -9.107kJ/mol. Activation energy and the average expansion rate describes the Ti (5h)-Al (4h) is the best compositional mixture for optimized expansion and feasibility. This also can be inferred from the above discussion that the above mixture is having Ti and Al particle size smaller enough to create ample fine capillaries of intrerparticulate voids with maximum traversing of Al melt.

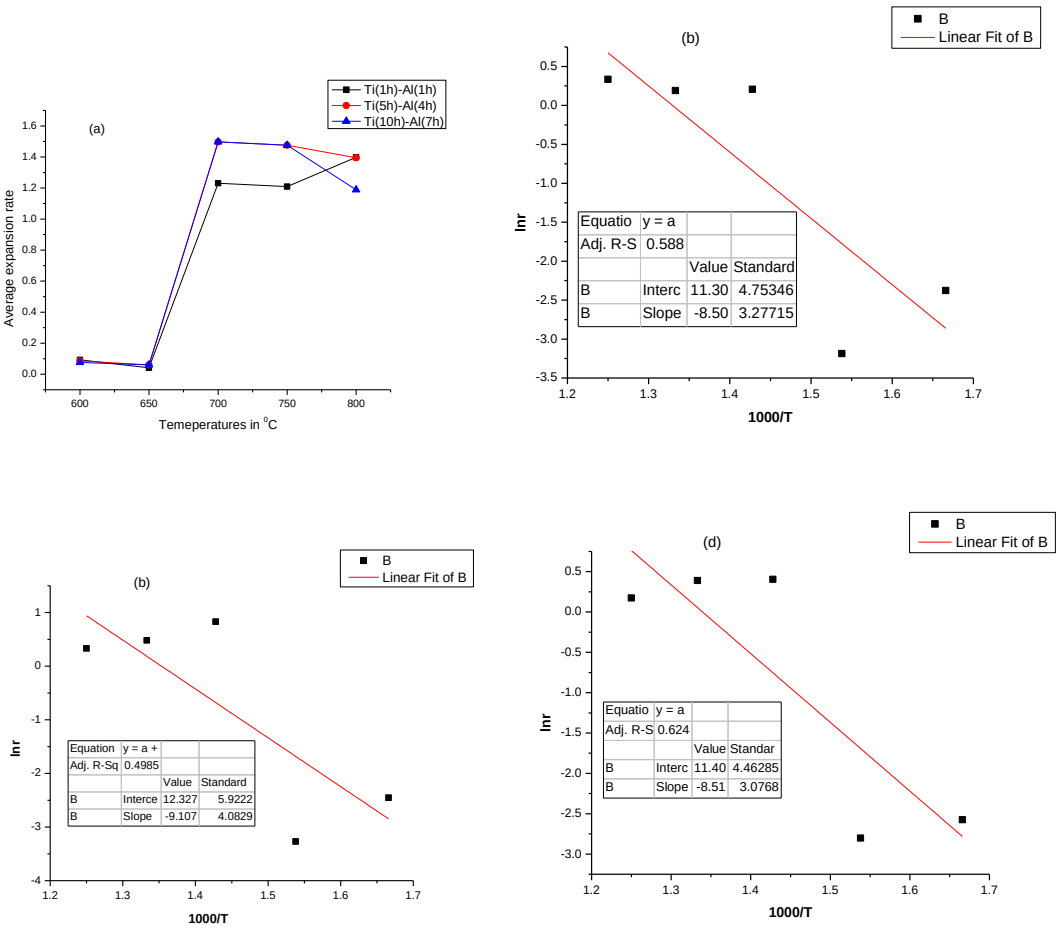

Fig 7.35 shows (a) comparative average shrinkage/expansion rate vs Temperature and activation energy of (b) Ti(1h)-Al(1h) (c) Ti(5h)-Al(4h) (d) Ti(10h)-Al(7h)

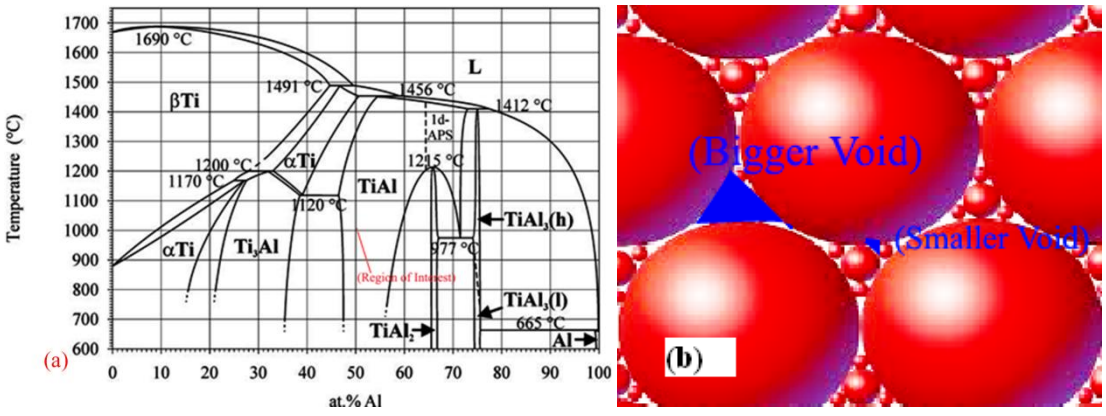

Fig 7.36 shows (a) A systematic phase diagram of Ti-Al binary system [28] (b) Thematic diagram explaining size of voids with change in particle sizes

7.4.3 *Summary*

Analyzing the exothermic peaks, activation energy and relative expansion of various mixtures of Ti-Al system with different particle size and various soaking temperatures, the Ti(5h)-Al(4h) mixture with an approximate particle size of 28μ shows the highest of activation energy. The activation energy (-9.107 kJ/mol) and the expansion rate of the above mixture shows the smoothness and the feasibility of the process, which concludes as the best of the composition with optimized characteristics.

CHAPTER 8

HYBRID SUBTRACTIVE CLUSTERING TECHNIQUE FOR ESTIMATION OF AVERAGE SHRINKAGE RATE

8.1 Introduction

The optimized density, high stiffness, oxidation resistance and high strength to weight ratio are the key characteristics in making the Ti-Al based intermetallics, a desired material for the industrial applications in gas turbines and aerospace industries.

Powder metallurgical processes have an edge upon other processes due to economical viability of the method and fabrication of near net shape product. Reaction synthesis and Mechanical alloying are two competitive processes for synthesis of aluminides. Work hardening during mechanically alloying and bulging of compacts during reaction sintering are the main drawbacks of the above processes. As mechanical alloying is a non equilibrium process, so work hardened materials will hardly show higher densification. When the starting materials were lowered in size, through reaction synthesis finer grain structures can be achieved. Dilatometric characterization will provide the idea of material which will have lowest bulging during sintering. Various researchers have carried out experimentation on linear shrinkage/expansion, onset of sintering and rate of expansion [Dabhade et al 2006 & Dabhade et al 2007]. Dabhade et al (2007) calculated the onset of sintering temperatures of Ti-TiN composite powders, linear shrinkage rate at constant rate of heating and sinterability. Wang et al studied the same for titanium aluminide compacts fabricated through cold extrusion and have various Al at% of 25-75. Though the dilatometric investigations provided data regarding thermal expansion, but hardly gave any idea about the linear shrinkage/expansion rate of the aluminides formed during the reaction synthesis process. There is rarely literatures available where the researchers have worked on the dilatometric investigations of titanium aluminides and determined expansion rate, activation energy and percentage linear expansion.

During this study, data has been processed for average shrinkage rate for Ti and Al powder mixtures with various particle sizes and various soaking temperature. A Model

has been developed using new emerging technique as Soft Computing Techniques (SCT). Three input data with one output has been used to develop this model using a tool of SCT as Artificial Neural Fuzzy Inference System (ANFIS). Subtractive Clustering Method (SCM) has been used to optimize the modeled output**.** Performance of the model is evaluated with checking/ validation data and found that the developed model can be used in future to estimate average shrinkage rate for same input parameters.

8.2 Methodology

Neuro-fuzzy modeling refers to the way of applying various learning techniques developed in the neural network literature to fuzzy modeling or to a fuzzy inference system (FIS). The basic structure of a FIS consists of three conceptual components: a rulebase, which contains a selection of fuzzy rules; a database which defines the Membership Functions (MF) used in the fuzzy rules; and a reasoning mechanism, which performs the inference procedure upon the rules to derive an output. FIS implements a nonlinear mapping from its input space to the output space. This mapping is accomplished by a number of fuzzy if-then rules, each of which describes the local behavior of the mapping. The parameters of the if-then rules definea fuzzy region of the input space, and the output parameters specify the corresponding output. Hence, the efficiency of the FIS depends on the estimated parameters. Flow chart for Fuzzy Inference System is given in Fig.8.1.

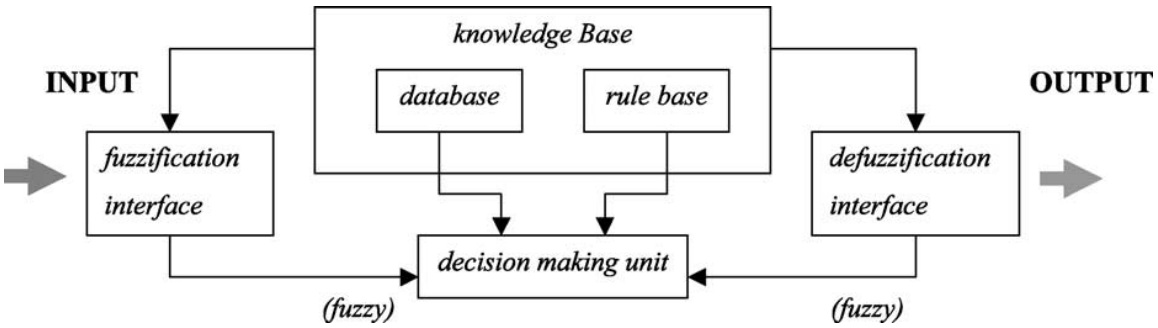

Fig. 8.1: Fuzzy Inference System with crisp output

8.2.1 ***Adaptive Neuro-Fuzzy Inference System (ANFIS)***

The Adaptive Neuro-Fuzzy Inference System (ANFIS), first introduced by Jang (1993), is a universal approximator and, as such, is capable of approximating any real

continuous function on a compact set to any degree of accuracy (Jang et al., 1997). Thus, in parameter estimation, where the given data are such that the system associates measurable system variables with an internal system parameter, a functional mapping may be constructed by ANFIS that approximates the process of estimation of the internal system parameter.

As a simple example, a fuzzy inference system with two inputs x and y and one output z is assumed. The first-order Sugeno fuzzy model, a typical rule set with two fuzzy if-Then rules can be expressed as:

Rule 1: IF x is A_1 AND y is B_1 THEN $f_1 = p_1 x + q_1 y + r_1 (1)$

Rule 2: IF x is A_2 AND y is B_2 THEN $f_2 = p_2 x + q_2 y + r_2 (2)$

The resulting Sugeno fuzzy reasoning system is shown in Fig8.2. Here, the output z is the weighted average of the individual rules outputs and is itself a crisp value.

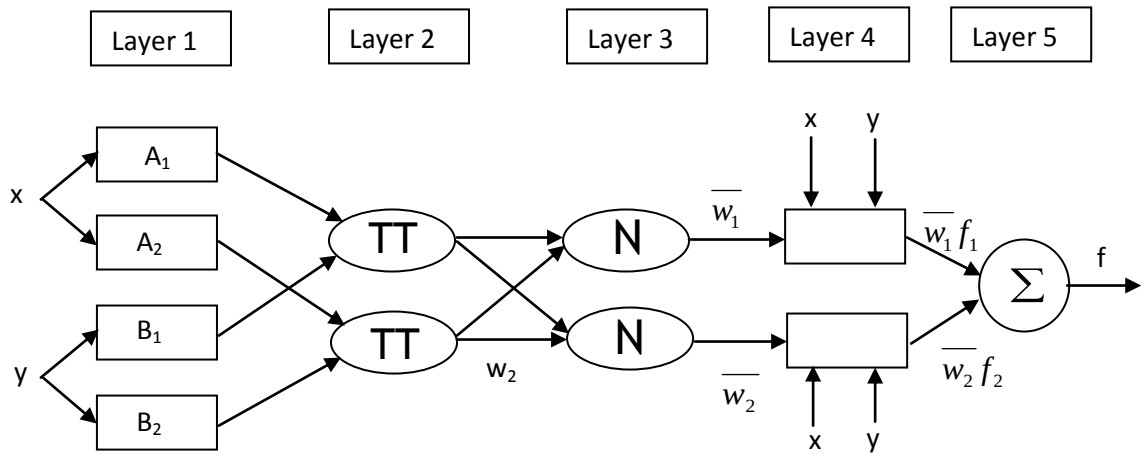

Fig 8.2: Equivalent ANFIS architecture

ANFIS is a tool of SCT with a combination of Fuzzy Logic Theory (FLT) with weights of Artificial Neural Network (ANN).

8.2.2 *Fuzzy Logic Theory (FLT)*

Fuzzy logic theory (FLT) is a convenient way to map an input to an output space. Fuzzy Systems, Linear System, Expert System, Neural Network, Differential Equations, Interpolated Multidimensional Look Up Tables etc. are numerous ways to handle a optimization problem. Among these, Fuzzy Systems are "easy to understand

and flexible". There are two types of fuzzy inference systems (FIS) that can be implemented in the FLT.

8.2.3 *Mamdani Type Inference*

Mamdani fuzzy inference method is the most commonly seen fuzzy methodology. This method is among the first control systems built using fuzzy set theory. Within this inference, the fuzzy rules are combined through the fuzzy operator, implication and aggregation methods (Jain and Srinivasulu (2004)). After the aggregation process, there is a fuzzy set for each output variable that needs defuzzification.

8.2.4 *Sugeno Type Inference*

Takagi-Sugeno (TS) method of fuzzy inference (Jang 1993) has been introduced in 1985. It is similar to the Mamdani method except the output, which is defined as constant or linear combination of inputs. A typical fuzzy rule in a zero-order Sugeno fuzzy model has the form:

If x is A and y is B then z = k

Where A & B are fuzzy sets in the antecedent, while k is a crisply defined constant in the consequent.

The more general first-order Sugeno fuzzy model has rules of the form:

If x is A and y is B then z = px + qy + r

Where A & B are fuzzy sets in the antecedent, while p, q & r are all constants.Due to the linear dependence of each rule on the system's input variables, the Sugeno method is ideal for acting as an interpolating supervisor of multiple linear controllers.

To initialize the FIS with ANFIS, there are two default partitioning methods as grid partitioning and subtractive fuzzy clustering. Due to wide use of this technique in the field of hydrology, the subtractive clustering approach has been used during this study.

8.2.5 *Subtractive Clustering Method (SCM)*

The purpose of fuzzy clustering is to identify natural grouping of the data from a large data set and to produce a concise representation of the behavior of a system. Various fuzzy clustering methods have been reported in the literature, such as fuzzy C- means clustering (Jang et al.(1997)) , mountain clustering (Johansen and Babuska (2002)),

subtractive clustering (Mamdani and Assilian(1975)), and Gustafson- Kessel (GK) fuzzy clustering (Mehta et al . 1997).

Fuzzy SCM is a data clustering technique wherein each data point belongs to a cluster to some degree that is specified by a membership grade. Clustering of numerical data forms the basis of many classification and system modeling algorithms. In this approach, the computation is simply proportional to the number of data points and is independent of the dimension of the problem under consideration. Nayak (Nash and Sutcliffe (1970) and Nayak et al. (2004)) have described the SCM model structure identification, each cluster centre D_i is considered as a fuzzy rule that describes the system behavior. The cluster centers are identified on the basis of the potential value (P_j) assigned to each data point x_i of a set of N data points in a p-dimensional space:

$$P_i = \sum_{j=1}^{N} \exp\left[-4 \frac{\left\| x_i - x_j \right\|^2}{r_a^2} \right] \tag{8.1}$$

where $r_a \geq 0$ and $\left\| x_i - x_j \right\|$ are cluster radius and Euclidean distance respectively at any point i. The data point with highest potential (p_i^*) is considered as the first cluster centre D_1^*. The potential of the remaining data points is modified by subtracting the influence of the first cluster centre. The point with the highest modified potential is considered as the second cluster centre (D_2^*) and the process is repeated to compute other cluster centres. Therefore, the modified potential of the data points after computation of the j[th] cluster centre is expressed as:

$$p_i = p_i - p_j^* \exp\left[-4 \frac{\left\| x_i - D_j^* \right\|^2}{r_b^2} \right] \tag{8.2}$$

Where $r_b \geq r_a \geq 0$ is the radius that results in measurable reduction in the potential of neighbourhood data points and avoids closely spaced cluster centre. The process is repeated until sufficient clusters are generated and the process is stopped if the following condition is fulfilled

$$P_k^* < \varepsilon P_i^* \tag{8.3}$$

Where ε is the reject ratio. These cluster centres $D_i^*, i = 1, k$ can be used as the centre of the fuzzy rules' premise of input data vector x and the degree to which rule i is fulfilled is defined by Gaussian membership function:

$$\mu = \exp\left[-4 \frac{\left\| x - D_i^* \right\|^2}{r_a^2} \right] \tag{8.4}$$

The cluster analysis assigns a set of rules and antecedent membership functions that model the data behavior. Using global linear least square estimation, the consequent equation of each rule is determined. The advantage of this method is that it generates Gaussian membership functions as fuzzy sets, which have infinite support for each input vector. Membership value of each fuzzy set is computed and hence every rule in the rule-base fires. This leads to the possibility of generating only a couple of rules capable of describing the relationship between input and output channels accurately.

8.2.6 *Data Processing*

The inputs are combination of various particle sizes of powder mixtures, soaking temperatures and relative percentage expansion. The out put data is nothing other than the average shrinkage rate of the compacts heated at various soaking temperatures. The various particle sizes studies the effect of particle sizes of Ti, Al and cumulative particle sizes of mixtures. The other input is soaking temperatures define the process in various steps. The temperatures provide the fact that the process significance, whether it signifies solid state sintering or transient liquid phase sintering or formation and completion of intermetallics. The third input parameter suggests the percentage relative expansion due to self propagating high temperature synthesis and the output is the averaged rate of shrinkage or expansion.

8.2.7 *Fuzzification of data*

The input & output data has been fuzzified with different membership functions within the grey range of data. Degree of membership is between 0 & 1. Gaussian membership functions have been used for all three input parameters as shown in Figures 3, 4 & 5. Fifteen categories of different ranges of MF have been defined for all three inputs. The output is treated as linear one for Takagi-Sugeno technique.

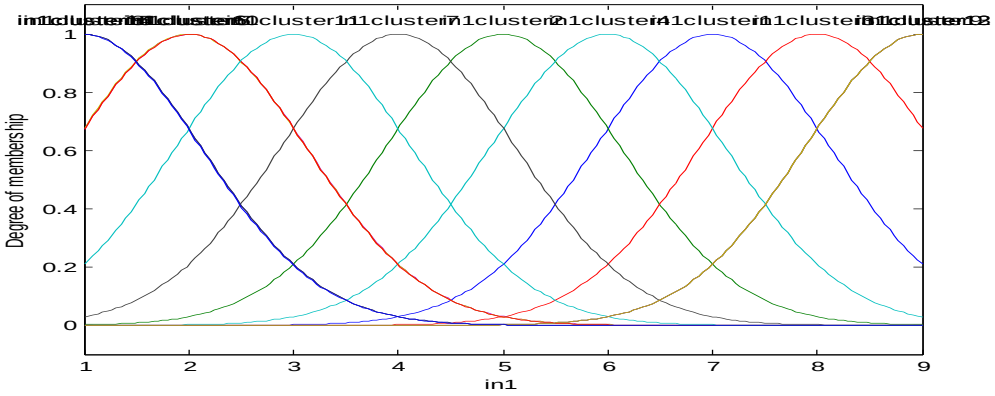

Fig 8.3: Gaussian membership functions for input data 1 as 'Composition'

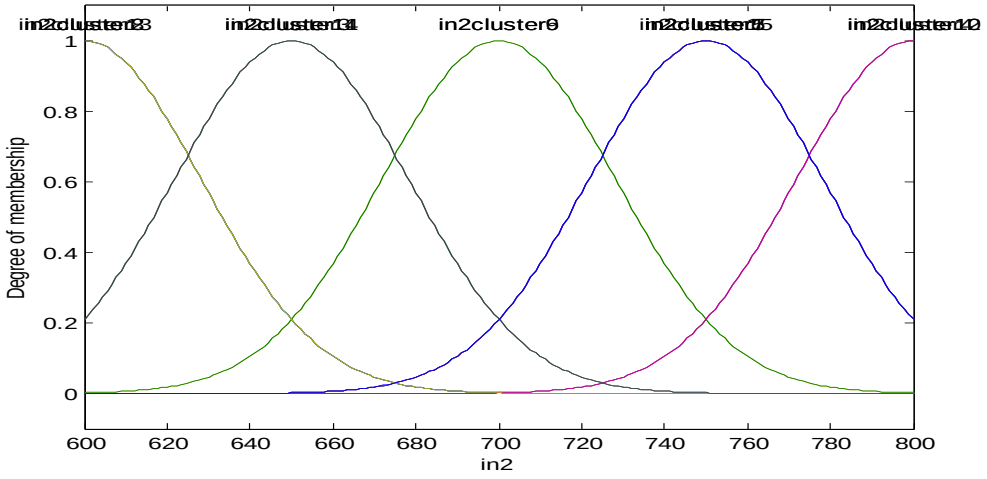

Fig 8.4: Gaussian membership function for input data 2 as 'Soaking Temperature'

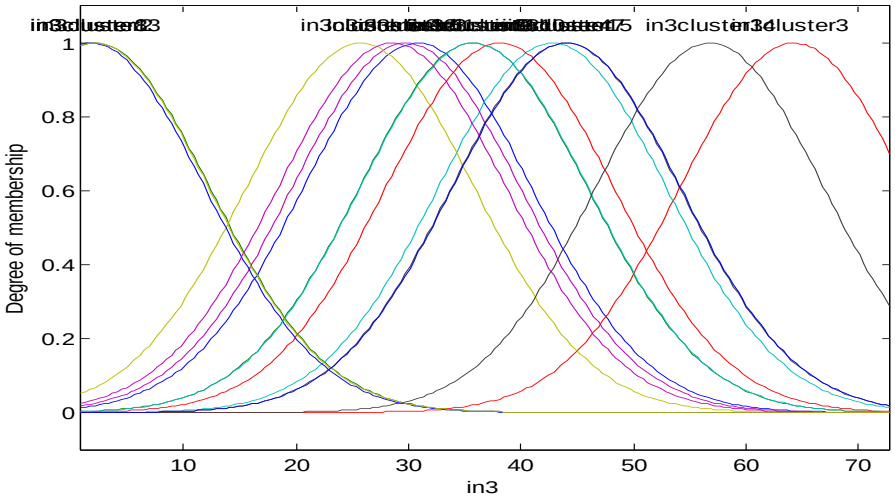

Fig 8.5: Gaussian membership function for input data 3 as '% relative expansion'

8.3 Formulation of Fuzzy Rule-Base

A fuzzy rule based model is a mathematical model based on a fuzzy rule system. A fuzzy rule system R, is defined as the set of rules which consist of sets of input variables or premises $A_{I,k}$ in the form of fuzzy sets with membership functions $\mu_{A\,I,k}$ and a set of consequences B, also in the form of a fuzzy set:

If a_1 is $A_{I,1}$& a_2 is $A_{I,2}$& ---------- a_k is $A_{I,k}$ then B_I is the set of consequences.

Assessment of rules is a procedure where knowledge and or available data are translated or encoded into rules described in the following form:

IF the value of variable x_1 is “large” AND variable x_2 is “medium” THEN the result y is “small”.

It is claimed that such rules more closely resemble the way we think than do more explicit mathematical rules.

Fuzzy rule-based modeling is centered on the definition and verification of a rule system. The different methods to do this, as described in Bardossy and Duckstein (1995), are as follows:

1. The rules are known by the experts and can be defined directly.
2. The experts can assess the rules directly, but available data should be used to update them.
3. The rules are not known explicitly, but the experts can specify the variables required for the description of the system.
4. Only a set of observations is available, and a rule system has to be constructed to describe the interconnections between the elements of the data set.

It was concluded that as the number of inputs in a fuzzy rule-base system increases, the number of rules quickly becomes too large, unidentifiable, and unmanageable. Rule system responses depend on the choice of both combination and defuzzification methods, which must thus be selected carefully. During the modeling, Fuzzy rules are defined as

IF (Composition is 1) AND (Soaking Temperature is High) AND (% rel. expansion is medium) THAN (Avg. Shrinkage rate is Low).

8.3.1 *Training of ANFIS Models*

The model identification was carried out in two steps: (1). Determining the number of fuzzy rules and their associated membership functions using fuzzy subtractive clustering approach, and (b) optimizing the TS fuzzy model through least squares estimation. The fuzzy clustering partitions a data set into a number of groups in such a way that the similarity within a group is larger than that among groups. The similarity matrices are generally highly sensitive to the range of elements in the output vectors. Therefore, the input-output data sets are normalized within the unit hypercube. The subtractive clustering approach is applied for computation of rule base and membership functions. The cluster centers, and thus the Gaussian membership function identified for each case, are used to compute consequent parameters through a linear least square method and finally, a TS fuzzy sub- clustering model is developed. Each fuzzy model has different number of rules. For every input vector, a membership degree to each fuzzy set greater than zero is computed from the Gaussian membership function. Therefore, all the rules fire simultaneously for each combination of inputs and a crisp output value is thus provided for a given data. The two ANFIS parameter optimization method options available for FIS training are hybrid (the default, mixed least squares and backpropagation). Error Tolerance as 0.001 is used to create a training stopping criterion, which is related to the error size. The training will stop after the training data error remains within this tolerance limit or after completing 10 epochs.

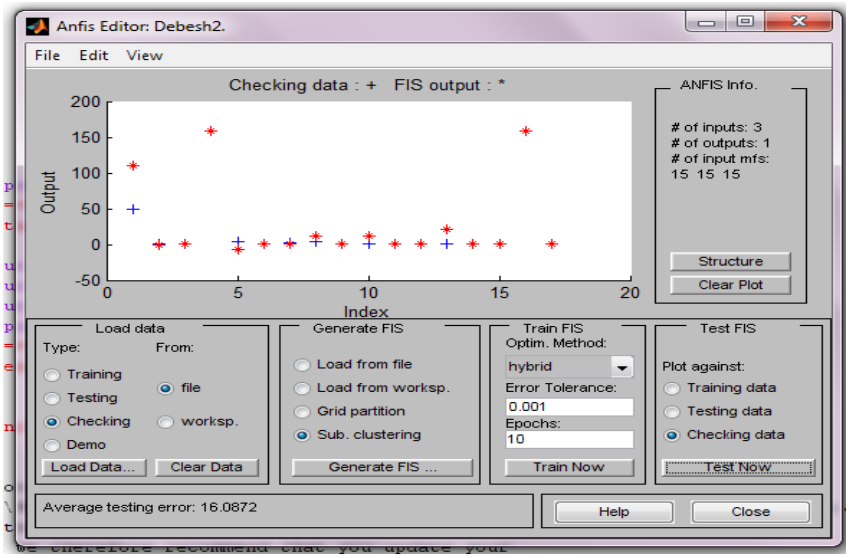

Fig 8.6: ANFIS editor for creating the model

A program codes, including ANFIS - subtractive cluster (SC) techniques, have been written in MATLAB language for simulation. Different ANFIS architectures are tried for optimum output. Then modelis tested and the results are compared by means of RMSE (root mean square error) and R^2 (coefficient of determination) statistics. The final architecture of ANFIS – SC models for is given in Table 8.1. The training and checking error for all models with all characteristics are given in Table 8.2.

Table 8.1: The training information for ANFIS- S-cluster methods

Features	SCM
Number of nodes	126
Number of linear parameters	60
Number of nonlinear parameters	90
Total number of parameters	150
Number of training data pairs	36
Number of checking data pairs	17
Number of fuzzy rules	15

The number of rules in the fuzzy rule base is $\prod_{i=1}^{n} c_i$, where c_i is the number of categories in the i^{th} variable and n is the number of variables. With increasing number of categories for the variables within a certain limit, a greater accuracy may be achieved. However, a very large rule base leads to dimensionality problems. Fifteen fuzzy rules have been developed for 36 training data.

Table 8.2: Training and Checking errors with input characteristics

Model training with 36 sets of input data			
Model	Training/ calibration error	Checking/ validation error	Characteristics of FIS files
SCM model	0.00263949	16.0872	Range of Influence=0.4, Squash factor = 1.25, Accept ratio = 0.5, Reject ratio = 0.15

Optimum outputs were obtained by models developed with characteristic of FIS files given in fourth column of Table 4. It shows that the validation errors for models is much higher than training error, it may be due to the short length of data. Ancreated ANFISsystem is shown in Fig. 7.

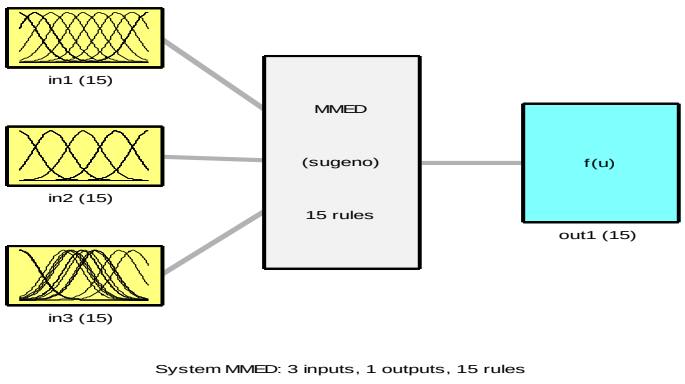

Fig 8.7: Created ANFIS system with three inputs and one output

8.4 Results and Discussions

The modeled output has been obtained by developed model for three input parameters. The calibrationsdata (36 sets of values) have been used to develop the model while 17 sets of values have been used for validate the model. Output results have been compared with observed values in Fig. 8.9

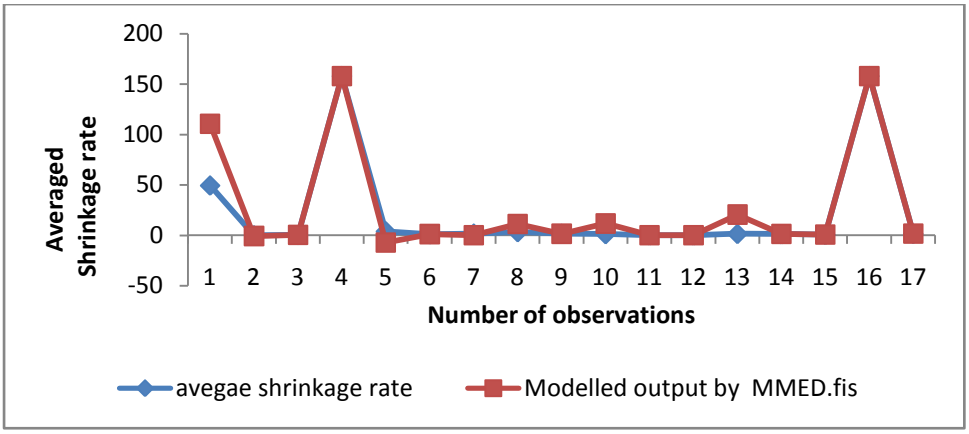

Fig 8.8 : Comparative plot of Modelled output and observed values

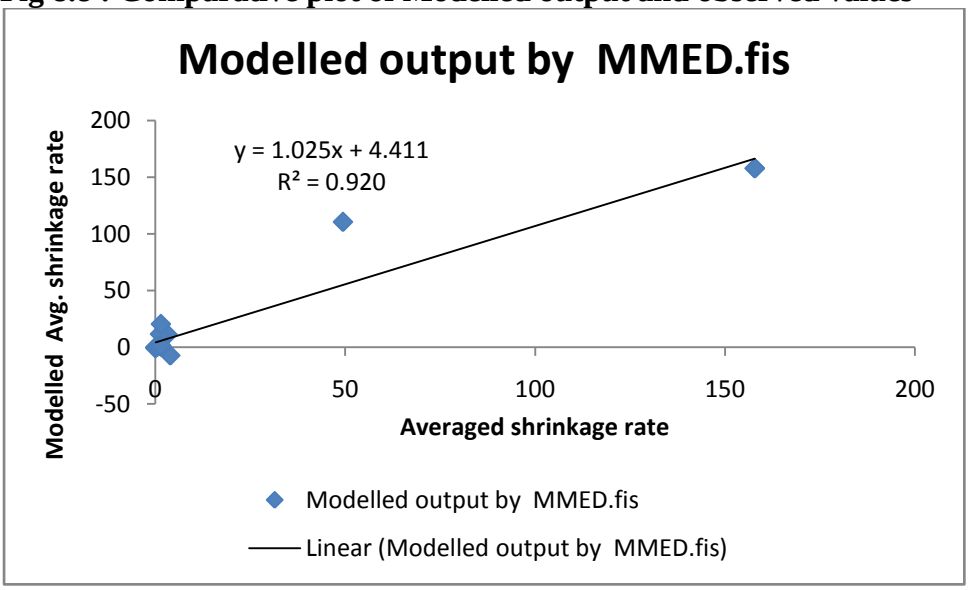

Fig 8.9: Linear relationship of ANFIS – SCM with observed output

The output for validation data seems very close with little error difference with observed values (Fig 8.8). The R^2 is very high (0.9209) for Subtractive cluster method as shown in Fig. 9. It is concluded that the ANFIS SCM model can be used for future analysis with little less error (Table 8.2) for same input parameters.

8.4.1 *Performance Indices of the Model*

Evaluations of model performance utilize number of statistics and techniques referred as "goodness of fit" statistics.To evaluate the model performance, different evaluation measures are considered and the resulting graphs from these models are analyzed statistically. Global error statistics, which include the RMSE between the computed and observed values, R^2, and the Nesh-Sutcliffe criterion (Nesh and

Sutcliffe, 1970), provide relevant information on overall performance.Finally, the error distribution at different threshold levels for all models is compared.

The models performance is evaluated by using Nash-Sutcliffe criterion of percent variance explained (VAREX) as given below:

$$VAREX = \left[1 - \frac{\sum_{t=1}^{N} (O_t - P_t)^2}{\sum_{t=1}^{N} (O_t - \overline{O})^2} \right] x100 \qquad (8.5)$$

Where N is number of observations; O_t is observed value at time t (m^3/s); $\bar{O}$ is mean of the observed values (m^3/s); and P_t is predicted value at time t (m^3/s). The value of VAREX ranges from 0 (lowest performance) to 100 (highest performance).

The training error is the difference between the training data output value, and the output of the fuzzy inference system corresponding to the same training data input value, (the one associated with that training data output value). The training error (trnError) records the RMSE of the training data set at each epoch. The ANFIS Editor GUI plots the training error versus epochs curve as the system is trained.

The values of performance indices of all the models are presented in Table 8.3.

Table 8.3: The values of performance indices of all the models

Models	**ANFIS- subtractive cluster**	
	Calibration data	**Validation data**
RMSE	0.00194	16.08717902
R^2	1	0.9209
VAREX	100	91.25677018

RMSE: Root mean squared error, R^2: Coefficientof determination, VAREX: percent variance

8.5 *Summary*

This model has been developed with ANFIS subtractive clustering technique of MATLAB software. During this process all three input data has been fuzzified with membership functions and output is treated as linear output. Figure 8.2 shows its comparative results with observed values. Graph has been drawn only for validation data. With respect to the performance indices of the model, it is strongly recommended that this developed model for shrinkage rate can be used for future analysis with same input parameters.

CHAPTER 9

CONCLUSION

1. Ni-P coating on carbon and graphite powders is possible using alkaline EL bath and can be used for making homogeneous coating on the irregular surfaces of carbon and graphite powders of the size of 5-10 microns. Atleast 75 hours to 100 hours of mechanical alloying with 300rpm, 5:1 ball to charge to ratio with agate balls and jars and toluene as PCA is needed for the synthesis of nanograined TiAl and Ti_3Al with an extra phase of Ti_3AlC.From the particle size analysis, it is seen that the particle size and the corresponding standard deviation decreased with increase in milling time, uniform and reduced size (140 to 189 nm) is obtained after 250 h milling for both the composition. The study of XRD patterns of compositions Ti-48Al-1Cr-1Nb-1(Ni-P) coated carbon and Ti-48Al-1Cr-1Nb-1(Ni-P) coated graphite, reveal that after about 75 h milling respectively the broadening of peaks occur. This is because the particles are in amorphous state and it infers that after such time of milling, one could go for sintering and reaction synthesis for further study of mechanical behaviors.
2. Titanium aluminide powders can be produced by mechanical alloying of elemental Ti and Al for 80 h. On Increasing MA time the particle size decrease down to less than 160 nm and further decrease in the range of 12-18 nm after 100 h of milling. According to the results the non-reactive sintering process displays better physical properties than reactive sintering.
3. The results of this study show that titanium aluminide based intermetallic matrix composites with AlNb2 phases as reinforcement can be produced by mechanical alloying of elemental Ti and Al powders for times longer than 80 h followed by hot pressing. Increasing mechanical alloying time to 100h lead to a decrease in the particle size of titanium aluminide powders down to about less than 160 nm and crystallite size in the range 12-18 nm after 100 h of milling. The prealloyed powders show lower hot pressing temperature (non reactive) and show comparative physical properties with fine grains.

4. The exothermic temperatures, heating rates, activation energy and density with various Al particle size containing TiAl mixtures have been compared. After the study of above results, Ti-Al (4h) mixtures show the optimized result for 30^0C/min heating rate. The above TiAl mixture records activation energy of -73.98kJ/mol and highest density of 3.129g/cm^3. The exothermic temperatures recorded for 30^0C/min is 761^0C. The Exothermic temperature range for Ti-Al (4h) for different heating rates is considerably low in comparison to that of the Ti-Al (0h) and Ti-Al (1h) and also not that much higher than that of the Ti-Al (7h) mixtures.
5. In this study the comparison of exothermic temperatures, heating rates, effect of particle size and determination of activation energy were carried out. After the study of the above results, Ti (5h)-Al provides optimized results for 6^0C/min rate of heating. Ti (5h)-Al powder blends records-11.57914kJ/mol kJ/mol activation energy and optimized density of 3.188g/cm^3. The reaction sintering temperature observed for the above mixture is 671^0C for heating rate of 6^0/min. The temperature range for exothermic peaks is the lowest for Ti (5h)-Al with respect to Ti (0h)-Al, Ti (1h)-Al and Ti (10h)-Al mixtures.
6. In this study the comparison of exothermic temperatures, heating rates, effect of particle size and the determination of activation energy were done. After studying above results, Ti (5h)-Al (4h) provides optimized results for 6^0C/min rate of heating.Ti (5h)-Al (4h) powder blends provides lower activation energy and optimized density of 3.193g/cm^3. The reaction sintering temperature observed for the above mixture is 670^0C for the heating rate of 6^0/min. The temperature range for exothermic peaks is lowest for Ti (5h)-Al (4h) as compared to Ti (0h)-Al (0h), Ti (1h)-Al (1h) and Ti (10h)-Al (7h) mixtures.
7. The exothermic temperatures, heating rates, activation energy and density with various Al particle size containing TiAl mixtures have been compared. After the study of the above results, Ti-Al (4h) mixtures show the optimized behavior for percentage relative expansion with highest of activation energies. The above TiAl mixture evolves

activation energy of - 40.11 kJ/mol. The microstructures also provide the information of lack of pores in case of Ti-Al(4h) mixtures .

8. Here we have compared the exothermic temperatures, activation energy, and percentage relative expansion with various particle sizes of Al in TiAl mixtures. After the study of the above results, Ti (5h)-Al mixtures show the optimized behavior for percentage relative expansion with highest of activation energies. The above TiAl mixture evolves activation energy of – 15.5 kJ/mol. The microstructures also provide the information of lack of pores in case of Ti (5h)-Al mixtures.
9. Analyzing the exothermic peaks, activation energy and relative expansion of various mixtures of Ti-Al system with different particle size and various soaking temperatures, the Ti (5h)-Al(4h) mixture with an approximate particle size of 28μ shows the highest of activation energy. The activation energy (-9.107 kJ/mol) and the expansion rate of the above mixture shows the smoothness and the feasibility of the process, which concludes as the best of the composition with optimized characteristics.
10. This model has been developed with ANFIS subtractive clustering technique of MATLAB software. During this process all three input data has been fuzzified with membership functions and output is treated as linear output. Figure 8.2 shows its comparative results with observed values. Graph has been drawn only for validation data. With respect to the performance indices of the model, it is strongly recommended that this developed model for shrinkage rate can be used for future analysis with same input parameters.

SCOPE OF FUTURE WORK

Based on the present study on reaction kinetics and dilatometric characterizations the following research activities are suggested:

1. DTA kinetic studies with applied pressure would be useful in calculation of activation energy and avrami parameter n for Ti-50at%Al aluminide formation.
2. Reaction kinetics study for binary compositions like Ti-48at%Al with variation of particle size will be helpful in providing facts for good densification.
3. Reaction kinetics studies of ternary compositions, quaternary compositions and composites with compositions of Ti-48Al-2Nb,Ti-48Al-2Nb-2Cr and Ti-48Al-2Nb-2Cr-SiC respectively will provide the idea for the route to achieve highly dense components.
4. With variations of particle sizes of Ti, Al, Cr, Nb, SiC and dilatometric investigations of the above compositions will provide the best components to work with.
5. Reaction hot pressing with the parameters calculated through dilatometric investigations will have a greater effect on achieving components to be used in higher temperature conditions.
6. Reaction sintering of gamma aluminides after degassing of elemental powders will display the actual amount of dilation to be reduced.
7. Hot stage microscopic studies of various stages of reaction sintering process with different particle size may be a useful method to determine the quantity and types of phases formed.

REFERENCES

1. Agarwala V., Agarwala R. C. and Kumar P. (2000), Intermetallics, 8, 85-87.
2. Appel F. and Wagner R. (1998), Mater Sci Eng, A22, 187-268.
3. Appel F., Oehring V and Wagner V. (2000), Intermetallics, 8, 1283-1312.
4. Appel F., Paul J. D. H., Oehring M., Frobel U. and Lorenz U (2003), Met Mater Trans A, 34A. 2149.
5. Austin C. M. and Kelly T. J. (1993), Proc Int Symp on Structural Intermetallics, Eds Darolia R., Lewandowski J. J., Liu C. T., Martin P. L., Miracle D. B. and Nachal M. V., TMS, Warrandale, PA, 143.
6. Baczewska Karwan J, Dymkowski T. and Seetharaman S. (2000), Proc Int Conf on Non Ferrous Metals and alloys 99, Archives of Metallurgy, No.3.
7. Baczewska Karwan J., Dymkoski T. and Seetharaman S. (1996), Adv in P M and Particulate Mater, 4, Part 15, 15-3.
8. Bahadur A., Kumar B. R. and Mohanty O. N. (1995), J Mater Sci, 30, 3690.
9. Baker I. and Gaydosh D. J. (1987), Mater Sci Eng, 96, 147.
10. Baker I. and Munroe P. R. (1990), High Temp Aluminides and
11. Banerjee D. (1994), Intermetallic Compounds, Eds J. H. Westbrook and R. L. Fleisher, John Wiley and Sons Ltd., 2, 91-131.
12. Bertolino N., Monagheddu M., Tacca A., Giuliani P., Zanotti C. and Tamburini Anselmi U. (2003) Intermetallics, 1_L, 41 -49.
13. Blackburn M. J. and Smith M. P. (1982), Technical report no. AFWAL- TR82-4086, U. S. Air Force Wright Laboratories.
14. Bondarev B., Anoshkin N., Molotkov A., Notkin A. and Elagin D. (1991), Intermetallic Compounds- Structure and Properties, Eds Izumi O., The Japan Inst of Metals, Sendai, 1009.
15. Bose A., Rabin B. H. and German R. M. (1988), P M Int, 20, 25.
16. C. Suryanarayana and C.C. Koch (2000), Nano crystalline Mater - Current Research and Future Directions, Hyperfine Interactions, 130. 5-44.
17. C. Suryanarayana, S.H. Yoo and J.R. Groza, (2001), J Mater Sci Let, 20, 2179-2181.

18. Cantor B. (2001), Proc 22nd Risoe Int Symp Mat Sci: Sci of Met^stable and NanocrystallineAlioys, Eds Dinesen A. R., Eldrup M., Juul Jensen D. and Linderoth S., Risoe National Laboratory, Denmark.
19. Chan K. S. (1992), JOM, 44, 30.
20. Chraponski J. Szkliniarz W., Koscielna A. and Serek B (2003), Mater Chemistry and Physics 8L 438-442.
21. Christman T.and Jain M.(1991), Scr Met Mater, 25, 767.
22. Copley S. M. and Kear B. H. (1967), TMS- AIME, 239, 977.
23. Crimp M. A. and Vedula K. (1986), Mater Sci Eng, 78, 193.
24. Cullity B. D. (2001), Elements of X-Ray Diffraction, Addison-Wiley Publishing Comapnay, Inc., USA.
25. Dahms M., Seeger J., Smarsly W. and Wildhagen B., (1991), ISIJ Int, 31, 1093-1099.
26. Darolia R. and Watson W. S. (1996), Intermetallics, 4, 505.
27. Darolia R., Lehman D.F. and Field R. (1992), Scr Met Mater, 26, 1007.
28. Das Gopal; Kestler H.; Clemens H and Bartolotta P.A.(2004), JOM, 56, No. 11,42-45.
29. Deevi S. C., Hajaligol M. R, Sikka V. K., Scorey C. R. and McKemon J. (1999), Proc Mater Res Soc Symp, 552, KK4.6.1.
30. Deevi S. C,, Sikka V. K. and Liu C. T. (1997), Prog Mater Sci, 42, 177.
31. Dimcic B, Vilotizevic M., Bozic D., Rajnovic D. and Jovanovic M. T. (2005), Mater Sci Forum, 494, 211-216.
32. Dimiduk D. M. (1999), Mater Sci Eng, A263. 281-288.
33. Djanarthany S., Viala J. and Bouix J. (2001), Mater Chemistry and Physics, 72, 301-319
34. Dogan B., Wagner R. and Beaven P. A. (1991), Scr Met, 25, 773-778.
35. Doychak J. (1994) Intermetallic Compounds, Eds Westbrook J. H. and Fleischer R. L., John Wiley and Sons, i, 977-1016.
36. Dwivedi D.K., A. Sharma, T.V. Rajan Journal of Materials Processing TechnologyVolume 196, Issues 1–3, 21 January 2008, Pages 197–204
37. Eelman D. A., Dahn J. R., Mckay G. R. and Dunlop R. A. (1998), J Alloys and Compounds, 266. 234.

38. EgryI., Brooks R., Holland-Moritz D, Novakovic R, Matsushita T, Ricci E., Seetharaman S. , Wunderlich R and Jarvis D. Int J Thermophys (2007) 28:1026–1036.
39. ener U. R., Lin J. C. and Chang Y. A. (1992), Met Trans A, 23A, 2081.
40. Eriksson R., Hayashi M., and Seetharaman S. International Journal of Thermophysics, Vol. 24, No. 3, May 2003 (© 2003).
41. Froes F. H., Suryanarayana C., Russel K. and Li C. G. (1995), A192/193, Mater Sci Eng, 612-623.
42. Fuchs G. E. (1993), Ti 92, Science and Technology, Eds Froes F. H. and Chaplan I. L., TMS, II, 1275.
43. Gedevanishvili S. And Deevi S. C. (2002), Mater Sci and Eng, A325, 163- 176.
44. George E. P. and Liu C. T. (1990), J Mater Sci, 5, 754.
45. German R. M. (1985), Liquid Phase Sintering, Plenum Press, NY.
46. German R. M. (1990), Advances in P M, Part 2,, 115.
47. German R. M., Bose A., and Stolloff N. S. (1989), High TempOrdered Intermetallic Alloys 111, Eds Liu C. T., Taub A.I., Stoloff N.S. and Koch C. C., MRS Proc, 133, 403-414.
48. Ghosh Dulal C. and Biswas Raka (2002), Int J Mol Sci, 3, 87-113.
49. Guo J. T. and Cui C. Y. (2002), Key Eng Mater, 2T7, 117-128.
50. Gupta R. K., Pant Bhanu, Agarwala Vijaya, Agarwala R.C. and Sinha P. P. Transactions of the Indian Institute of Metals Vol. 62, Issue 1, February 2009, pp. 21-24
51. Gupta R. K., Pant Bhanu, Agarwala Vijaya, and Sinha P. P. Metal Science and Heat Treatment, Vol. 55, Nos. 7 – 8, November, 2013 (Russian Original Nos. 7 – 8, July – August, 2013)
52. Gupta R. K., Pant Bhanu, Agarwala Vijaya, Ramkumar P. and Sinha P. P. Transactions of the Indian Institute of Metals Vol 63,issue 4,August 2010, 715-718
53. Hahn Y. D. and Lee Y. T. (1992), Adv in P M and Particulate Mater, 9, 309 318.
54. Hajaligol M. R., Deevi S. C., Sikka V. K. and Scorey C. R. (1998), Mater SciEng, A258. 249.

55. Hamada S., Hamada H., Suzuki H. and Nozue A. J. (2002), J Mater Sci,37, 1107-1113.
56. Hanamura T., Ikematsu Y., Morikawa H., Tanino M. and Takamura J. (1991), Proc Int Symp on Intermetallic Compounds, Eds Isumi O., Sendai, Japan, 179-183.
57. Hansson T., Kamaraj M., Mutoh Y. and Patterson B. (2000), ASTM, STP 1367, Eds Hoeppner D. W., Chandrasekhran V. and Elliott C. B., American Society of Testing and Mater, 85-69.
58. Haubold T., Bohn R., Birringer R. and Gleiter H. (1992), Mater Sci Eng, A153. 679-683.
59. He Xiaodong, Han Jiecai and Zhang Xinghong (2002), Key Eng Mater, 217. 51-54.
60. Henaff G. and Tonneau A (2001) Met and Mater Trans A, 32A , 557-567.
61. Hiroyuki Y. Yasuda, Takayoshi Nakano, Jun Nakazawa and Yukichi Umakoshi, (1997) ISIJ Int,37, No. 1 2, 1210-1217.
62. Huang S. C. (1992), Met Trans A, 23A, 375.
63. Huang S. C. and Chesnutt J. C. (1994), Intermetallic Compounds, Eds Westbrook J. H. and Fleisher R. L., John Wiley and Sons, 2, 73 - 90.
64. Huang S. C. and Hall E. L. (1991), High Temp Ordered Intermetallic Alloys IV, Eds Johnson L. A., Pope D. P. and Stiegler J. O., Mater Res Soc Symp Proc, 213, 827-832.
65. Huang S. C. and Shih Donald S (1991), Micro-Property Relationships in Ti Aluminides and Alloys, Eds Kim Y. W. and Boyer Rodney R., TMS, 105- 121.
66. Huang S. C. and Siemers P. A. (1989) Met Trans 20A, 1899.
67. Huang S. C., Hall E. L. and Shih Donald S (1991), ISIJ Int, No. 10, 31, 1100-1105.
68. Ibrahim I. A., Mohammed F. A. and Lavernia (1991), J Mater Sci, 26, 1137-1156.
69. Imayev R. M., Imayev V. M. and Salischev G., (1993a) Scr Met Mater, 29, 713-718.
70. Imayev R. M., Imayev V. M. and Salischev G., (1993b) Scr Met Mater, 29, 719-724.
71. Imayev V. M., Salischev G.A., Imayev R M., Shagiev M. R., Gabdullin N. K.,

and Kuznestov A. V. (1997), Structural Intermetallics 1997, Eds Nathal M.V., Darolia R., Liu C. T., Martin P. L., Miracle D. B., Wagnor R. and Yamaguchi M., Minerals Metals and Mater Soc ConfProc, 505-514.

Intermetallics, Eds Whang S. H., Liu C. T., Pope D. P. and Stiegler J. O., TMS, Warrandale, 425-452.

72. Jang J-SR, Sun C-T, Mizutani E. 1997. Neuro-Fuzzy and Soft Computing: A Computational Approach to Learning and Machine Intelligence. Prentice Hall: Upper Saddle River, NJ.

73. Jang J-SR. 1993. ANFIS: adaptive network based fuzzy inference system, IEEE Transactions on Systems, Man and Cybernetics 23: 665–683.

74. Johansen TA, Babuska R. 2002. On multi-objective identification of Takagi–Sugeno fuzzy model parameters. In *Preprints 15th IFAC Word Congress,* Barcelona, Spain.

75. Kawabata T., Tamura T. and Izumi O. (1989), High Temp ordered Intermetallic Alloys III, 133, Eds Liu C. T., Taub A. I., Stollof N. S. and Koch C. C., Mater Research Society, 329-334.

76. Kawaura H., Kawahara H.,Nishino K and Saito T. (2002), Mater Sci Eng 331. 589-595.

77. Khanna Rita, McCarthy Fiona, Sun Haiping, Sahajwalla Veena and Simento Noel Metallurgical and Materials Transactions B December 2005, Volume 36, Issue 6, pp 719-729

78. Khanna Rita, Sahajwalla Veena, Rodgers Brenton, McCarthy Fiona Metallurgical and Materials Transactions B August 2006, Volume 37, Issue 4, pp 623-632

79. Kim J. K., Kin T. K., Lee T. K., Hwang S. K., Nam S. W. and Kim N. J.. (1999),Gamma Ti Aluminides, Eds Kim Y. W., Dimiduk D. M. and Loretto M. H., The Minerals, Metals and Material Society, 231-238.

80. Kim J.K, Rohatgi P.K., Acta Materialia Volume 46, Issue 4, 13 February 1998, Pages 1115–1123.

81. Kim Y. W. (1992), Acta Met et Mater, 40, 1121-1134.

82. Kim Y. W. and Froes F. H. (1990), High Temp Aluminides and Intermetallics, Eds Whang S. H., Liu C. T., Pope D. P., 465-492.

83. Kim Y.W. (1995) JOM, 46, (7), 39-41.

84. Kim Y.W. and Dimiduk D. M. (1991), JOM, 43, 40.
85. Kingery W.D., Woulbourn J. M. and Charvat F. R. (1963), J Amer. Ceramic Soc., 46, 391-395.
86. Koch C. C. (1988), Rapid Solidification of Intermetallic Compounds, Int Mater Rev, 33, (4), 201 -219.
87. Kongkarat Somyote, Khanna Rita and Sahajwalla Veena steel research international
88. Kuang J.P., Harding R.A., Campbell J. (2002), Mater Sci Eng, A329-331. 31-37.
89. Kumar Vikas, Germann L and Studel Jean-Loup (1999), Annual Report SNECMA/ARM1NE/TUBOMECA No. 940937, Lot2.
90. Lee Byeong-Joo and N. Saunders (1997), Z Met, 88, 152-161.
91. Lee D. J. and Yoon D. N. (1988), P M Int, 20, 15.
92. Lee T. K., Mosunov E. I. and Hwang S. K. (1997), Mater Sci Eng, A239- 240. 540-545.
93. Lipsitt H. A. (1985), High Temp Ordered Intermetallic Alloys, Eds Koch C. C. , Liu C. T. and Stolloff N. S., MRS, 39, 351 -364
94. Liu C. T. and White C. L. (1985), High Temp Ordered Intermetallic Alloys, Eds Koch C. C., Liu C. T. and Stoloff N. S., MRS Proc, 39, 365-380.
95. Liu C.T and Pope D.P. (1994), Intcrmclallic Compounds, Eds Westbrook J. H.and Fleischer R.L, John Wiley and Sons, 2, 17-51.
96. Liu C.T. (1991), Scr Met, 25, 1232-1288.
97. Liu Tong, Shao Huaiyu and Xingguo Li(2003) Nanotechnology JI4, 542.
98. Liu.C.T and George E. P. (1990), Scr Met, 24, 1285-1290.
99. London B. and Kelly T. J. (1991), Microstructure/ Property Relationships in Ti Aluminides and Alloys, Eds Y. W. Kim and RR Boyer, TMS, Warrandale, 285.
100. Mamdani, E. H., and Assilian S. 1975. An experiment in linguistic synthesis with a fuzzy logic controller, Int. J. Man MaChine Stud., 7(1), 1 – 13.
101. Martin P. I, Mendiratta M. G. and I-ipsitt H. A. (1983), Met Trans, 14A. 2170.
102. Martin P. L. and Hardwick D. A. (1994), Intermetallic Compounds, Eds J. H. Westbrook and R. L. Fleisher, John Wiley and Sons, 637-660.
103. Mckamey C. G., Whang S. H., and CT Liu, (1995) Scr Met Mater, 32, (3), 383-388.

104. McQuay Paul and Larsen Don (1997), Structural Intermetallics 1997, Eds Nathal M. V., Darolia R., Liu C. T. Martin P. L., Miracle D. B., Wagner R. and Yamaguchi M. The Minerals, Metals and Mater Society, 523-529.

105. Mehta R, Jain S.K., & Kumar Vipin 2005. Fuzzy technique for reservoir operation – effect of membership functions with different number of categories, 28 (3-4), 17-34.

106. Mei B., Lin J., Miyamoto Y. and Iwasa M. (2000), SIJ Int, 40, S77-S81.

107. Minay EJ, McShane HB and Rawlings RD (2004), Intermetallics, 12, 75 - 84.

108. Miracle D. B. (1993), Acta Met Mater, 39, 649.

109. Miracle D.B. and Darolia R. (1994), Intermetallic Compounds, EdsWestbrook J. H. and Fleischer R.L, 2, 53-72.

110. Mistier R. E., Sikka V. K., Scorey C. R., McKernan J. E., and Hajaligol M. R. (1998), Mater Sci Eng, A258,, 258-265.

111. Mohan B., Rajadurai A. and Satyanarayana K. G. (2004), J Mater Processing Tech, 153-154. 978-985.

112. Morales Ricardo, Aune Ragnhild E., Grinder Olle, and Seetharaman Seshadri JOM October 2003, Volume 55, Issue 10, pp 20-23 .

113. Morris D. G. and Morris M. A. (1991), High Temp Ordered Intermetallic Alloys IV, Eds Johnson L. A., Pope D. P. and Stiegier J. O., Mater Res Soc Symp Proc, 213. 847-852.

114. Munir Z. A. and Anselmi -Tamburini (1989), Mater Sci Rep, 3, 277.

115. Mutoh Y., Moriyal T., Zhu S. J. and Mizuhara Nagaoka Y. (1998), Third Pacific Rim Int Conference on Advanced Mater and Processing, Honolulu, Hawaii; July 12-16.

116. Naidich Y. V., Lavrinenko I. A. and Evdokmov V. A. (1974), Sov. Powder Met Metal. Ceram., jJ3, 26-30.

117. Nakagawa Y. G., Yokoshima S. and Mastuda K. (1992), Mater Sci Eng A, 153.722.

118. Nash P., Singleton AAM. F. and Murray J. L. (1991), Phase diagrams of binary nickel alloys (ed. Nash P.), i, ASM Int, 3.

119. Nash, J E and Sutcliffe J.V. 1970. River flow forecasting through conceptual models: 1. A discussion of principles, J. Hydrol., 10, 282 –290.

120. Nayak, P. C., Sudheer K. P., Rangan D. M., and Ramasastri K. S. 2004. A

neuro-fuzzy computing technique for modeling hydrological time series, J. Hydrol., 291(1 – 2), 52 – 66.

121. Nishimura C. and Liu C. T. (1993), Acta Met et Mater, 41, 113-120.
122. Nishiyama Y., Miyashita T., Isobe S. and Noda T. (1990) High Temp Aluminides and Intermetallics, Eds S. H. Whang, Liu C. T., Pope D. P. and Steigler J.O., The Minerals Metals and Mater Society, USA, 557-584.
123. Odone R. Robert and German R. M. (1989), Adv in PM, 3, 475.
124. Oleszak D. and Shingu P. H. (1994), Mater Sci Eng, A181/182, 1217.
125. Paidar V., Pope D. P. and Vitek V. (1984), Acta Met, 32, 435.
126. Park H. S., Park K. L. and Hwang S. K. (2002), Mater Sci Engg, A329- 331. 50-56.
127. Peacock D. K. (1989), Met Mater, 5,474.
128. Perkins R. A., Chiang K. T. and Meier G. H. (1987), Scr Met, 21, 1505.
129. Pillai Suresh C., Kelly John M., McCormack Declan E., O'Brien Paul and Raghavendra Ramesh (2003), J Mater Chemistry, 13(10), 2586 - 2590.
130. Planck S. K. and Rosenberger A. H. (2002), Mater Sci and Eng, A325. 270-280.
131. Prasanth N, Pillai R. M. and Pai B. C. (2004), Indian Foundry Journal 50(1), 50-57.
132. Priyadarshi A. and Balasubramaniam R. (2001), Bull. Mater Sci, Indian Academy of Sciences, 24, No. 5, 559-562.
133. Qian Wang, Zhengming Sun, Hitoshi Hashimoto, Shuji tada, Yong-ho Park, Se-Hyun Ko and Toshiko Abe (2000), Mater Trans JIM, 41_, No.5, 551-554.
134. Qin G.W., Wul L., Oikawa K. , Ikeshoji T., Sumi S., Zhao G., Jiang M., Mao D.W., Ma J.L., Hao S.M. (2001), Intermetallics, 9, 173- 177.
135. Rabin B. H. and Wright R. N. (1991), Met Trans A, 22A, 277.
136. Rajan T.V. , Sharma C.P. and Sharma Ashok"Heat Treatment Principles and techniques.Volume 84, Issue 4, pages 362–369, April 2013.
137. Ramaseshan R. (1998), PhD Thesis on Synthesis and Characterization of y-Tial/ Ti_2AlC Intermetallic Composites Made by Reactive Processing of Electroless Coated Ti Powders, Indian Institute of Technology Madras, Chennai, India.
138. Rawers J. C. and Wrzesinky, W. R. (1992), J Mater Sci, 27, 2877-2886.

139. Retallick W. B., Brady M. P. and Humphrey D.L (1998), Intermetallics, 6, 335-337.
140. Reuss S. and Vehoff H. (1990), Scr Met Mater, 24, 1021.
141. Rohatgi P. K., Ray S. and Liu Y. International Materials Reviews 1992 Vol. 37 NO.3 129.
142. Rowe R. G., (1990) High Temp Aluminides and Intermetallics, Eds Whang S. H., Liu C. T., Pope D. P. and Stiegler J. O., TMS, Warrandale, 465-492.
143. S.J. Hong, T.S. Kim, C. Suryanarayana and B.S. Chun, (2001), Met and Mater Trans A, 32A, 821 -829.
144. Salischev G., Imayev R M., Senkov O. N., and Froes F. H. (2000a), JOM, Dec., 46-48.
145. Salischev G., Imayev R M., Senkov O. N., Imayev V. M., Gabdullin N. K., Shagiev M. R., Kuznestov A. V. and Froes F. H. (2000b), Mater Sci Eng, A286. 236-243.
146. Sauthoff G. (1995) Intermetallics,VCH Verlagsgesellchaft mbH, Germany.
147. Savstkii A. P. and Brutsev N. N. (1981), Soviet P M Metal Ceramics, 20, 681-621.
148. Savstkii A. P.(1980), Soviet P M Metal Ceramics, J_9, 488.
149. Seetharaman Sankaranarayanan, Subramanian Jayalakshmi, Gupta Manoj and Hamouda Abdelmagid S. , Metals 2012, 2, 274-291.
150. Semiatin S. L. and Mcquay P. A. (1992), Met Trans A, 23A, 149.
151. Semiatin S. L., Lark K. A., Barker D. A., Seetharaman V. and Marquardt B. (1992), Met Trans A, 23A, 295-305.
152. Shagiev M.R., Salischev G., Imayev R. M., Imayev V. M. and Kuznestov A. V. (2004), Mater Sci Forum, 447-448. 317-322.
153. Sharma A., La Metallurgia Italiana, 2013 - gruppofrattura.it.
154. Sharma S. B., Agarwala R. C.; Agarwala V. and Ray S., Surface Engineering Volume 18 Issue 5 (01 October 2002), pp. 344-349.
155. Sharma S. B., Agarwala V., Agarwala R. C. and Satyanarayana k.g. metallurgical and materials transactions b volume 36b, february 2005,23-31.
156. Sharma S.B. PhD Thesis
157. Shechtman D., Blackburn M. J. and Lipsitt H. A. (1974), Met Trans, 5, 1373.
158. Shemet V., Tyagi A. K.., Singheiser L., Breuer Kamruddin U. and Quadakkers

W. J. (2000), Proc of Int Symp on Mater Ageing and Life Management (ISOMALM - 2000), Kalpakkam, India, Eds: Raj Baldev, Rao K.Bhanu Sankara, Jayakumar T.and Dayal R.K., 809-814.

159. Shih D.S. and Scarr G. K. (1991), High Temp Ordered Intermetallic Alloys IV, Mater Res Soc Symp Proc, 213, 727.
160. Shobana M.K, Sankar S. and Rajendran V. Journal of Alloys and Compounds 472 (2009) 421–424.
161. Shobana M.K, Sankar S. and Rajendran V. Materials Chemistry and Physics 113 (2009) 10–13.
162. Shobana M.K., Rajendran V., Jeyasubramanian K. and Suresh Kumar N. Materials Letters Volume 61, Issue 13, May 2007, Pages 2616–2619.
163. Sikka V. K. (1990), High Temp Aluminides and Intermetallics, Eds Whang S. H., Liu C. T., Pope D. P. and Stiegler J. O., TMS, Warrandale, 505-520.
164. Sikka V. K. (1991), High Temp Ordered Intermetallic Alloys IV, Mater Res Soc Symp Proc, 213, 907.
165. Skrotzki W., Kegler K.., Tamm R., and Oertel C.G. (2005), Cryst Res Technol 40, 1/2, 90-94.
166. Sohn H. Y. and Wang X. (1996), J Mater Sci, 3J, 3281 -3288.
167. Springgate Mark Edwin, Nikolas Douglas Gene ,Sturgis; David H. and Yasrebi Mehrdad (2000), United States Patent No. 6,024,163 dated February 15, 2000.
168. Srinivasan S., Desch P. B. and Schwartz R. B. (1991), Scr Met Mater, 25, 2513.
169. Sujata M., Sastry D. H. and Ramachandra C. (2004), Intermetallics, 12, 691-697.
170. Surappa M. K and Rohatgi P. K. JOURNAL OF MATERIALS SCIENCE. 16 (1981) 983-993.
171. Suryanarayana C. (2001) Progress in Mater Sci, 46 , 1-184.
172. Suryanarayana C., Froes F. H. and Riowe R. G., (1990), Int Mater Rev, 9 (11), 948-957.
173. Takahashi T., Nagai H. and Oikawa H. (1990) Mater Sci Eng A, 128A. 195.
174. Taub A. I. and Fleischer R. L. (1989), Science, 243, 616-621.
175. Taub A.I. Huang S. C. and Chang K. M. (1984), Met Trans, 15A, 399.
176. Tetjukhin V.V., Levin I.V., Kozlov A.N., Poljanskij S.N. (2002), US Patent

No. 2179899 dated 9 Apr 2002.

177. Tetsui T. (1997), Structural Intermetallics 1997, Eds Nathal M. V., Darolia R., Martin P. L., Miracle D. B., Wagner R. and Yamaguchi M., The Minerals, Metals and Mater Society , 489-493.
178. Tetsui T. (2002a), Intermetallics, 10, 239-245.
179. Tetsui Toshimitsu (2002b), Mater Sci Eng, A329-331. 582.
180. Thakur Sanjay Kumar, Srivatsan T.S., Gupta Manoj Materials Science and Engineering A 466 (2007) 32–37.
181. Thakur Sanjay Kumar, Kwee Gan Tai and Gupta Manoj J Mater Sci (2007) 42:10040–10046.
182. Thornton P. H., Davies R.G. and Johnston T.L. (1970), Met Trans A, JA, 207.
183. Tsuzimoto T. and Hashimoto K. (1989), High Temp Ordered Intermetallic Alloys III, Eds Liu C. T., Taub A. I., Stollof N. S. and Koch C. C,, Mater Research Society, 133, 391-396.
184. V. Seetharaman and Semiatin S. L (1998), Met Mater Trans A,29A, 1991.
185. Vedula K. (1994) Intermetallic Compounds, Eds Westbrook J. H. and Fleischer R. L., John Wiley and Sons, 2, 199-209.
186. Vujic D,, Z. Li and S. H. Wang (1988), Met Trans A, 9A, 2445- 2455.
187. Wang G. X. and Dahms M. (1992), Scr Met Mater, 26, 717-722.
188. Wang X., Sohn H. Y. and Schlesinger M. E. (1994), Mater Sci Eng, A186. 151-155.
189. Wegmann Gerhard, Maruyama Kouichi (2000), Phil Mag A, 80, 2283 - 2298.
190. Wei Zhao and David E. Luzzi, (2000), 2000 Fall Meeting Symposium on Influences of Interface and Dislocation Behavior on Microstructure Evolution; http://www.mrs. org/members/proceedings/fall2000/y/Y 10_4.pdf.
191. Wen C. E., Yasue K. and Yamada Y. (2001), J Mater Sci, 36> 1741-1745.
192. Westbrook J. H. (Ed) (1959), Mechanical Properties of Intermetallic Compounds, John Wiley and Sons, Inc., NY.
193. Westwood A. R. C. (1988), Met Trans A, 19A, 749-758.
194. Whittenberger J. D. (1990), Solid State Powder Processing, Eds Clauer A. H. and Barbadillo J. J., The Minerals, Metals and Mater Society, 137-155.
195. Xia J. (2005) Surface Eng, 2J_, No. 1, pp. 6-11(6).
196. Yamagata T. and Yoshida H. (1973), Mater Sci Eng, J_2, 95.

197. Yamaguchi M., Nishitani S. R. and Shirai Y. (1990), High Temp Aluminides and Intermetallics, Eds S. H. Whang,Liu C. T., Pope D.P. and Steigler J.O., The Minerals Metals and Mater Society, USA, 63-90.
198. Yamaguchi M. (1992), Mater Sci Tech, 8, 299.
199. Yamaguchi M., Inui H. and Ito K. (2000), Acta Mater, 48 , 307-322.
200. Yi H. C. and Moore J. J. (1988), Scr Met, 22, 1889-1892.
201. Yi H. C. and Moore J. J. (1990), J Mater Sci, 25, 1159.
202. Zhang P., Baczewska Karwan J, Du S. and Seetharaman S. (1996), Met Mater Trans A, 27A, 2978-2984.
203. Zhao I., Beddo J., Morphy D. and Wallace W., (1995), Mater Sci Eng, A192/193. 957-964.
204. Zhao J.C. and Westbrook J. H. (2003), Ultrahigh-Temp Mater for Jet Engines and Westbrook, MRS Bulletin/ September, 622-630.
205. Zhenbin Ge, Kexin Chen, Junming Guo, Heping Zhou and Jose M. F. Ferreira (2003), J European Ceramic Soc, 23, 567 -574.

LIST OF PUBLICATIONS

(i) List of Reviewed Publications

1. Synthesis of Nanograined Ti-Al-Cr-Nb-X [X = Ni-P-Coated Graphite and Carbon] Intermetallic Matrix Composites by Mechanical Alloying, by **D.D. Mishra**, V.Agarwala, R.C Agarwala, Journal of Particulate Science and Technology Particulate Science and Technology: An International Journal Volume 31, Issue 4, pages 313-318 2013.
2. Sintering behavior of mechanically alloyed Ti-48Al-2Nb Aluminides, by **D.D. Mishra**, V.Agarwala, R.C Agarwala, published in High Temperature, 2014, Vol. 52, No. 1, pp. 65–71. © Pleiades Publishing, Ltd., 2014
3. Effect of Al particle size on the reaction kinetics and densification of TiAl intermetallics by **Debesh Devadutta Mishra**, Vikram.V.Dabhade, Vijaya Agarwala and R.C.Agarwala, Journal of Phase Transitions. 2014 Vol. 87, No. 4, 344–356.

(ii) List of papers presented in Conferences

1. Synthesis of Nanograined Ti-Al-Cr-Nb-X [X=Ni-P coated Graphite and Carbon] Intermetallic Matrix Composites by Mechanical Alloying by **Debesh Devadutta Mishra**, Vijaya Agarwala and R.C.Agarwala is presented in International Conference NANO-2010 during December11-13,2010 at Centre for Nanoscience and Technology ,KSR College of Technology, Thiruchengodu - 637215
2. Synthesis of Titanium Aluminides by Mechanical Alloying and their Sintering Behavior by **Debesh Devadutta Mishra**, Vikram.V.Dabhade Vijaya Agarwala and R.C.Agarwala is presented in International Conference PM-11, during February 2-4,2011 held at Pune by PMAI.
3. Synthesis Of Titanium Aluminides and their further sintering by **Debesh Devadutta Mishra**, Vijaya Agarwala and R.C.Agarwala is presented in One day Workshop on Thermo-Mechanical Simulator on February 3, 2010 at IIT Roorkee.

4. Synthesis of Titanium Aluminides based Intermetallic Matrix Composites by Mechanical Alloying and their Consolidation by Hot Pressing by **Debesh Devadutta Mishra**, Vijaya Agarwala and R.C.Agarwala is presented in International Conference ICCM-18, during June 20--26, 2011 held at Jeju, South Korea.
5. Synthesis of Titanium Aluminides and their Consolidation by Hot Pressing in Thermo –Mechanical Simulator by **Debesh Devadutta Mishra**, Vijaya Agarwala and R.C.Agarwala is presented in One day workshop on Thermo-Mechanical Simulator on February 3, 2011 at IIT Roorkee.
6. Effect of Aluminium particle size on the Reactive Sintering and Mechanical properties of Ti-Al Intermetallics by **Debesh Devadutta Mishra**, Vikram.V.Dabhade Vijaya Agarwala and R.C.Agarwala is presented in International Conference PM-12, during February 2-4, 2011 held at Mumbai by PMAI.

7. Effect of Ti Particle Size on the Reaction Kinetics and Densification of TiAl Intermetallics **D.D.Mishra**[*], V. Agarwala and R.C. Agarwala, presented in International Conference PM-13, during February 7-8, 2013 held at Pune,India by PMAI.

8. Effect of Ti and Al Particle Size on the Thermal analytical behavior and Densification of TiAl Intermetallics **D.D.Mishra**[*], V. Agarwala and R.C. Agarwala, presented in International Conference AFTMME in PTU, Punjab.

9. Effect of Ti and Al Particle Size on the Dilatometric behavior of TiAl Intermetallics, **D.D.Mishra**[*], V. Agarwala and R.C. Agarwala, presented in International Conference PFAM XXII,Singapore , December 2013

(iii) List of papers communicated in Journals

1. Effect of Ti Particle Size on the Reaction Kinetics and Densification of TiAl Intermetallics D.D.Mishra[*], V. Agarwala and R.C. Agarwalaunder review in Journal of Advanced Powder Technology (Under review)